

UNIVERSITY OF TECHNOLOGY, SYDNEY

Nanoparticle Transport Modelling in Saturated Porous Media

A dissertation submitted in partial satisfaction of the requirements for the
degree
Doctor of Philosophy

in
Engineering Science with Specialization in Groundwater Modelling

by

Sara Moghadas Mehrabi

Principal Supervisor:
Dr William Milne-Home
Co- Supervisor:
Dr Robert McLaughlan

2014

CERTIFICATE OF ORIGINAL AUTHORSHIP

I certify that the work in this thesis has not previously been submitted for a degree nor has it been submitted as part of requirements for a degree except as fully acknowledged within the text.

I also certify that the thesis has been written by me. Any help that I have received in my research work and the preparation of the thesis itself has been acknowledged. In addition, I certify that all information sources and literature used are indicated in the thesis.

Signature of Student:

Date: 01/04/2014

Acknowledgments

It is with incredulity that I face the end of this very interesting and eventful journey. The time has come to express gratitude to those who made it such an enjoyable ride.

It's customary to give thanks to the advisor first for their help, though, I pride myself on breaking tradition. I will not follow such convention. Instead, I will thank an idol who showed me how to be humble, a friend who stuck by me when the times were tough, and a teacher who taught me everything I know. Thank you for your never-ending support. Thank you for believing in me and my wild and ambitious ideas. Thank you for tolerating my juvenile stubbornness. Thank you for taking my whines and whinges with a smile on your face. Thank you for meeting me whenever I needed you. Thank you for the many cups of delicious hot chocolate. They were the most delightful treat and kept me energised to do more and more. Thank you for being there for me when I was in a dark place. Thank you for all I have achieved, because they would not be possible without you. Thank you Bill (Dr William Milne-Home) for everything you have been, still are, and will be for me.

To my co-supervisor Dr Robert McLaughlan, my external advisor, Mr Hugh Middlemis, and the remarkably accommodating Dr Henning Prommer, I thank you for your generosity with your time and knowledge.

The ongoing support of several others is deeply appreciated. Ms Phyllis Agius, Ms Belinda Lee, Ms Bianca Azar, and Associate professor Barry Jay are amongst those exceptionally giving and supportive individuals.

To my closest friends Dr Thomas Given-Wilson and [soon to be] Dr Jose Vergara who continually challenged my ideas, no matter what I said; thank you for making our conversations so interesting and thank you for keeping me sane. You guys deserve a trip to Las Vegas!

I offer my most sincere thanks to Mrs Marjorie James for proof reading this document and providing excellent advice on improving the manuscript. Also to Mr Eric Sanderson for generously sharing his expertise in 3D visualisation of special/temporal data.

Finally, thanks to my loving family. My mother for the countless times she asked me:” just how much longer are you going to take dear?” which kept me motivated to push on as hard as I could. My beautiful sister and her family for their enduring emotional support. My cheeky brother for always dismissing my complaints, including the legitimate ones. To my parents-in-law for their encouragement. And to Mr and Mrs Mal and Carole Brown who filled the void of my distant parents ever so delightfully. Last but not least my soul mate, Mr Craig McClelland for simply being who he is; The Best!

Dedications

I wish to dedicate this work to my father who was the most significant influence on me growing up. An intellectual man who encouraged me to better myself in every way possible, who taught me critical thinking, who heartened me to use logic in arguments and who introduced me to man's best friend; book!

My heart is broken by his sudden and unexpected passing last year, coming to terms with the bitter fact that he won't share with me the happiness of achieving what he dreamed for me. But his memory is always with me and his legacy will live on.

Vita and publications

This document features the following papers, posters, and presentations, either accepted or submitted for consideration at the time of submission. The dissertation author was the primary investigator and author of these publications.

Mehrabi, S., Milne-Home, W., 2014, *Modelling the transport of cylindrical nanoparticles in saturated porous media*, Environmental modelling & software, under preparation.

Mehrabi, S., Milne-Home, W., 2014, *Reducing the uncertainty in nanoparticle transport modelling by inclusion of natural heterogeneity of the porous media*, International Journal of Hydrology Science and Technology, Submitted.

Mehrabi, S., Milne-Home, W., 2013, *Optimization of Nanoparticle Delivery to Subsurface Contaminated Zone*, the 4th International Conference on Nanotechnology: Fundamentals and Applications, Toronto, Ontario, Canada.

Mehrabi, S., Milne-Home, W., 2012, *Representation of Heterogeneity in Single Collector Efficiency Equation for Multi-Walled Carbon Nanotubes*, International Journal of Theoretical and Applied Nanotechnology (IJTAN), 1-75-86pp.

Mehrabi, S., Milne-Home, W., 2012, *The Importance of Particle Orientation in the Transport of Carbon Nanotubes through Porous Media*, IAH 2012 International Congress: Confronting Global Change, Niagara falls, Canada.

Mehrabi, S., Milne-Home, W., 2012, *Representation of Heterogeneity in Single Collector Efficiency Equation for Multi-Walled Carbon Nanotubes*, the 3rd International Conference on Nanotechnology: Fundamentals and Applications, Montreal, Quebec, Canada.

Mehrabi, S., 2011, *Groundwater Protection Using Advanced Modelling Techniques*, Innovative Solutions for Environmental Challenges (ISEC 2011), Southern Cross University, Lismore, QLD.

Mehrabi, S., Milne-Home, W., 2011, *Applications of Nano-Size Zero Valent Iron Particles for Groundwater Remediation in NSW*, NSW IAH Symposium 2011 - Uncertainty in Hydrogeology, Sydney, NSW.

Table of Contents

CERTIFICATE OF ORIGINAL AUTHORSHIP	I
ACKNOWLEDGMENTS	II
DEDICATIONS	IV
VITA AND PUBLICATIONS	V
TABLE OF CONTENTS	VII
LIST OF FIGURES	XI
LIST OF TABLES	XV
ABSTRACT	1
1 INTRODUCTION	3
1.1 UNDERSTANDING TRANSPORT PRINCIPLES	8
1.1.1 <i>Groundwater Remediation</i>	11
1.1.1.1 Pump and Treat	12
1.1.1.2 Air Sparging	12
1.1.1.3 Permeable Reactive Barriers	13
1.1.1.4 Chemical Oxidation	13
1.1.1.5 Nanoremediation	13
1.2 KNOWLEDGE GAPS AND RESEARCH NEEDS	14
1.3 SCOPE OF PROPOSED IMPROVEMENTS	15
1.4 OVERVIEW	15
2 NANOPARTICLES AND THEIR TRANSPORT	19
2.1 FUNDAMENTALS	20
2.1.1 <i>General Information and Definitions</i>	20
2.1.2 <i>Carbon Nanotubes</i>	22

2.1.2.1	Discovery	22
2.1.2.2	Properties	25
2.2	DISPERSIVITY OF NANOPARTICLES	25
2.3	TRANSPORT PRINCIPLES	31
2.3.1	<i>Advection</i>	32
2.3.2	<i>Dispersion</i>	33
2.3.3	<i>Filtration</i>	34
2.4	EFFECTS OF PARTICLE SHAPE ON FILTRATION COEFFICIENT	36
2.5	EFFECTS OF PARTICLE ORIENTATION ON FILTRATION COEFFICIENT	39
2.6	EFFECTS OF PHYSICAL HETEROGENEITY OF POROUS MEDIA ON FILTRATION COEFFICIENT	40
2.6.1	<i>A Question of Scale</i>	44
2.6.2	<i>Representation of Heterogeneity</i>	45
2.6.2.1	Grainsize Distribution and Hydraulic Conductivity	45
2.6.2.2	Selection of the Best Suited Equation	47
2.7	EFFECT OF COLLECTOR EFFICIENCY ON PARTICLE FILTRATION	53
3	COLLOID TRANSPORT MODELLING	56
3.1	MODELLING HISTORY	57
3.2	MODELLING THEORIES: OLD AND NEW	58
3.2.1	<i>Advection-Dispersion Equation</i>	58
3.2.2	<i>Irreversible Attachment</i>	59
3.2.3	<i>Equilibrium Adsorption</i>	60
3.2.4	<i>Kinetic Adsorption-Desorption</i>	61
3.2.5	<i>Hypothesis Development</i>	61
3.3	MODELLING TOOLS	65
3.3.1	<i>Selected Software</i>	66
3.3.1.1	Flow and Transport simulation software	66
3.3.2	<i>Finite Element vs. Finite Difference</i>	68
3.4	THEORY COMPARISON AND BENCHMARKING	69

3.5	A REAL-WORLD 3D EXAMPLE	86
3.5.1	Site description	87
3.5.2	Regional Groundwater Regime	88
3.5.3	Grid Design	90
3.5.4	Boundary Conditions	93
3.5.5	Parameterisation	94
3.5.5.1	Hydraulic Conductivity	95
3.5.5.2	Recharge and Evapotranspiration	98
3.5.5.3	Temporal Discretisation	100
3.5.6	Model Calibration	100
3.5.6.1	Targets	100
3.5.6.2	Calibration statistics	101
3.5.7	Transport model	102
4	UNCERTAINTY ANALYSIS: STOCHASTIC MODELLING	107
4.1	A QUESTION OF UNCERTAINTY	109
4.1.1	Where does uncertainty come from?	109
4.1.2	Types of errors	111
4.1.2.1	Systematic errors	111
4.1.2.2	Extreme errors	112
4.1.2.3	Random errors	114
4.2	PARAMETER SENSITIVITY AND UNCERTAINTY	117
4.2.1	Particle Diameter Sensitivity	120
4.2.1.1	Model Parameterization	120
4.2.1.2	Key Observations	122
4.2.1.3	Additional discussions	123
4.2.2	Particle Length Sensitivity	124
4.2.2.1	Model Parameterization	124
4.2.2.2	Key Observations	125
4.2.2.3	Additional discussions	126

4.2.3	<i>Collector Diameter/Hydraulic Conductivity Sensitivity</i>	126
4.2.3.1	Model Parameterization.....	126
4.2.3.2	Key Observations	127
4.2.3.3	Additional discussions	128
4.2.4	<i>Particle Density Sensitivity</i>	129
4.2.4.1	Model Parameterization.....	129
4.2.4.2	Key Observations	130
4.2.4.3	Additional discussions	131
4.3	DEALING WITH UNCERTAINTY IN GROUNDWATER TRANSPORT MODELLING	132
4.4	REDUCTION AND ESTIMATION OF UNCERTAINTY	133
4.4.1	<i>Uncertainty Reduction</i>	133
4.4.2	<i>Uncertainty Estimation</i>	134
4.5	METHOD APPLICATION	135
5	CONCLUDING REMARKS	167
5.1	RECAPPING THE STORY	169
5.2	OBSERVATIONS AND RESULTS.....	173
5.3	CONCLUSIONS AND DISCUSSIONS	175
5.4	FUTURE RESEARCH	179
	APPENDIX A- ORIGINAL PHT3D RATES DATABASE	180
	APPENDIX B- SIMULATED WATER TABLE POST-CALIBRATION	206
	APPENDIX C- FLOW MODEL RAW OUTPUT	207
	APPENDIX D- GLOSSARY	224
	BIBLIOGRAPHY	227

List of Figures

Figure 1-1 Water availability on planet earth	4
Figure 1-2 World population growth.....	5
Figure 1-3 Material spillage opportunities during transfer	9
Figure 1-4 Introduction of contaminants through MAR.....	11
Figure 1-5 Dissertation structural design.....	18
Figure 2-1 Size guide chart	20
Figure 2-2 Detergent function (adapted from Encyclopedia Britannica, 2005)	21
Figure 2-3 Molecular structures of a single-walled carbon nanotube (SWNT) and of a multi-walled carbon nanotube (MWNT)	23
Figure 2-4 TEM image of what could be a SWCNT specifically from the bare part between arrows, yet unlikely. Monthioux and Kuznestoy scanned this image from Endo's original thesis (adapted from Monthioux and Kuznetsov, 2006).....	24
Figure 2-5 CNT dispersion methods	28
Figure 2-6 main collision/contact mechanisms	35
Figure 2-7 Ellipsoids of Revolution (Formed By Rotating an Ellipse about Either Its Major Axis (Prolate) or Minor Axis (Oblate) (Adapted from Harding & Colfen 1995).	37
Figure 2-8 Side and end contact between a cylindrical particle and collector. Where d_p is particle diameter and l is particle length.....	38
Figure 2-9 Particle orientation, speculated based on a) high velocity and b) low velocity	40
Figure 2-10 Particle flow model in a homogeneous porous medium; a) particles position , b) day 100, c) day 300, d) day 500, e) day 800, f) day 885, when all particles move out of the system on day 895. The green and blue arrows show the centre of the mass as the particles move through the porous medium.	42

Figure 2-11 Particle flow model in a randomly heterogeneous porous medium; a) particles position , b) day 100, c) day 300, d) day 500, e) day 610 when the first particle leaves the system, f) day 940 when the last particle is just about to leave the system, when all particles move out of the system on day 945. The green and blue arrows show the centre of the mass as the particles move through the porous medium.....	43
Figure 2-12 SCE calculated based on d10 and d50 for 10 heterogeneous samples.....	49
Figure 2-13 Comparison of SCE results using Eq. 2-10 with d10, d50, and Eq. 2-27.....	53
Figure 3-1 Title image in McCarthy's publication, Nature, 1989	57
Figure 3-2 Random heterogeneity field of hydraulic conductivity in the 2D model.....	70
Figure 3-3 Scenario comparison results for Tracer, Particle shape inclusion, and Heterogeneity inclusion.....	82
Figure 3-4 Site location.....	87
Figure 3-5 Site elevation	88
Figure 3-6 these velocity vectors show the flow pattern across the model domain	89
Figure 3-7 Grid design	91
Figure 3-8 Row cross-sections	92
Figure 3-9 Column cross-sections	93
Figure 3-10 Boundary conditions.....	94
Figure 3-11 recovery curve or rising head curve for A-BH-1011.....	96
Figure 3-12 Spatial map of recharge/ET zones	99
Figure 3-13 Observed VS simulated values	101
Figure 3-14 Water table contours.....	102
Figure 3-15 a-i series of 3D illustration of particle movement	106
Figure 3-16 final time step contour map	106
Figure 4-1 An example of a systematic error	112
Figure 4-2 An example of extreme error	114

Figure 4-3 Random errors distribution scenarios (a) where the true value can be estimated based on a normal distribution of errors (b) where the true value can only hold positive values and the normal distribution of errors is disturbed. In b, the black shaded part is cut off from the data set.	115
Figure 4-4 A chart of errors during a standard groundwater modelling process.....	116
Figure 4-5 Sensitivity log chart for 'a'	118
Figure 4-6 Standard normal distribution, probability density function	119
Figure 4-7 Conductivity field (m/day)	121
Figure 4-8 Relationship between particle diameter and lambda	123
Figure 4-9 Relationship between particle length and lambda	125
Figure 4-10 Relationship between grain size and lambda	128
Figure 4-11 Relationship between particle density and lambda	131
Figure 4-12 Examples of random realizations of hydraulic conductivity field using Fast Fourier transform-based analysis.....	137
Figure 4-13Probability distribution density vs concentration for observation point 1 and 1'	140
Figure 4-14Probability distribution density vs concentration for observation point 6 and 6'	141
Figure 4-15Probability distribution density vs concentration for observation point 7 and 7'	142
Figure 4-16Probability distribution density vs concentration for observation point 10 and 10'	143
Figure 4-17Probability distribution density vs concentration for observation point 14 and 14'	144
Figure 4-18Probability distribution density vs concentration for observation point 17 and 17'	145
Figure 4-19Concentration realisation: Observation Point 1	146

Figure 4-20	Concentration realisation: Observation Point 2.....	147
Figure 4-21	Concentration realisation: Observation Point 3.....	148
Figure 4-22	Concentration realisation: Observation Point 4.....	149
Figure 4-23	Concentration realisation: Observation Point 5.....	150
Figure 4-24	Concentration realisation: Observation Point 6.....	151
Figure 4-25	Concentration realisation: Observation Point 7.....	152
Figure 4-26	Concentration realisation: Observation Point 8.....	153
Figure 4-27	Concentration realisation: Observation Point 9.....	154
Figure 4-28	Concentration realisation: Observation Point 10.....	155
Figure 4-29	Concentration realisation: Observation Point 11.....	156
Figure 4-30	Concentration realisation: Observation Point 12.....	157
Figure 4-31	Concentration realisation: Observation Point 13.....	158
Figure 4-32	Concentration realisation: Observation Point 14.....	159
Figure 4-33	Concentration realisation: Observation Point 15.....	160
Figure 4-34	Concentration realisation: Observation Point 16.....	161
Figure 4-35	Concentration realisation: Observation Point 17.....	162
Figure 4-36	Concentration realisation: Observation Point 18.....	163
Figure 4-37	Concentration realisation: Observation Point 19.....	164
Figure 4-38	Concentration realisation: Observation Point 20.....	165
Figure 5-1	Proposed framework for assessment of emerging contaminants.....	178

List of Tables

Table 2-1 Reported size distribution of selected engineered nanoparticles in water.....	29
Table 2-2 Characterised Australian soil samples.....	48
Table 2-3 Validation scenarios.....	51
Table 2-4 Single Collector Efficiency (SCE) calculation results and their standard deviation from SCE with homogeneity assumption	52
Table 2-5 Filtration attachment rate calculations for sample No. 10	55
Table 3-1 Cylindrical nanoparticle retardation rate calculation code	83
Table 3-2 Hydraulic conductivity calculations	97
Table 3-3 Permeability zoning	97
Table 3-4 Weather stations in the area	98
Table 3-5 Recharge/ET zones	99
Table 3-6 Calibration statistics.....	101
Table 4-1 sensitivity chart data for b and c multipliers	118
Table 4-2 Model parameters- Case 1.....	121
Table 4-3 Statistical characterisation of the hydraulic conductivity field	122
Table 4-4 Multipliers and values for Particle diameter sensitivity analysis.....	122
Table 4-5 Model parameters- Case 2.....	124
Table 4-6 Multipliers and values for Particle length sensitivity analysis.....	125
Table 4-7 Model parameters- Case 3.....	127
Table 4-8 Multipliers and values for grain size sensitivity analysis	127
Table 4-9 Model parameters- Case 4.....	129
Table 4-10 Multipliers and values for particle density sensitivity analysis	130
Table 4-11 Statistical information: Observation Point 1	146
Table 4-12 Statistical information: Observation Point 2	147

Table 4-13Statistical information: Observation Point 3	148
Table 4-14Statistical information: Observation Point 4	149
Table 4-15Statistical information: Observation Point 5	150
Table 4-16Statistical information: Observation Point 6	151
Table 4-17Statistical information: Observation Point 7	152
Table 4-18Statistical information: Observation Point 8	153
Table 4-19Statistical information: Observation Point 9	154
Table 4-20Statistical information: Observation Point 10	155
Table 4-21Statistical information: Observation Point 11	156
Table 4-22Statistical information: Observation Point 12	157
Table 4-23Statistical information: Observation Point 13	158
Table 4-24Statistical information: Observation Point 14	159
Table 4-25Statistical information: Observation Point 15	160
Table 4-26Statistical information: Observation Point 16	161
Table 4-27Statistical information: Observation Point 17	162
Table 4-28Statistical information: Observation Point 18	163
Table 4-29Statistical information: Observation Point 19	164
Table 4-30Statistical information: Observation Point 20	165

Abstract

This research deals with multi-scale descriptions of nano-colloidal transport in saturated porous media. Colloidal transport has been simulated, historically, by employing a pore-scale model. I argue that the use of such simulations on a continuum-scale where formulations are generally phenomenological, may be unsuitable if at all possible due to requirements for pore-scale parameterization.

I propose to up-scale the pore-scale equation by inclusion of natural heterogeneity of porous media which consequently substitutes the pore-scale parameters (often unobtainable in real cases) with continuum-scale parameters (measurable at field). This approach transforms the pore-scale formulation into a Darcy-scale formulation, making it usable for real-world simulations.

I demonstrate a closer agreement with experimental data once porous media's natural heterogeneity is considered compared with the use of a mean value for media grain size in the conventional methods. These results can be explained by noting the fact that hydraulic conductivity of a porous medium is not controlled by the coarser or the median size grains. Rather, it is the smaller grains which ultimately determine (or in other words, restrict) the permeability of any given porous medium.

By comparing various modelled scenarios, I also assess the magnitude of difference in predicted results which displays a significant divergence from the case where the porous medium is assumed to be homogeneous.

Finally I aim to estimate the uncertainty associated with scenarios A (Yao's equation) and B (Mehrabi_ Milne-Home equation) in the absence and presence of natural heterogeneity, respectively. The results showed a noticeable decrease of 9% to 87% in the uncertainty caused by the most prominent source of uncertainty in groundwater modelling; porous media's

heterogeneity. The uncertainty is generally lower closer to the contaminant release point and increases as the plume moves away from the source point. The more substantial improvements (reduction of uncertainty) was observed at selected point which were located further away from the release point.

A framework for the assessment of nanoparticle transport in aquifers follows in which the extent of movement is estimated based on available field measured data and the probabilities of various potential realizations can be measured. This will help provide a much needed set of information for the policy-making processes with regards to new and emerging contaminants including engineered nanoparticles.

1 INTRODUCTION

“Water, like religion and ideology, has the power to move millions of people. Since the very birth of human civilization, people have moved to settle close to it. People move when there is too little of it. People move when there is too much of it. People journey down it. People write, sing and dance about it. People fight over it. And all people, everywhere and every day, need it” (Mikhail Gorbachev, quoted in Peter Swanson's Water: The Drop of Life, 2001BBC News). .

.. What more can be said to highlight the importance of water, without which, no human civilizations would have come to exist.

Almost 70% of earth is covered with water, 97.5% of which is saline. This leaves us with approximately 2.5% fresh water supplies. These resources include a significant 69% glacier and permanent snow, 30% groundwater, and a small proportion of 1% surface water that exists mainly in lakes, swamps, and rivers. While rivers host the most available form of freshwater to humans, they form less that 2% of surface water resources. That is less than 0.01% of all forms of fresh water. The following graph (Figure 1-1) illustrates water availability on planet earth.

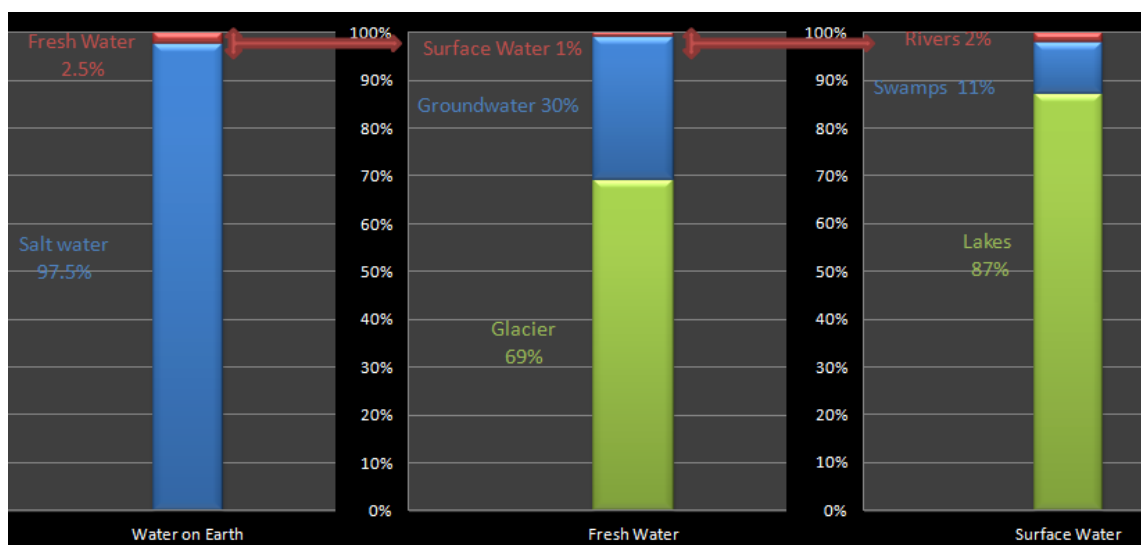


Figure 1-1 Water availability on planet earth

When early civilizations formed around major rivers in the Middle East, East and South Asia, Africa, and Western Europe, rivers could support the relatively small human populations allowing them to live, grow, reproduce and expand.

It took humans almost all of human history to reach one billion but it took only a little over a century to double that population. The third billion was added in 30 years and the fourth billion in only 15 years. In the year 2000, world population was estimated at around 6 billion. Based on the US Bureau of Statistics, our planet currently hosts approximately 6.9 billion humans (statistics for 2012). This swift and exponential growth (shown in Figure 1-2) has placed an enormous stress on our limited water resources and has brought up the question of water security for humans, animals, and the environment, both now and in the future.



Figure 1-2 World population growth

As well as population growth, global warming, amplified urban areas (low recharge areas), rising industrial water requirements and escalating water pollution are forcing us to improve the ways we store, manage and use water.

Many arid and semi-arid areas dealt with water availability issues by utilising groundwater resources when surface water was sparse. In turn, the unsustainable usage of groundwater imposed a great risk on groundwater quality and quantity in many countries. Once thought to be an enormous source of water, aquifers started to show severe signs of stress in some parts of the world (Wada et al. 2012).

“When the well is dry, we know the worth of water” (Benjamin Franklin, 1746). It has become evident we are once again faced with an issue of water security. Many ideas have been raised by the scientific community and many studies have explored the feasibility of those ideas. Groundwater is once again identified as a more secure source of fresh water which is protected from intensive evaporation, severe microbial and urban pollution (due to natural filtration through soil), in contrast to expensive infrastructural developments such as dams. It was, therefore, brought to the communities’ attention that not only the water table needs to be monitored and maintained at an acceptable level, but also groundwater quality should be observed regularly to avoid complications due to contamination. Some artificial recharge and/or urban runoff were also to be injected into the subsurface for safekeeping of the water under Managed Aquifer Recharge (MAR) schemes.

The introduction of foreign contaminants into the groundwater systems through injection of surface runoff has always been a possibility. However, pre-treatment was suggested to minimise the likelihood of this spread.

While the well-established methods of water treatment and pre-treatment are designed to remove the known contaminants from artificial recharge, they leave a path open to a group of new but emerging contaminants. Previously rare and hence seemingly undeserving of expensive treatment attempts, some of these contaminants can also act as facilitators for other pollutants to find their way into a formerly improbable territory (Monteiro & Boxall 2009).

One group of these so-called emerging contaminants, on which this dissertation will focus, is engineered nanomaterials. The term nanomaterial refers to a variety of materials with external dimensions, or an internal structure, measured in nanometres. Nanomaterials often display different chemical, physical, and biological characteristics, and thus behave differently, with respect to materials of a coarser structure with the same elemental or molecular composition (Lövestam et al. 2010). Their significantly increased surface area makes them much more efficient at reacting with their surrounding environment. Products using nanomaterials are

made to be lighter, stronger, cleaner, less expensive, more efficient, more precise, or more aesthetic. Examples of manufacturing areas with products containing nanomaterials are:

- cosmetics and personal care products
- paints & coatings
- household products
- catalysts & lubricants
- sports products
- textiles
- biosensors and electrochemical electrodes
- medical & healthcare products
- food and nutritional ingredients
- food packaging
- agrochemicals
- veterinary medicines
- construction materials
- weapons & explosives
- consumer electronics (Lövestam et al. 2010; Aravind & Ramaprabhu 2012).

New applications are found every day for various types of nanomaterials and greater volumes of these materials are produced and sold day after day due to high demand.

Several monitoring studies, which looked for these emerging contaminants, have detected them in a range of environmental sections including surface waters, groundwaters, drinking waters, fish and earthworms across the globe (Juhler, Sorensen & Larsen 2001; Lagana et al. 2001; Banfield & Zhang 2001; Li 2002; Kolpin et al. 2002; Zimmerman, Schneider & Thurman 2002; Battaglin et al. 2003; Diallo et al. 2005). These findings raise an important question: is it safe to have these engineered materials in our environment? Moreover, do we have enough information on their transport and fate in the natural environment?

1.1 Understanding Transport Principles

There are several answers to the question: “what is the importance of understanding transport principles for nanoparticles?” Well, the selection of an appropriate response derives from the context in which the question is asked. In the remainder of this section, I will attempt to elaborate on these answers.

Transport principles or equations that govern the movement of nanoparticles are tools, which facilitate predictive modelling of the movement of these particles. To delve into the importance of establishing and understanding these equations, I will firstly consider various situations under which it is useful to know how far, how long, and in what direction(s) these nanoparticles will travel.

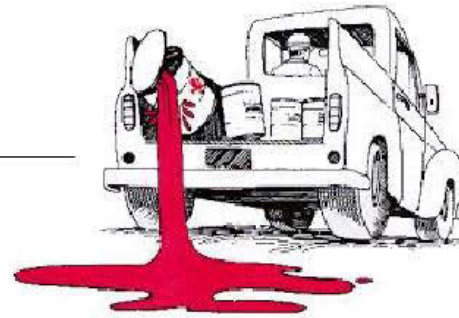
Let P be a single engineered particle with an assumed set of characteristics. Let it be very small (nano sized), toxic or potentially toxic and able to be stabilised in a water-based dispersion. These characteristics make P a highly mobile particle that can travel for a considerable distance. As a potential user of water or food that contains P, you will be concerned about its toxic or potentially toxic properties.

Now imagine several tons of material P is being transferred from the production plant A to the target location B in a truck. At a number of points during the transfer process, there is a chance for material P to be released into the environment, as illustrated in Figure 3. Since P is an engineered and toxic material, there would be a significant value in predicting just how far it will travel, how long it takes until it reaches potential recipients, and, what concentrations will survive the distance. These matters are necessary to answer in order to design a risk management or a damage control plan. Understanding the transport principles of material P is the key to answering these very important questions. In this scenario, P plays the role of a contaminant that is potentially harmful to the health of the receivers including humans, animals and the environment. Hence, it is crucial to be able to predict its transport and fate to minimise the risk of hazardous exposure.



Target Location B

Spillage during transport



Spillage as a result of a road accident



Production Plant A



Spillage during loading

Figure 1-3 Material spillage opportunities during transfer

Now, let us look at material P with a fresh pair of eyes. Let material P be an innovative, engineered material, specifically designed to remediate a contaminant in a hard to reach territory such as aquifers. In order to maximise the effectiveness of this remedial material, it has to be delivered to the desirable depth (where the plume is believed to reside) in optimal concentrations.

In this scenario, it is desired that P travels optimally through the soil profile and reaches the plume. However, there are key factors such as reactivity, dispersivity, porosity of the pathway media, pH, IS, and more involved in the delivery of this material. This scenario sketches another situation under which understanding the transport principles of material P is vital in creation of a successful remedial design.

In the above mentioned scenarios, material P could be any one of the number of engineered nanomaterials that are mass produced today. These versatile materials have many various applications and are used in many products. This guarantees their release in the environment one way or other. Ignoring the opportunities for accidental spillage during transport, the products will eventually be disposed of. The leachant from the waste will contain nanomaterials and has the potential to disperse in surface runoff and/or reach groundwater.

This brings us to the last scenario I will discuss here to highlight the importance of predictive tools for nanomaterial transport and fate. Assume material P has found its way into urban runoff (grey water). The area suffers from water shortage due to a semi-arid climate and below-average rainfall over the past 3 years. An efficient scheme has been put in place for managed aquifer recharge (MAR). In this picture, urban runoff is injected into the aquifer after pre-treatment for known and expected contaminants (Figure 1-4). Material P is new and extremely small; it is unanticipated in the recharge water. In addition, it will pass through the usual filters and survive the treatments that were not designed to remove material P. Later, P particles are found in grey water and reported in a new study. It is suspected they have been introduced into

the aquifer and hence, it is essential to estimate and predict the extent of their spread and remaining concentrations since the injection. Once again, governing equations come handy.

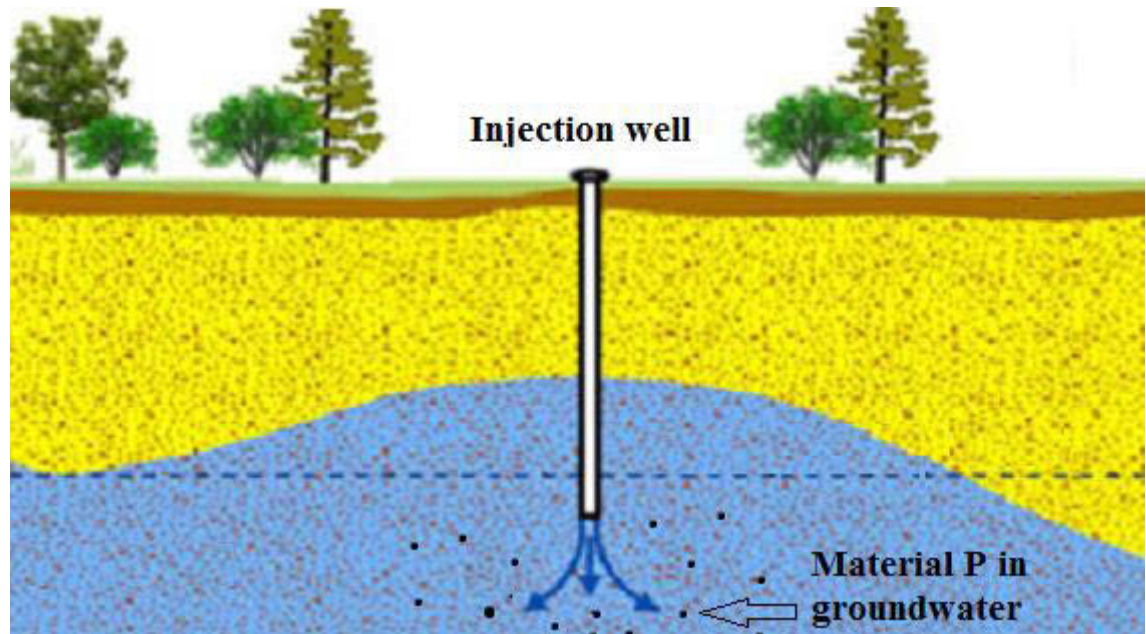


Figure 1-4 Introduction of contaminants through MAR

1.1.1 Groundwater Remediation

Water and groundwater pollution issues are amongst the most challenging areas in sustainable development. A combination of an ever-growing population, need for continual development, and historical mistakes poses a risk on the aquatic environment and offsets clean-up attempts. Compromises are often made to balance the high costs and long times associated with remediation projects. In most cases, remediation only offers a temporary decrease in contaminant concentration to meet the guidelines for the proposed beneficial use.

Nanotechnology can change this picture for many suitable contaminated sites as it promises effective, relatively cheap and quick results. Nevertheless, some key issues are still faced when assessing the feasibility of such methods under real-scale field conditions. Delivering suspensions of nanoparticles (nanosuspensions) is one of the more challenging matters in this regard. As mentioned in the previous section, predicting the extent of suspension transport is vital for a successful remedial design.

Groundwater remediation in a more conventional context is usually associated with high cost, long periods, need for continual management, and production of highly polluted waste which has to be safely disposed of. Let us have a look at more traditional groundwater remediation techniques, their strengths and limitations. I will then briefly compare those methods with nanoremediation technology.

1.1.1.1 Pump and Treat

Pump and treat is an ex-situ method which involves the extraction of groundwater, followed by various types of treatments. These treatments are selected based on the type of contaminant(s) (Khan et al., 2004) and the treated water is then released or re-injected into rivers or aquifers respectively. The remaining waste has high concentrations of the contaminant(s) and often has specific disposal requirements which are typically costly.

In addition to cost/time constraints, other issues such as partial capture of the plume, continued desorption of contaminants from the solid phase back into the water and the need for constant supervision of the operation detract from this method's desirability.

1.1.1.2 Air Sparging

Air sparging is an in-situ remedial technology that reduces concentrations of volatile constituents in petroleum products that are adsorbed to soils and dissolved in groundwater. This technology, which is also known as "in situ air stripping", involves the injection of contaminant-free air into the subsurface saturated zone, enabling a phase transfer of hydrocarbons from a dissolved state to a vapour phase. The air is then vented through the unsaturated zone (USEPA, 1994).

This method is only effective for volatile contaminants with low water solubility in a high permeability soil. It can cause accumulation of potentially dangerous gasses in confined subsurface spaces as well as spreading the contaminant in the aquifer.

1.1.1.3 Permeable Reactive Barriers

Permeable reactive barriers (PRBs) are treatment zones composed of materials that degrade or immobilize contaminants as the groundwater passes through them. They can be installed as permanent, semi- permanent or replaceable barriers within the flow path of a contaminant plume. The material chosen for the barrier is based on the contaminant(s) of concern. These barriers can only remediate contaminant plumes that pass through them; they do not address dense non aqueous-phase liquids (DNAPLs) or contaminated groundwater that is beyond the barrier (Gavaskar et al. 1998; Powell et al. September 1998; Rajan 2011).

1.1.1.4 Chemical Oxidation

Chemical oxidation technologies (in-situ) are predominantly used to address contaminants in the source area saturated zone and capillary fringe. Cost concerns can preclude the use of chemical oxidation technologies to address large and dilute petroleum contaminant plumes (USEPA, 2004, USEPA, 2008).

1.1.1.5 Nanoremediation

Nanoremediation methods entail the application of reactive nanomaterials for transformation and detoxification of pollutants (Karn, Kuiken & Otto 2011). These techniques have proven to be effective alternatives to the conventional practices for site remediation. Nanoparticles such as zero-valent iron, metal oxides, carbon nanotubes and metalloporphyrinogens have been tested in terms of their suitability for various types of contaminants.

Nano-scale Zero valent Iron particles (NZVI) are the most extensively studied and used nanoparticles in the remediation field. These particles have been used for cleaning up various types of contaminants such as DNAPLs and uranium (Arnold & Roberts 2000; Brooks 2000; Geiger et al. 2003; Quinn et al. May 2004). Carbon nanotubes (CNTs) are super adsorbent and can uptake various types of chlorinated hydrocarbons (Yang et al. 2006). Moradi and Zare (2011) reported on CNT adsorption of Pb(II), Cd(II) and Cu(II). Gold nanorods are used as mercury sensors, magnesium oxide nanorods are used in toxic waste remediation, while zinc

oxide nanorods (Jattasingh 2009) and titanium dioxide nanorods are utilized in waste water and groundwater remediation (Grassian et al. 2008; Guo et al. 2008).

1.2 Knowledge Gaps and Research Needs

There are many identified knowledge gaps when it comes to engineered nanoparticles (ENPs). Alistair Boxall (2012) reviews these new materials in his report for the OECD's committee for agriculture and the environment policy and offers his list of gaps. He suggests the following questions should be addressed through future research:

- What are the risks of substances that have yet to be studied?
- How can we analyse certain emerging contaminants in environmental media?
- Are we considering all the main exposure pathways?
- How will ENPs interact with a) each other; and b) other contaminants?
- What do the ecotoxicity data mean? How can we better assess ecotoxicity?
- What are the mechanisms determining fate and transport of ENPs?
- How can we mitigate against any identified risks?

This work focuses on the question of transport and how it can help with risk assessment and risk management plans. Despite establishing the importance of understanding nanoparticle transport governing equations in the previous sections, one has to admit there are significant knowledge gaps in this area. One of the biggest challenges put forward by Maynard et al. (2006) is "*developing models for predicting engineered nanomaterial behaviour in the environment*".

To identify the gaps and limitation, a review of scientific literature was carried out to examine the existing methods of modelling the movement of nanoparticles. Since ENPs are a relatively new group of materials, there is not sufficient data available on their transport and fate in the saturated sub-surface environment. Very few studies have explored the behaviour of engineered nanoparticles with soil particles under saturated conditions (e.g. Li et al., 2008).

However, based on information for other processes, it is likely that the behaviour of these materials will be different from non-particulate contaminants. Therefore, new models and paradigms will need to be developed for ENPs in saturated porous environment (Boxall 2012). Theories previously used to explain and ultimately model the transport of ENPs have limitations due to the assumptions under which they stand. The particularly small size, geometrical shape, and -when applicable- the orientation of ENPs are often overlooked in these theories. These theories, their strengths and their limitations will be extensively discussed in upcoming chapters.

1.3 Scope of Proposed Improvements

This work focuses on the matter of nanoparticle transport. Moreover, it will specifically address some of the present shortcomings in modelling the transport of cylindrical nanoparticles. These improvements include introduction of heterogeneity to the governing equations, developing a modelling tool and establishing a framework in which the uncertainties of a transport model can be considered.

I will also provoke the matter of particle orientation through theoretical calculations. These scenarios will establish a range of outcomes resulting from various orientational combinations of dispersed nanoparticles. Due to lack of real data for nanoparticle orientation in water matrix, benchmarking this theory was not possible. However, it crafts a new query for future research.

1.4 Overview

Thus far, the problem has been outlined and the importance of solving it, has also been highlighted. Together, we took it step by step from the matter of protecting our water resources, to emerging contaminants that are hard to detect or predict, then to what we need to know to deal with the issue more effectively and finally what I will do in this study to partially address the listed limitations.

The remainder of this dissertation can be sketched in three main sections each one of which will build foundations for their sequel section. The first and most fundamental section will concentrate on nanoparticles, their characteristics and their applications. This part will lay foundations for the following section which will focus on modelling tools and theories.

A comprehensive review of the history of particle movement modelling, various theories and tools will be presented in this section. A discussion of selection criteria for modelling tools and industry-standard codes will be put forward. Theories will be assessed and modifications will be suggested. Subsequently, I will present details of how the new theory was developed as well as how the modelling tool (code) was implemented. This section will conclude with a discussion on how the new modifications affect the result of predictive modelling benchmarked against previous work done by the USGS.

In the third and last structural section of this dissertation, stochastic modelling is examined. Probabilities are important in predictions and I consider that they should be a part of any predictive modelling. Hence, this part is dedicated to exploring the uncertainties inherent in the transport equation and how they can vary the outcomes of the model. I will also show how much reduction of uncertainty is resulted from the modifications suggested by us. This is seen as a step towards more sophisticated modelling practices.

At the end, the major findings, discussions and future research suggestions are presented; a bibliography is provided and several appendices are attached for those who would like to review the work in more details.

In brief, the structural design of this report can be defined as a flowchart. It starts with an introduction to the problem. This multidimensional problem consists of water scarcity, pollution, and the unknown risks of emerging contaminants. It documents why this problem is important, why it is worth solving, what needs to be done and how I am going to do it. At the next level, fundamental concepts of nanoscience and nanotechnology are discussed. Without this understanding, the reader would find it hard to appreciate the difficulties faced

when it comes to modelling the transport of nanoparticles. It will shed light on the definition of nanoparticle, their properties and their various types. By the end of this segment, the reader will understand why it is important to have specific equations for this group of particles, and what challenges it presents.

Building on the foundations laid, the next segment is dedicated to modelling theories and tools. This mathematically oriented part outlines the details of equation modifications proposed by the writer and will benchmark the results for validation purposes.

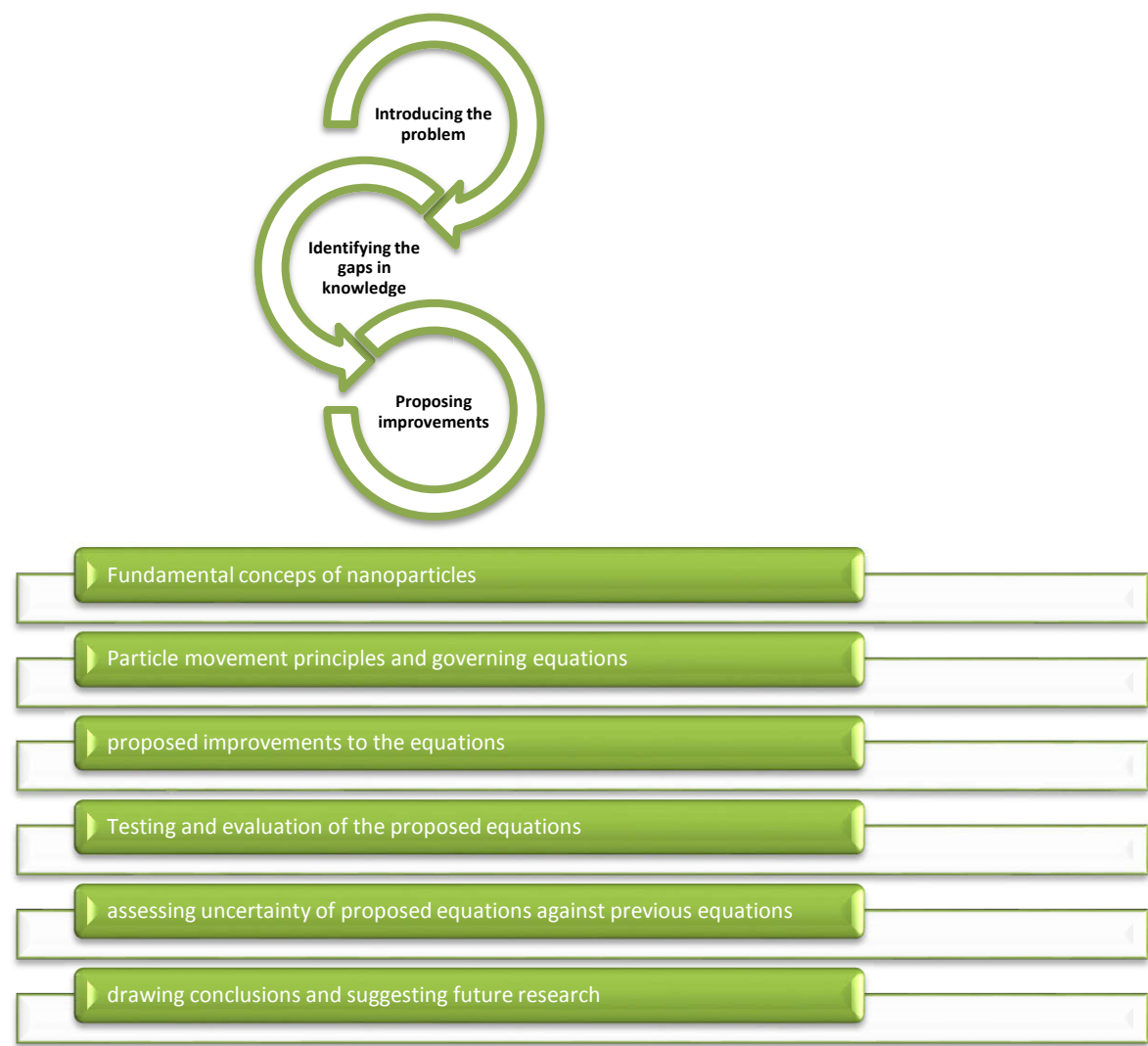
A succinct, yet very important segment represents the stochastic modelling section. In this exercise, the Monte Carlo method is used to determine the range of likelihoods as model outcomes for a nanoparticle transport model. This section focuses on the uncertainty of the modelling results, comparing old and new approaches for a solid evaluation of the proposed improvements.

At the end, conclusions are drawn, discussions are presented and the author's suggestions for future research are made.

For better illustration of the structure designed for this report, a graph has been sketched schematically on

Figure 1-5.

Figure 1-5 Dissertation structural design



2 Nanoparticles and their transport

“Learn from yesterday, live for today, hope for tomorrow. The important thing is to not stop questioning. If we knew what it was we were doing, it would not be called research, would it?”

Albert Einstein

2.1 Fundamentals

In this section the basics of nano-science are discussed. Our aim is to lay a common understanding for the nano-specific terminology to avoid confusion.

2.1.1 General Information and Definitions

In nanoscience, particles are defined as small units that behave similarly to the entire unit.

Based on their size, these particles are divided into three categories:

- coarse particles (between 10,000nm and 2,500nm)
- fine particles (between 2,500nm and 100nm)
- ultra-fine particles or nanoparticles (between 100nm and 1nm) (Granqvist et al. 1976).

Figure 2-1 provides a size-guide chart to put these particles in context.

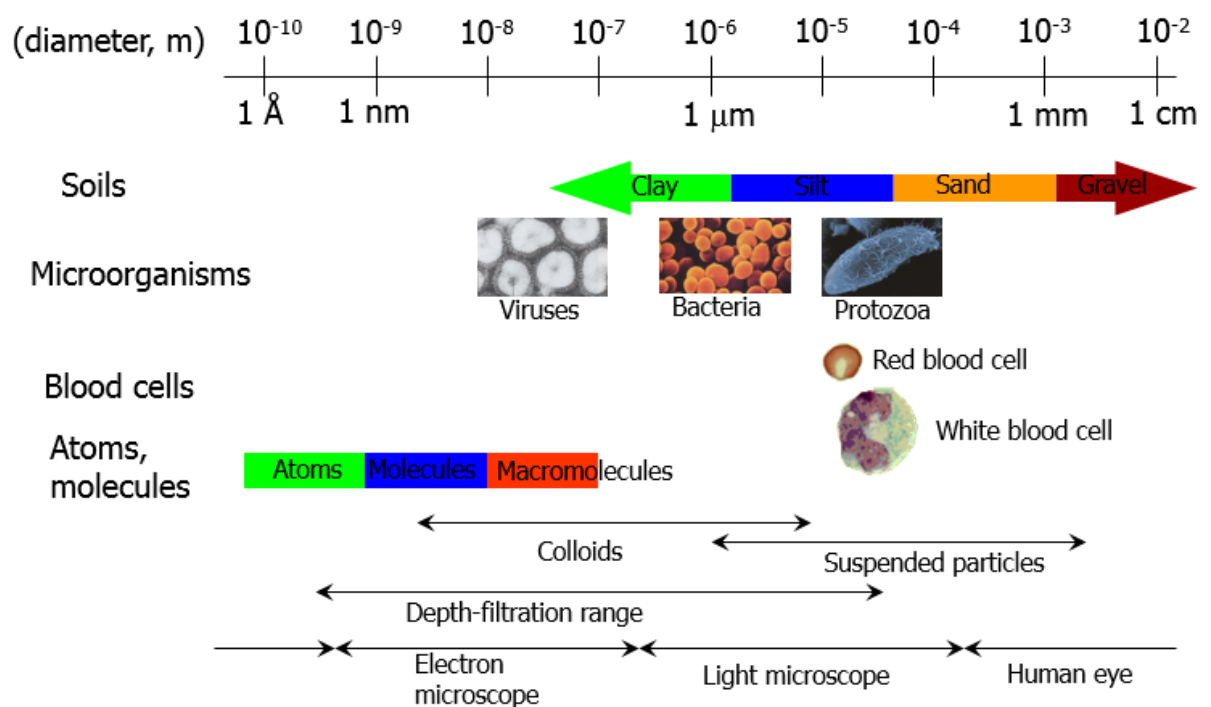


Figure 2-1 Size guide chart

Nanoparticles are subject to intensive scientific research because of their extraordinary properties. Unlike a bulk material, which displays constant characteristics (size-independent), nanoparticles often exhibit size-dependent properties. The outstanding features of nanoparticles are typically due to their very large surface area. This means, the number of atoms at the surface of a nanomaterial is significantly higher than that in a bulk material in relation to the total number of atoms in the bulk of the material. For example, the surface area of 1kg of 1mm^3 particles is the same as the surface area of 1mg of 1nm^3 particles. You can picture a block of soap, washing powder and washing nano-powder. The role of a detergent is to form bonds with non-polar molecules of dirt and grease with its non-polar (hydrophobic) tail and dissolve it into the water with its polar (hydrophilic) head Figure 2-2. In this context, soap has an effective area of the cube surface into which it has formed, whilst washing powder has a significantly larger surface area to carry on the task of cleaning. Our previous example implies what a kilogram of washing powder does could potentially be achieved with one milligram of the nano-powder of the same material.

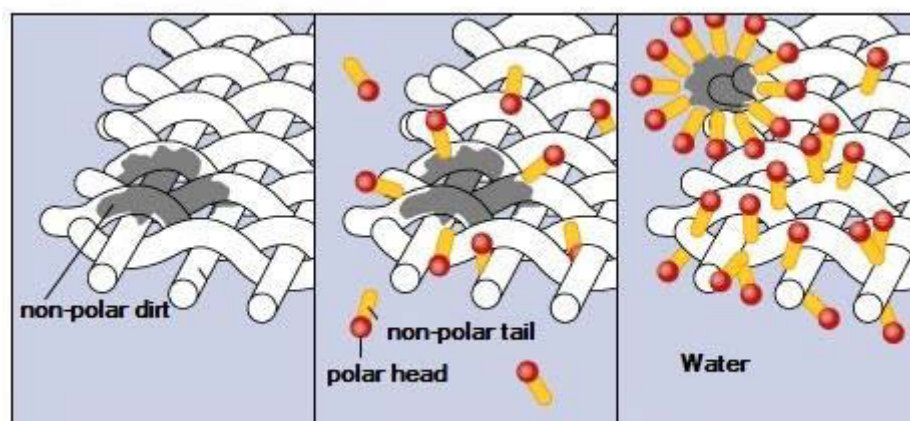


Figure 2-2 Detergent function (adapted from Encyclopedia Britannica, 2005)

In relation to their production processes, nanoparticles fall into two categories:

- natural nanoparticles
- engineered nanoparticles

As their names suggest, natural nanoparticles are the naturally occurring particles that fit in the 1 to 100nm size whereas engineered nanoparticles (ENPs) are produced by humans. ENPs are usually designed for a specific application and are very well characterised in relation to their uniformity, size, shape and any other property of interest as determined by the purpose of production.

2.1.2 Carbon Nanotubes

Since this work will later focus on the transport of cylindrical nanoparticles, Carbon nanotubes (CNTs) are selected as an example for the purpose of illustration. Moreover, CNTs are among the most widely used nanoparticles in nanotechnology, henceforth, we will become familiar with CNTs, their history of discovery, their properties and their applications in more details.

2.1.2.1 Discovery

1991, Sumio Iijima, Nature: *“Here I report the preparation of a new type of finite carbon structure consisting of needle-like tubes. Each needle comprises coaxial tubes of graphite sheets ranging from 2 up to about 50 in number. On each tube the carbon-atom hexagons are arranged in a helical fashion about the needles axis. The helical pitch varies from needle to needle and from tube to tube within a single needle”* (Iijima 1991).

Professor Iijima is often considered as the discoverer of CNTs due to the high impact of his paper on global carbon nanostructure research. However, this is very neglectful of other scientists who preceded this citation in relation to carbon nanotubes.

To tell the story of CNT’s discovery, we have to first distinguish between single walled and multi walled carbon nanotubes (SWCNT and MWCNT respectively- Figure 2-3).

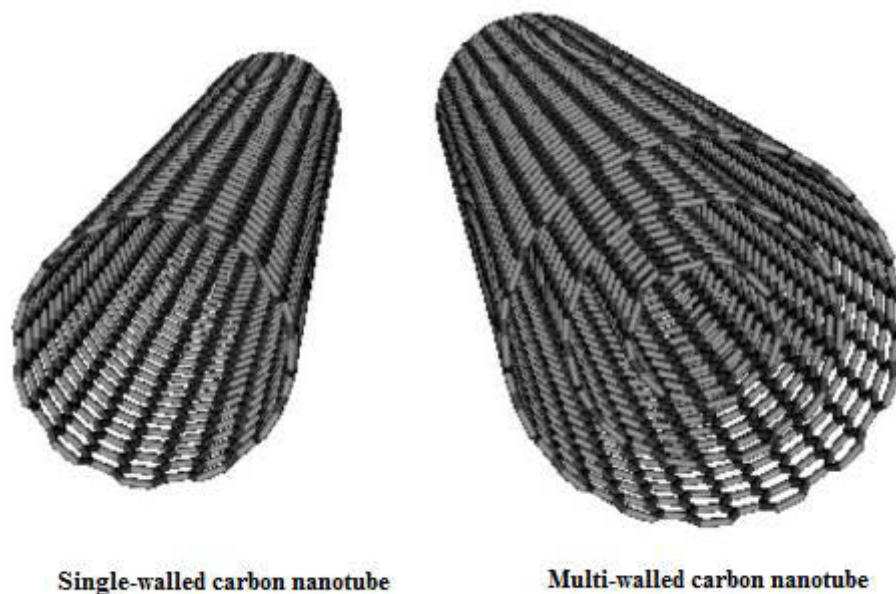


Figure 2-3 Molecular structures of a single-walled carbon nanotube (SWNT) and of a multi-walled carbon nanotube (MWNT)

It is fair to state the first clearly identified SWCNT was reported in 1993 (Nature) by two independently submitted papers. One by Iijima and Ichihashi, at the time affiliated at NEC¹, and the other by Bethune et al. from IBM, California. The only other potential earlier observation of SWCNT is just about impossible to verify. An image from Oberlin et al. (1976) shows a nanotube, resembling a SWCNT (Figure 2-4), but never claimed to be so by the authors. In fact, nobody from the carbon material community at that time was ready to admit that nanotubes built up using a rolled single graphene could ever exist (Monthioux & Kuznetsov 2006). It is, however, more likely that this image shows a MWCNT based on the diameter of the tube (5nm). Unfortunately, the number of the walls could not be determined in the course of image examination that Monthioux and Kuznetsov conducted in 2006. Was this the first single or double walled CNT ever imaged? We will never know.

¹ The company was known as the Nippon Electric Company, Limited, before rebranding in 1983 as just NEC.

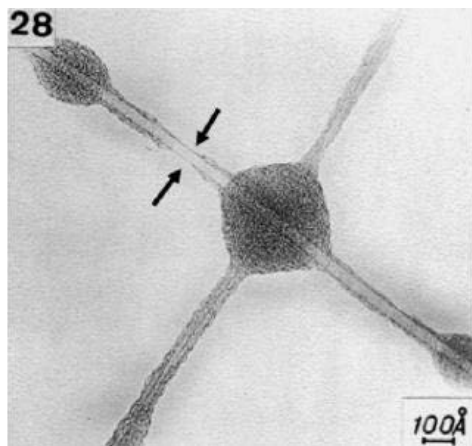


Figure 2-4 TEM image of what could be a SWCNT specifically from the bare part between arrows, yet unlikely. Monthioux and Kuznestoy scanned this image from Endo's original thesis (adapted from Monthioux and Kuznetsov, 2006).

When it comes to MWCNTs the story becomes even more remarkable. The possibility of forming carbon filaments was mentioned in the nineteenth century by Hughes and Chambers (1889) in a patent at the same time as Edison presented the light bulb at the Paris Universal Exposition. Nevertheless, due to the lack of suitable imaging tools and techniques, there is no evidence of these structures being nanotubes. Later in 1939, Siemens produced the first transmission electron microscope (TEM) which made imaging of these structures possible.

The first scientific evidence of tubular carbon nanostructures was presented in the Journal of Physical Chemistry of Russia in 1952 (Radushkevich & Lukyanovich 1952). This indeed is the earliest scientific report presented on MWCNTs. However, owing to the cold war, Russian science was not accessible for western scientists, hence, not much of this work and what followed it, is mentioned in the scientific literature of the time. Since then, many dedicated scientists have studied and reported on various tubular structures of carbon. Baird, Boehm, Endo, Harris, Oberlin, and many more have reported their experiments and observations, but it wasn't until the early 1990s that the scientific community was truly ready for nanoscience. This mentality coincided with the availability of better tools and methods for imaging ultra-fine nano-structures. The combination of these factors resulted in a high impact paper by Iijima in 1991, when it described the CNT structure even though it was not the first time such

structures were being mentioned. After the publication of Iijima's paper, CNT became the hottest research topic of the 20th century (Monthieux & Kuznetsov 2006).

2.1.2.2 Properties

Carbon nanotubes are in fact one or more graphene sheets seamlessly rolled into a cylindrical tube (Figure 2-3) with a diameter of few nanometres and a tube length of up to two millimetres (Pan et al. 1998). They exhibit unique electronic, mechanical, optical and thermal properties owing to their unique and diverse structure. CNTs can show metallic, semi-metallic, or semi-conductive features (Saito et al. 1992). Wong et al. (1997) described MWCNT as a distinctively strong, energy-absorbing material with an interesting elastic collapsing characteristics. CNTs' electronic, mechanical, optical and thermal properties have been studied by many scientists (Mintmire & White 1995; de Heer et al. 1995; Dresselhaus, Dresselhaus & Eklund 1996; Odom et al. 1998; Saito, Dresselhaus & Dresselhaus 1998; Smith et al. 2000; Kong et al. 2000). In the extremely promising presence of many potential applications for these nanoparticles, scientists face three main challenges. As outlined by Hilding and co-workers, (Hilding et al. 2003) these challenges are:

- purification and separation of nanotubes by chemistry and morphology,
- making uniform and reproducible dispersion,
- controlling orientation of these particles in liquid and melt phases.

When CNTs are produced, the final product is usually a mixture of various morphologies. In addition, CNTs are highly hydrophobic and have a tendency to cluster together due to electrostatic forces, or simply become physically entangled. However, for most of their applications, CNTs need to be dispersed.

2.2 Dispersivity of Nanoparticles

Dispersion of nanoparticles deserves our special attention in the context of contaminant/remediant transport in aquifers. In other words, if these particles are not dispersed

in a stable or semi-stable manner, they are most likely to form large aggregates and consequently be mechanically filtered in the vadose zone before reaching the saturated zone at the water table. On this basis, I will discuss the dispersivity properties of nanoparticle as well as various laboratory and natural processes that could lead to the formation of stable dispersions of nanoparticles.

In general, one of three main methods or mechanisms is used for dispersion:

- mechanical methods
- chemical methods
- electrical mechanisms

I will briefly write about each method and shed some light on their advantages as well as their limitations.

Mechanical methods are commonly used in the purification of nanoparticles. During the mechanical dispersion of cylindrical nanoparticles, they are often broken into shorter pieces, which in turn, increases their dispersivity. In fact the shorter the nanotubes or nanorods are, the less likely they will become tangled and form aggregates. However, this breakage can cause some damage to the structure of the nanotubes. This might have a significant impact on their functionality. Hence, if the intended application requires the cylindrical nanoparticles to be long, mechanical methods are not the best choice for dispersing them.

Frequently used mechanical methods are: ultrasonication, high impact mixing, grinding /rubbing, and high shear mixing. Rubbing is the most damaging method to the structure of NPs and can result in ragged walls, cuts, permanent bends and irreversible twists. Note that these types of damages can also happen during any of the other mechanical methods as well as some of the chemical treatments.

Chemical methods focus on surface coating and/or surface functionalization. Coating the surface (Jiang, Gao & Sun 2003; Jung, Ko & Jung 2004; Lisunova et al. 2006)(Jiang, Gao & Sun 2003; Jung, Ko & Jung 2004; Lisunova et al. 2006)(Jiang, Gao & Sun 2003; Jung, Ko & Jung 2004; Lisunova et al. 2006) as well as attaching functional groups can change the ways CNTs interact with their surrounding and hence can lead to their dispersion. Acid treatment (Chen et al. 1998), fluorination and use of various surfactants are common chemical treatments for dispersion. Many have studied the impact of various functional groups on CNT dispersion such as some polymers (Sano et al. 2001b) and (Zhao et al. 2005), DNA (Hazani et al. 2003) and (Zheng et al. 2003), some proteins (Huang et al. 2002), crown ethers (Kahn, Banerjee & Wong 2002), and glucosamine (Pompeo & Resasco 2002). Many studies have observed breakage of CNTs as a result of acid treatment (Garg & Sinnott 1998; Monthieux et al. 2001; Hilding et al. 2003; Salzmann et al. 2007).

In the electrical mechanism, an external electrical field is applied. If the electrical field energy exceeds atomic bond energy, nanoparticles such as CNTs can break and be reshaped shorter open-ended tubes. However, in most cases these broken tubes will fuse and form new and longer close-ended tubes within seconds of breakage.

The following chart (Figure 2-5) summarises the main methods of dispersion.

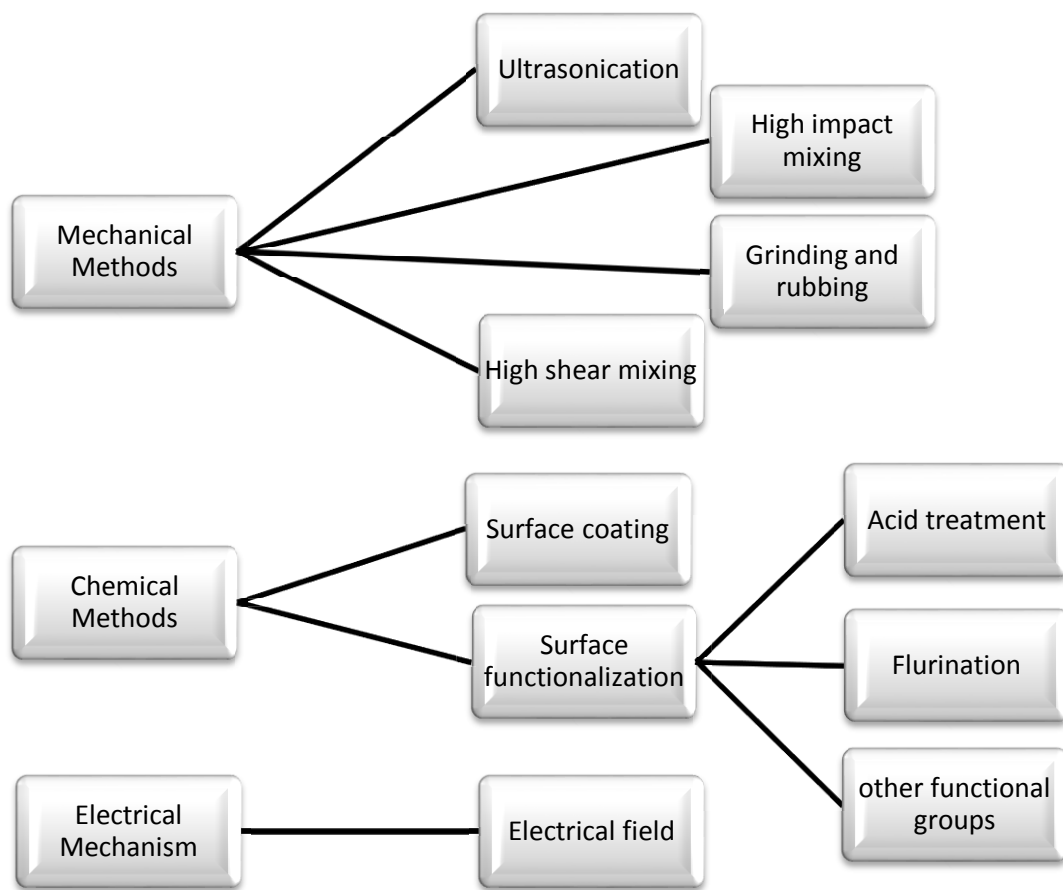


Figure 2-5 CNT dispersion methods

Let us, once more, evoke the importance of stably dispersed nanoparticles. Many engineered nanoparticles display significant attractive forces towards each other and form large aggregates as soon as they are suspended in an aqueous phase. In fact, a number of laboratory studies on ENPs showed the hydrodynamic particle size is much greater than the individual particle size in the dry phase, indicating that the aggregation is a common process for ENPs in water. The aggregation process is subject to the properties of the ENPs (e.g., size, chemical composition, and surface characteristics) and water chemistry parameters (e.g., ionic strength, pH and DOM content). Aggregation reduces the overall specific surface area of ENPs and interfacial free energy and therefore will limit the reactivity of ENPs (Lin et al. 2010). Table 2-1 shows the reported size distribution of selected ENPs in water. However, when they are

dispersed using chemical methods, this suspension is often stable. This will provide optimal conditions for their transport in aqueous environments.

Table 2-1 Reported size distribution of selected engineered nanoparticles in water

ENP	Individual Particle Size	Hydrodynamic Particle Size	Reference
	nm		
Ag	26.6 ± 8.8	216	Griffitt et al. (2008)
Ag	20–30	~100	Gao et al. (2009)
Cu	15–45	~10,000	Gao et al. (2009)
Cu	26.7 ± 7.1	94.5–447.1	Griffitt et al. (2008)
Al	41.7 ± 8.1	4442	Griffitt et al. (2008)
Al	41	215 ± 99	Darlington et al. (2009)
Co	10.5 ± 2.3	224–742	Griffitt et al. (2008)
Ni	6.1 ± 1.4	44.9–446.1	Griffitt et al. (2008)
NiO	10–20	750 ± 30	Zhang et al. (2008)
TiO2	20.5 ± 6.7	220.8–687.5	Griffitt et al. (2008)
TiO2	15–40	200–530	Zhang et al. (2008)
TiO2	11	284–612	Xia et al. (2008)
TiO2	15–27	90–290	J.K. Jiang et al. (2009)
TiO2	66	330	Adams et al. (2006)

ENP	Individual Particle Size	Hydrodynamic Particle Size	Reference
	nm		
TiO2	11	40	Kiser et al. (2009)
TiO2	4–5	50–60	French et al. (2009)
TiO2	50	550	H.H. Wang et al. (2009)
ZnO	67	480	Adams et al. (2006)
ZnO	13	36–413	Xia et al. (2008)
ZnO	50–70	320 ± 20	Zhang et al. (2008)
ZnO	20	759	H.H. Wang et al. (2009)
SiO2	14	205	Adams et al. (2006)
SiO2	10	740 ± 40	Zhang et al. (2008)
Fe2O2	5–25	200 ± 10	Zhang et al. (2008)
Fe2O2	9.2	46.2	Baalousha et al. (2008)
Fe2O4	<10	120	Illés and Tombácz (2006)
CeO2	8	323–2610	Xia et al. (2008)
Al2O2	60	763	H.H. Wang et al. (2009)
CdSe/ZnS	2.1	~12.5	Slaveykova et al. (2009)

It is important to note, dispersion is not necessarily a process which only takes place in laboratories and under controlled conditions. Saleh et al. (2008) studied the effects of the

presence of natural humic acid on the stability of multi-walled carbon nanotubes and reported that it markedly enhanced the colloidal stability of MWCNTs by reducing the aggregation rate by nearly two orders of magnitude. The increased stability was attributed to steric repulsion imparted by absorbed humic acid macromolecules. Their results suggest that, in general, MWCNTs are relatively stable at solution pH and electrolyte conditions typical of natural aquatic environments. Such studies provide scientifically robust proof that typically-aggregating nanoparticles could become mobile in the natural aqueous environments and hence can travel for considerable distances from the discharge point.

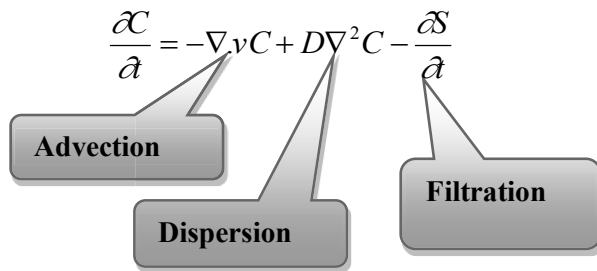
2.3 Transport Principles

Transport of particles through porous media is an important matter in several fields.

Some problems involving particle transport through porous media are:

- water treatment systems
 - Deep Bed Filtration (DBF)
 - membrane-based filtration
- transport of contaminants in aquifers
 - colloidal particles transport
 - nanoparticle transport
- transport of colloidal remedants in aquifers
 - nanoremediation technology
- transport of microorganisms
 - pathogen transport in groundwater
 - bio-remediation of aquifers
- clinical settings
 - blood cell filtration
 - bacterial and virus filtration
 - drug-delivery using nanoparticles

Transport of a suspension (of micron and nano sized particles) in a saturated porous medium under uniform flow is generically expressed through Eq. 2-1. The terms of this equation are defined in sections 2.3.1 to 2.3.3.

$$\frac{\partial C}{\partial t} = -\nabla \cdot vC + D\nabla^2 C - \frac{\partial S}{\partial t} \quad \text{Eq.2-1}$$


2.3.1 Advection

Advection describes the movement of miscible or suspended contaminants at the same velocity as the groundwater flow. In many field cases advection is the dominant mechanism of transport. To measure the degree of its dominance, the Peclet number, P_e , is calculated through:

$$P_e = \frac{|v|L}{D} \quad \text{Eq. 2-2}$$

Where:

$|v|$ is the magnitude of seepage velocity (LT^{-1})

L is characteristic length (L)

D is dispersion coefficient (L^2T^{-1})

When transport is advection-dominated (sharp front transport), the Peclet number is large. A small dispersion coefficient will result in P_e numbers approaching infinity.

The seepage velocity magnitude is calculated through:

$$|v| = \sqrt{v_x^2 + v_y^2 + v_z^2} \quad \text{Eq. 2-3}$$

Where v_x , v_y , and v_z are velocities in x, y, and z direction respectively. When the flow vector is aligned with one of the coordinate axes, the other velocity vectors are reduced to zero.

2.3.2 Dispersion

Dispersion describes the spreading of the contaminant over a larger area than would be predicted solely from the average groundwater velocity vectors (Anderson 1979; Anderson 1984).

Dispersion happens based on both mechanical dispersion and molecular diffusion. Mechanical dispersion is caused by velocity deviations from the actual velocity vector while molecular diffusion is caused by the concentration gradient. While mechanical dispersion is often more significant than diffusion, the latter mechanism becomes more important at very low velocities.

The hydrodynamic dispersion tensor, D_{ij} for an isotropic porous medium, is defined, according to Bear (1972; 1979):

$$D_{xx} = \alpha_L \frac{v_x^2}{|v|} + \alpha_T \frac{v_y^2}{|v|} + \alpha_T \frac{v_z^2}{|v|} + D^* \quad \text{Eq. 2-4}$$

$$D_{yy} = \alpha_L \frac{v_y^2}{|v|} + \alpha_T \frac{v_x^2}{|v|} + \alpha_T \frac{v_z^2}{|v|} + D^* \quad \text{Eq. 2-5}$$

$$D_{zz} = \alpha_L \frac{v_z^2}{|v|} + \alpha_T \frac{v_x^2}{|v|} + \alpha_T \frac{v_y^2}{|v|} + D^* \quad \text{Eq. 2-6}$$

$$D_{xy} = D_{yx} = (\alpha_L - \alpha_T) \frac{v_x v_y}{|v|} \quad \text{Eq. 2-7}$$

$$D_{xz} = D_{zx} = (\alpha_L - \alpha_T) \frac{v_x v_z}{|v|} \quad \text{Eq. 2-8}$$

$$D_{yz} = D_{zy} = (\alpha_L - \alpha_T) \frac{v_y v_z}{|v|} \quad \text{Eq. 2-9}$$

Where:

D_{xx} , D_{yy} , D_{zz} are the principal components of the dispersion tensor (L^2T^{-1})

D_{xy} , D_{xz} , D_{yx} , D_{yz} , D_{zx} , D_{zy} are cross terms of the dispersion tensor (L^2T^{-1})

α_L is the longitudinal dispersivity (L)

α_T is the transverse dispersivity (L)

D^* is the effective molecular diffusion coefficient (L^2T^{-1})

v_x , v_y , v_z are the components of the velocity vector along the x, y, and z axes (LT^{-1})

$|v|$ is the magnitude of velocity vector (LT^{-1})

2.3.3 Filtration

Particle filtration through saturated porous media is mainly affected by Single Collector Efficiency (SCE), sticking factor (α), particle and grain size, and approach velocity.

SCE is the theoretical value which estimates the likelihood of collision between particles and grains (collectors). The assumed three mechanisms through which a particle comes into contact with a collector are; inertial impaction (interception), settling due to gravity (sedimentation), and diffusion (Brownian diffusion). SCE (η_0) is calculated as:

$$\eta_0 = \eta_D + \eta_I + \eta_G \quad \text{Eq. 2-10}$$

where η_D, η_I, η_G represent theoretical values for the SCE when the only transport mechanisms are diffusion, interception, and sedimentation, respectively (Figure 2-6).

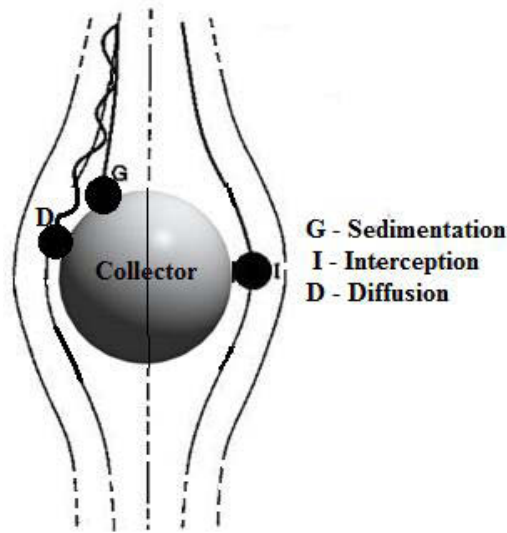


Figure 2-6 main collision/contact mechanisms

For a spherical particle, each component of SCE is calculated through:

$$\eta_D = 4.04Pe^{-\frac{2}{3}} = 0.9 \left(\frac{KT}{\mu d_p d_c v_0} \right)^{\frac{2}{3}} \quad \text{Eq. 2-11}$$

Where:

K is the Boltzmann Constant ($1.3806488 \times 10^{-23}$ (J K⁻¹))

T is the absolute temperature (Kelvin)

μ is fluid viscosity (ML⁻¹T⁻¹)

v_0 is fluid velocity (LT⁻¹)

d_p is particle diameter (L)

d_c is collector diameter (L)

$$\eta_I = \frac{2}{3} \left(\frac{d_p}{d_c} \right)^2 \quad \text{Eq. 2-12}$$

$$\eta_G = \frac{(\rho_p - \rho) g d_p^2}{18 \mu v_0} \quad \text{Eq. 2-13}$$

Where:

ρ_p is particle density (ML⁻³)

ρ is baulk density (ML⁻³)

(Yao 1968).

2.4 Effects of Particle Shape on Filtration Coefficient

By change of geometry, more contact types (with different contact areas) are conceivable as the particle is no longer a symmetrical sphere. The assumption of spherical shape was identified as a limiting factor in applicability of the CFT. Therefore new relationships for the theoretical collector efficiencies due to interception, gravitational sedimentation and diffusion were developed for cylindrical particles to broaden the applicability of colloid filtration theory (Yao 1968; Harding & Colfen 1995; Liu et al. 2009).

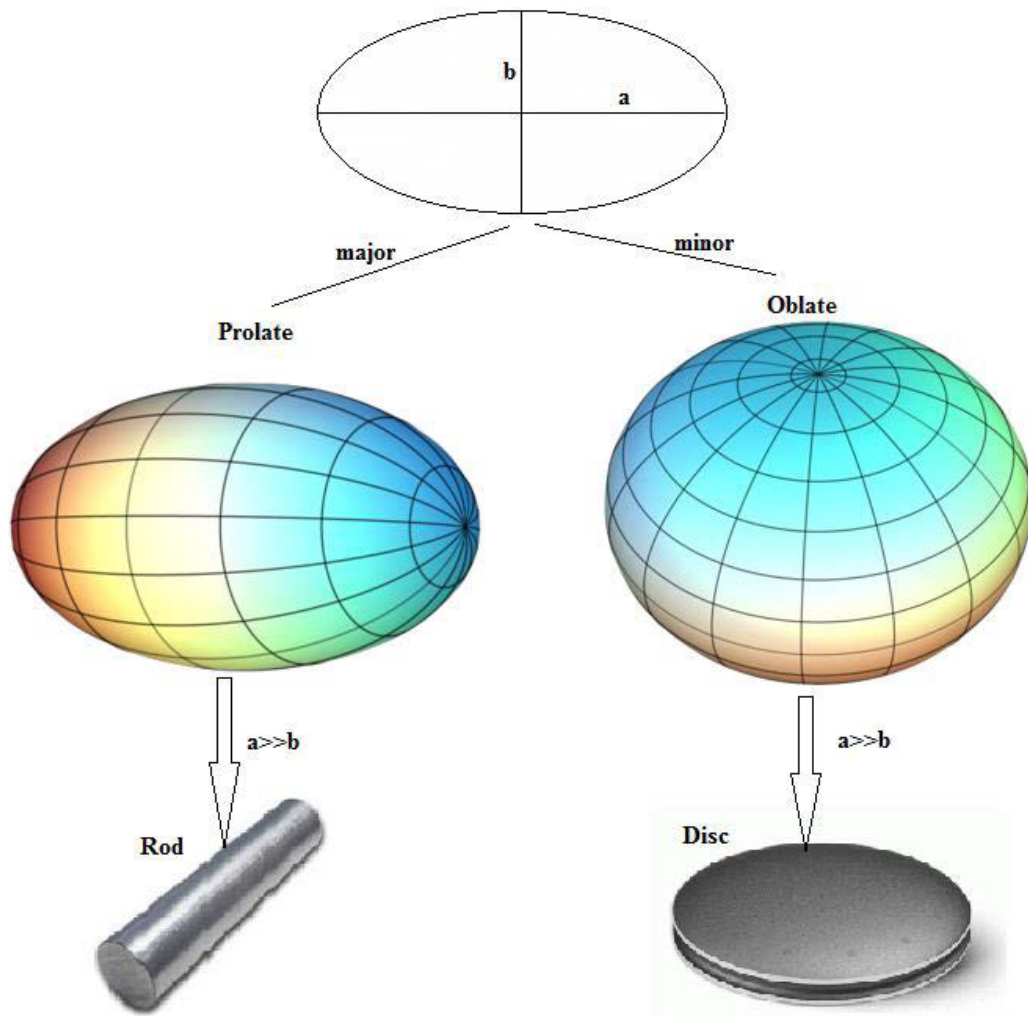


Figure 2-7 Ellipsoids of Revolution (Formed By Rotating an Ellipse about Either Its Major Axis (Prolate) or Minor Axis (Oblate) (Adapted from Harding & Colfen 1995).

When it comes to cylindrical particles (the focus of this study), two main contact types are conceivable (Figure 2-8): side contact (similar contact area to that of a prolate ellipsoid) and end contact (similar contact area to that of an oblate ellipsoid) (Figure 2-7).

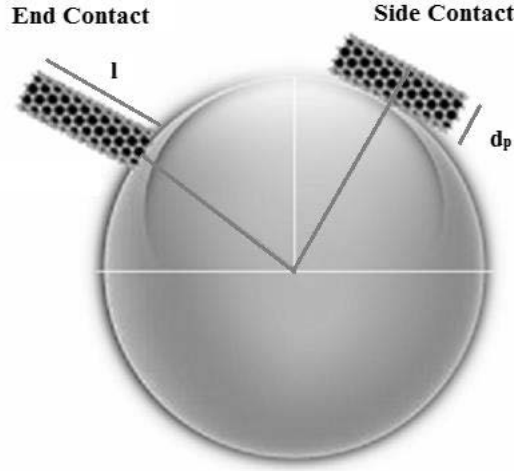


Figure 2-8 Side and end contact between a cylindrical particle and collector. Where d_p is particle diameter and l is particle length.

For a cylindrical particle, each component of SCE is calculated through:

$$\eta_D = 4.03 \left[kT \ln \left(\frac{1 + \left[1 - \left(\frac{d_p}{l} \right)^2 \right]^{\frac{1}{2}}}{\frac{d_p}{l}} \right) \right]^{\frac{2}{3}} \left(3\pi\mu d_c v_o \left(\frac{3}{2} d_p^2 l \right)^{\frac{1}{3}} \left(\frac{l}{d_p} \right)^{\frac{2}{3}} \left(1 - \left(\frac{d_p}{l} \right)^2 \right)^{\frac{1}{2}} \right)^{-\frac{2}{3}}$$

Eq. 2-14

$$\eta_G = \left(\frac{d_p}{l} \right)^{\frac{2}{3}} \left(\frac{0.146(\rho_p - \rho)g(d_p^2 l)^{\frac{2}{3}}}{\mu v_o \left[1 - \left(\frac{d_p}{l} \right)^2 \right]^{\frac{1}{2}}} \right) \ln \left(\frac{1 + \left[1 - \left(\frac{d_p}{l} \right)^2 \right]^{\frac{1}{2}}}{\frac{d_p}{l}} \right) \quad \text{Eq. 2-15}$$

$$\eta_l(side - contact) = \left[\frac{1}{2} \left(\frac{d_p}{d_c} \right)^2 \left(3 - \frac{d_p}{d_p + d_c} \right) \right] \quad \text{Eq. 2-16}$$

$$\eta_l(end - contact) = \left[\frac{1}{2} \left(\frac{l}{d_c} \right)^2 \left(3 - \frac{l}{l + d_c} \right) \right] \quad \text{Eq. 2-17}$$

Details on mathematical modelling equations for calculating filtration coefficient will be extensively discussed in Chapter Three.

2.5 Effects of Particle Orientation on Filtration Coefficient

For non-spherical particles, where more than one contact type is probable, orientation can become a deciding factor. Determining the orientation of cylindrical nanoparticles in water is a challenging task due to their very small size which favours random Brownian motion over predictable alignment and/or movement. However, some studies in synthetic compositions and polymer science, suggest that carbon nanotubes showed a higher degree of alignment in the longitudinal flow direction under high velocity rates. While the morphological analysis, using SEM, TEM and AFM, showed that the nanotubes were randomly oriented in the plane of the compression moulded samples, which were subjected to low velocities (Fan & Advani 2005; Abbasi, Carreau & Derdouri 2010). Their results alert us to expect higher alignment with the average velocity vector of groundwater flow when the magnitude of the velocity is large. Random orientation is, however, expected where velocity is very low.

Based on this hypothesis, under higher velocities, more end contacts are perceivable and hence less filtration will occur. Vice versa, when velocity is low, side contact become more probable and hence filtration rate is expected to increase (see Figure 2-9).

Further research and experimental work is needed to observe non-spherical suspended nanoparticles in motion in order to establish relationships between particle orientation and other potentially effective parameters such as velocity, pore size, pore connectivity, surface

roughness, particle size, and particle shape. No documented work was found to have studied this phenomenon in a water matrix to the best of my knowledge.

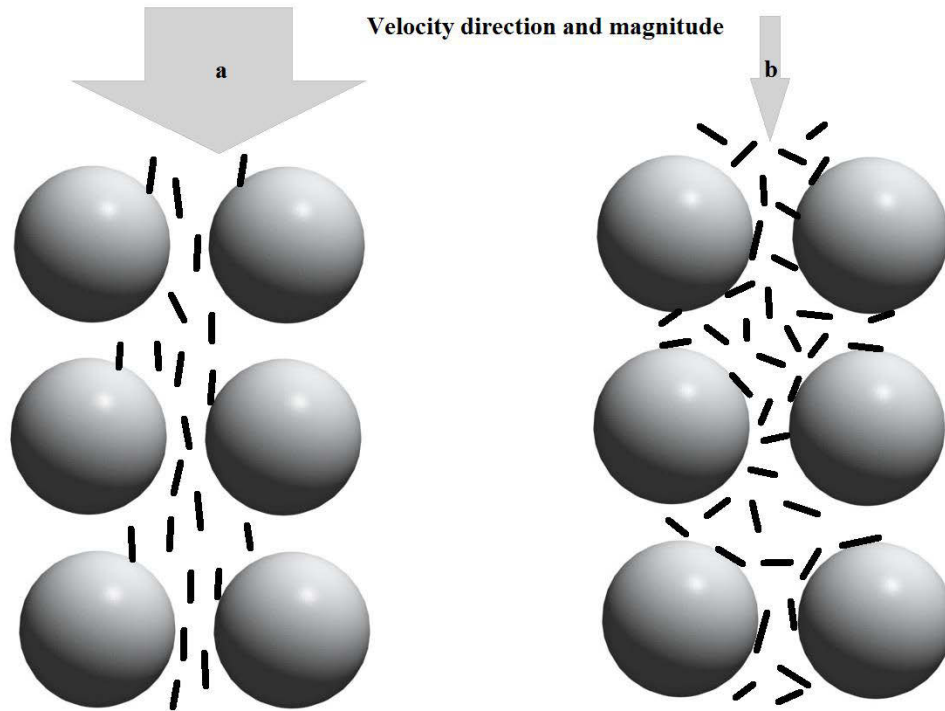


Figure 2-9 Particle orientation, speculated based on a) high velocity and b) low velocity

2.6 Effects of Physical Heterogeneity of Porous Media on Filtration Coefficient

While (equations 2-14 to 2-17) were shown to provide improved results for cylindrical nanoparticle filtration (Liu et al. 2009; Yao 1968), they fail to represent the heterogeneity of a natural porous medium. Natural porous media, such as alluvial layers, volcanic rocks, and other commonly found geological formations are characteristically heterogeneous (Le Gallo, Bildstein & Brosse 1998). They feature combinations of pores of various shapes, sizes, surface areas, and connectivity.

Equations 2-16 and 2-17 require the assignment of collector diameter [d_c]. This parameter has been traditionally represented by d_{50} or the mean grain size (Yao 1968; Liu et al. 2009; Nelson

& Ginn 2011). In other words, by using a single value in single collector efficiency equation, the porous media has been traditionally assumed to be homogeneous with uniform grains of average diameter. Since in these cases the experimental setting has been on laboratory scale (pore-scale) and the experimental soil columns have been packed by well characterized and homogeneous material, the equations have been deemed suitable. However, it is evident that the presence of heterogeneity changes the particle transport pathways as a result of property changes within porous media. A simple particle flow model (P-FLOW by USGS) can be used to illustrate this concept further.

This model is initially developed as a homogeneous system. A group of particles are then introduced to the system and their movement through this medium is tracked until they move out of this box system. Two arrows, each on one axis, locate the centre of the mass as the particles move through the porous media.

The same setup is used for tracking the particles in a randomly heterogeneous system. In this scenario, particles become dispersed as they move through the medium. The blue arrow grows in length, showing the dispersion of the plume mass as a result of heterogeneity of the physical properties of the solid matrix.

Another observation made through comparing these two systems indicates that the overall transport time has increased in the heterogeneous system. Ironically, the first particle leaves the box model earlier in the heterogeneous system (day 610).

Conceptually, dispersion becomes more and more important with increasing level of heterogeneity. In a particle transport scenario, filtration also becomes more significant in the presence of heterogeneity by creating small and local flow fields, eddies, dead corners where molecular diffusion replaces dispersion, and disconnected pores where the particles are trapped and finally sorbed onto the surface area.

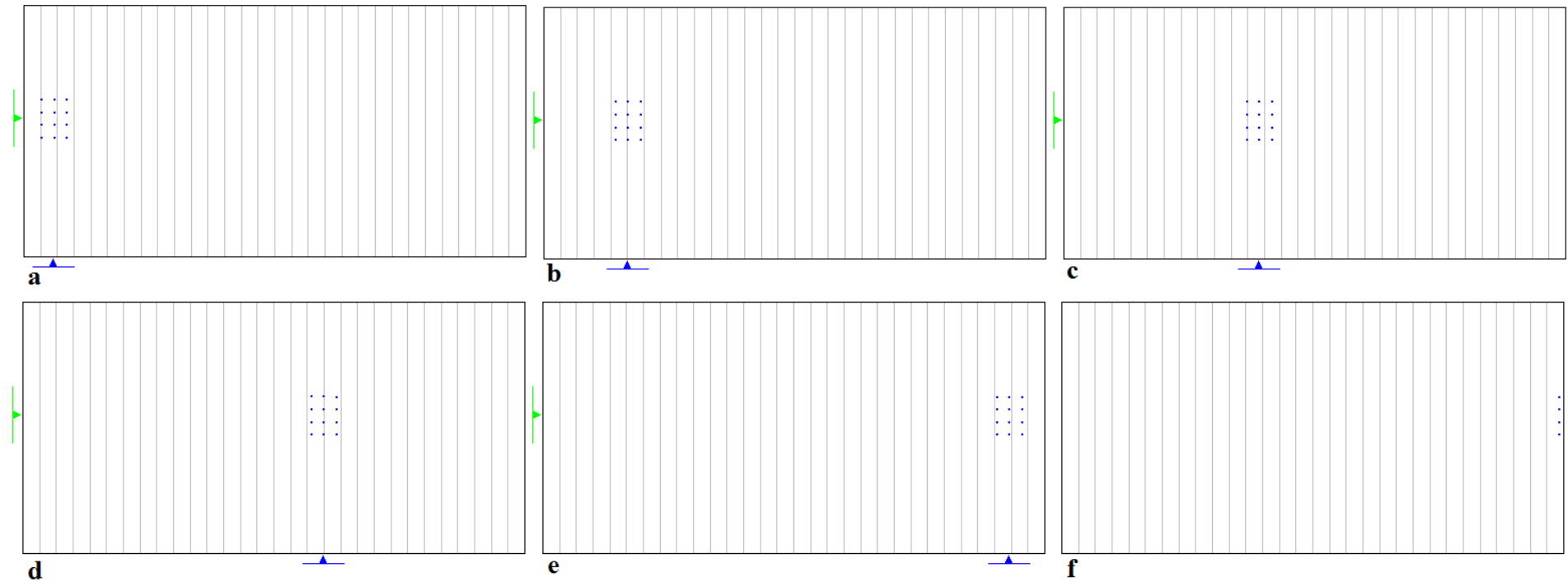


Figure 2-10 Particle flow model in a homogeneous porous medium; a) particles position , b) day 100, c) day 300, d) day 500, e) day 800, f) day 885, when all particles move out of the system on day 895. The green and blue arrows show the centre of the mass as the particles move through the porous medium.

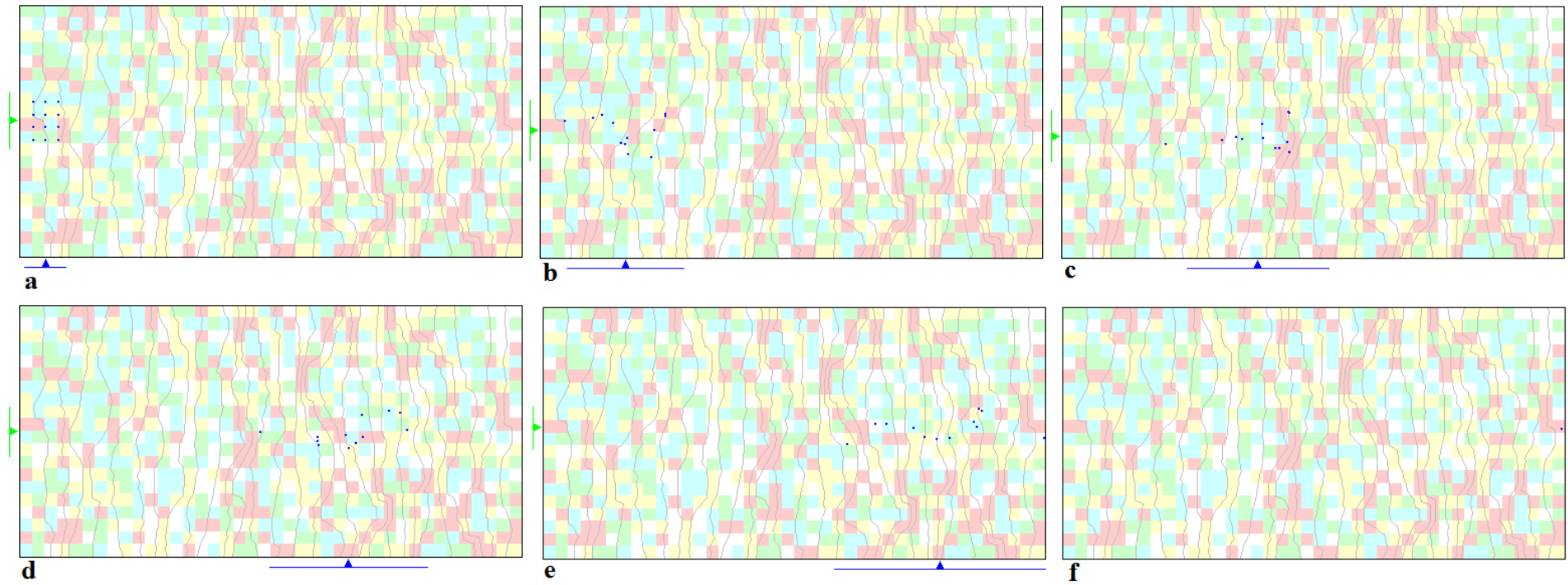


Figure 2-11 Particle flow model in a randomly heterogeneous porous medium; a) particles position , b) day 100, c) day 300, d) day 500, e) day 610 when the first particle leaves the system, f) day 940 when the last particle is just about to leave the system, when all particles move out of the system on day 945. The green and blue arrows show the centre of the mass as the particles move through the porous medium.

Previous particle filtration modelling studies suggest that particle size, heterogeneity of the porous media and attachment efficiency are important factors in particle mobility (Sun et al. 2001; Bhattacharjee, Ryan & Elimelech 2002; Loveland et al. 2003; Jaisi et al. 2008). Complex modelling of colloid transport has been done by a number of researchers (Maxwell, Welty & Thompson 2003; Tufenkji, Redman & Elimelech 2003; Tufenkji & Elimelech 2004; Scheibe, Dong & Xie 2007; Tartakovsky et al. 2007; Tufenkji 2007) where the results showed much improvement following the utilization of field hydraulic conductivity data and a better representation of field heterogeneities. In many cases the behaviour of the porous media has been termed “non-classical” as it cannot be predicted by existing laboratory-scale theories (Bryant & Thompson 2001). These studies highlight the importance of inclusion of heterogeneity for particle filtration modelling. Scaling effects have been observed to be very significant in many cases and the need for developing new theories to overcome these effects has been highlighted in many cases. For example, Szecsody et al. (Szecsody et al. 1998) observed that only through stochastic modelling, by incorporating natural heterogeneity of the system, could they reproduce the observations for reactions of CoII/III/EDTA with Fe oxide-containing sediments. Volume-averaging methods was used to upscale the reaction rate constants for quartz suspension by Lichtner and Tartakovsky (Lichtner & Tartakovsky 2003), incorporating the heterogeneity in mineral grain size and by Battiato (Battiato 2010) to advance flow simulations in CNT forests which are both attributed to heterogeneous distribution of grain/pore sizes.

2.6.1 A Question of Scale

Any equation models a simplified case of a real system at a particular scale which only holds under a specific set of assumptions. These simplifications make it possible to formulate an otherwise much more complex system behaviour and use this equation as a predictive tool. Predictive equations and models are only accepted if precision is in an acceptable balance against simplifications and the system behaviour can be simulated with enough accuracy while the simulation times/costs remain realistic.

Different models may be suitable for various systems depending on their limitation, assumptions, accuracy, and scale. The main challenge is applicability of the scientifically rigorous equations which are well defined and understood on a much smaller scale than that of a real field. Under such tightly controlled conditions, natural heterogeneities are not a concern. Ironically, predictions are often desired in complex natural systems much larger and inherently heterogeneous. These complex systems cover a variety from subsurface aquatic environments, to human blood, and nanotechnology products.

Flow and transport can be modelled for a pore-scale or a continuum-scale case (using specific models for each scenario). Equations that have a solid physical foundation based on the first principles (e.g., Stokes equations for fluid flow and Fick's law of diffusion for solute transport) usually satisfy the needs of the most demanding theoretician, however the use of such microscopic models requires the knowledge of pore geometry (that is hardly ever available in real applications). Macroscopic models (e.g., Darcy's law for fluid flow and an advection-dispersion equation for transport), which treat a porous medium as an "averaged" continuum, overcome these limitations by relying on phenomenological descriptions and a number of simplifications (Battiato 2010).

2.6.2 Representation of Heterogeneity

In order to represent the physical heterogeneity of the porous media soil measurements such as grain size distribution, porosity, and hydraulic conductivity can be used to replace the grain size (collector diameter [d_c]) in equations 2-16 and 2-17.

2.6.2.1 Grainsize Distribution and Hydraulic Conductivity

The relationship between grain size distribution and hydraulic conductivity has been studied by numerous scientists and there are, therefore, many attempts to offer a robust relationship between grain size and hydraulic conductivity. Some of the more commonly used methods and theories are discussed subsequently.

In 1893 Hazen developed a relationship between hydraulic conductivity and grain size distribution. His method has been vastly used since, however, many ensuing studies refined and improved his methods and extended the limitations of his equation. Alyamani and Sen (1993), Carmen (1937), Kozeny (1927), Masch and Denny (1966), Uma et al. (1989), and many more have developed empirical equations, all of which performs best under a given set of conditions assumed for the soil of interest. Vukovic and Soro (1992) have summarised several methods from these studies and have commented on each one's limitations and inherent assumptions. Most of these equations apply to granular aquifers and include the grain size distribution of the component particles from mechanical sieving. The grain diameter is d_x , where x is the size fraction (by weight) finer than a given sieve size. The uniformity coefficient, C_μ , is defined as the ratio of d_{60} to d_{10} and is a measure of the distribution's spread.

Hazen's equation (Eq. 2-18) can be applied when effective diameter (d_{10}) is between 0.1 and 3 mm and C_μ is less than 5.

$$K = Cd_{10}^2 (0.70 + 0.03T) \quad \text{Eq. 2-18}$$

Where:

K is hydraulic conductivity (m/day)

C is Hazen Coefficient calculated based on porosity [Eq. 2-19]

d_{10} is effective grain diameter (mm).

T is temperature in °C

$$C = 400 + 40(n - 26) \quad \text{Eq. 2-19}$$

Where;

n is porosity as a percentage (not as a fraction)

For a typical groundwater sample with a temperature of 10 °C, Eq. 18 can be re-written as:

$$K = Cd_{10}^2 \quad \text{Eq. 2-20}$$

Eq. 2-20 is also known as the Beyer equation when temperature is not taken into consideration.

In the Beyer equation hydraulic conductivity is estimated in m/s units and C is calculated as:

$$C = (4.5 \times 10^{-3}) \log \left[\frac{500}{C_{\mu}} \right] \quad \text{Eq. 2-21}$$

The Kozeny-Carman equation (Eq. 2-22) also considers porosity as well as the effective grain diameter:

$$K = 5400 \frac{n^3}{(1-n)^2} d_{10}^2 \quad \text{Eq. 2-22}$$

Alyamani and Sen (1993) introduced a new variable to their equation: *intercept*, I_o , is the value at which no material passes from the set of sieves. This value is usually very close to zero and is less than d_{10} . Intercept has a direct relationship with hydraulic conductivity. They also suggested a relationship between hydraulic conductivity and the slope which defines the rate of grain diameter change within the sample. They derived a relationship as:

$$K = 1300 [I_o + 0.025(d_{50} - d_{10})]^2 \quad \text{Eq. 2-23}$$

The use of Intercept makes Alyamani-Sen equation applicable to a much wider range of soil types with various size distribution properties.

2.6.2.2 Selection of the Best Suited Equation

In a homogeneous porous medium such as those used in the soil column laboratory experiments of Liu et al. (2009), d_{10} is the same or very similar to d_{50} and d_{60} as a result of

near-perfect sorting in preparations. Hence, C_μ tends towards 1 and any of the given equations can be rewritten with d_{10} , d_{50} , and d_{60} replaced by a single value for the grain size (collector diameter).

I state that using d_{50} as the representative average grain-size, will under-estimate collector efficiency. To further demonstrate this concept ten characterised soil samples from Australia were used (

Table 2-2). The SCE for each sample was calculated using d_{50} based on the common practice of taking the average value as a representative measurement, followed by calculations using d_{10} as the most frequently used “effective grain size” reported in the literature.

Note that using d_{50} virtually assumes a larger grain size as a representative diameter. On the other hand, it is widely accepted that the finer grains control the hydraulic conductivity (and hence the ease of water flow) of a porous medium. It is also observed that SCE shows a very clear inverse relationship with hydraulic conductivity (plotted on a secondary axis) when effective grain size (d_{10}) is used (Figure 2-12).

Table 2-2 Characterised Australian soil samples

* Sample	Hydraulic Conductivity (m/d)	d_{10} (mm)	d_{50} (mm)	d_{60} (mm)	St. Dev. (mm)	C_μ	Porosity (n)**
1	950.4	0.91	1.04	1.07	0.11	1.18	0.46
2	864	0.65	0.75	0.79	0.11	1.22	0.46
3	777.6	0.54	1.75	1.97	0.63	3.65	0.38
4	172.8	0.33	0.46	0.48	0.08	1.45	0.45
5	86.4	0.32	0.36	0.37	0.04	1.16	0.46
6	69.1	0.24	0.29	0.3	0.03	1.25	0.46
7	25.9	0.18	0.45	0.51	0.56	2.83	0.41
8	17.3	0.18	0.37	0.45	0.4	2.5	0.42
9	17.3	0.19	0.57	0.94	0.69	4.95	0.36
10	17.3	0.16	0.21	0.22	0.03	1.38	0.45

* Data taken from Alyamani and Sen (1993)

** Porosity of each sample was calculated from the Vukovic and Soro (1992) equation; $n = 0.255 (1+0.83^{C_\mu})$

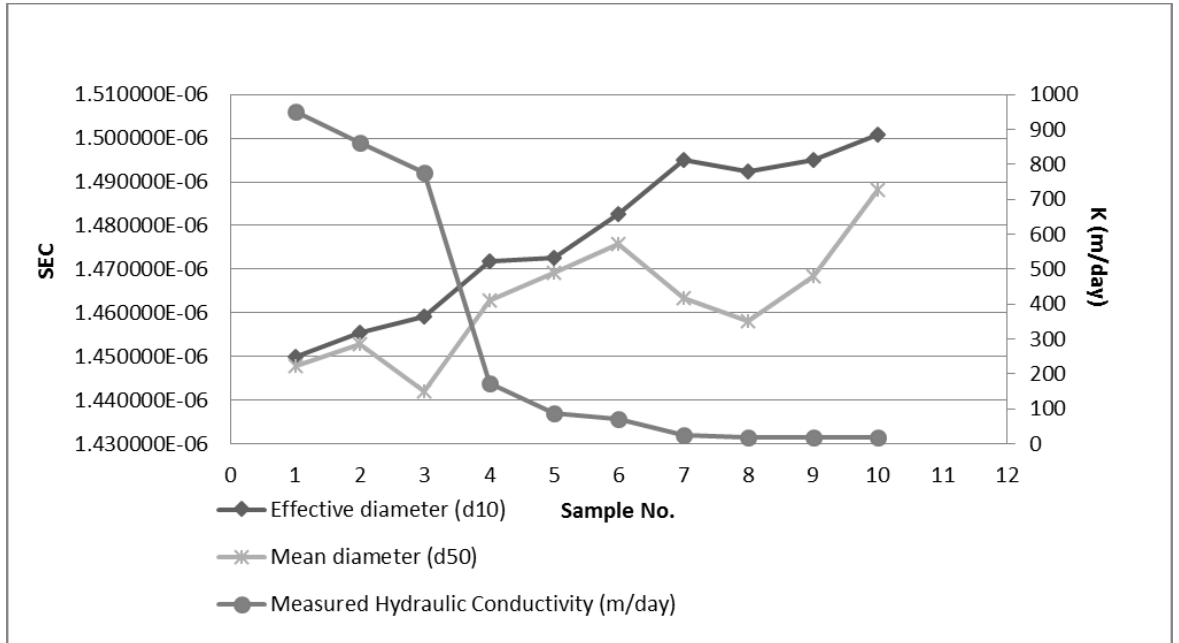


Figure 2-12 SCE calculated based on d10 and d50 for 10 heterogeneous samples

Assuming a poorly sorted (well graded), homogeneous porous medium at 10 °C, each one of Equations 2-20 (for both Hazen and Beyer), 2-22, and 2-23 can be rearranged as Equations 2-24, 2-25 and 2-26 in terms of d_c (equivalent to d_{10}).

The Hazen equation (Eq. 2-20) at 10 °C can be expressed as:

$$K = (400 + 40.(n - 26))d_{10}^2$$

$$\Rightarrow d_{10} = d_c = \sqrt{\frac{K}{400 + 40(n - 26)}} \quad \text{Eq. 2-24}$$

The Beyer equation (Eq. 2-21) can be rearranged as:

$$K = 4.5 \times 10^{-3} \log \frac{500}{C_\mu} \times d_{10}^2$$

$$\Rightarrow d_{10} = d_c = \sqrt{\frac{K}{4.5 \times 10^{-3} \log \frac{500}{C_\mu}}} \quad \text{Eq. 2-25}$$

The Kozeny-Carman equation becomes:

$$K = 5400 \frac{n^3}{(1-n)^2} d_{10}^2$$

$$\Rightarrow d_{10} = d_c = \sqrt{\frac{K(n-1)^2}{5400n^3}}$$
Eq. 2-26

The Alyamani and Sen equation (Eq. 2-23) does not consider porosity. Instead it is concerned with the difference between the mean and effective grain sizes. This difference defines a slope which, in turn, defines the *intercept* (I_0) at the plot origin. In a well-sorted (homogeneous) porous medium, the trend line between d_{10} and d_{50} is essentially a vertical line parallel to Y axis. In such a case I_0 , d_{10} , and d_{50} will have the same value as d_c .

Hence d_c can be expressed as;

$$K = a[I_0 + 0.025(d_{50} - d_{10})]^b$$

$$\Rightarrow d_{50} = d_c = \frac{\sqrt[b]{\frac{K}{a}} - I_0 + 0.025d_{10}}{0.025}$$
Eq. 2-27

Where:

a is 2 for the data in hand

b is 1300 for the same database.

Note that in this empirical equation, hydraulic conductivity unit is m/day while grain diameter values are in mm.

Each one of these replacement equations offers a different level of representation for the natural heterogeneity of the porous media. In order to evaluate the deviation from the original theoretical SCE equation, d_c has been replaced by equations 2-24 to 2-27 for a set of soil

samples. Table 2-3 shows a list of various scenarios for which these calculations were carried out. In these scenarios, grain size changes between 0.001 and 1 millimetre. These scenarios cover a range of very fine to coarse grain size.

By developing these scenarios, the deviation of each method's result can be calculated from the theoretical value of SCE. Selected method can be then evaluated using laboratory measurements of real samples.

Table 2-3 Validation scenarios

Collector Diameter (mm)	Hazen K (m/day)	Beyer K (m/day)	Kozeny-Carman K (m/day)	Alyamani-Sen K (m/day)
0.001	0.0012	1.05	1.80	0.0013
0.01	0.12	10.5	18.02	0.13
0.1	12	104.9	180.25	13
1	1200	1049.36	1802.5	1300

For all scenarios particle diameter, particle length, temperature, and all other relevant parameters are the same and the uniformity coefficient is always 1 as the material is assumed to be homogeneous.

Table 2-4 contains the results of the SCE calculations for each method and the standard deviation from the SCE equation (Eq. 2-10) with homogeneity assumption. Results presented in Table 2-4 strongly favour the Alyamani and Sen equation which has replicated the SCE calculations most closely. Based on this validation of the various options available, I adapted this equation for introducing heterogeneity into SCE equation.

Table 2-4 Single Collector Efficiency (SCE) calculation results and their standard deviation from SCE with homogeneity assumption

Grain size (mm)	Eq. (2-10) Results	Hazen		Beyer		Kozeny-Carman		Alyamani-Sen	
		Results	Std. Dev.	Results	Std. Dev.	Results	Std. Dev.	Results	Std. Dev.
0.001	7.68E-5	1.047E+1	7.40E+0	2.41E-1	1.70E-1	5.49E+0	3.88E+0	3.50E-6	5.18E-5
0.01	2.61E-6	1.04E-1	7.42E-2	2.41E-2	1.70E-2	5.36E-1	3.79E-1	1.87E-6	5.19E-7
0.1	1.53E-6	1.05E-3	7.42E-4	2.41E-3	1.70E-3	5.50E-2	3.89E-2	1.52E-6	5.20E-9
1	1.44E-6	1.19E-5	7.42E-6	2.43E-4	1.70E-4	5.50E-3	3.89E-3	1.44E-6	5.34E-11

The values of SCE for the previously mentioned Australian soil samples have been compared between Eq. 2-10 -with the limitation of assuming d_{50} or d_{10} as d_c and hence neglecting the heterogeneity- and the proposed modified equation where the Alyamani and Sen Equation (Eq. 2-27) has replaced d_c in Eq.2-10. Figure 2-13 illustrates the results of this comparison.

The Alyamani and Sen equation offers an even more interesting observation: despite following a general inverse relationship with hydraulic conductivity, it estimates SCEs below and above those calculated based on d_{10} only. This is believed to be due to other characteristics of the soil such as uniformity, porosity, and size distribution.

Note that the Hazen, Beyer, and Kozeny-Carman equations calculated values of approximately 1, 2, and 3 orders of magnitude larger than those calculated by Alyamani and Sen. The Hazen equation has been recommended for conditions under which $0.1 < d_{10} < 3$ mm and $C_u < 5$ (Vukovic and Soro, 1992). While these conditions are true for all ten soil samples tested in this paper, the Hazen method predicts much higher values for SCE.

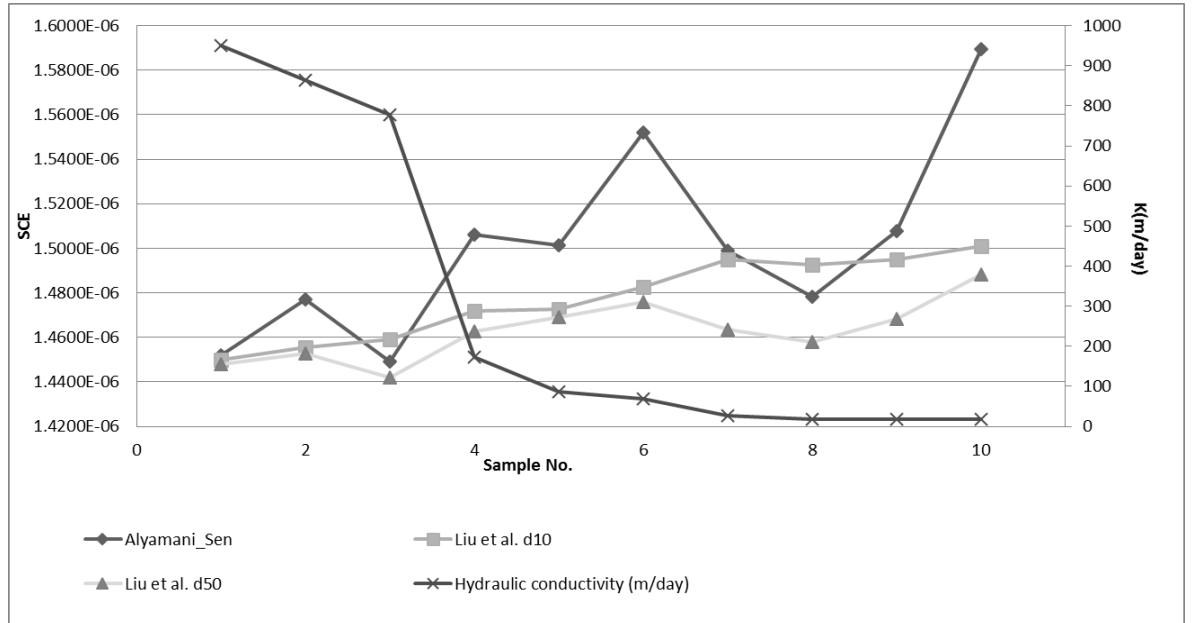


Figure 2-13 Comparison of SCE results using Eq. 2-10 with d10, d50, and Eq. 2-27

Virtual and real scenarios tested here, illustrated a difference in values estimated with and without the heterogeneity represented in the predictions. These observations plant the seeds for a plausible argument that the mobility of cylindrical nanoparticles can be significantly different from those estimated under the assumption of uniformity and homogeneity of the saturated porous media.

2.7 Effect of Collector Efficiency on particle Filtration

To recap what was presented earlier in this chapter, the main concepts and equations are summarised here, before the effects of collector efficiency on filtration are explored.

A “collector” represents the solid phase grain (in the porous medium). A fraction η_0 of the particles are brought to surface of the collector by the mechanisms of Brownian diffusion, Interception and/or Gravitational sedimentation. η_0 is calculated through:

$$\eta_0 = \eta_I + \eta_G + \eta_D \quad \text{Eq. 2-28}$$

A fraction α of the particles that reach the collector surface attach to the surface. Sticking factor or attachment efficiency α is usually determined by normalising K_{att} by the experimentally

determined deposition rate coefficient under favourable electrostatic conditions ($\alpha = \frac{k_d}{k_{d,fav}}$)

(Jaisi et al. 2008).

Total theoretical number of particles collected by a single collector is:

$$\eta_o \times \alpha \quad \text{Eq. 2-29}$$

The single collector efficiency is then scaled up to a macroscopic filtration coefficient, which can be related to first-order attachment rate of the particles to the solid phase of the medium.

Where filtration coefficient is:

$$\lambda = \frac{3(1-n)}{2d_c} \alpha \eta_o \quad \text{Eq. 2-30}$$

Equation 2-30 can be rearranged as followed to include heterogeneity:

$$\lambda = \frac{0.0375(1-n)}{-\sqrt{\frac{K}{1300}} + I_0 + d_{50}} \alpha \eta_o \quad \text{Eq. 2-31}$$

And the first-order deposition rate is:

$$k_{att} = \lambda v_0 \quad \text{Eq. 2-32}$$

For sample No. 10 (as seen in Table 2-2) under conditions outlined in Table 2-5 attachment rate has been calculated assuming three different scenarios:

In scenario 1 d_c is represented by d_{10}

In scenario 2 d_c is represented by d_{50}

In scenario 3 d_c is represented by Alyamani-Sen replacement equation or d_{AS}

Table 2-5 Filtration attachment rate calculations for sample No. 10

Scenario		α (mm)	Velocity mm/s	K_{att}
1	dc=d10	1.12	0.01157	1.00E-07
2	dc=d50			7.58E-08
3	dc=d _{AS}			1.23E-09

Based on the scenarios tested here, it is shown that particles could become more mobile when natural heterogeneity is represented.

3 Colloid Transport Modelling

“A thinker sees his own actions as experiments and questions-as attempts to find out something. Success and failure are for him answers above all.”

Friedrich Nietzsche

3.1 Modelling History

Early modelling of colloidal particles was driven by the need to understand the performance of deep-bed filters used in chemical engineering and waste-water treatment (Yao, Habibian & O'Melia 1971; Iwasaki 1937). It was as recently as some two decades ago that colloids were recognised as a possible facilitator for contaminant transport in groundwater systems (McCarthy 1989). This new way of looking at colloids, positioned them as a mobile solid phase on which contaminants could be attached and hence travel further than they would have without the assistance of the colloids (Figure 3-1). Many subsequent studies focused on colloidal movement, transport of contaminants with colloids, colloidal filtration, changes of porosity caused by colloids, and transport of biocolloids (ie. bacteria and virus transport) (Corapcioglu & Jiang 1993; Ibaraki & Sudicky 1995; Kessler & Hunt 1994; Lührmann, Noseck & Tix 1998; Swartz & Gschwend 1999; Wan & Wilson 1994; Granqvist et al. 1976; McCarthy 1989; McDowell-Boyer 1992; Robert & Powellet 1992; Lindqvist, Cho & Enfield 1994; Saiers & Hornberger 1996; Pang 1996; Seaman & Bertsch 1997; Roy & Dzombak 1997; Kersting et al. 1999; Honeyman 1999).

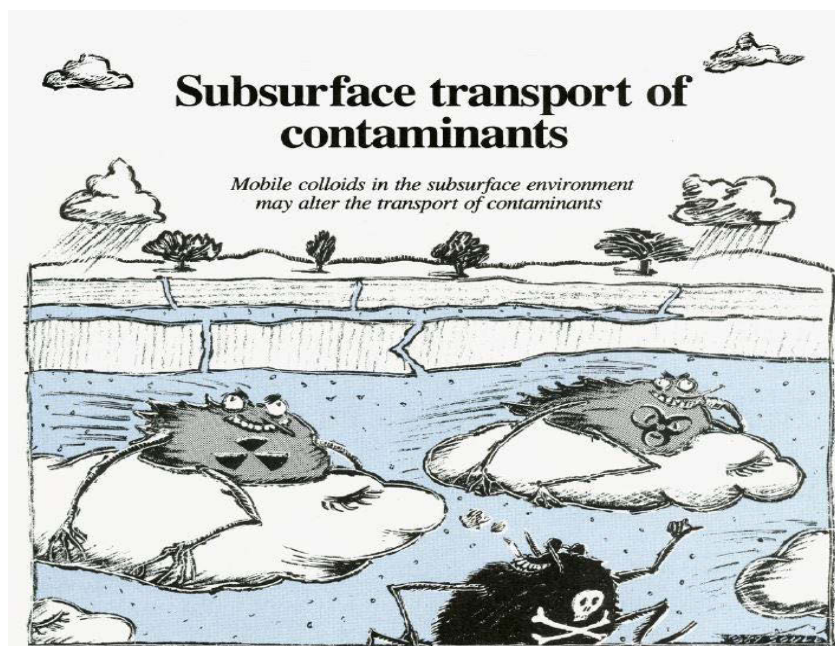


Figure 3-1 Title image in McCarthy's publication, *Nature*, 1989

Understanding colloidal transport is a complex matter and many factors play a role in determining the fate of a colloidal particle in saturated porous media (Elimelech & Ryan 2002).

Colloidal particles such as mineral colloids can be generated under various physical and chemical conditions and change the transport dynamics of any present contaminant. These colloids can change the porosity and pore network connectivity of the solid phase through which they flow. Other important colloids which add even more weight to colloid transport modelling significance include microbial colloids, viruses, new pesticides, and engineered nanoparticles (Mawdsley, Bardgett & et al. 1995; Smith & Perdek 2004; Medema & Juhasz-Holterman 2000). According to Gerba (1975), between 1946 and 1960, 61% of waterborne disease outbreaks were attributed to contaminated groundwater in the USA. Some matters of security such as potential for bioterrorism attacks to the drinking water supply have further promoted the need to develop improved mathematical models of colloids and biocolloids migration (Tufenkji 2007).

3.2 Modelling Theories: Old and New

The mobility of nanoparticles as a group of colloids in saturated subsurface is dependent on their distribution between the solid matrix (soil network) and the liquid matrix (water). Hence the theory of transport considers these two phases when it comes to colloid transport.

In general terms, colloid transport in a porous medium is modelled as a combination of (1) advection, (2) dispersion, and (3) attachment to the solid matrix surface (Loveland et al. 2003).

There are various methods which have been used to model the attachment of colloids to the granular porous media.

3.2.1 Advection-Dispersion Equation

A simplified way of predicting the general transport of colloidal particles is the ordinary advection-dispersion equation:

$$\frac{\partial C}{\partial t} = D \frac{\partial^2 C}{\partial x^2} - v \frac{\partial C}{\partial x} \quad \text{Eq. 3-1}$$

Where:

C is the concentration of the colloidal particles

D is the hydrodynamic dispersion

v is the velocity

In this equation, the special concentration of colloids over time is described by advection and dispersion as described in Chapter 2.

To be able to consider the removal of colloids through physiochemical filtration, an attachment term is added to the advection-dispersion equation (Eq. 3-1) to obtain Eq. 3-2.:

$$\frac{\partial C}{\partial t} = D \frac{\partial^2 C}{\partial x^2} - v \frac{\partial C}{\partial x} - \frac{\rho_b}{n} \frac{\partial S}{\partial t} \quad \text{Eq. 3-2}$$

Where:

S is sorbed concentration of colloids

n is porosity

ρ_b is bulk density of the soil matrix.

The filtration of particles has been modelled as both reversible and irreversible process. In the case of reversible attachment, both equilibrium and kinetic mechanisms have been considered (Schijven & Hassanizadeh 2000; Rajagopalan & Tien 1976; Tufenkji 2007).

3.2.2 Irreversible Attachment

Filtration theories have been developed from theoretical considerations and experimental results for the transport of monodisperse micro (or nano)-spheres through columns packed

with spherical collector grains (Yao, Habibian & O'Melia 1971; Rajagopalan & Tien 1976). Colloid Filtration Theory (CFT) is the most commonly approach for colloid transport modelling since it was developed by Yao et al. in 1971. It has been used for modelling transport and retention of colloids in both laboratory and field-scale studies (Schijven & Hassanizadeh 2000; Tufenkji, Redman & Elimelech 2003).

CFT defines attachment as a two-step process:

- the first step is quantified by single collector efficiency (η), which represents the frequency at which the particles come in contact with the solid phase
- the second step defines α , the frequency at which contacting particles actually get attached to the solid phase (collectors).

While single collector efficiency (η) is a theoretical value and is calculated using a closed-form equation (Yao 1968; Rajagopalan & Tien 1976; Nelson & Ginn 2005), α is measured for each given environment as described in Chapter 2 (2.7).

3.2.3 Equilibrium Adsorption

To improve the older methods of modelling colloidal particles, advances have been made by considering two-site attachment, Langmuir-type reaction kinetics (Lindqvist, Cho & Enfield 1994) as well as Freunlich isotherm (Yates, Yates & Gerba 1988).

In an equilibrium adsorption, the sorbed concentration is directly related to concentration in liquid phase and the equilibrium constant rate.

$$S = k_{eq} C \quad \text{Eq. 3-3}$$

where k_{eq} is the equilibrium constant.

3.2.4 Kinetic Adsorption-Desorption

Before an equilibrium is reached in any system, the attachment and detachment of colloids is controlled by a kinetic process. This process happens in two steps: in the first step, the colloids come into contact with the surface of the solid matrix (mass transfer of the colloids), and in the second step they get adsorbed onto these surfaces by physiochemical interactions. Attachment is directly related to colloid concentration in the fluid as well as available surface area of the solid matrix.

The desorption (detachment) of the sorbed colloids may also be controlled by a kinetic process. The detachment rate correlates with the sorbed concentration of the colloids onto the solid matrix.

The overall change in concentration of attached colloids can be described as:

$$\frac{\rho_b}{n} \frac{\partial S}{\partial t} = K_{att} C - \frac{\rho_b}{n} K_{det} S \quad \text{Eq. 3-4}$$

Where:

K_{att} is attachment rate coefficient

K_{det} is detachment rate coefficient

3.2.5 Hypothesis Development

Kretzschmar et al., 1997 conducted a series of short-pulse injection experiments to study the kinetics of colloid deposition rate in soil columns and concluded that the kinetic rate coefficients were independent of column dimensions, confirming their assumption of first-order colloid deposition kinetics. Whereas colloid deposition describes the retardation of colloids as they travel through porous media, use of advection-dispersion equation is deemed not sufficient as it will predict colloid behaviour to be the same as that of a conservative tracer.

Equilibrium adsorption and kinetic attachment methods have been used for many laboratory and field studies but do not result in removal of the colloids from the fluid matrix. This is a major shortcoming when it comes to defining irreversible retention and/or inactivation (for biocolloids).

Using a combined method where colloid deposition rate is calculated by using CFT's single collector efficiency, together with the Langmuir isotherm as well as implementation of a blocking factor can be a step towards better simulation of colloid transport. This method is investigated here.

Assuming an irreversible attachment (no or negligible detachment) of colloids (observed by Liu et al. 2010 and Jaisi et al, 2008 with MWCNTs), the following could be presented:

$$S \frac{\rho_b}{n} = K_{att} C \quad \text{Eq. 3-5}$$

Where:

S is sorbed concentration of colloids

n is porosity (which is usually assumed to be equal to ϵ or volumetric water content)

ρ_b is bulk density of the soil matrix.

While the Langmuir isotherm is expressed as:

$$S(1 + K_L C) = K_L \bar{S} C \quad \text{Eq. 3-6}$$

Where:

\bar{S} is the total concentration of adsorption sites

K_L is the Langmuir constant

As many have suggested, the particle deposition rate is calculated far more accurately when single collector efficiency is used and Brownian motion is incorporated into the particle trajectory as well as the other transport mechanisms (Nelson & Ginn 2005; Molla 2009; Tufenkji & Elimelech 2004; Nelson & Ginn 2011). It was also suggested that considering the limitation of adsorption sites, will simulate the slowing deposition rate over time as less adsorption sites become available (Tufenkji 2007; Tufenkji, Redman & Elimelech 2003; Johnson & Elimelech 1995; Ko & Elimelech 2000; Saleh, Pfefferle & Elimelech 2008; Jaisi et al. 2008; Cullen et al. 2010; Liu et al. 2009). This mechanism is considered in the Langmuir isotherm as it limits the deposition to the maximum concentration of adsorption sites \bar{S} . In order to incorporate the more desirable deposition rate calculations as well as the limitations of adsorption due to adsorption site availability, I have combined the two approaches as follows:

Eq. 3-5 and 3-6 can be solved for S and combined to form Eq. 3.7 as follows:

$$1- S = \frac{K_{att} C n}{\rho_b}$$

$$2- S = \frac{K_L \bar{S} C}{1 + K_L C}$$

$$\Rightarrow \frac{K_{att} C n}{\rho_b} = \frac{K_L \bar{S} C}{1 + K_L C} \rightarrow K_{att} C n + K_{att} n K_L C^2 = \rho_b K_L \bar{S} C$$

$$\Rightarrow \frac{K_{att} n}{K_L} = \rho_b \bar{S} - K_{att} n C$$

$$\Rightarrow K_L = \frac{K_{att}n}{\rho_b \bar{S} - K_{att}Cn} \quad \text{Eq. 3-7}$$

With this approach, K_L can be replaced by a new term which uses K_{att} that incorporates η_o and hence will be a better representative value for particle deposition rate.

While the impact of straining depends on the degree of agglomeration, which itself depends on characteristics of nanocolloids, I have chosen to ignore this mechanism as a filtration mechanism - as have others (Cullen et al. 2010; Liu et al. 2009). Hence, the attachment rate is calculated based on traditional mechanisms of filtration as the most significant mechanisms (Tufenkji & Elimelech 2004; Liu et al. 2009; Li et al. 2008).

$$K_{att} = \frac{3\alpha\eta_o\nu(1-n)}{2d_c} \quad \text{Eq. 3-8}$$

Where:

α is sticking coefficient (as defined in Sections 2.3.3, 2.7 and 3.2.2)

η_o is the calculate single collector efficiency

d_c is the collector diameter often replaced by the mean collector diameter or d_{50}

Equation 3-9 is essentially a mass balance statement, i.e., the change in the mass storage (both dissolved and sorbed phases) at any given time is equal to the difference in the mass inflow and outflow due to transport mechanism.

$$n \frac{\partial C}{\partial t} + \rho_b \frac{\partial S}{\partial t} = \frac{\partial}{\partial x_i} \left(n D_{ij} \frac{\partial C}{\partial x_j} \right) - \frac{\partial}{\partial x_i} (n v_i C) \quad \text{Eq. 3-9}$$

This equation presented by Zheng and Wang (Zheng & Wang 1999) can be rearranged as:

$$\frac{\partial C}{\partial t} = \frac{\partial}{\partial x_i} \left(D_{ij} \frac{\partial C}{\partial x_j} \right) - \frac{\partial}{\partial x_i} (v_i C) - \frac{\rho_b \partial S}{n \partial t} \quad \text{Eq. 3-10}$$

Where:

$\frac{\rho_b \partial S}{n \partial t}$ represents the solid phase mass balance (over time) which equals to $K_{att}C$ as seen in

Eq.3-5.

Previously, the solid phase mass balance was calculated based on the above equation when CFT has been assumed to simulate the transport. Replacing this equation by combining the Langmuir isotherm and the general transport equation, a new way of computing the solid phase mass balance can be presented as follows:

$$S = \frac{\left(\frac{K_{att}n}{\rho_b \bar{S} - K_{att}Cn} \right) \bar{S} C}{1 + \left(\frac{K_{att}n}{\rho_b \bar{S} - K_{att}Cn} \right) C} \quad \text{Eq. 3-11}$$

Where K_{att} is calculated by **Eq.3-8** and η_o is calculated by **Eq. 2-10**.

3.3 Modelling Tools

One of the previously mentioned purposes of this study was to build a bridge between the science produced in the laboratory and the industry where these results can help solve a real-world problem.

By modifying the pore-scale equations and up-scaling them, I took the first step in making these equations applicable to field scale problems. However, making the equations readily available for use in conjugation with industry standard modelling packages would promote the use of these newly developed equations.

Here, I will identify the selected software and briefly explain how the equations were implemented to be compatible with these codes.

3.3.1 Selected Software

To encourage the use of new knowledge in the industry, I have selected the most widely used packages for groundwater modelling, with priority given to Australia. It is noticeable, however, that Australia shows a significant resemblance in this regard with Asia and the north Americas.

Here I review existing noteworthy commercial tools, their modelling applications, and will eventually focus on the selected software for both flow and transport modelling.

3.3.1.1 Flow and Transport simulation software

- MODFLOW, MODFLOW-2005, and related programs: Three-dimensional finite-difference groundwater model. Codes included on this link include MODPATH, RADMOD, and ZONEBUDGET
- FEFLOW: A finite element computer program for simulating groundwater flow, mass transfer and heat transfer in porous media
- HydroGeoSphere: A 3D control-volume finite element groundwater model, simulating surface and subsurface water flow and solute and thermal energy transport
- MicroFEM: A finite-element program for multiple-aquifer steady-state & transient ground-water flow modelling
- Hydrus: A suite of Windows-based modelling software that can be used for analysis of water flow, heat and solute transport in variably saturated porous media
- MF2K-GWT: Three-dimensional groundwater flow and solute-transport model integrated with -2000
- MODFE (DG/Sun): Modular finite-element model for areal and axisymmetric ground-water flow problems
- MODFLOW-NWT: A Newton formulation for MODFLOW-2005

- MODFLOW-USG: An Unstructured Grid Version of MODFLOW for Simulating Groundwater Flow and Tightly Coupled Processes Using a Control Volume Finite-Difference Formulation
- MT3DMS: A Modular 3-D Multi-Species transport model for simulation of advection, dispersion, and chemical reactions of contaminants in groundwater systems
- CRT: Cascade Routing Tool to define and visualize flow paths for grid-based watershed models
- GSFLOW: Coupled Groundwater and Surface-water FLOW model based on the USGS Precipitation-Runoff Modelling System (PRMS) and Modular Groundwater Flow Model (MODFLOW-2005)
- HST3D: Three-dimensional flow, heat, and solute transport model
- HYDROTHERM: Three-dimensional finite-difference model to simulate multiphase groundwater flow and heat transport in the temperature range of 0 to 1,200 degrees Celsius
- INFIL3.0: A grid-based, distributed-parameter watershed model to estimate net infiltration below the root zone
- PHAST: A program for simulating ground-water flow, solute transport, and multicomponent geochemical reactions
- PHREEQC: A computer program for speciation, batch-reaction, one-dimensional transport, and inverse geochemical calculations
- SEAWAT: A computer program for simulation of three-dimensional variable-density groundwater flow and transport
- RT3D: A software for modelling multi-species reactive transport in groundwater
- PHT3D: A reactive multicomponent transport model for saturated porous media
- SEAM3D: A numerical model for three-dimensional solute transport coupled to sequential electron acceptor-based biological reactions in groundwater

- SHARP: A quasi-three-dimensional, numerical finite-difference model to simulate freshwater and saltwater flow separated by a sharp interface in layered coastal aquifer systems
- SUTRA and related programs: 2D, 3D, variable-density, variably-saturated flow, solute or energy transport
- TopoDrive and ParticleFlow: two computer models for simulation and visualization of groundwater flow and transport of fluid particles in two dimensions.

3.3.2 Finite Element vs. Finite Difference

The two most commonly used numerical modelling software are MODFLOW and FEFLOW, a finite difference and a finite element code respectively.

While the finite element method finds approximate solutions to boundary value problems for differential equations, finite-difference methods approximate the solutions to differential equations by approximating derivatives of these equations. In fact, finite difference method was later developed as a variation of finite element method (Fornberg 1998; Tinsley Oden 2010).

There are many advantages to using either of the above mentioned modelling programs. For example MODFLOW offers time efficiency and is an open-source code which can be relatively easily modified to suit specific needs for a given site/user. It is also free and because of the significant number of users, has been well tested over time and various scenarios. There are many forums where modellers share their experience and ask questions (Macdonald & Harbaugh 2003).

FEFLOW on the other hand, offer great flexibility for grid discretisation. With irregular shaped cells, refining areas of interest is made easy and the number of cells are kept to what's needed for a desirable resolution (Trefry & Muffels 2007).

The strictly rectangular shaped cells in MODFLOW grids, was always a limiting factor and refinement often a challenge. Many methods of refinement were developed and tested over time and each had its own disadvantages. Such methods introduced numerical errors, computational burden, or much additional effort when used (Macdonald & Harbaugh 2003). With the development of the latest version of MODFLOW code (MODFLOW-USG), this issue has been solved. MODFLOW-USG supports irregular-shaped grid cells and overcomes the refinement matter (Panday et al. 2013).

For the above mentioned reasons, MODFLOW family of programs (also compatible with many other packages developed for transport modelling and visualisation) have become industry standard in Australia, USA, Canada, large parts of Asia, and parts of Africa. Hence I used MODFLOW and its most commonly used compatible solute transport package MT3DMS in this study. I will also utilise PHT3D which couples MT3DMS with PHREEQC for a more detailed rate calculation capability through direct programming.

3.4 Theory Comparison and Benchmarking

To cap all the theories and approaches mentioned in the previous sections, I will compare the transport of cylindrical nanoparticles against a spherical tracer species and, furthermore, compare the results of CNT transport modelling based on Yao's improved equation (inclusive of the particle shape effect) as well as our suggested improved equation (inclusive of natural heterogeneity of the porous media). So the three cases illustrated here are:

- conservative tracer
- execution of Yao's modifications in order to represent the geometrical shape of cylindrical particles
- implementation of physical heterogeneity of the porous media as well as particle shape.

Previous work has revealed that considering the shape and the limited adsorption site availability do, in fact, improve the predictions (Yao, Habibian & O'Melia 1971; Johnson & Elimelech 1995; Szecsody et al. 1998; Tufenkji & Elimelech 2004; Liu et al. 2009; Cullen et al. 2010). It has also been highlighted time and time again that inclusion of heterogeneity has delivered improvement to the results of the transport model (Bales et al. 1991; Bhattacharjee, Ryan & Elimelech 2002; Elimelech & Ryan 2002; Loveland et al. 2003; Tufenkji, Redman & Elimelech 2003).

An injection well was defined in a 2D model with random isotropic heterogeneity (Figure 3-2) and a range in hydraulic conductivity from 0.01 to 30 m/d, consisting of 40 columns (total length of 200 meters), 1 row, and 20 layers (total depth of 100 meters). This well injects a suspension of 1 mg/l (of CNT) under a 0.1 m³/d flux into the system and its screen is located at layer 8.

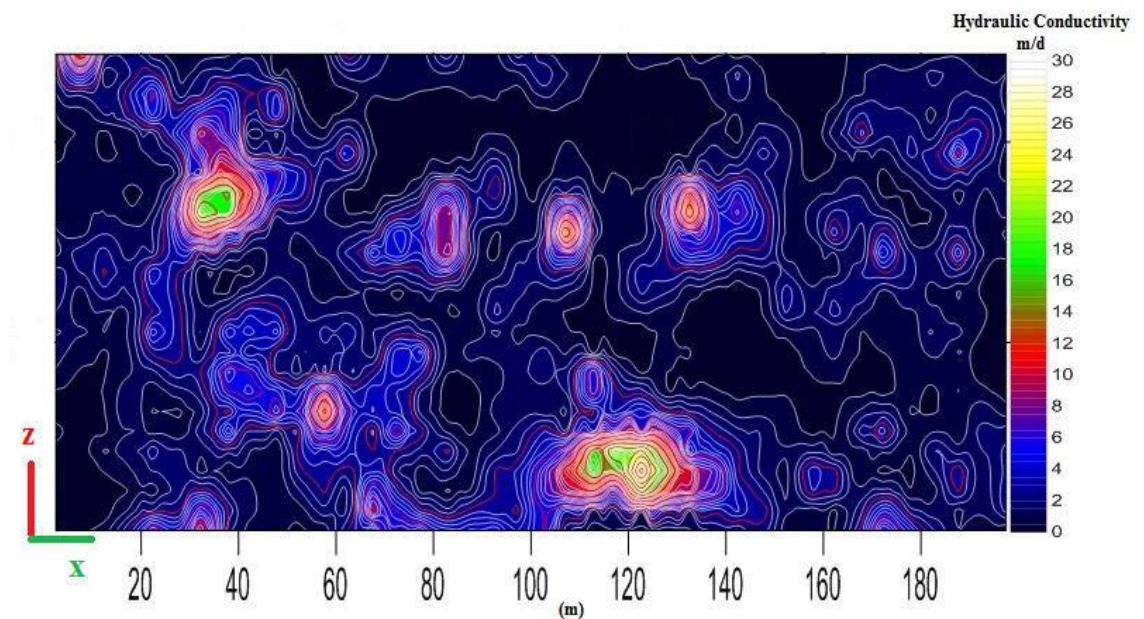


Figure 3-2 Random heterogeneity field of hydraulic conductivity in the 2D model

Firstly, let us have a look at the movement of a non-reactive tracer. This will show the movement pattern and extent where no reaction occurs between the plume and the porous media. What is expected to be observed is that preserved concentrations will move based on

advection and dispersion with no retardation. Movement pattern and extent will be controlled by flow vectors (determining advective movement) and molecular dispersivity assigned to the tracer. Concentration is expected to remain high and the centre of the mass will be moving under advective forces with delay (density dependent).

The second case will model the movement of a cylindrical nanoparticle dispersion (such as CNTs) where retardation rate is calculated based on Yao's equation (as explained in Chapter 2) while neither adsorption site limitation, nor the role of natural heterogeneity in retardation rate is considered. This scenario was designed to illustrate the importance of considering particle shape based on how significantly it changes the movement pattern and adsorption rate.

In the third scenario, retardation (adsorption) rate is calculated considering adsorption site limitation as well as porous media heterogeneity. Based on Sun et al. (2001), representing natural heterogeneity significantly improves the agreement between observed and modelled results. Other researchers have also confirmed this fact for various types of natural heterogeneity (Bales et al. 1991; Bhattacharjee, Ryan & Elimelech 2002; Elimelech & Ryan 2002; Loveland et al. 2003; Tufenkji, Redman & Elimelech 2003). While other work focused on geochemical, particle, surface charge, and other types of heterogeneity, our work aims at representing physical heterogeneity under the same assumption.

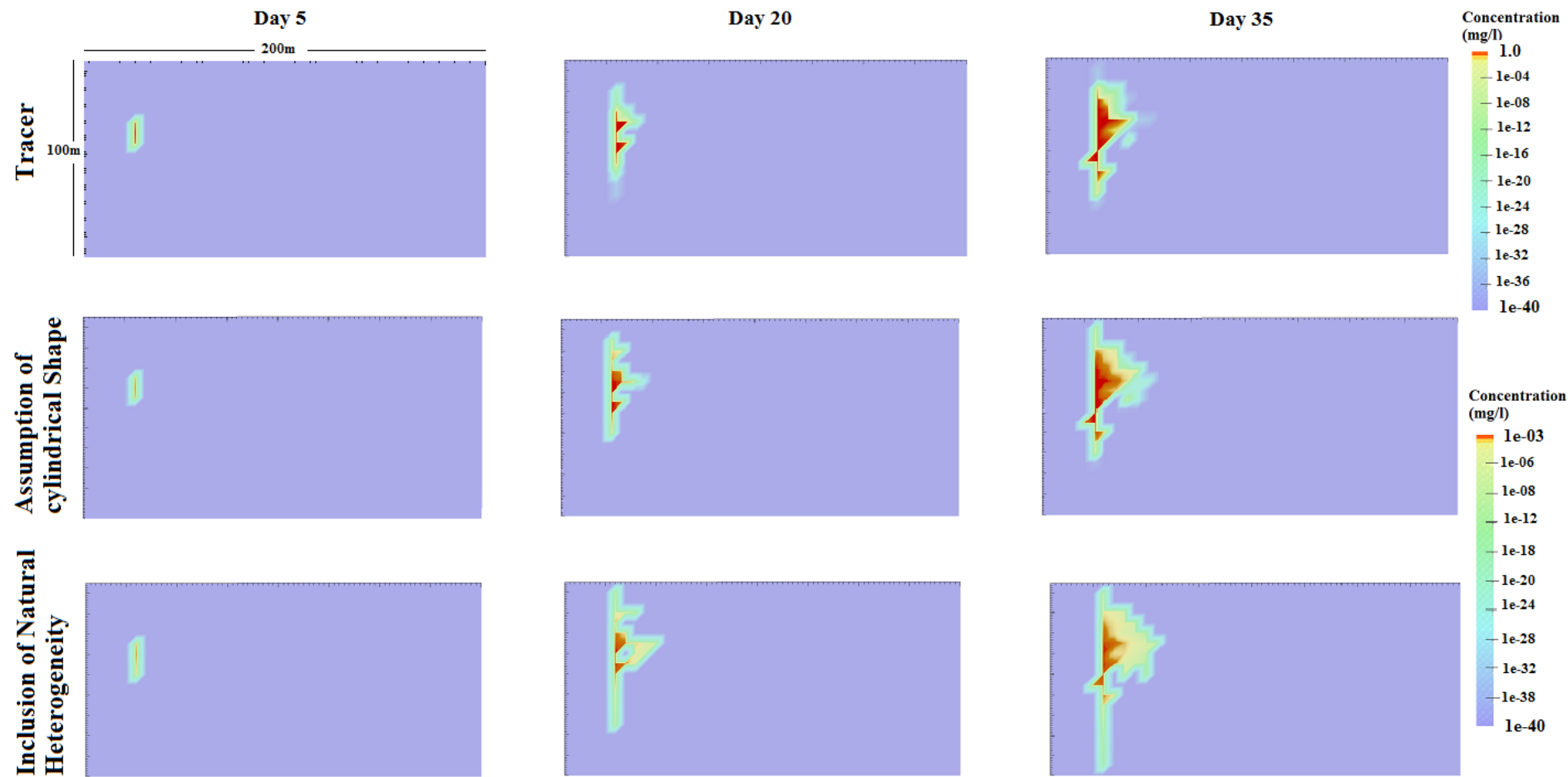
Let us observe the following real-time series of visualisations for three cases (Figure 3-3). Tracer movement is affected by the natural heterogeneity of the system. This is observed through the pattern of movement where the mass of the plume spreads and moves unevenly under advective forces. With transport of particles (as well as bacteria, viruses, and solutes) downward movement is just as significant as forward movement, therefore, it is important to show the movement from a cross section in x direction rather than just the plan view. In this case, the movement of the non-reactive tracer is a bench mark which shows how a plume would move in this heterogeneous environment if no retardation happened in the system. Also

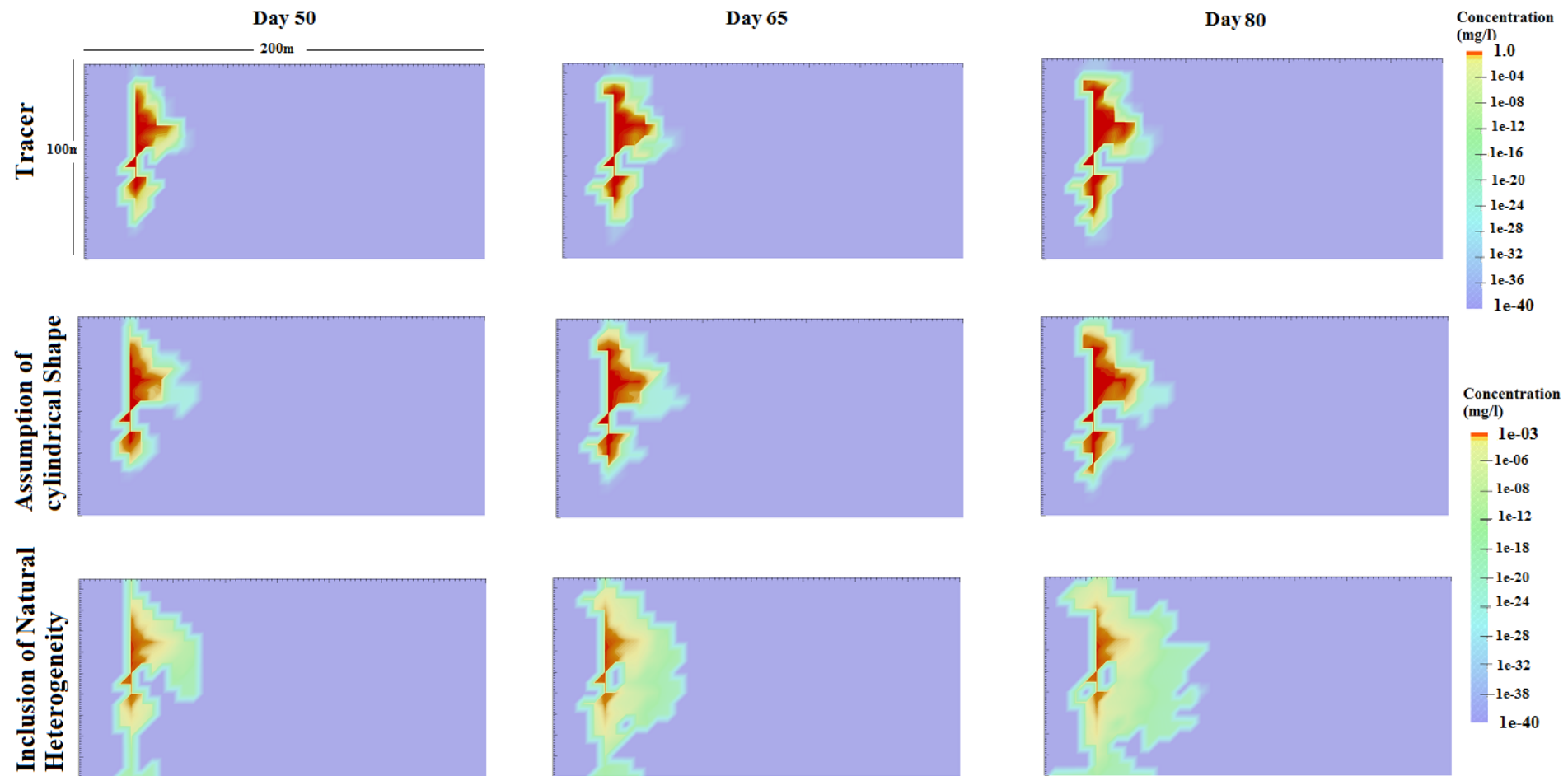
note the scale legend for the first case has a maximum value three orders of magnitude bigger than the scale legend for the second and third cases.

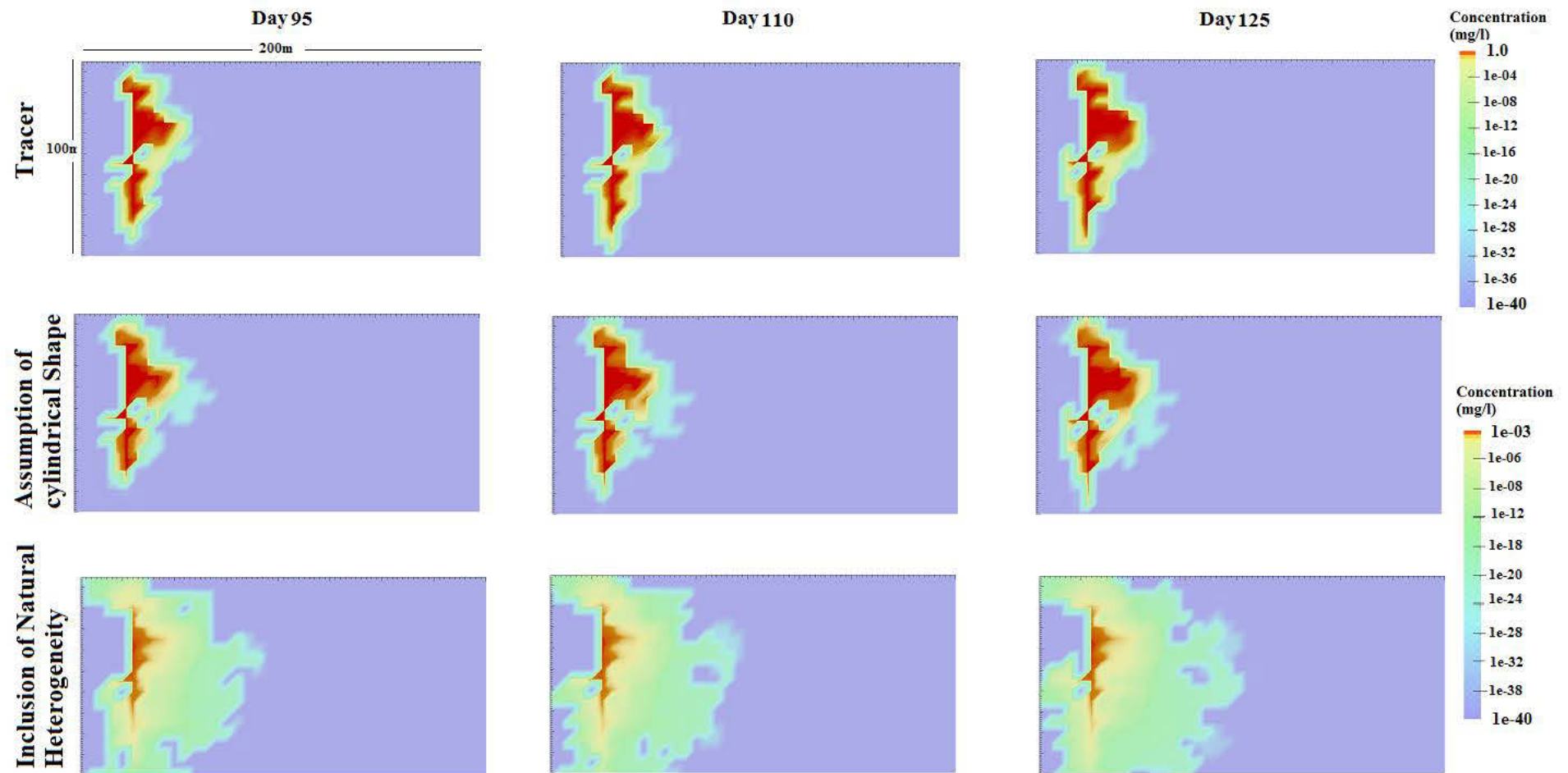
When calculating retardation rate based on Yao's equation, in the second case, the pattern of particle movement remains more or less similar to that of the tracer specie. However, simulated concentrations are 2-3 orders of magnitude smaller than those of the tracer simulation. Retardation of the particles as they pass thorough the porous media results in smaller concentration of particles moving forward and laterally in the system over time. However, since I am yet to define the heterogeneity of the porous media into retardation rate calculation, I'm only allowing advection to be affected by it and not other mechanisms, hence observing the same pattern as tracer simulation is expected. Though it is worth pointing out that there is more smearing at the front of the moving plume in the second case which once again confirms the previous work done by others claiming the ease of movement for cylindrical nanoparticles compared with spherical particles through a porous media such as cell membrane and human blood veins (Bianco, Kostarelos & Prato 2005; Hilder & Hill 2008; Srinivasan 2008).

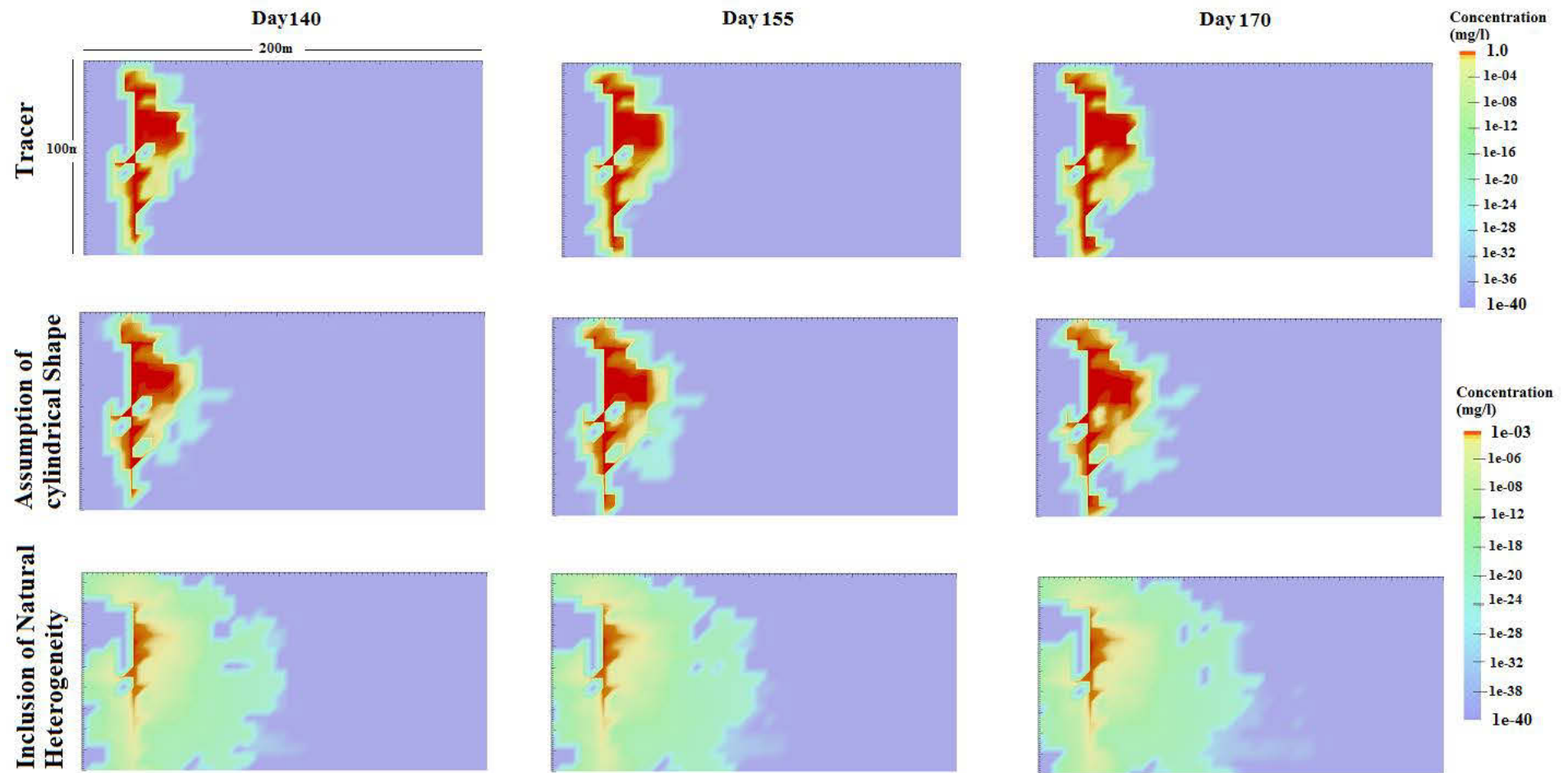
The third case images clearly point to a much larger spreading with much smaller concentrations. Note that in this scenario the retardation is being calculated based on an equation which takes natural heterogeneity into account while accounting for adsorption instead of relying on a median grain size. I showed in Chapter 2 that an average grain size is not representative of a porous medium's heterogeneity and hence the equation was modified to consider this phenomenon. The result is a much larger area of exposure over a comparative period of time to that of the other approaches. I believe this is an important and alarming finding when it comes to exposure assessment studies for transport of cylindrical nano particles. It is, however, somewhat comforting to observe rapid retardation of the particles as sorption sites become available leading to concentrations 2-5 orders of magnitude smaller than the rate calculated based on Yao's equation. Saturation of adsorption sites results in spreading

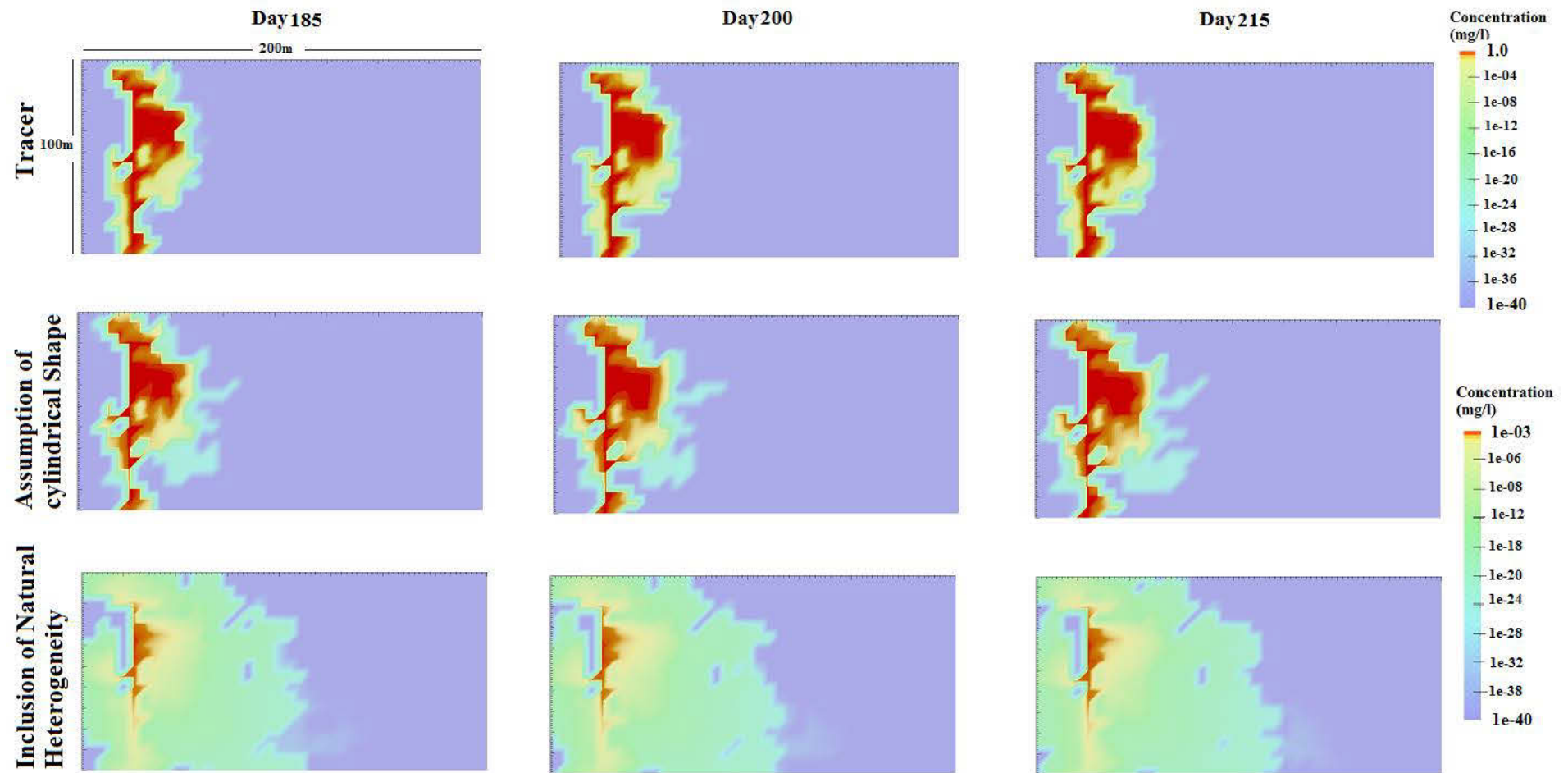
of the particles which highlights a significant difference between Case 2 and 3. This is because (as mentioned before) Case 2 assumed unlimited sorption sites for the particles to retard on.

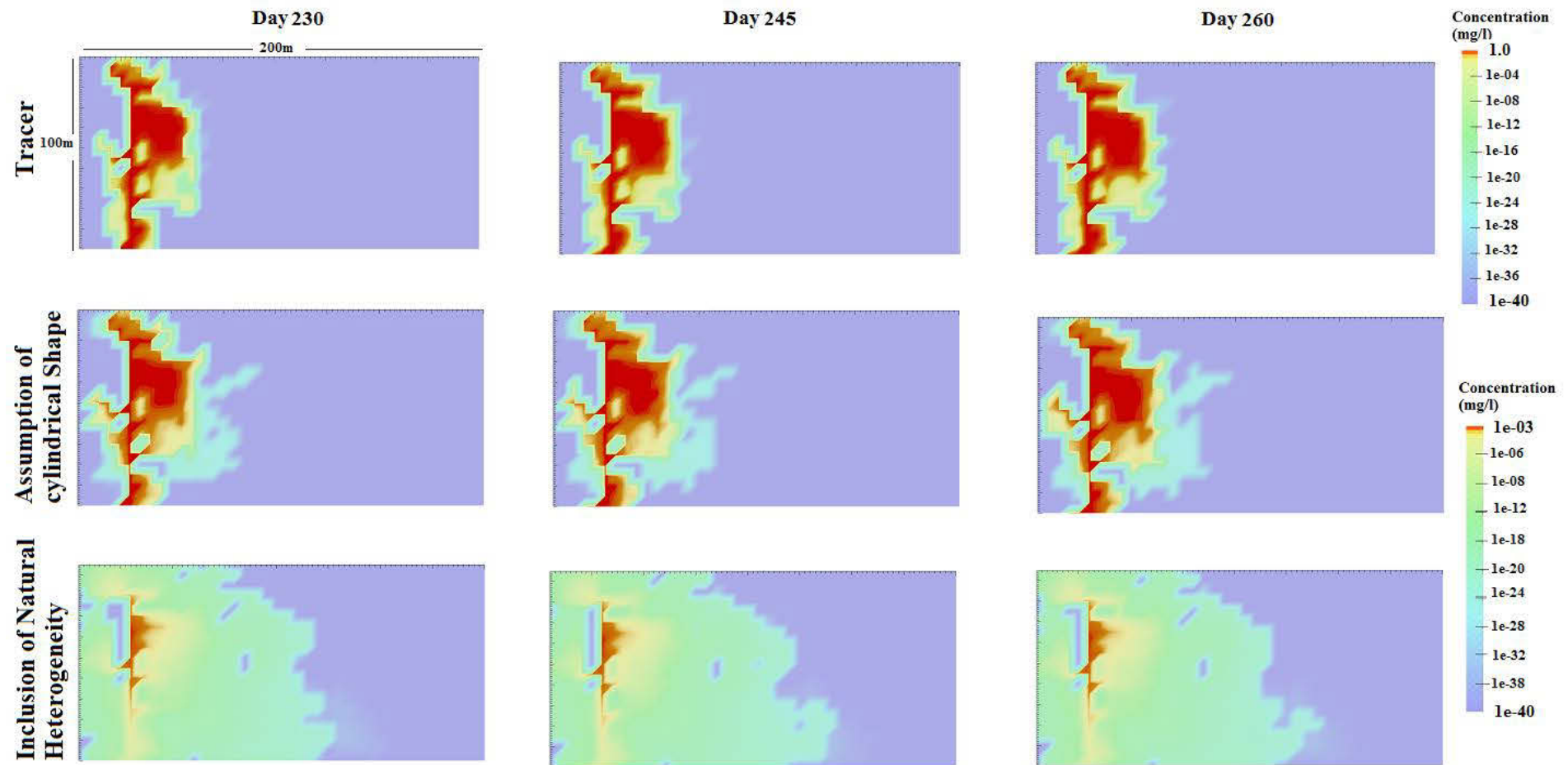


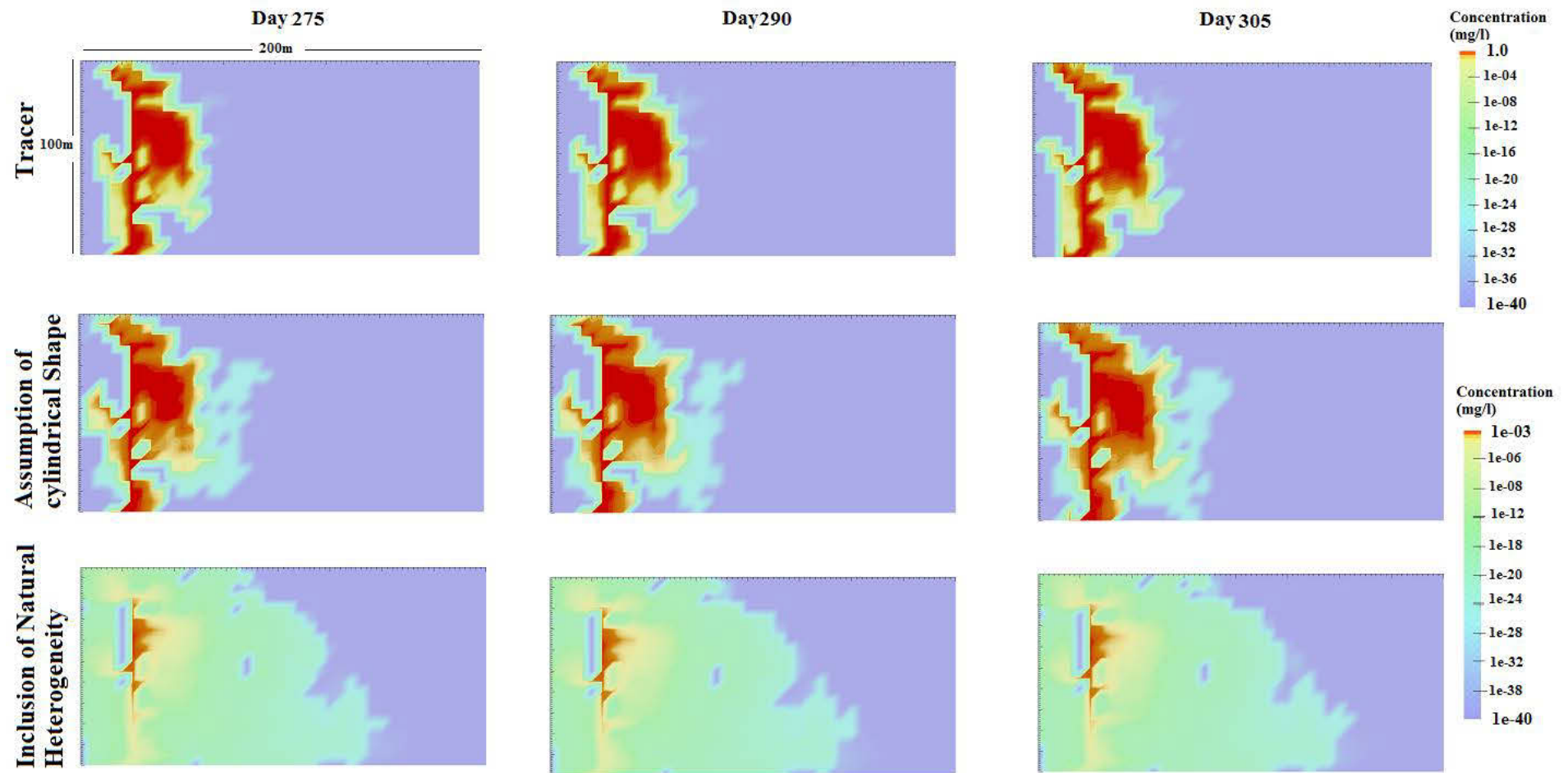


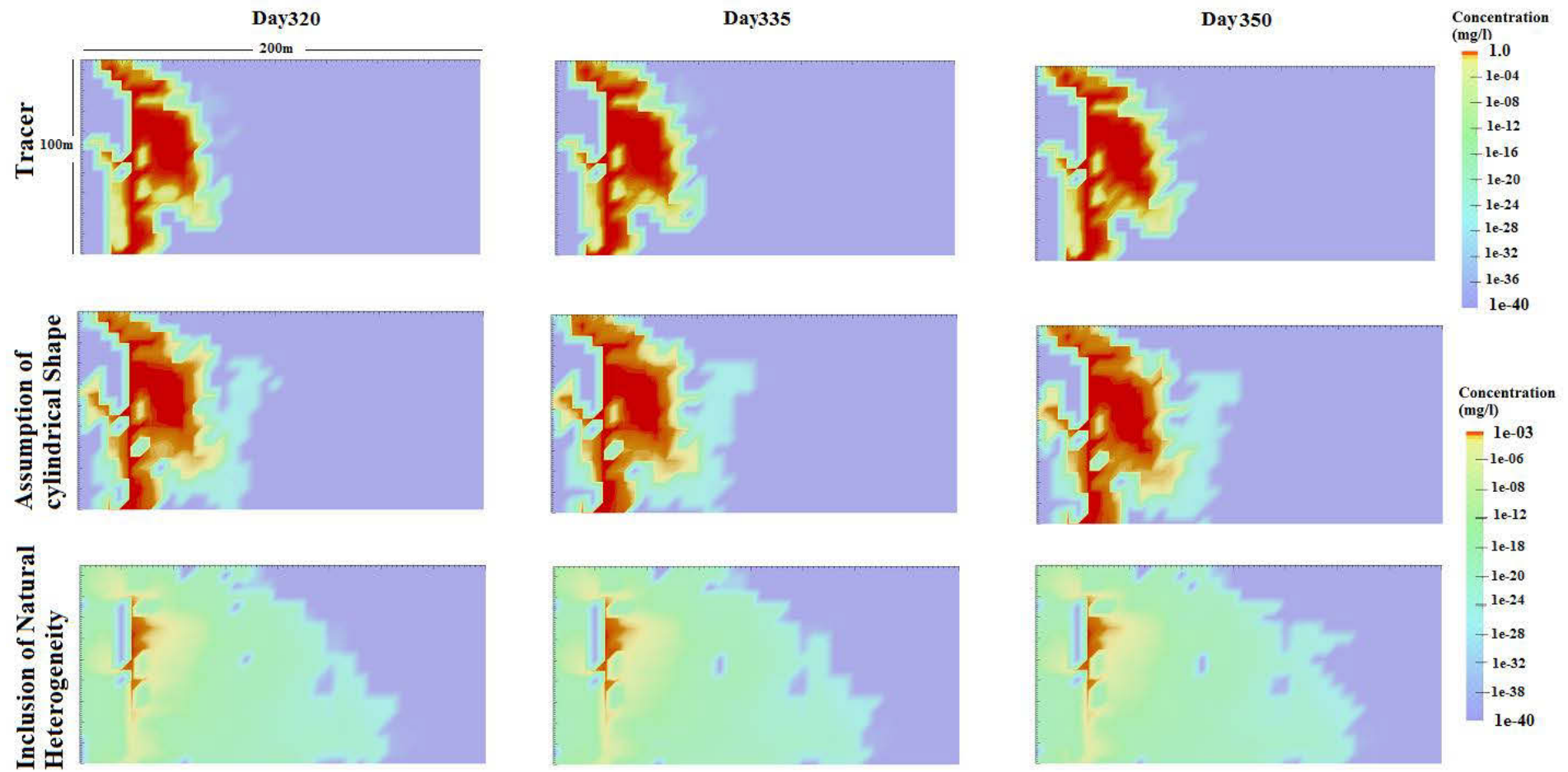












Day 365 - Final Day

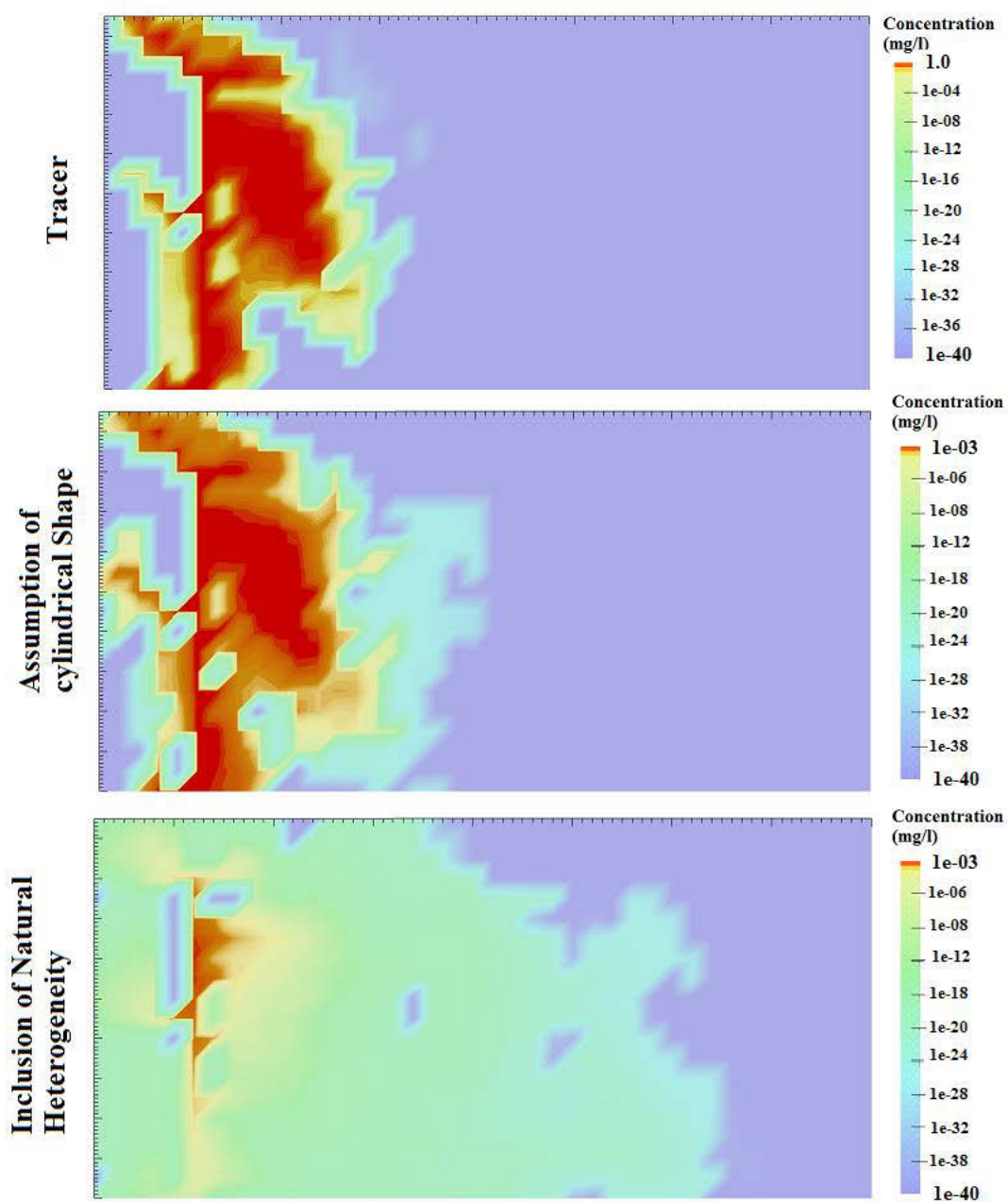


Figure 3-3 Scenario comparison results for Tracer, Particle shape inclusion, and Heterogeneity inclusion

Retardation rate for CNT (applicable to any other cylindrical nanoparticle) was coded into the database file for PHT3D which couples PHREEQC with MT3DMS. This database can be viewed in full in Appendix A- Original PHT3D Rates Database.

Please note that this is a new contribution to the PHT3D database and therefore, is not yet available from the official website of PHT3D. However, it is envisaged that these rates may become available in 2014-2015 (upon approval). Table 3-1 contains this rate calculation.

Table 3-1 Cylindrical nanoparticle retardation rate calculation code

<pre>##### Carbnano_m ##### -start 1 PR = parm(1) 2 DR = parm(2) 3 DC = parm(3) 4 DH = parm(4) #----- # TIME UNIT in MT3D = DAYS - TRANSLATE INTO SECONDS #----- 5 qx = parm(5) /86400 6 qy = parm(6) /86400 7 qz = parm(7) /86400 8 lambda = parm(8) 9 HC = parm(9)</pre>	
<pre># Get fluxes, cell dimensions and porosity from mt3d #----- 11 vx = qx / (DH * DR) / PR 12 vy = qy / (DH * DC) / PR 13 vz = qz / (DC * DR) / PR 14 v_abs = sqrt(vx*vx+vy*vy+vz*vz) #----- 19 I = 397*1e-08 20 AL = 2*1e-6 # 200 nanometres (length of CNT) 21 Ap = 2*1e-08 # 20 nanometres (radius of CNT 10nm) 22 Ac = 397*1e-06 #(median of grain size distribution) 24 AR = Ap/AL #Particle's aspect ratio 25 AAs = ((sqrt(HC/1300))+I+AC)/0.025 #Alyamani/Sen equation 26 mTmp = mol("Tmp")*1000 27 T = 273.15+mTmp # T = absolute temp in Kelvin 28 omega = 9.85*10^15 * T^(-7.7) # omega= dynamic viscosity 29 k = 1.2806*10^(-23) # Boltzmann's Constant JK^(-1) 30 Pi = 3.14159 # Pi number #31 Print "T, Omega, AAS=", T, omega, AAS</pre>	


```

# Calculating the Gravity number
# grav =accln due to gravity m/s^2
52     grav  = 9.81
53     paden = 1050          # kg/m3 particle density
54     fluden = 1000         # kg/m3 fluid density
55     exp7  = 0.146*(paden-fluden)*grav*((AP*AP*AL)^(2/3))

```

```

# Calculating collector efficiency
#-----
# Calculating the diffusion number
39     exp1  = 1+(1-((AR)^(2)))^(0.5)
40     exp2  = (k*T*LOG(exp1))^(2/3)
41     exp3  = ((3/2)*AP*AP*AL)^(1/3)
42     exp4  = 3* Pi*omega*AC*v_abs*exp3
43     exp5  = (1-(AR^(2)))^(0.5)
44     exp6  = (exp4*exp5*(AR^(-2/3)))^(2/3)

```

```

# straining efficiency
71 nstr  = 2.7*(Ap/Ac(OR AAS))^(3/2)  #ok
72 alpha_str = 0.01 #straining correction factor #ok

80 k_str   = (sp_area*v_abs*PR/4)*(nstr*alpha_str)
82 k_stick = (sp_area*v_abs*PR/4)*(n0*alpha_tot)

```

```

#Calculating Efficiency Factor
60     n01 = exp2*exp6
61     n02 = ((AR)^(2/3))*(exp7/(omega*v_abs*exp5))*log(exp1)
62     n03 = 0.5*((Ap/AC (OR AAS))^(2))*(3-(AP/(AP+AC (OR AAS))))
63     n0  = n01 + n02 + n03
#Overall sticking effciience
65     alpha_f = 1.0  # sticking eff at favorable sites = 1
66     alpha_u = 0.0007 # sticking eff at unfavorable sites
68     alpha_tot = lambda*alpha_f+(1-lambda)*alpha_u

```

```

# straining rate (= irreversible)
84 str_rate = k_str * TOT("Carbnano_m")
# decay rate (= attachment to sediments)
85 stick_rate = k_stick * TOT("Carbnano_m")
# decay rate in aqueous phase: default k_dec = ~ 0.2 per day
90 dec_rate = k_dec * TOT("Carbnano_m")

# save sticking (attachment) rate for use
# in rate expression of immobile Carbnano
91 put(stick_rate,20)
# retrieve detachment rate from rate
# expression of immobile Carbnano
92 det_rate = get(21)
# negative sign is introduced to induce removal of mobile Carbnano
# straining and decay decrease conc, detachment increases
# concentrations of mobile Carbnano
94 rate = - stick_rate - dec_rate - str_rate + det_rate
95 moles = rate * TIME
100 if (moles > m) then moles = m
200 SAVE moles
-end

```

```

#####
# Carbnano attached
#####
Carbnano_im
-start
1 m Carbnano_im = TOT("Carbnano_im")
# 2 if (m Carbnano_im <= 1e-14) then goto 200
7 k_dec = parm(1)/86400
8 k_det = parm(2)/86400
20 dec_rate = m Carbnano_im * k_dec
25 det_rate = m Carbnano_im * k_det
# save detachment rate so it can be used in the
# rate expression for the mobile Carbnano
28 put(det_rate,21)
# retrieve straining_rate from rate
# expression for mobile Carbnano
30 str_rate = get(20)
# positive str_rate causes immobile Carbnano to increase
# while positive decay rate decreases concentrations
40 rate = stick_rate - dec_rate - det_rate
# 45 print "Carbnano: str_rate - dec_rate - det_rate", str_rate, -dec_rate, -det_rate
95 moles = rate * TIME
100 if (moles > m) then moles = m
200 SAVE moles
-end

```

Note that two versions of this rate calculation were used for models:

- the first version uses AC as collector diameter (user-defined value in the code) and this value is the median value of grain size (d_{50}).
- the second version replaces AC by AAS which implements the modifications suggested by us to include natural heterogeneity of the natural media.

Straining is negligible due to the size ratio of nanoparticles to collector grains, however it has been coded in for those who wish to use the first version of this code for laboratory conditions where grains are small and the soil pack is homogeneous. Detachment is also included in the code despite the reported “no detachment” situation (Tufenkji 2007; Liu et al. 2009). In the break-through-curves, after the passing of the pulse, no release of CNTs were observed by Liu et al. (2009). This indicates either a no-detachment system, or an equilibrium between detachment and attachment. Either way, calculation of detachment can be ignored for CNTs, but might be relevant to and needed for other nanorods or nanotubes.

A decay rate is also included to increase the versatility of the code and broaden its applications even though CNTs do not decay. Decay rate would be relevant when modelling the transport of tubular bacteria or viruses to deal with the inactivation rate of the species in hand.

3.5 A Real-World 3D Example

A real-world model is chosen to show-case the new and modified equations in a three dimensional real setting. In this section, I will go through the model set up, site specification and data availability before the design of the grid, parameterization, and boundary set up is explained.

Please note that while this model is set up and calibrated based on field measured data, the plume of CNT suspension is a hypothetical scenario. The theory of it is, however, based on the already laid foundations of previous sections in this chapter as well as Chapter 2. This example can be used as a template framework for exposure assessment studies in a large scale model.

3.5.1 Site description

This site stretches from south of Port Macquarie to the north of Kempsey. It features elevated parts in the West and the northwest corner, sloping down to flat sandy fields towards the coast line (Figure 3-4). The elevation profile ranges from 0 and 232 mAHd (Figure 3-5).



Figure 3-4 Site location

Many rivers and waterways meander around the little hills and create winding valley ways across the site. This site features variable gradient, rivers, coast, and a small lake all together. These condition will provide an opportunity to see particle transport over a much steeper gradient than in the 2D comparative models. It will also show how rivers, wells, wetlands, and hills affect particle movement.



Figure 3-5 Site elevation

3.5.2 Regional Groundwater Regime

There are two main types of aquifers in the modelled area:

- the unconfined alluvial aquifers under the floodplains of the Hastings and Wilson rivers, as well as adjacent to other water ways such as Cooperabung Creek, Smiths Creek, Pipers Creek and the Maria River, and
- the semi confined bedrock aquifers in the Cooperbung Hill area and Maria River State Forest area.

Groundwater within the bedrock aquifers generally flows from areas of high elevation (the recharge zones), to areas of low elevation (the discharge zones). Along the site, the higher elevation areas of Cooperabung Hill, Cairncross State Forest and Maria River State Forest are likely areas of recharge, and groundwater area divides, for the bedrock aquifers with discharge trending towards the Hastings and Wilson Rivers. Movement of groundwater through the

alluvium is from recharge zone down gradient towards a stream or river for discharge (see Figure 3-6).

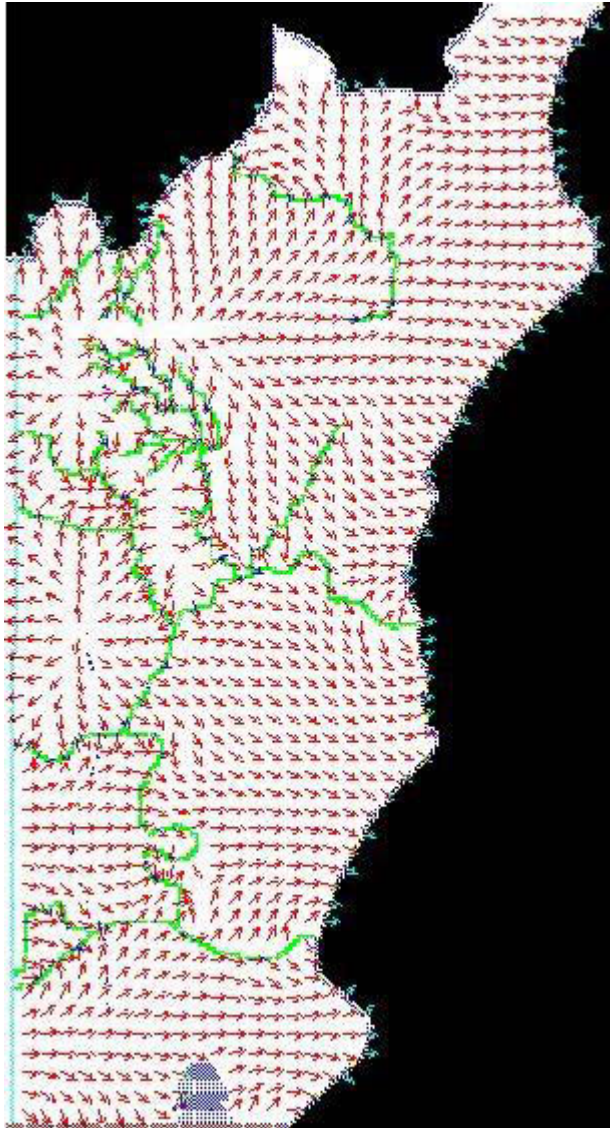


Figure 3-6 these velocity vectors show the flow pattern across the model domain

Recharge to the alluvium occurs through the land surface from rainfall and lateral movement from fractured rock aquifers.

The direction of the alluvial is generally north-south, and the groundwater flows perpendicular to the major rivers.

3.5.3 Grid Design

This model covers an area of 1,980 km² starting from (bottom left corner) Cowarra Dam [477776 E, 6514281 S] and extending 33 kilometres east and 60 kilometres north. The grid is presented in Figure 3-7.

Based on a simplified conceptual model, a three-layered grid was developed. The third layer is inactive and represents the deep impermeable bedrock, the two top layers are active and represent the alluvial and the fractured elevated aquifers. The grid consists of 300 rows, 165 columns, displaying 148500 cells of 200m by 200m in 3 layers (49,00 cells in each layer). Out of all cells, a total of 80319 cells are active cells while the rest define no-flow boundaries as inactive cells.

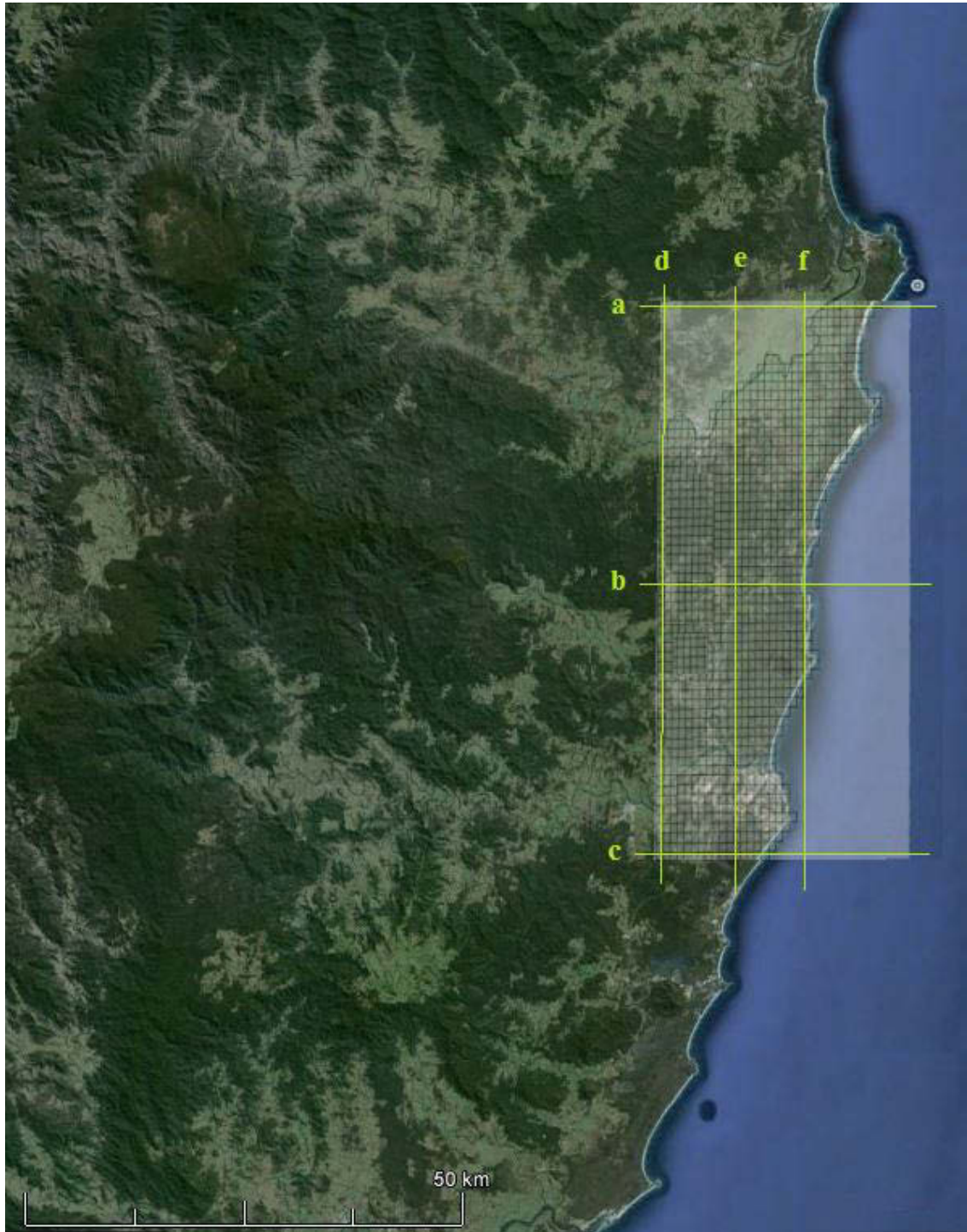


Figure 3-7 Grid design

For a general grid design illustration a series of cross sections (also shown in Figure 3-7) in both north-south and east-west directions are presented in Figure 3-8 and Figure 3-9. In these

figures, a strong decline in elevation is observed from west to east. Groundwater flow direction obeys this gradient and groundwater eventually discharges into the ocean.

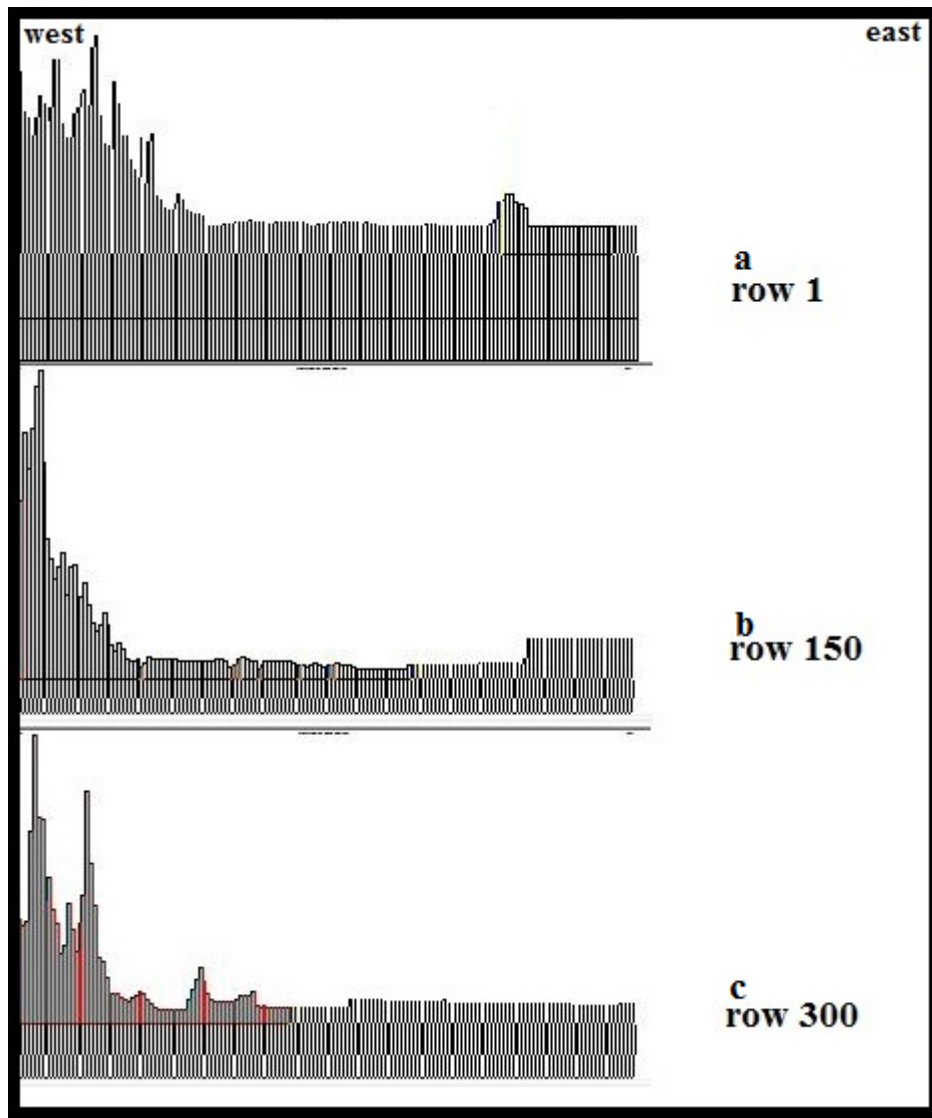


Figure 3-8 Row cross-sections

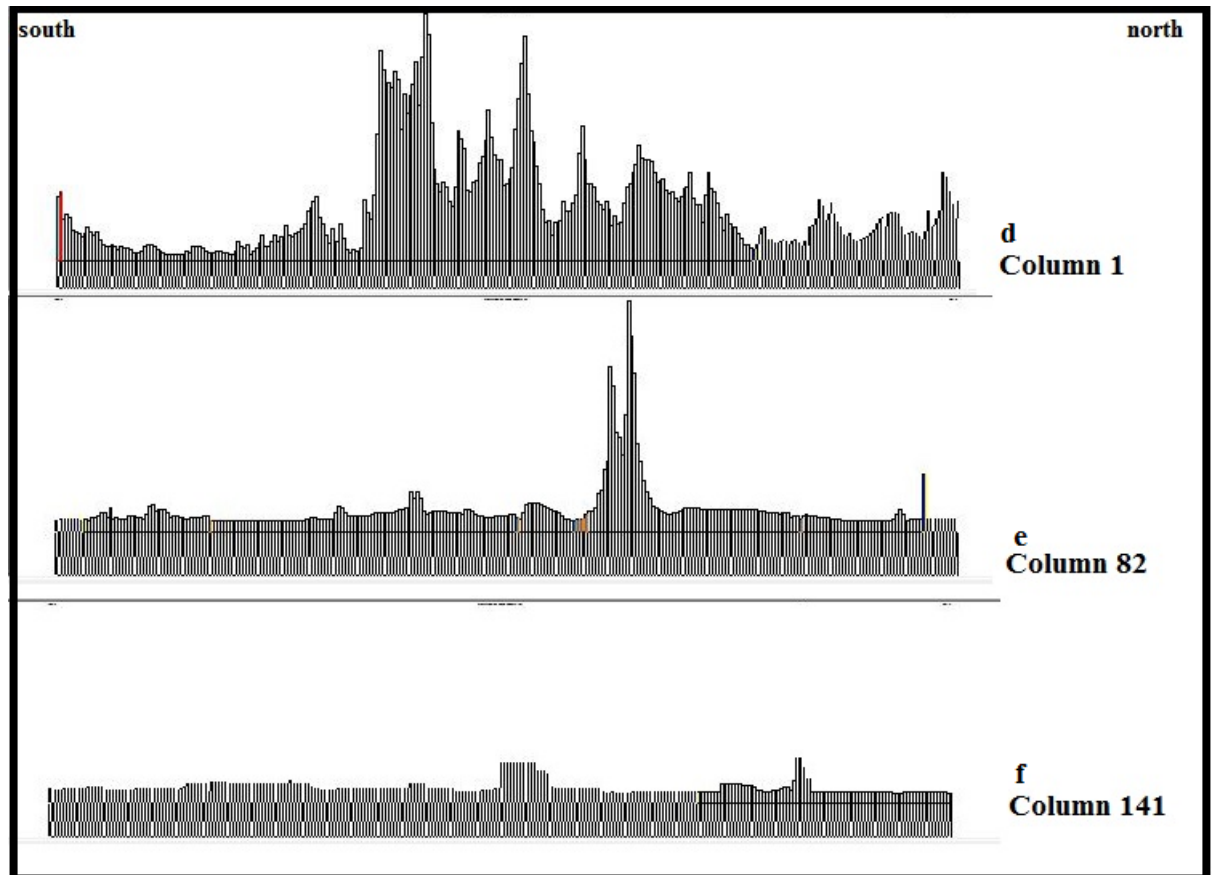


Figure 3-9 Column cross-sections

3.5.4 Boundary Conditions

To simulate the boundaries of the model, the ocean (east), Innes lake (south), and Macleay River (north) were used as natural boundaries beyond which was set to no flow boundary (Figure 3-10).

The coast line (east) is set as a constant head boundary with a value of 0 m AHD to closely simulate the gradient of groundwater flow towards the ocean. Lake Innes (south) is also set as a constant head boundary (2.8 mAHD) and helps with maintaining the integrity of the model's southern boundary.

“River boundary” represents rivers and creeks in the model area. This type of boundary is used for major rivers as well as smaller creeks on the skirts of the elevated areas where the groundwater table is constantly fed from the higher elevation recharge areas.

General Head boundary is used along the western and southern borders of the model in the absence of any natural boundary.

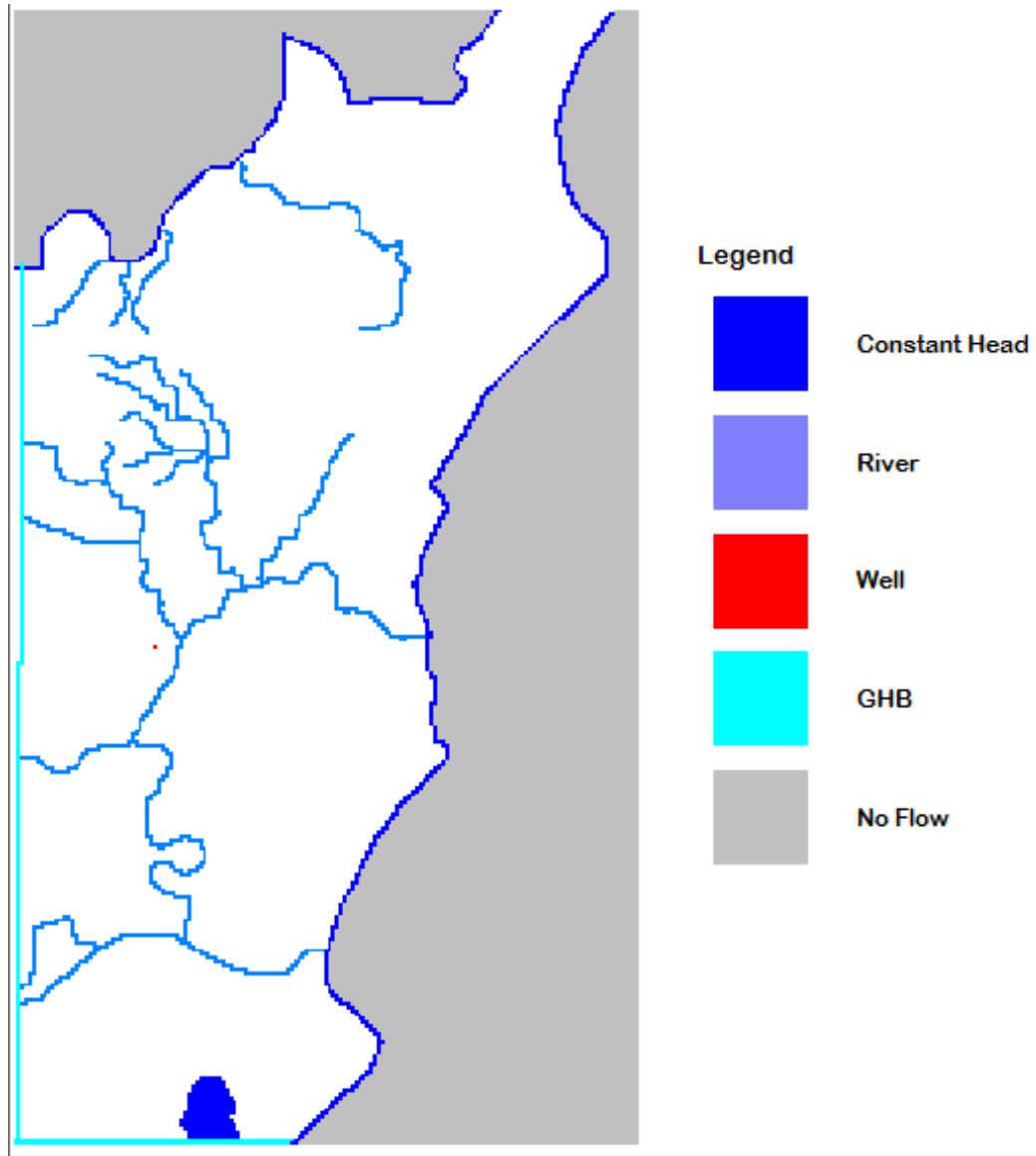


Figure 3-10 Boundary conditions

3.5.5 Parameterisation

To parameterize this model, a combination of field measured data, logger data, and literature data were used.

3.5.5.1 Hydraulic Conductivity

A series of recovery curves (recorded by loggers) of several piezometers were used to estimate the permeability of the aquifer.

In cases where piezometers are installed to monitor head and for quality sampling, but do not fully penetrate the aquifer, the Hvorslev method is considered a suitable method to approximate hydraulic conductivity (K). In addition, the type of recovery information available from data loggers in some bores is also appropriate to the Hvorslev method. .

Hvorslev equation calculates K through:

$$K = \frac{r^2 \ln(L_e / R)}{2L_e t_{37}} \quad \text{Eq. 3-12}$$

Where:

K is hydraulic conductivity (L/T)

r is the radius of the well casing (L)

R is the radius of the well screen (L)

L_e is the length of the well screen (L)

t_{37} is the time it takes for the water level to rise or fall to 37% of the initial change (T)

Where the porous media is low permeability, and the well screen is gravel-packed around to fill the gap between the wall of the excavation and the screen, $R=r$ and L_e is the length of the gravel pack (Fetter 2001).

The recovery curve (rising head) for A-BH-1011 after bailing for a sampling event is provided on Figure 3-11. The analysis method is as follows:

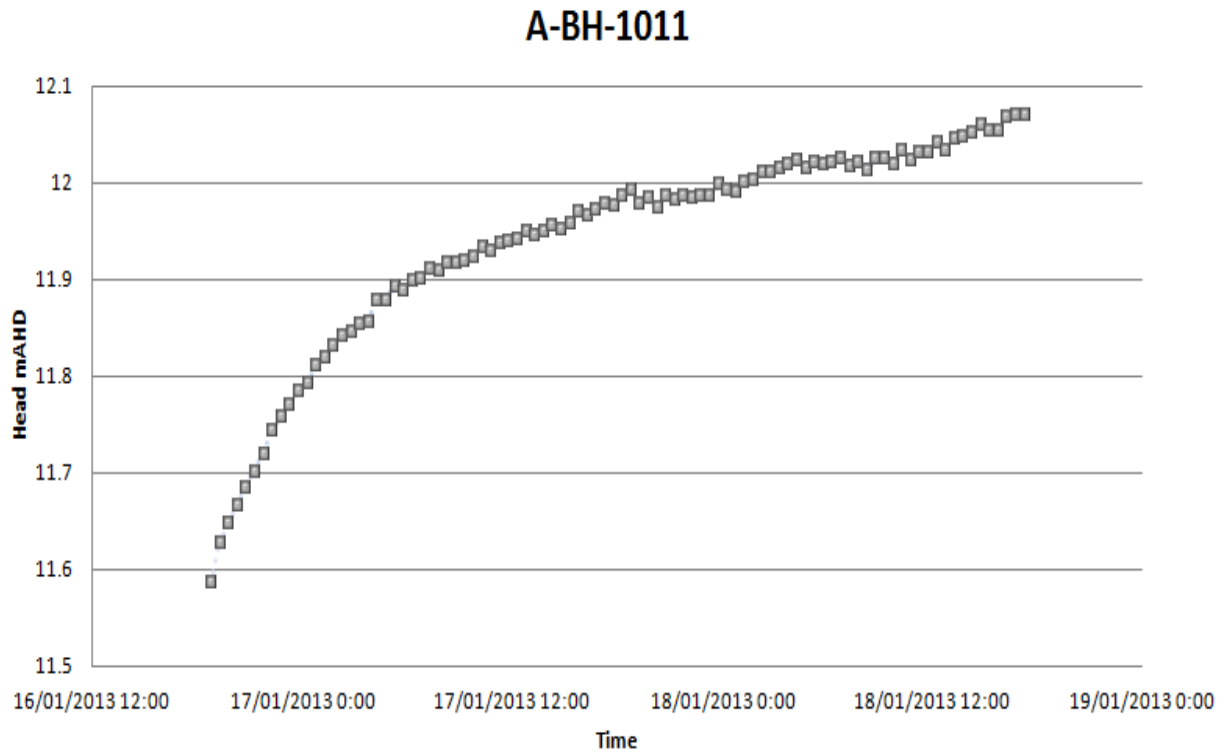


Figure 3-11 recovery curve or rising head curve for A-BH-1011

Based on the logger data, total head change after sampling is 0.48 m; 37% of which is approximately 0.18. Where the lowest head is recorded at 11.58 m AHD, t_{37} is the time at which the water head rises to $11.58 + 0.18$ or 11.76 m AHD.

Based on the recovery curve (Figure 3-11), the water head rises to 11.76 m after 4.5 hours (0.1875 day). With a screen radius of 62.5 mm (pipe diameter is 125 mm), and a gravel pack length of 8350 mm, hydraulic conductivity is approximated at:

$$K = \frac{(62.5)^2 \ln(8350/62.5)}{2 \times 8350 \times 0.1875} \Rightarrow K = 6.1 \text{ mm/day} \Rightarrow K = 0.006 \text{ m/day}$$

Other suitable logger data were analysed based on this method and provided a range of values between 0.002 and 8.01 m/d (refer to Table 3-2). An average value of hydraulic conductivity was assigned to various areas of the model and calibration was done within the calculated range of values.

Table 3-2 Hydraulic conductivity calculations

Bore name	Hydraulic conductivity(m/d)
A-LCD-1002	0.035
A-BH-1011	0.006
A-BH-1018	6.15
A-BH-1044	0.002
B-BH-1017	0.27
B-BH-1031	2.87
B-BH-1056	3.64
BSR-BH-1006	3.75
B-LCD-1012	4.16
C-BH-1030	0.0028
C-BH-1037	0.056
CSR-BH-1025	0.0075
D-BH-1035	8.01
D-BH-1060	6.43

Some bores showed rapid recovery after bailing. Most of these bores are located in the upper portion of fractured elevated areas where higher permeability is expected.

Permeability was, therefore directly linked to elevation profile and three zones were digitized to represent the various permeability profiles. Note the values and zones presented in Table 3-3 are post-calibration values.

Table 3-3 Permeability zoning

Zone No.	Hydraulic conductivity(m/d)	Location
1	3.16	Most of layer 1 and all of layer 2
2	6	Fractured high grounds in layer 1
3	0.02	High ground skirts featuring many small creeks and waterways in layer 1

3.5.5.2 Recharge and Evapotranspiration

Rainfall data from four weather stations near the domain were used to assess the reasonable range for recharge values. Recharge values were assigned as a net balance of recharge minus evapotranspiration (ET).

Recharge values were determined through calibration within a reasonable range of values. The reasonable range was assessed based on the data available from the stations named in Table 3-4.

Table 3-4 Weather stations in the area

Station name	Station number	Average daily rainfall (mm) (2012-2013)	Average rainfall (m/d) (2012-2013)
Port Macquarie AirPort	60139	11.1	0.0111
Telegraph Point	60031	10.3	0.0103
Kundabung	60018	15.4	0.0154
Kempsey (Wide Street)	59017	9.8	0.0098
Average value		11.7	0.0117

A total of 8 zones (shown in Figure 3-12) were designed to allow for variations based on altitude/latitude, and expected permeability which are key factors in precipitation and recharge respectively. These values were later refined through calibration and post-calibration values are listed in Table 3-5.

Net recharge varies between approximately 17 and 0.001 percent of the rainfall. In wetlands and swamp areas, recharge can be very small or zero. Based on field information, some of these areas consist of very low permeability formations.

Higher recharge values apply to elevated areas where evaporation is less, due to the depth to water table and lower temperatures. In addition, infiltration exceeds that of the lower elevation areas, due to the higher number of fractures observed in these formations.

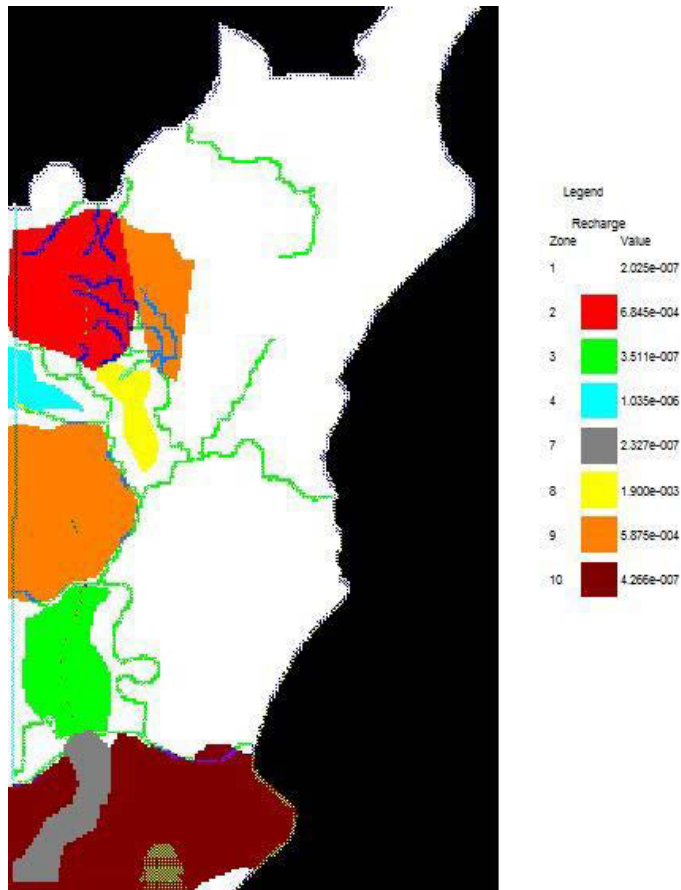


Figure 3-12 Spatial map of recharge/ET zones

Table 3-5 Recharge/ET zones

Zone number	Net recharge (m/d)
1	2.025E-07
2	6.845E-04
3	3.511E-07
4	1.035E-06
5	2.327E-07
6	1.900E-03
7	5.875E-04
8	4.266E-07

3.5.5.3 Temporal Discretisation

This model is set to run for 16 years (5844 days) to simulate the current water table equilibrium (see Appendix B- Simulated Water Table Post-Calibration). While the flow model is a steady state (see Appendix C- Flow Model Raw Output) the transport model is set as a transient model. The setup of the transport model will be discussed later in this chapter.

3.5.6 Model Calibration

The model was calibrated using PEST (Doherty 2014) which is one of the most commonly used model-independent non-linear parameter estimation packages. Pest has the ability to reverse-calculate the parameters in order to achieve the closest set of parameters to a user-defined result. The user also defines the boundaries in which PEST can vary each parameter. This capability keeps the calibration-derived parameters realistic and plausible.

3.5.6.1 Targets

This model was calibrated using 38 targets, all of them groundwater level recordings. While the main calibrated parameter is net recharge, hydraulic conductivity was also minimally altered (within the range of calculated/estimated values from recovery curves) to achieve the best possible agreement between the observed and computed data.

Calibration results display a very close agreement with the observed targets. As illustrated on Figure 3-13, the trend line forms a 45° angle with the axis and the correlation coefficient is 0.99. It is also noticed that higher heads (above 20 mAHD) match their observed values better than lower head observation (under 10 mAHD).

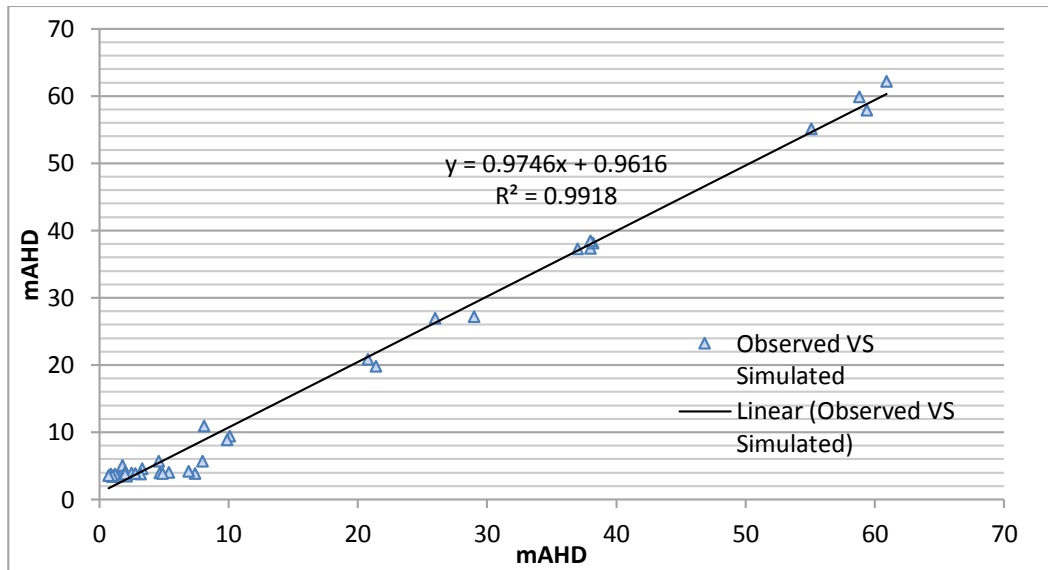


Figure 3-13 Observed VS simulated values

3.5.6.2 Calibration statistics

More information about calibration statistics are presented in Table 3-6. Note that the targets available for calibration have a limited areal extend and hence good calibration results do not necessarily reflect a high level of accuracy over the entire model domain.

Table 3-6 Calibration statistics

Statistical element	Value
Residual mean	0.5 m
Range of observations	60.6 m
Scaled residual standard deviation	0.035
Scaled absolute mean	0.03
Scaled RMS	0.03

These results meet the criterion (Scaled RMS < 10%) in the Australian modelling guidelines (Barnett et al. 2012) with a very good agreement between observed and computed values with the scaled RMS of 3%.

Following PEST calibration, calibrated parameters were updated and the model was run for a period of 16 years to simulate the current hydrogeological regime in the area of interest.

3.5.7 Transport model

In the transport model, a location on the elevated parts of the western side was chosen to be the point source of CNTs. The rationale behind this choice was to contrast the very low gradient of the 2D models in the previous section to simply broaden our understanding of CNT movement under varying conditions. Water elevations (mAHD), highlighting the gradient between the source point and the final destination is illustrated in Figure 3-14.

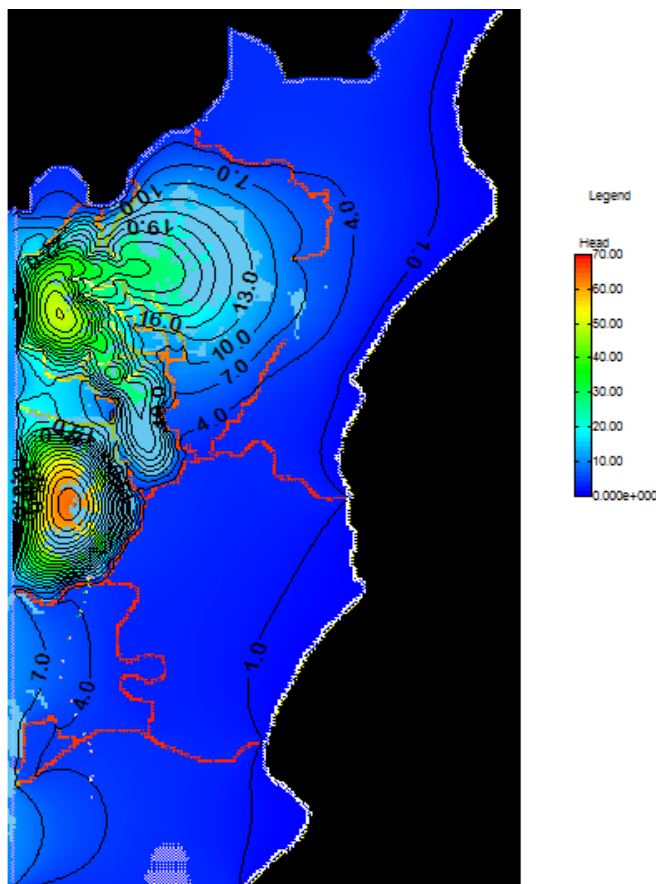


Figure 3-14 Water table contours

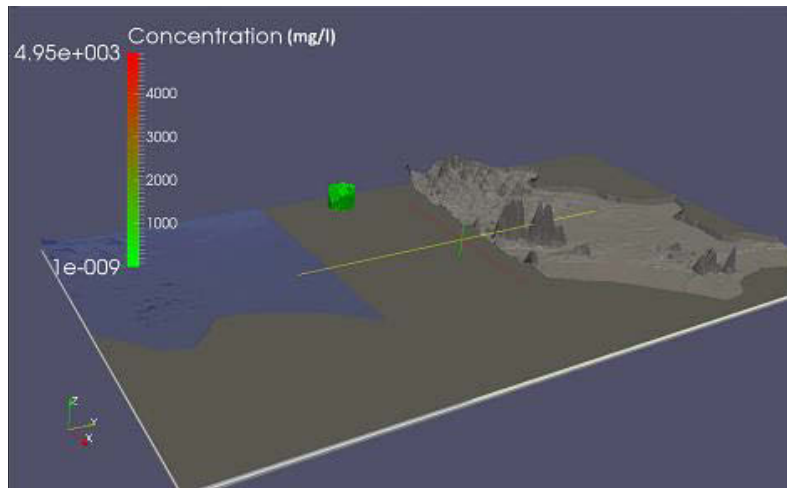
Another significant difference is the concentration of the continuous point source. Here I have defined a zone of recharge for the suspension which continues to recharge a suspension of 5 g/l (5000 mg/l) into the shallow aquifer.

It can also shed light on how natural boundaries such as rivers can help contain or spread the nanoparticles in a natural setting.

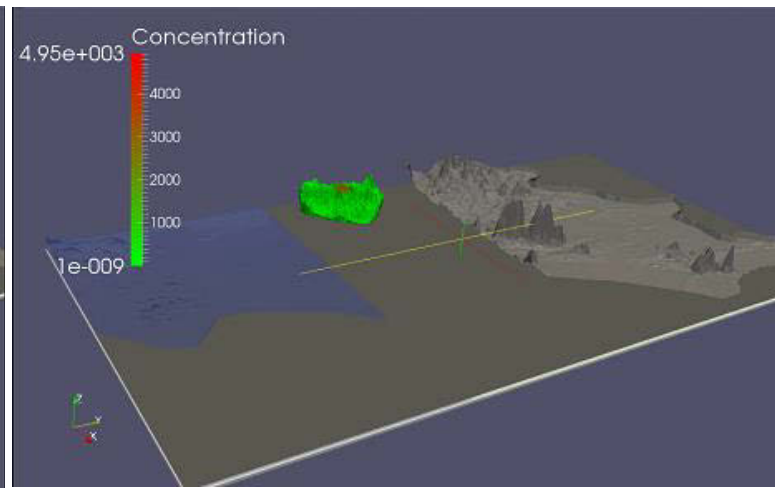
Temporal discretization displays 92 time steps for the transport model and the results were saved for every time step. For the purpose of illustration, results were extracted and contoured every 300 days to show the movement of the plume over time in an animation. An interesting point to notice is varying rate of movement as the gradient changes (ie. faster during the initial steps while the plume moves towards the hill slopes and slower when it reaches the less steep slopes).

Figure 3-15 (a-i) is a series of snap-shots of the animation with equal time intervals of 600 days. The model has been peeled off to expose the plume in its bare essential form for better comprehension of movement rate and plume outline. As a result of the varying transport rate, the final images have to be carefully examined to detect the movement. This can be done by using the x axis in the middle of the model domain as a reference line.

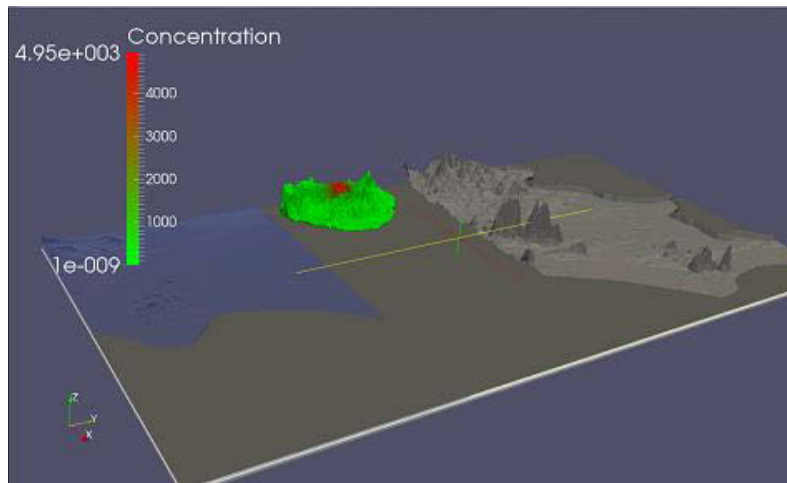
In order to show the smearing effect observed in the 2D comparative models, a separate contour map of the final time step appears at the end to highlight the small concentration movement across from the river(s). Please bear in mind that I have not accounted for the concentration released in the rivers although it is easy to predict that the connected water bodies have exchanged water and particles in it. This would be discussed in the last chapter as a potential suggested field for further research to investigate particle movement from groundwater to surface water bodies.



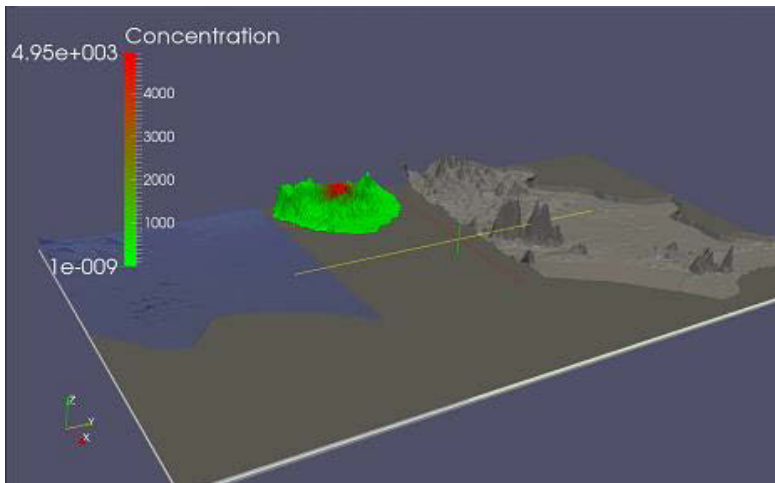
a



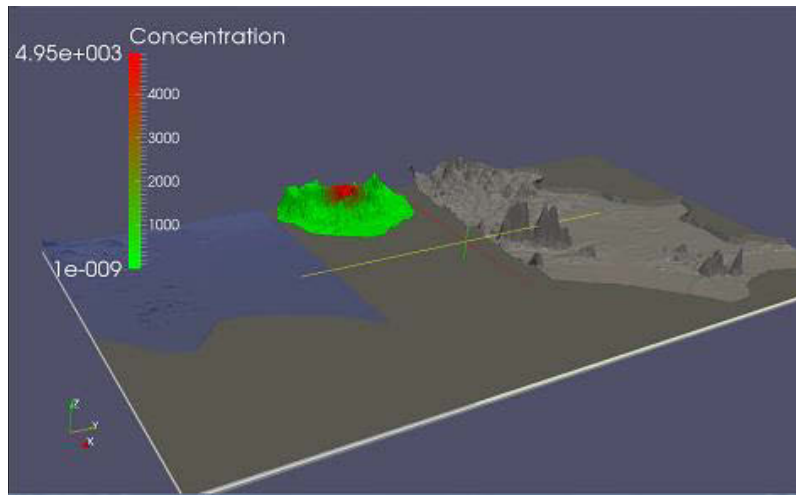
b



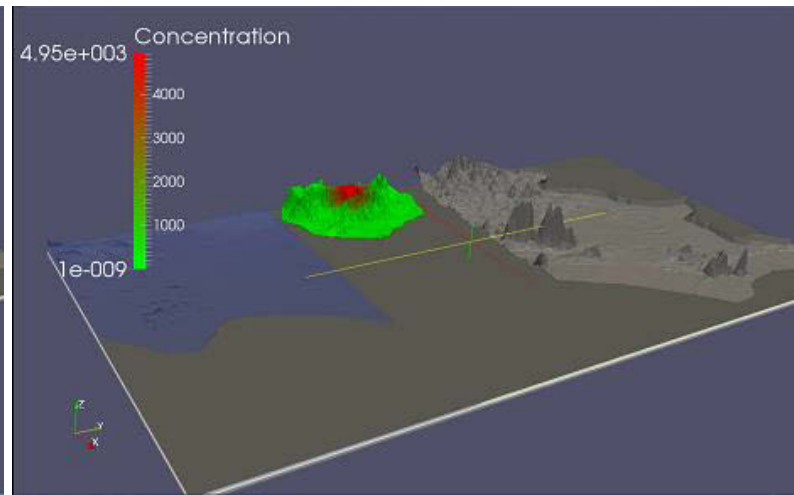
c



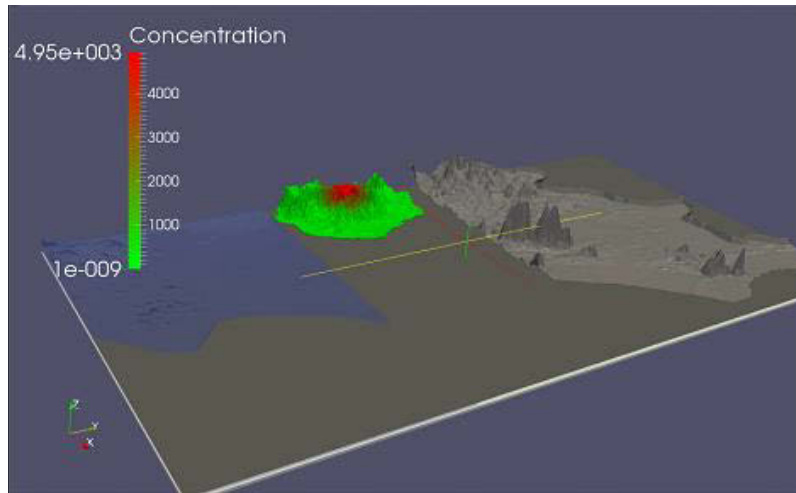
d



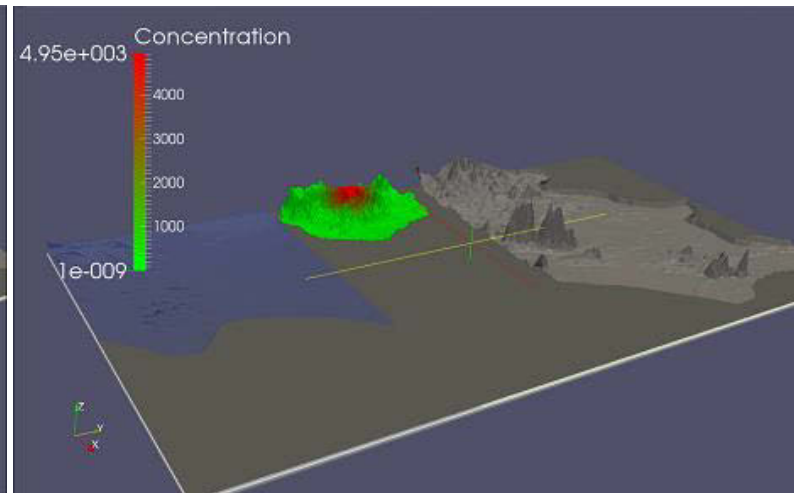
e



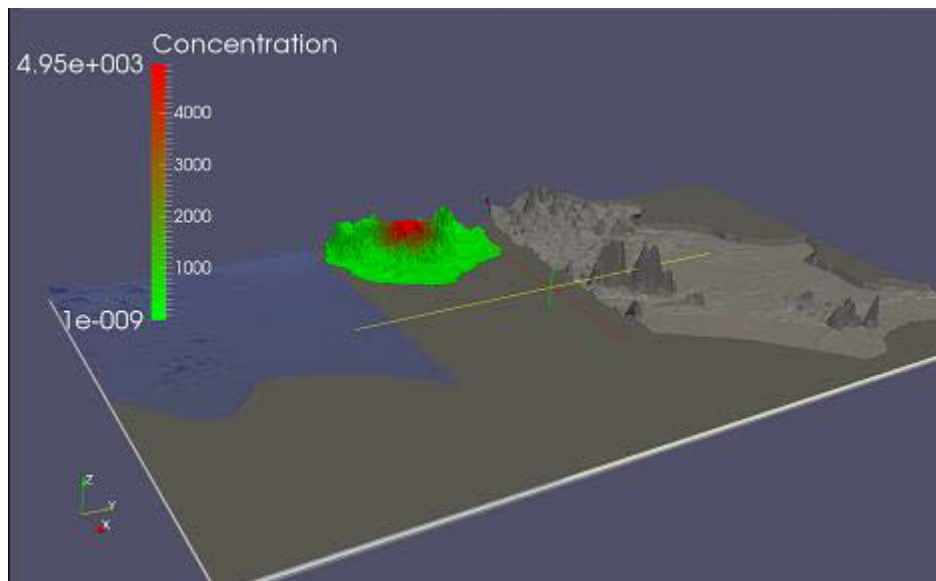
f



g



h



i

Figure 3-15 a-i series of 3D illustration of particle movement

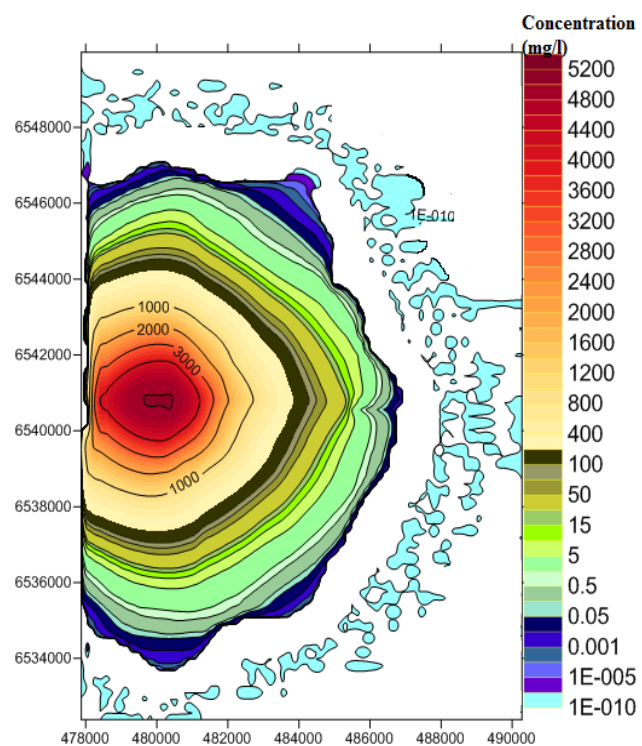


Figure 3-16final time step contour map

4 Uncertainty Analysis: Stochastic Modelling

“Even if it were possible to cast my horoscope in this one life, and to make an accurate prediction about my future, it would not be possible to 'show' it to me because as soon as I saw it my future would change by definition. This is why Werner Heisenberg's adaptation of the Hays Office—the so-called principle of uncertainty whereby the act of measuring something has the effect of altering the measurement—is of such importance. In my case the difference is often made by publicity.

Christopher Hitchens, Hitch-22: A Memoir

One basic aspect of human cognition is partiality. Partial -in this perspective- means incomplete, more or less, or fuzzy. Therefore, uncertainty goes hand in hand with human cognition. A conventional way of dealing with uncertainty is trying to reduce it by increasing accuracy where possible. However, it is wrong to believe we can completely eliminate uncertainty. In the context of natural systems (which forms our ultimate interest in this work), error is not just an inaccuracy that can be removed but is a fundamental aspect of nature (Burrough 1986). The remaining uncertainty (which cannot be removed) can be measured within defined constraints, under a defined set of assumptions. These constraints can be possibilistic, probabilistic, or veristic (Zadeh 2005).

The centrepiece of the framework presented in this chapter is a concept of probabilistic constraint and its basic premise is that many realisations can lead to a similar solution and hence, predictions based on a single realisation should not be treated as a deterministic answer to a question. By defining probable ranges for observed and measured data and concurrent runs of the predictive scenario, a band of confidence can be drawn, on which decisions can be subsequently made.

In fact, presenting probabilities of a set of predicted potential results, is a much more sophisticated approach compared with presenting a single result as a deterministic scenario. Predictive modelling of long term climatic changes and even the daily weather forecast reports are presented probabilistically. Based on all the unknowns and all fluctuations in a natural system, we will never be able to predict “the true answer”. It is therefore more appropriate that groundwater modelling also follows suit.

Over the past few decades, various approaches were employed for stochastic modelling. These methods are either conditioned on calibrated models or independent of them. First-order uncertainty estimates (Neuman & Yakowitz 1979; Townley & Wilson 1985; Draper & Smith 1998; Hill 1998; Zimmerman et al. 1998; Tyagi & Haan 2001; Hill & Tiedeman 2007), Bayesian uncertainty analysis, and simultaneous uncertainty analysis (Vecchia & Cooley

1987; Vasco, Peterson & Majer 1996; Gomez-Hernandez, Sahuquillo & Capilla 1997; Poeter & Hill 1998; Christensen & Cooley 1999a; Christensen & Cooley 1999b; Woodbury & Ulrych 2000; Doherty 2003; Moore & Doherty 2005; Tonkin, Doherty & Moore 2007) are placed in the first group while Monte Carlo simulation (Smith & Charbeneau 1990; Ballio & Guadagnini 2004; Gaganis & Smith 2006), generalised likelihood uncertainty estimation (or GLUE) (Beven K.J. & Binley 1992), and Bayesian model averaging (or BMA) (Carrera & Neuman 1986; Gupta, Sorooshian & Yapo 1998; Madsen 2003; Vrugt et al. 2003; Neuman & Wierenga 2003; Neuman 2003) are examples of the second.

Here, I will lay a common foundation for the concept of uncertainty, various approaches to deal with it, and its significance and applications in groundwater modelling. Then, I'll specifically focus on the cylindrical nanoparticle transport modified equation and estimate the uncertainty associated with it.

4.1 A Question of Uncertainty

Complicated numerical modelling tools with advanced and detailed visualisation capability in the modern times can give a rather false impression of accuracy. It is essential to understand that to mathematically model any natural system, simplifications must be made and assumptions must be introduced. Simplification, often denotes compromise, which –in turn– introduces uncertainty to the model, while making it computationally (and usually also commercially) viable. Accepting all human concepts are partial and hence have an inherent uncertainty, at the same time as errors occur because of dynamic and ever-changing characteristics of any natural system, uncertainty may well be viewed as a permanent part of this picture.

4.1.1 Where does uncertainty come from?

Uncertainty is rooted in fluctuations and errors. Errors can occur in a variety of situations, from a selection of sources and on a range of matters. Error is defined as deviation from the true value or in a more mathematical sense it is:

Error = |measurement (or observation) – true value|.

In addition to natural fluctuations which make it impossible to have a single value as the true value for many parameters, errors occur because of limitations of methods, instruments, and human involvement. In groundwater modelling context, from the start which is conceptualisation of the system, human judgment will introduce bias and errors through knowledge gaps and/or misinterpretation of the obtainable information. The field-measured parameters will not be devoid of errors caused by a measuring instrument with not enough accuracy or one that hasn't been calibrated recently or accurately enough, an unrepresentative sampling point, and/or a biased operator who is also susceptible to misreading the instrument or mistaken transcription of the data.

Then all data is assigned into a mathematical model which is a simplification of the natural system and only holds under a particular set of assumptions which may or may not be met for every case. These simplifications can (and will) bring their fair share of errors into the model. A more mechanical mistake can happen in the process of importing the input data.

The system is simulated based on the information and the data. This model will be showing some deviation from observed data (this is expected) and will undergo calibration in order to show a higher level of agreement with the observed data. Calibration is often carried out through inverse modelling practices. While in principle calibration may be seen as a corrective process that will single out the most suitable set of parameters to proximate the simulation to reality, considering the possibility of target values containing errors [a fair assumption] would suggest a faultiness in this belief.

The complex concept of non-uniqueness also suggests that more than one set of parameters can simulate the present state of the system -to the same level of agreement- while each set might simulate different results for the same predictive scenario(s). This concept goes to show even a very close calibration cannot be taken as less uncertain in the predictive results (Moore and Doherty, 2005, Tonkin and Doherty, 2006).

I intend to further expound the types of errors and the uncertainties associated with them, before examining the methods of reducing uncertainty and ultimately measuring and presenting the remaining uncertainty.

4.1.2 Types of errors

Errors can be categorized into three major types:

- systematic errors
- extreme errors
- random errors (Velikanov 1965)

When trying to identify and measure the errors, the total error would be a function of all error types.

4.1.2.1 Systematic errors

Systematic errors happen as a result of a recurring mistake or a misjudgement. For example if a logger is not calibrated and water level data is being recorded higher than the actual elevation, it will lead to a systematic error which could be corrected by adding or subtracting a constant value from all data points over time.

Systematic errors can also happen spatially. For example if all water levels have been recorded against a wrong datum. Or as seen in Figure 4-1, if the data has been processed incorrectly and depth to water level has been measured from top of the casing and assigned as depth to water from ground surface, where casings have a constant value of 30 cm stick up. In this case all various points of data across the well field should be corrected to bring back the whole network to a realistic level.

Although these errors can be corrected to a large extent, Velikanov (1965) argues that they are virtually impossible to completely eliminate. He points out that any attempt to identify systematic errors are ultimately restricted by human judgement and it is safe to assume that other types of errors have in fact occurred.

In the context of groundwater modelling, systematic errors could occur as a result of a erroneously assumed conceptual model (Carrera & Neuman 1986; Refsgaard et al. 2006), inaccurate model input (Kavetski, Franks & Kuczera 2002; Vrugt et al. 2005; Gaganis & Smith 2006; Huard & Mailhot 2006), or poor representation of heterogeneity (Cooley 2004; Cooley & Christensen 2006; Moore & Doherty 2005; Mehrabi & and Milne-Home 2012).

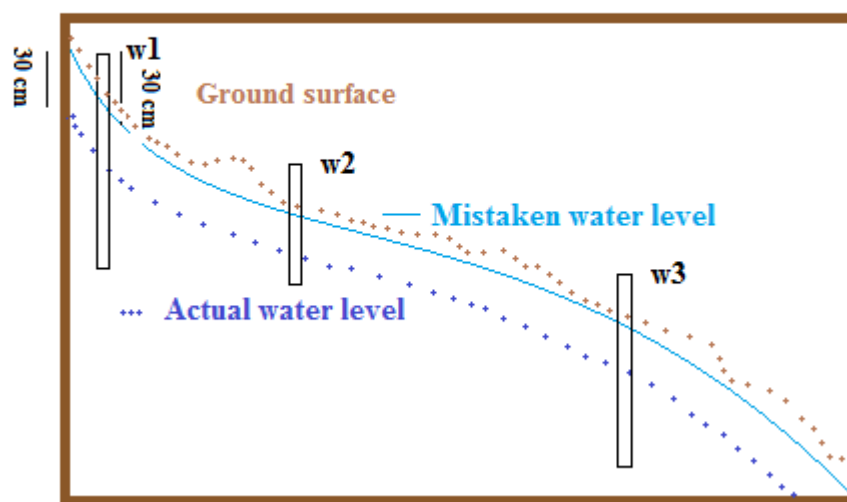


Figure 4-1 An example of a systematic error

4.1.2.2 Extreme errors

Extreme or chaotic errors are, as the name suggest, values which differ from the rest of the measurements in an extreme and unpredictable manner. Combining the views of Velikanov (1965) and Parratt (1961), the following, lists the causes of chaotic errors:

- Sampling networks are developed based on human judgment. Considering the ever-limited number of sampling locations as well as sampling frequency, interpolation between to sampling points (both spatially and temporally) is commonly used to determine what lies in between. If a sample is taken at a point (a locale or a point in

time) where unrepresentative characteristics are present, it can lead to significant deviations from the true values where it has been taken into account for interpolation.

- Accidental misreading of an instrument by the operator will also result in a single or a series of values which display deviation from the true value.
- In case where collected data need to be analysed and/or interpreted, there will be scope for sporadic misinterpretation or misunderstanding.
- If conversion of units or any other mathematical processing needs to be performed, arithmetic mistakes and misplaced decimal point can be of concern as possible causes for an extreme error to occur.
- Last but not least, an extreme deviation of a single data point or a small series of points, could be a result of human error while recording the data (writing down or recoding it digitally).

The conventional way of dealing with such errors, when detected, is to neglect the outliers as “noise”. In other words, cleaning the data off the unrepresentative values is done before any further use of data is made. Figure 4-2 illustrates a case of an extreme error where one data point shows a significant deviation from the rest of the data set.

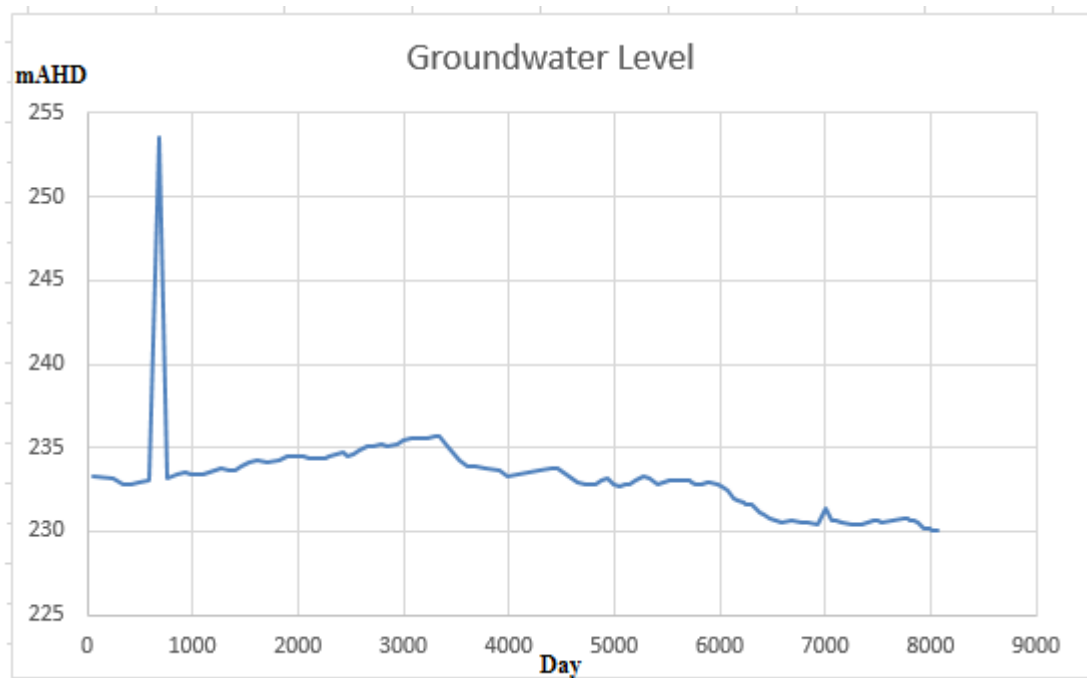


Figure 4-2 An example of extreme error

It is important to be very cautious of not neglecting a true value, since natural systems present such complexity that it is possible (even if not highly probable) that these apparent outliers may in fact be true values. It is recommended that any such error, more so if it occurs as a series rather than a single point, be further investigated if possible to clarify the situation. The possibility of the outlier shown in Figure 4-2 being a true recording of the groundwater level, can be examined by looking at precipitation data or any other activity that could have potentially caused a temporary and rapid rise in the well. Although in the absence of any supporting evidence, it is advisable that this value be cut off.

4.1.2.3 Random errors

As mentioned earlier in this chapter, total errors will be a function of all three types categorised here. Hence, random errors can be presented as total errors, less systematic and extreme errors.

Random errors occur as a result of disturbances of human performance and because they are random, they often follow a normal distribution curve (a symmetrical distribution either side of the true value) which leads to a more or less justified result. However, Velikanov (1965)

and Gould (1970) argue this may not always be the case. The rationale behind this argument is where small values are being measured (such as soil moisture, porosity, permeability of a tight structure, dispersivity, etc.). In these instances, random errors might initially display a symmetrical distribution, however, the negative end of the values will be cut off since these parameter cannot be represented as a negative value. Consequently, the natural and symmetrical distribution of the random errors will be disturbed and a bias is introduced into the dataset (Figure 4-3).

As these errors are random and there is no model to predict them and they are not so significant as to display a large deviation from the other data points in the dataset, they are extremely difficult to detect and therefore nearly impossible to correct. They should simply be assumed to exist under any conditions.

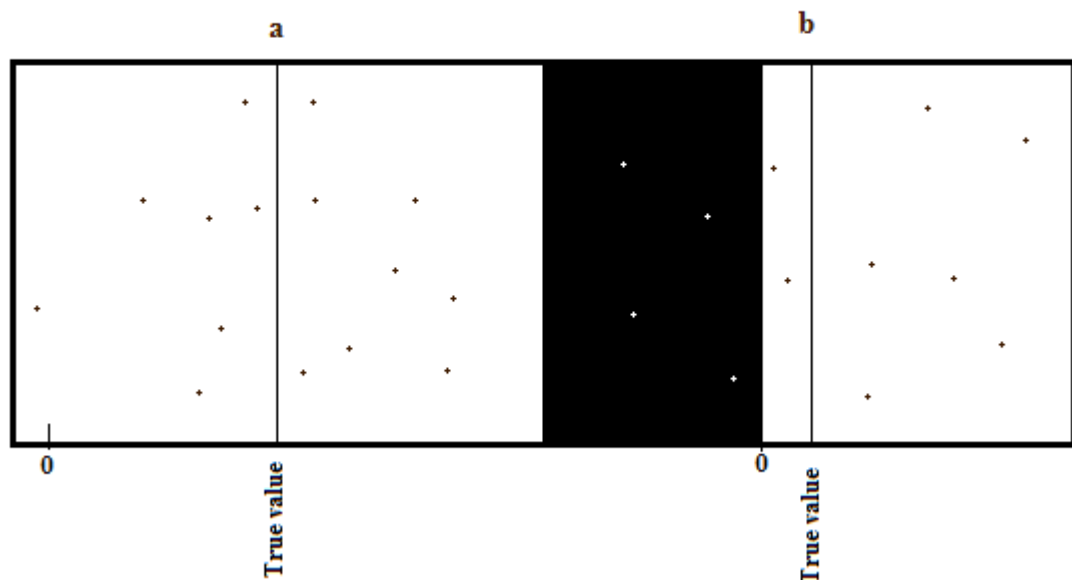


Figure 4-3 Random errors distribution scenarios (a) where the true value can be estimated based on a normal distribution of errors (b) where the true value can only hold positive values and the normal distribution of errors is disturbed. In b, the black shaded part is cut off from the data set.

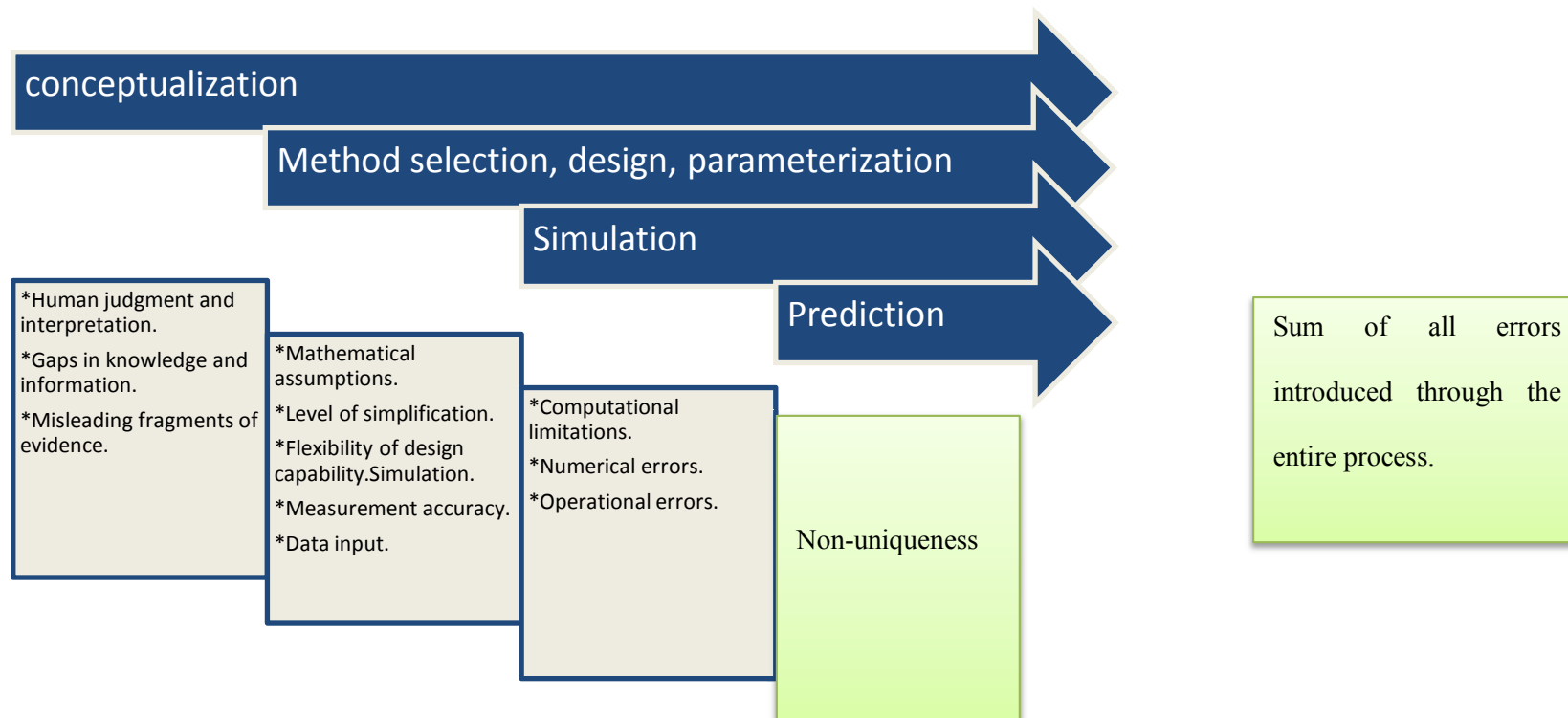


Figure 4-4 A chart of errors during a standard groundwater modelling process

As can be seen in this chart (Figure 4-4) errors can occur at every step of the process and the earlier errors are likely to become systematic errors which will have an impact on the subsequent steps.

4.2 Parameter Sensitivity and Uncertainty

In any given mathematical equation, a set of variables determine the solution. Each one of these variables carry a weight based on which their impact on the final solution is determined. The magnitude of this impact is measured as sensitivity of that variable in the context of that equation.

In a more complex setting where many equations are in use, parameter impact on the final result of a particular calculation is estimated and used to fine-tune the simulation results. The basic and simplified rationale behind this theory can be explained as follows:

If $a=3b+c$, then the impact of changes in variable 'b' is more significant than the impact of changes in variable 'c' on the value of 'a' as seen in Figure 4-5. Table 4-1 lists the chart data where initial values for 'b' and 'c' are assumed to be 1 (resulting in a value of 4 for 'a').

It is evident from this chart that smaller changes to 'b' result in bigger changes in the overall result (or the value of 'a'). Please note that this example is a simple linear case and there are many other examples where as a result of a much more complex relation between the parameters and the result there are thresholds for sensitivity response. In other words, changes in parameter value up to a point might result in changes in result but beyond that specific point, it may be of no impact on the result. The magnitude of impact can also change in various relationships. This means that the ratio of change in result for every unit change of a parameter may not remain the same over a range of multipliers.

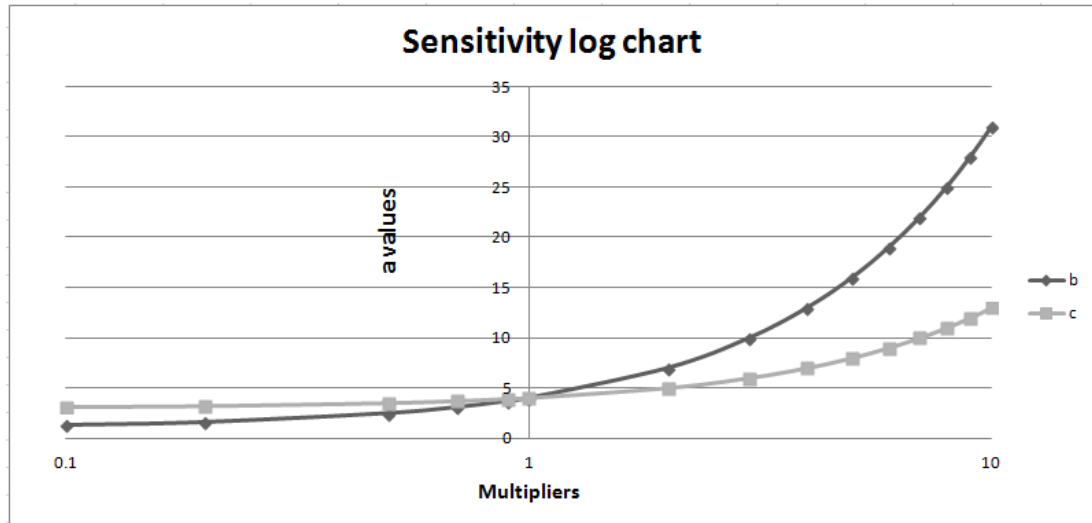


Figure 4-5 Sensitivity log chart for 'a'

Table 4-1 sensitivity chart data for b and c multipliers

b \ c	0.1	0.2	0.5	0.7	0.9	1	2	3	4	5	6	7	8	9	10
0.1						1.3									
0.2						1.6									
0.5						2.5									
0.7						3.1									
0.9						3.7									
1	3.1	3.2	3.5	3.7	3.9	4	5	6	7	8	9	10	11	12	13
2						7									
3						10									
4						13									
5						16									
6						19									
7						22									
8						25									
9						28									
10						31									

Suppose we have a true value for ‘a’ and based on the initial estimations of ‘b’ and ‘c’, this value is not met. Since ‘b’ and ‘c’ have been estimated and are assumed to differ from their true values, they can be changed in their probable range of possible values in order to simulate the true value of ‘a’ as a target. This process is called calibration. Now suppose (as in our example case) every unit change in ‘b’ changes ‘a’ by 3 units while every unit change in ‘c’ changes ‘a’ by one unit; indicating more sensitivity towards ‘b’ than ‘c’. Under the assumption of random errors in assuming initial values for ‘b’ and ‘c’, we can assume a normal distribution for the possible values which will contain the true value of each one of these parameters. A normal distribution in a parameter ‘b’ with mean ‘x’ and variance σ^2 is a statistic distribution with probability density function.

$$P(b) = \frac{1}{\sigma\sqrt{2\pi}} e^{-(b-x)^2 / (2\sigma^2)} \quad \text{Eq. 4-1}$$

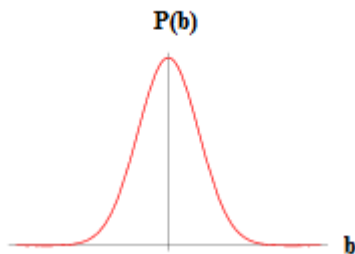


Figure 4-6 Standard normal distribution, probability density function

While the parameters have been selected based best available information, it is highly desired to keep the parameters as close as possible while fine-tuning the results to achieve a good agreement.

Based on these assumptions, the best way forward to reduce uncertainty in the result by tuning it closer to the known ‘true value’ (i.e. observed data), is to impose changes as small as possible to sensitive parameters. By doing this, parameter values will remain in a high probability range

and the results will be in better agreement with the targets. This highlights the importance of sensitivity analysis and its role in reducing (and ultimately measuring) uncertainty.

During his studies on the effects of physical heterogeneity of the porous media on uncertainty, Gelhar (Gelhar 1993) found the observed deviations from stochastic theories is much larger in contaminant concentration than that in hydraulic head, indicating a strong sensitivity of solute transport to small scale heterogeneity of hydraulic conductivity.

While our modified equation specifically targets physical heterogeneity of the porous media, it would be valuable to examine how sensitive the parameters involved in this equation are, and how this changes the overall sensitivity of transport results.

4.2.1 Particle Diameter Sensitivity

In this section I aim to investigate the effect of particle diameter on plume movement via its effect on filtration coefficient (λ) which in turn determines the retardation of particles as they move through the porous media. This is carried out by a series of calculations where all parameters remain constant while particle diameter changes.

4.2.1.1 Model Parameterization

Model parameters are listed in

Table 4-2. Hydraulic conductivity of the model is a randomly generated field (which was also used in the previous chapter to model the movement of cylindrical nanoparticles under various mathematical assumptions). The heterogeneous conductivity field (Figure 4-7) is distinctively characterized by a set of statistical parameters such as mean, geometrical mean, root mean square, variance, standard deviation, range, average absolute deviation, relative mean difference, and standard error.

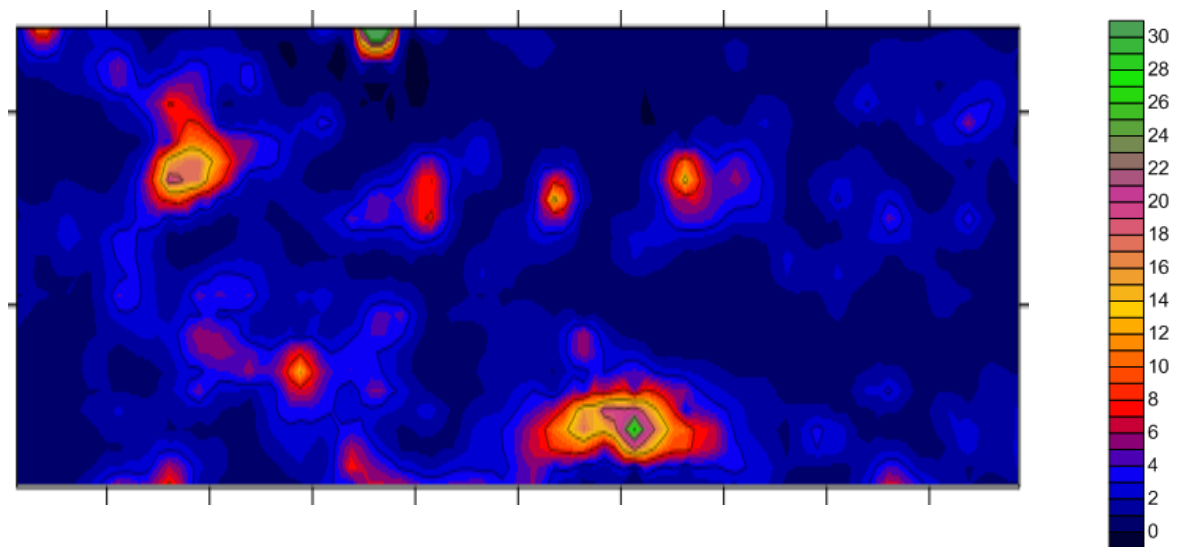


Figure 4-7 Conductivity field (m/day)

Table 4-2 Model parameters- Case 1

Grid	1 (R) 40 (C) 20 (L)
Cell Size (m)	5 by 5
Time Steps (day)	365
Porosity	0.3
Particle Diameter (nm)	Varied
Particle Length (nm)	200
Particle Density (kg/m ³)	1500
Intercept (μm)	170
Median Collector Diameter (μm)	379
Dynamic Viscosity (ω)	0.001

Table 4-3 Statistical characterisation of the hydraulic conductivity field

Hydraulic Conductivity Field Statistics	
Mean	1.23
Geometrical Mean	1.99
Root Mean Square	3.25
Variance	6.62
Standard Deviation	2.57
Range	27.91
Average Abs. Deviation	1.33
Relative Mean Difference	1.03
Standard Error	0.054

Table 4-4 Multipliers and values for Particle diameter sensitivity analysis

Multipliers	Particle Diameter (nm)
0.1	2
0.2	4
0.5	10
1	20
2	40
5	100
10	200

4.2.1.2 Key Observations

- Filtration coefficient (λ) calculated by Yao's equation (Eq. 2-16 and Eq. 2-17) is larger than those calculated by our suggested modified equation (where d_c is replaced by Eq. 2-27), justifying less smearing observed in chapter 3 model results.

- Sensitivity relationship differs in these two cases for multipliers between 1 and 10.
- Neither of the methods displays a linear relationship with lambda.
- Neither of the methods displays a constant trend with lambda, indicating both inverse and direct correlation over various ranges of parameter.

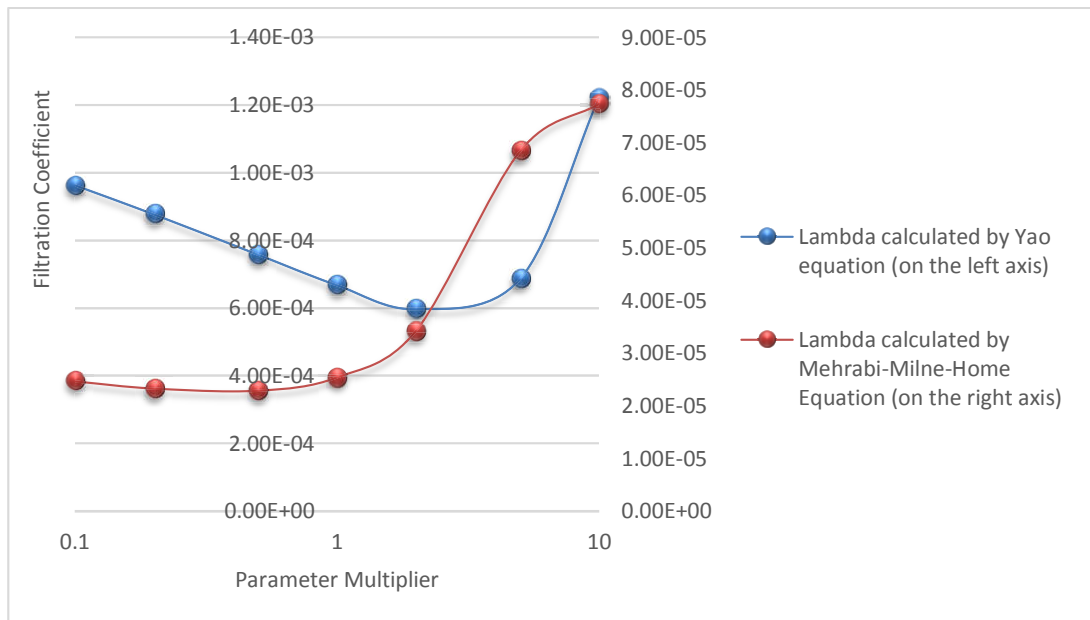


Figure 4-8 Relationship between particle diameter and lambda

In Figure 4-8, Yao-based calculations have been plotted against the first, and our calculations, against the second vertical axis.

4.2.1.3 Additional discussions

The values in the two series plotted in Figure 4-8, are an order of magnitude different. As pointed out in the previous chapter, consideration of heterogeneity introduces more smearing into the transport phenomenon by reducing the filtration coefficient, confirming the observations of Sampath (2006).

The minimum points of each series are different, indicating a potential major difference between the methods. The effects of particle diameter size change can vary based on the particle orientation distribution which determines the ratio of side contact/end contact.

4.2.2 Particle Length Sensitivity

In this section I aim to investigate the effect of particle length on plume movement through its effect on filtration coefficient (λ) which in turn determines the retardation of particles as they move through the porous media. This is carried out by a series of calculations where all parameters remain unchanged as shown in Table 4-5 while particle length changes based on the multipliers shown in Table 4-6.

4.2.2.1 Model Parameterization

Model parameters are listed in Table 4-5. Hydraulic conductivity field characteristics are the same as case 1 as seen in Table 4-3 and Figure 4-7.

Table 4-5 Model parameters- Case 2

Grid	1 (R) 40 (C) 20 (L)
Cell Size (m)	5 by 5
Time Steps (day)	365
Porosity	0.3
Particle Diameter (nm)	20
Particle Length (nm)	Varied
Particle Density (kg/m ³)	1500
Intercept (μm)	170
Median Collector Diameter (μm)	379
Dynamic Viscosity (ω)	0.001

Table 4-6 Multipliers and values for Particle length sensitivity analysis

Multipliers	Particle length (nm)
0.1	20
0.2	40
0.5	100
1	200
2	400
5	1000
10	2000

4.2.2.2 Key Observations

- Filtration coefficient (λ) calculated by Yao's equation is larger than those calculated by our suggested modified equation.
- Sensitivity relationships are very similar in trend for both equations, but somewhat different in magnitude.
- Both approaches show a generally steady decline in lambda when length increases. The decline gets slighter as the multiplier grows bigger.

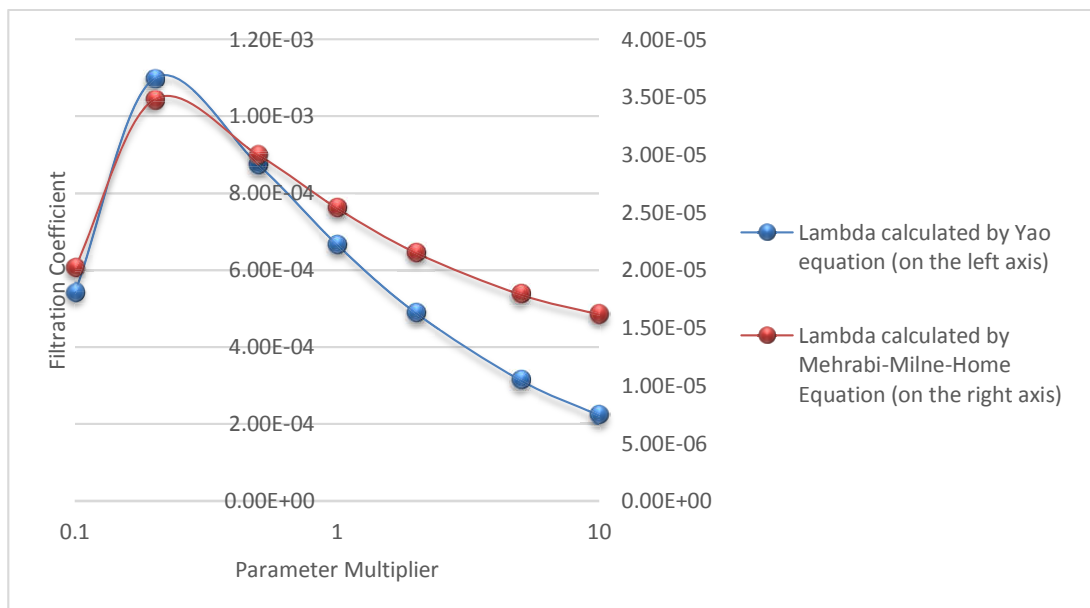


Figure 4-9 Relationship between particle length and lambda

In Figure 4-9, Yao-based calculations have been plotted against the first, and our calculations, against the second vertical axis.

4.2.2.3 Additional discussions

Particle length at its smallest value in this series of simulations takes a value of 20 (same as particle diameter) so effectively the particle behaves as a spherical object. In this scenario, the particle has a ratio of one for particle diameter over particle length. Following the correction of this ratio to effectively resurrect the ratio of a cylindrical particle (subsequent to a multiplier of 0.2), the relationship between increase in length and decrease in filtration coefficient is evident.

Note that without the consideration of heterogeneity (i.e. Yao's equation), sensitivity is higher while the other curve, graphing the results based on our suggested equation results has a lesser slope indicating lower levels of sensitivity.

4.2.3 Collector Diameter/Hydraulic Conductivity Sensitivity

In this section I aim to investigate the effect of the porous medeum's physical characteristics on plume movement through its effect on filtration coefficient (λ) which in turn determines the retardation of particles as they travel. This is carried out by a series of calculations where all parameters remain unchanged while grain size changes are based on the multipliers shown in Table 4-8.

Note that the parameter of investigation is median grain diameter which is a term in Yao's equation and is used to calculate Intercept in our equation (along with effective grain size or d_{10}) so it is of potential sensitivity in both of the approaches.

4.2.3.1 Model Parameterization

Model parameters are listed in Table 4-7. Hydraulic conductivity field characteristics are the same as case 1 and case 2 as listed in Table 4-3 and Figure 4-7.

Table 4-7 Model parameters- Case 3

Grid	1 (R) 40 (C) 20 (L)
Cell Size (m)	5 by 5
Time Steps (day)	365
Porosity	0.3
Particle Diameter (nm)	20
Particle Length (nm)	200
Particle Density (kg/m ³)	1500
Intercept (μm)	170
Median Collector Diameter (μm)	Varied
Dynamic Viscosity (ω)	0.001

Table 4-8 Multipliers and values for grain size sensitivity analysis

Multipliers	Median grain size (d50) (μm)
0.1	0.0000379
0.2	0.0000758
0.5	0.0001895
1	0.000379
2	0.000758
5	0.001895
10	0.00379

4.2.3.2 Key Observations

- Filtration coefficient (λ) calculated by Yao's equation is larger than those calculated by our suggested modified equation.
- Sensitivity relationships for both approaches are very similar in trend, but somewhat different in magnitude.

- Both approaches show a steady decline in lambda when grain size increases. On a non-log plot, this decline displays an almost linear relationship.

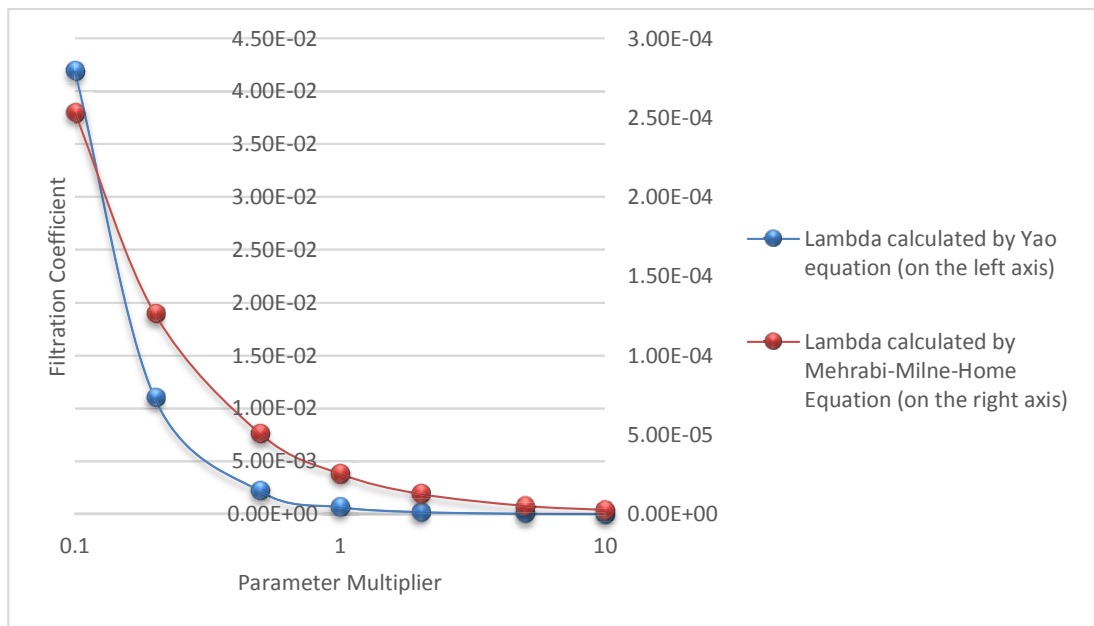


Figure 4-10 Relationship between grain size and lambda

In Figure 4-10, Yao-based calculations have been plotted against the first, and our calculations, against the second vertical axis.

4.2.3.3 Additional discussions

Figure 4-10 shows a clear inverse relationship between grain size and filtration coefficient. Expectedly, as the grain size decreases, the surface area of the porous media (capable of adsorbing particles) increases which in turn, increases the filtration coefficient. It is just as well expected that an increase in grain size will decrease the sorption sites (surface area) and will result in a decreased filtration coefficient as more particles pass through the medium without being filtered.

Note that, once more inclusion of heterogeneity of the porous media has slightly decreased the level of sensitivity towards grain size as it had with particle length.

4.2.4 Particle Density Sensitivity

In this section I aim to investigate the effect of particle density on plume movement through its effect on filtration coefficient (λ) which in turn determines the retardation of particles as they transfer. This is carried out by a series of calculations where all parameters remain the same while particle density changes based on the multipliers shown in Table 4-10.

It is important to note that the density of water has been inputted as 1000 kg/m^3 and as a result some of the multipliers have produced particle density lower than that of water. Although this is not a realistic realization for CNTs, it is useful to establish the sensitivity of the parameter density. In addition, some synthetic materials have lower densities than water and can be produced as nanorods or nanotubes.

4.2.4.1 Model Parameterization

Model parameters for case 4 are listed in Table 4-9. Hydraulic conductivity field characteristics are the same as case 1 and case 2 as listed in Table 4-3 and Figure 4-7.

Table 4-9 Model parameters- Case 4

Grid	1 (R) 40 (C) 20 (L)
Cell Size (m)	5 by 5
Time Steps (day)	365
Porosity	0.3
Particle Diameter (nm)	20
Particle Length (nm)	200
Particle Density (kg/m^3)	Varied
Intercept (μm)	170
Median Collector Diameter (μm)	379
Dynamic Viscosity (ω)	0.001

Table 4-10 Multipliers and values for particle density sensitivity analysis

Multipliers	Particle Density (kg/m³)
0.1	150
0.2	300
0.5	750
1	1500
2	3000
5	7500
10	15000

4.2.4.2 Key Observations

- Filtration coefficient (λ) calculated by Yao's equation is larger than those calculated by our suggested modified equation.
- Sensitivity relationships for both approaches are very similar in trend, but somewhat different in magnitude, particularly for lesser values of density. This difference vanishes as density increases.
- Both approaches show a steady upsurge in λ by increases in density value.

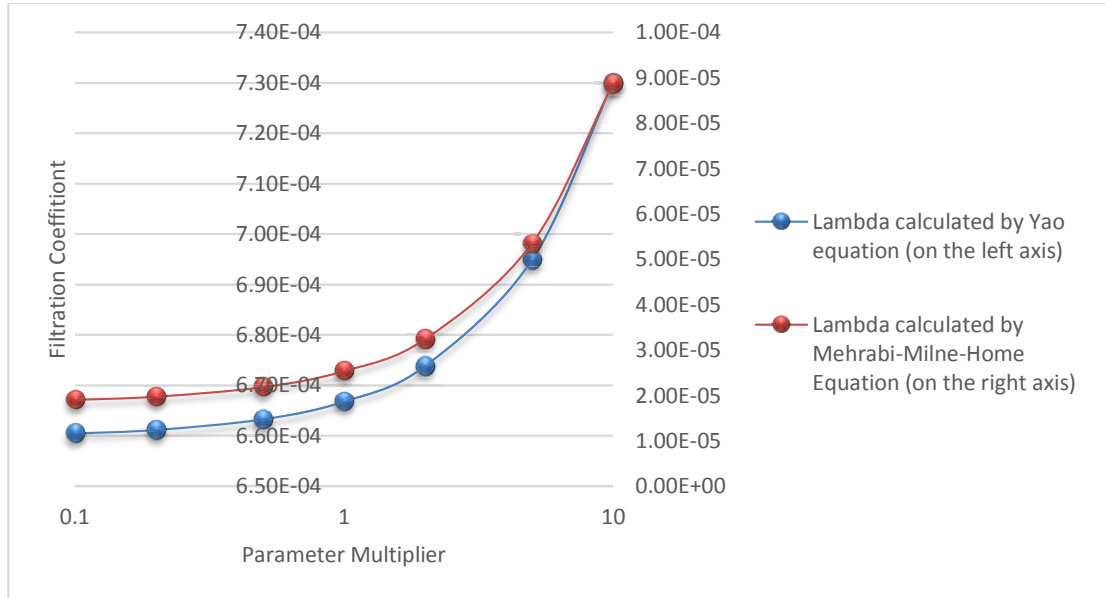


Figure 4-11 Relationship between particle density and lambda

4.2.4.3 Additional discussions

The exponential growth in filtration coefficient by increasing density is a shared symptom in both series plotted in Figure 4-11. An increase in density will amplify sedimentation of the particles (one of the three mechanisms of filtration considered in filtration theory) and consequently escalate filtration. This behaviour is expected to affect both approaches in more or less the same manner as is illustrated above.

A noteworthy statement here is the generally decreased sensitivity of investigated parameters when using Mehrabi-Milne-Home equation. By bringing in heterogeneity of the porous media into the equation, I aimed at reducing the uncertainty associated with using an average grain size value which I proved not to be a representative value for permeability. In simple terms, decreased sensitivity indicates that if the input data on any of the investigated parameters in this section is within small random error zone, the overall uncertainty imposed on the final result would be smaller if our equation is used. Using Yao's equation can introduce more uncertainty as a result of a bigger deviation from the true value result.

4.3 Dealing with Uncertainty in Groundwater Transport Modelling

Over the past few decades, a significant effort has been made to identify sources of uncertainty with groundwater pollution sources and plume distribution based on various system heterogeneities. Gorelick et al. (1983) carried out their work by considering only measurement errors as a source of uncertainty and tried to achieve better agreement between computed and observed data by using an optimisation model. While Datta et al. (1989) focused on various disposal conditions for the contaminant as a source of uncertainty. Other researchers such as Bagtzoglou et al. (1992) and Wagner (1992 and 1999) used inverse modelling methods to determine the most probable contaminant disposal location by examining various realizations of the permeability distribution and head/concentration measurements respectively. More source identification approaches were developed and investigated by using Tikhonov regulation (Skaggs & Kabala 1994), and a combination of Bayesian analysis and randomised geo-statistical parameter distribution (Snodgrass & Kitanidis 1997; Michalak & Kitanidis 2003).

While the above mentioned methods are generally focused on determining contaminant source and its disposal conditions, other methods attribute a much greater significance to natural heterogeneities of the system when it comes to uncertainty. These methods examine the probabilities based on various realisations of heterogeneous parameters such as hydraulic conductivity and porosity. Many researchers have stressed that groundwater velocity and solute transport are significantly impacted by small-scale heterogeneity of hydraulic conductivity (Gelhar, Gutjahr & Naff 1979; Gelhar 1993; Kapoor & Kitanidis 1997; Salandin & Fiorotto 1998; Salandin & Fiorotto 2000; Darvini & Salandin 2006; Morales-Casique, Neuman & Guadagnini 2006a; Morales-Casique, Neuman & Guadagnini 2006b). It is also because of a typical lack of robust data on plume distribution and concentration. In those few case where an acceptable amount of concentration data are available, measurement errors can introduce significant biases in uncertainty estimations. It seems however, permeability heterogeneity can set satisfactory constraints to capture the various realisations of a plume

transport scenarios. So in 1989 Wagner and Gorelick developed an optimisation model with the purpose of minimizing pumping volumes (for a pump and treat remedial design) while ensuring compliance with the water quality guidelines by using hydraulic conductivity as the main decoder of probabilities.

There were others who also considered hydraulic conductivity distribution a major source of uncertainty in their efforts to capture probabilities for optimisation of remedial designs (Andricevic & Kitanidis 1990; Mulvey, Vanderbei & Zenios 1995; Watkins Jr. & McKinney 1997).

4.4 Reduction and Estimation of Uncertainty

As explained earlier in this chapter, elimination of uncertainty, especially in the context of natural systems, is not possible. However it is possible to reduce and minimise the errors and consequently the uncertainty. There are several ways through which errors in measurement and interpretation can be reduced but our main goal in this work is to estimate the existing uncertainties.

4.4.1 Uncertainty Reduction

To briefly discuss some of the approaches in regard to uncertainty reduction, I'll point out some of the common recommendations in the followings. These recommendations are unanimously set to increase the accuracy of the data and post-processing practices.

- Collect as much information and data as possible. This will help with forming a better, more accurate conceptual model. More information on other indirect aspects will reduce the bias, while more data points will ensure a more realistic interpolation between the data points.
- Use accurate instruments. The accuracy of an instrument is decided based on the technology it uses and the frequency of its calibration. Calibrate accurately and frequently to avoid deviations in recorded data.

- Use best practice sampling methods. Sampling must be carried out methodically, correctly, and diligently. Go through the processes of sampling for each parameter of interest and make sure the sample is taken in an appropriate way. For example, right filters should be used for filtered metals analysis. An inappropriate mesh size for the filter will alter the results and introduces large errors.
- Repeat measurements either consecutively with the same instrument or simultaneously with multiple instruments to avoid errors. Average all the readings to balance random errors.
- Analyse and post-process data diligently and put it all through quality assurance and quality control processes as many time as possible.

For a full suite of guidelines and best practices refer to relevant government policies and environmental protection authority (EPA) guidelines.

4.4.2 Uncertainty Estimation

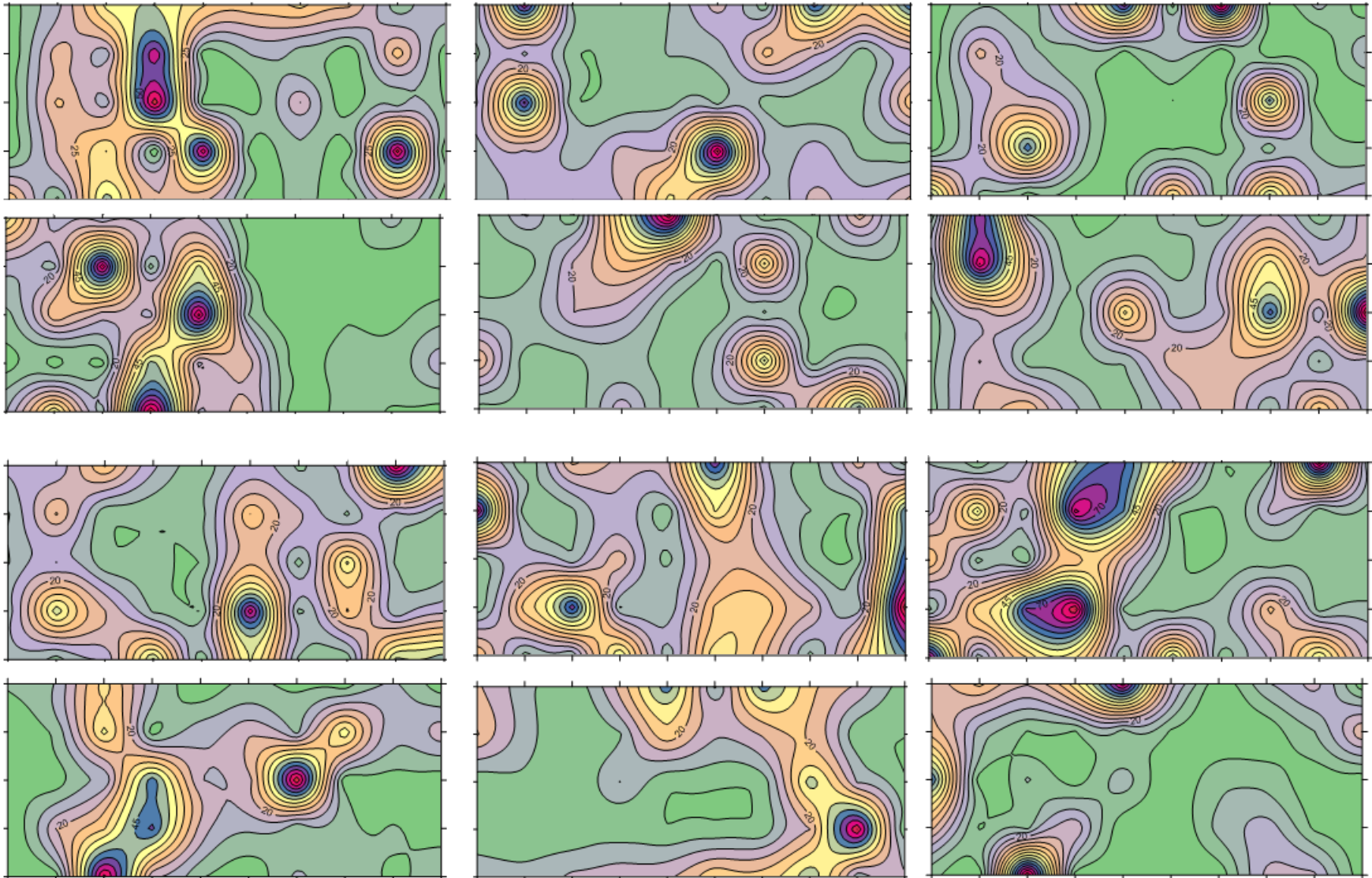
Monte Carlo Simulation is commonly used to analyse uncertainty due to model parameters. It delivers a comprehensive distribution of potential model predictions, which is then used to quantify the upper and lower bounds of prediction uncertainty.

The conventional Monte Carlo method involves three steps:

1. random field generation: generating a probability distribution for uncertain parameters in the model (examples are shown in Figure 4-12)
2. numerical modelling: repeatedly running the model with a randomly selected value for each uncertain parameter from the probability distribution pool
3. and to finish, statistical post-processing: constructing the probability distributions of model outputs.

4.5 Method Application

Let us go through the process of a Monte Carlo Simulation for the transport model of carbon nanotubes defined and outlined in chapter 3. A series of random fields of hydraulic conductivity were produced (some examples are shown in Figure 4-12). The number of realizations were limited to 1000 to 2000.



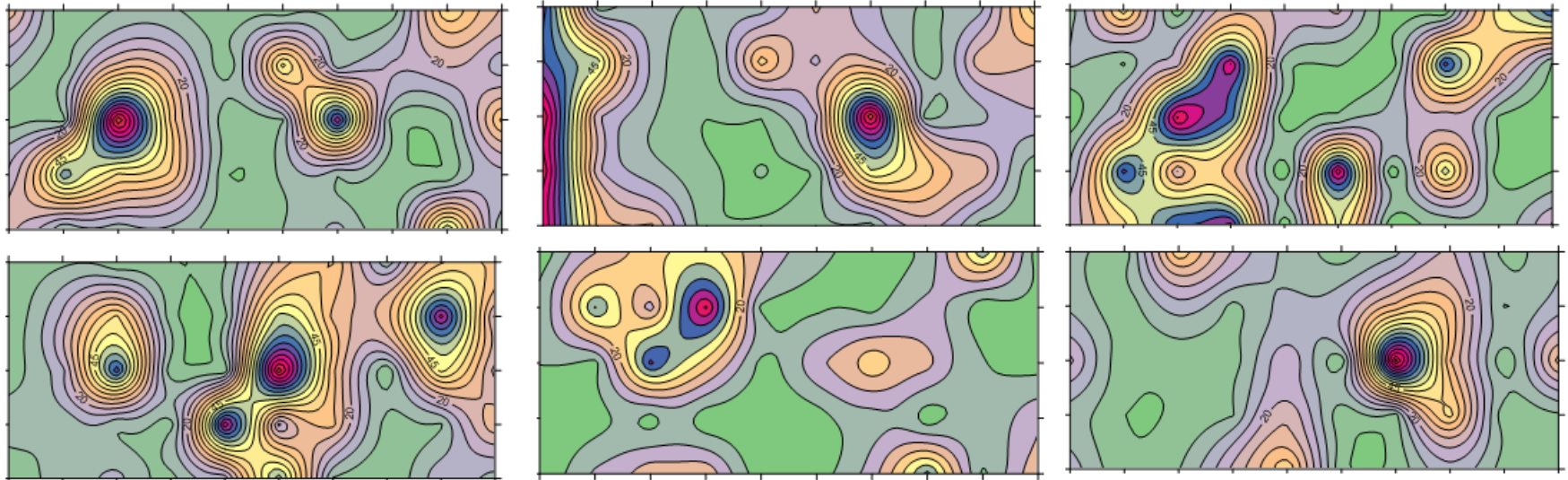
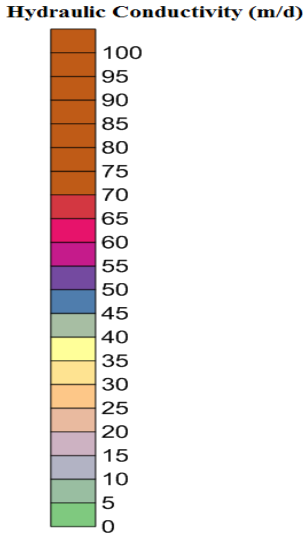


Figure 4-12 Examples of random realizations of hydraulic conductivity field using Fast Fourier transform-based analysis



The underlying assumptions were:

- hydraulic conductivity is assumed to be the main source of uncertainty (as hydraulic conductivity heterogeneity is the main focus of this work, this assumption will allow a pure investigation of this parameter's heterogeneity without
- extreme errors are cut out of the dataset ,
- random errors associated with hydraulic conductivity follow a normal distribution,
- source contaminant conditions are known and will be maintained in all realizations,
- particles are uniform and will not aggregate during their transport through porous media.

The result of interest in this study is the concentration of the particles simulated during a 365-day modelling period. For this purpose, twenty points were selected within the model grid. The probability distribution of concentration value (on day 365) at each point was analysed based on just over 1000 realizations. Selected results are shown in Figure 4-13 to Figure 4-18. In these series of figures, the top figures relate to Yao's equation while the bottom figures display the results of our equation and its various realisations. In all cases our equation covers a smaller range of values with higher probability density, indicating lower levels of uncertainty.

The plots shown in Figure 4-19 to Figure 4-38, display over one thousand realisations for each point on day 365. In these plots you can see the upper and lower bound for calculated concentrations (gr/m^3) in each realisation for a given observation point (obs 1 to obs 20). The statistical information for each set of concentration calculations is also presented in the relevant tables (Table 4-11 to Table 4-30) associated with these plots.

Each plot shows two benchmark lines for each one of the deterministically calculated (1) Yao (blue line) and (2) Mehrabi-Milne_Home (orange line) cases. Calculations for Monte Carlo realisations are plotted for each case; where Yao's realisations are colour coded grey and Mehrabi-Milne-Home data points are yellow. Equal distance from the benchmark line

indicates a normal and symmetrical distribution and widely different bounds on either side of the line indicates a bias in calculations.

For ease of understanding the results despite the different scale of the data points (often smaller in Mehrabi Milne-Home case), all relevant statistical information have been listed in associating tables to show the range of the calculations as well as standard deviation and mean values.

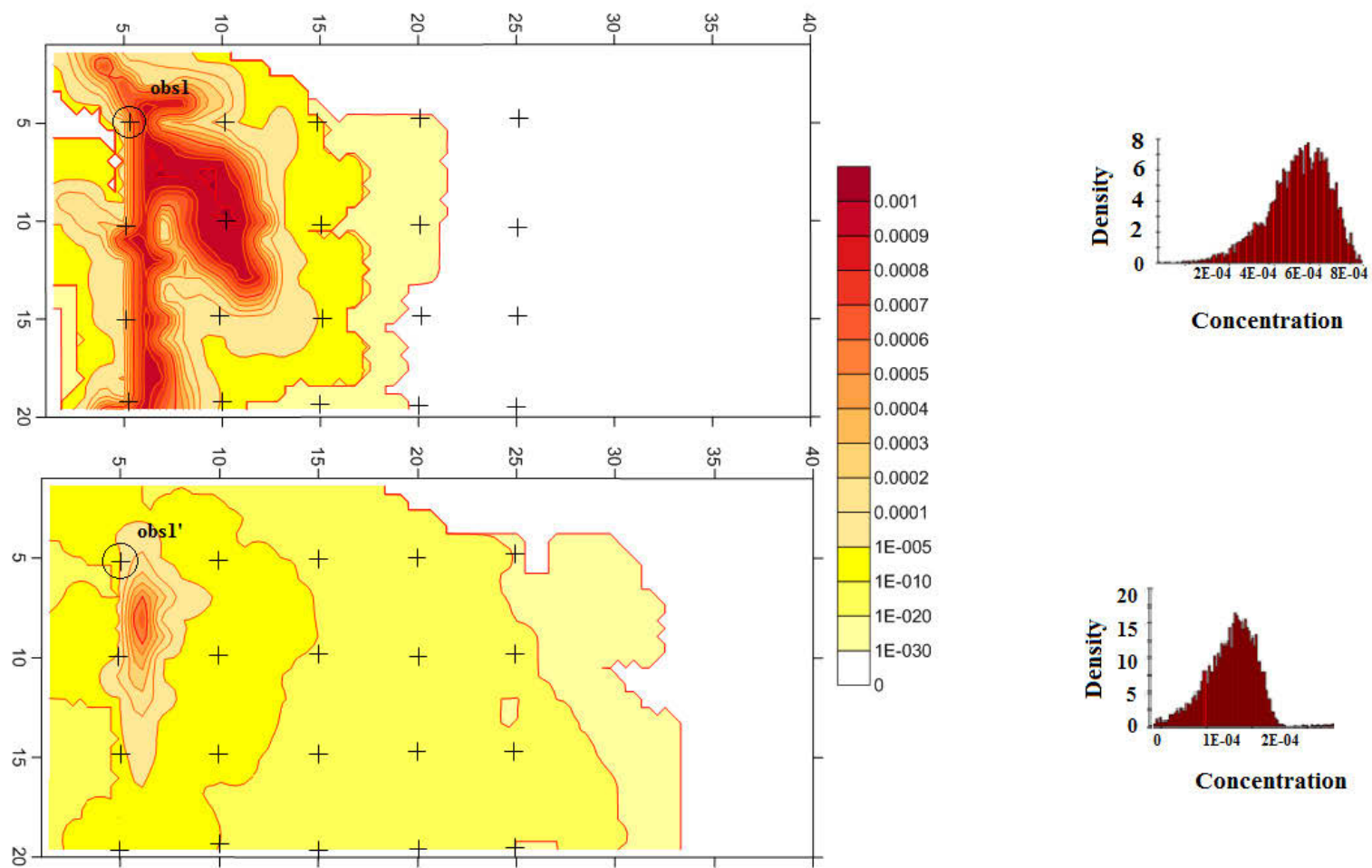


Figure 4-13 Probability distribution density vs concentration for observation point 1 and 1'

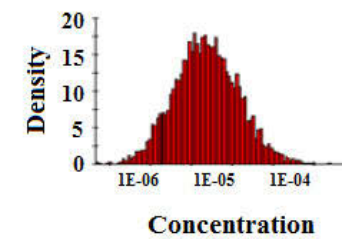
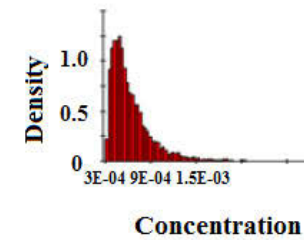
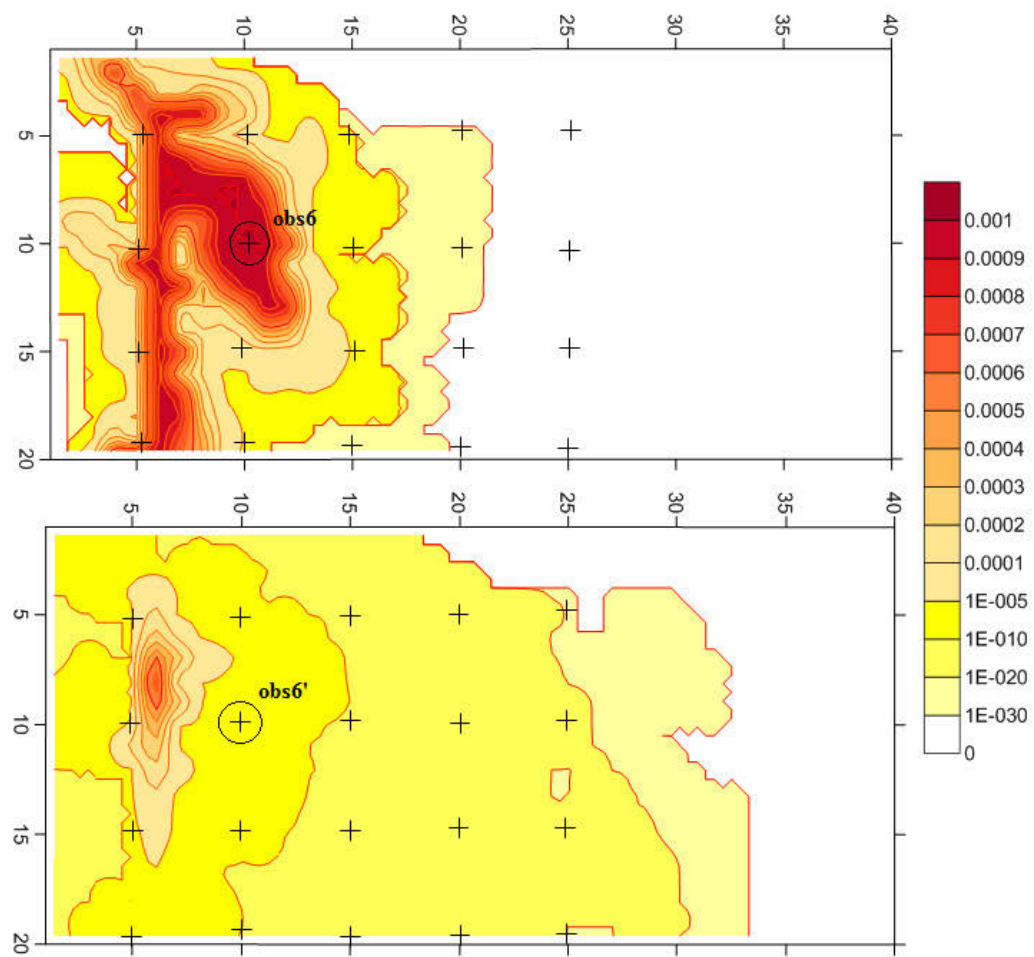


Figure 4-14 Probability distribution density vs concentration for observation point 6 and 6'

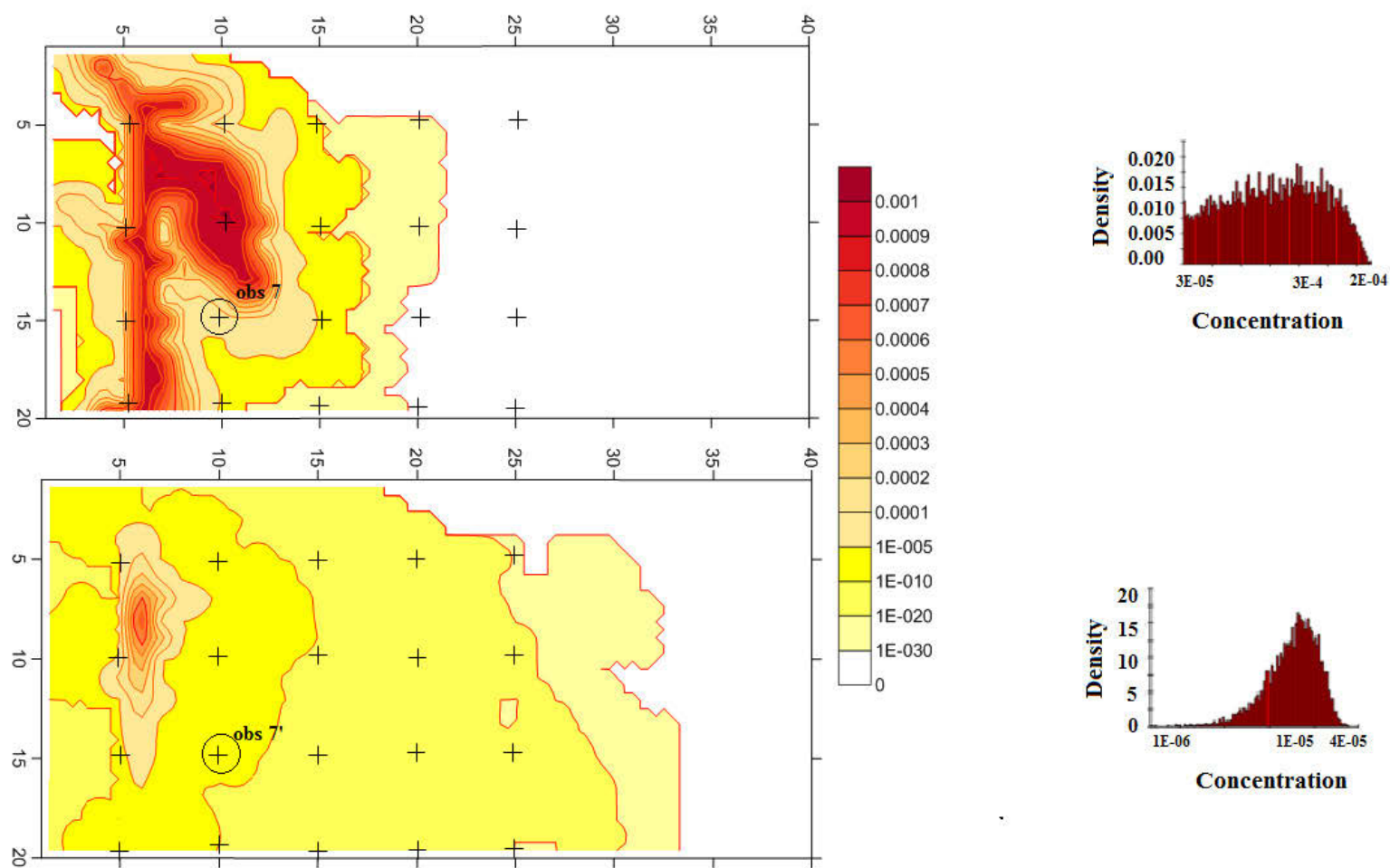


Figure 4-15 Probability distribution density vs concentration for observation point 7 and 7'

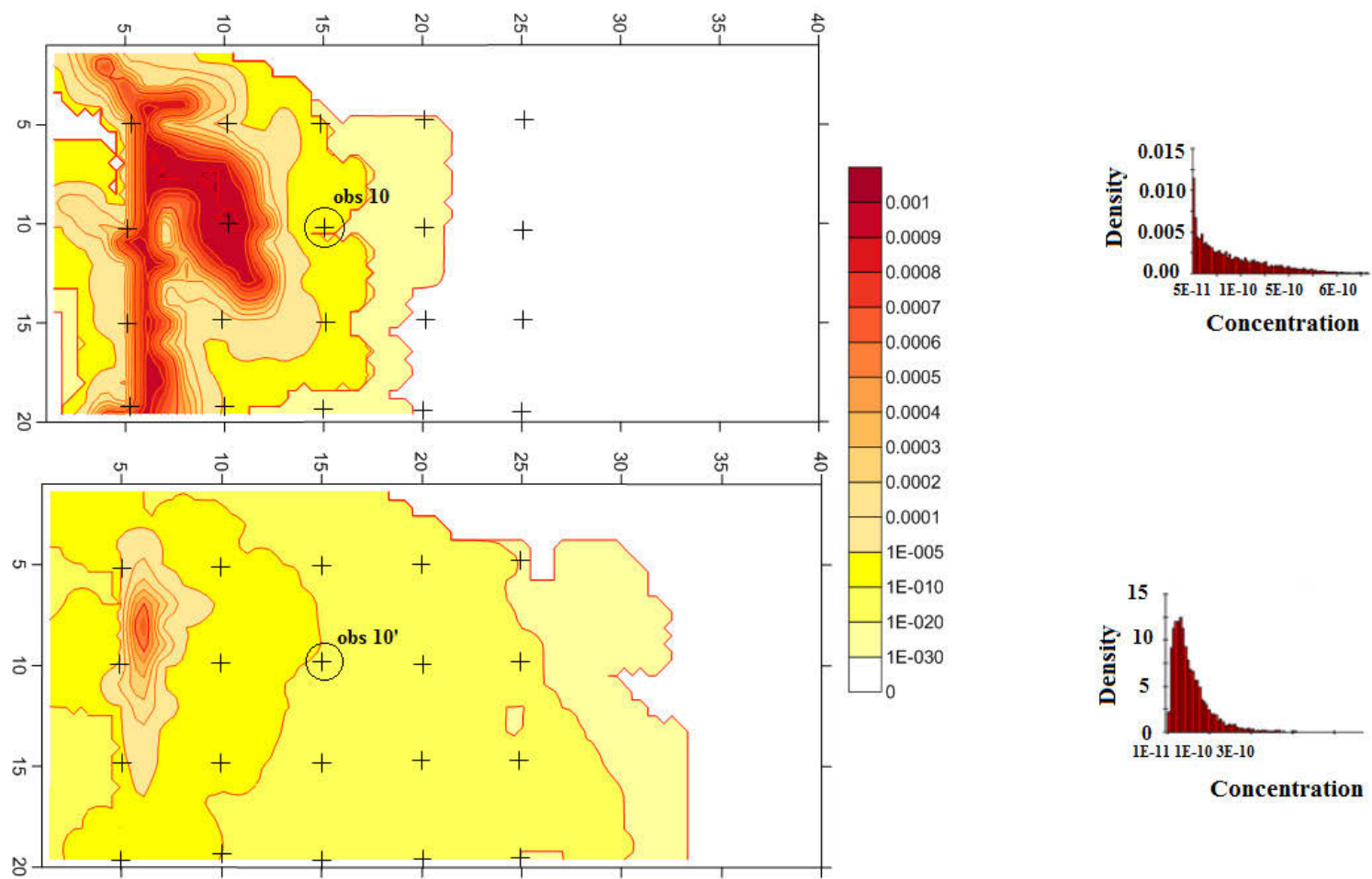


Figure 4-16 Probability distribution density vs concentration for observation point 10 and 10'

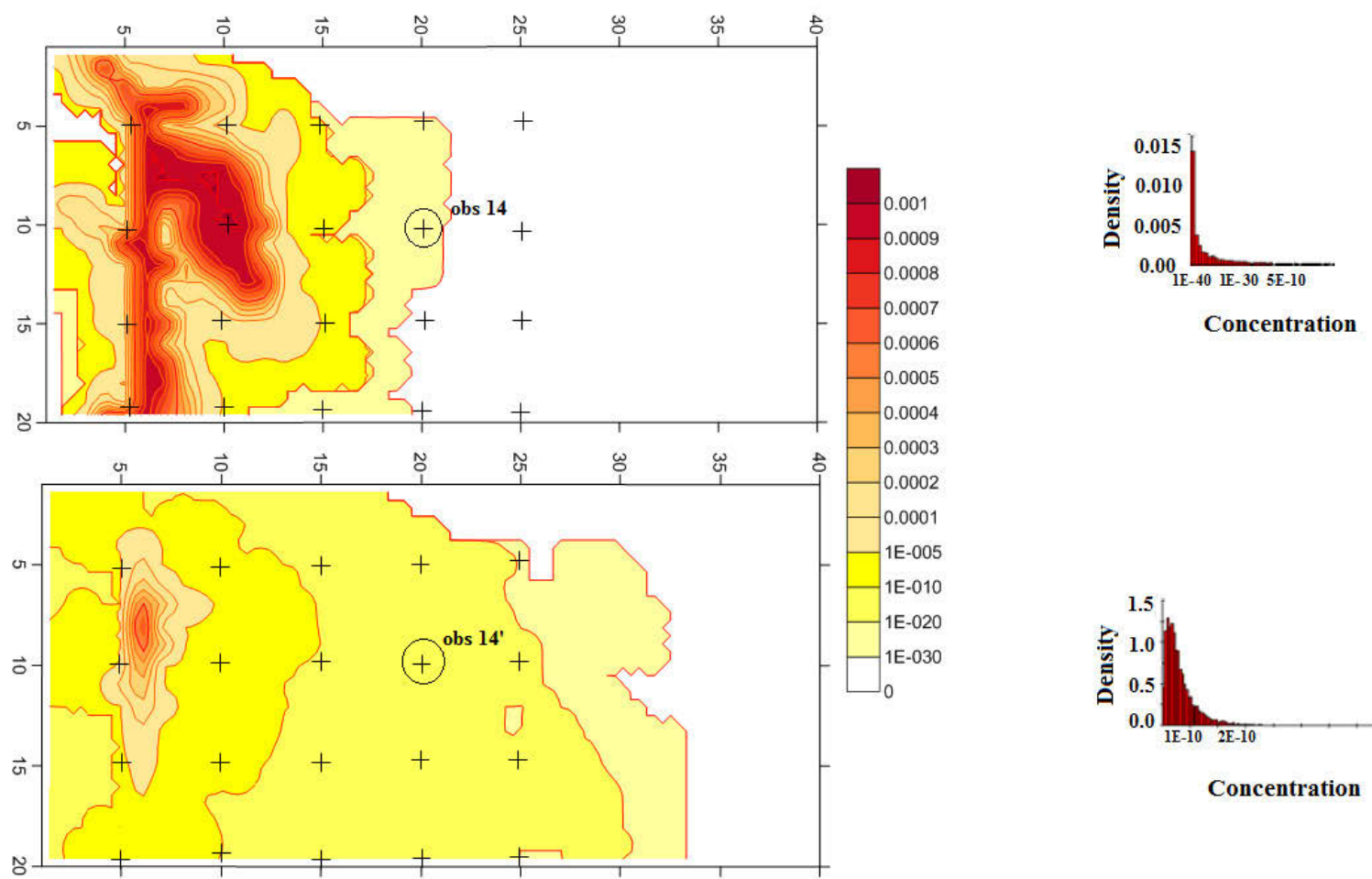


Figure 4-17 Probability distribution density vs concentration for observation point 14 and 14'

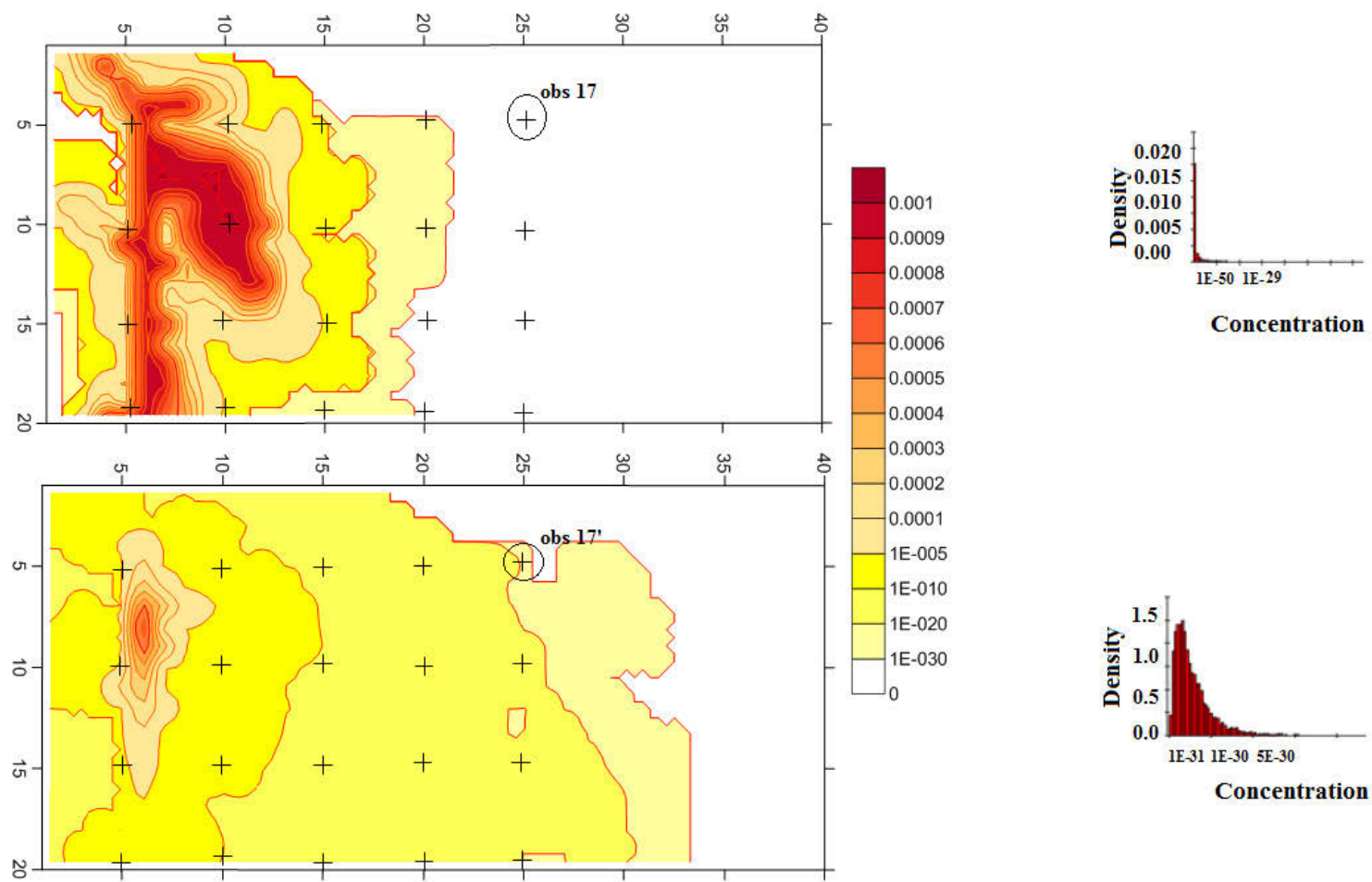


Figure 4-18 Probability distribution density vs concentration for observation point 17 and 17'

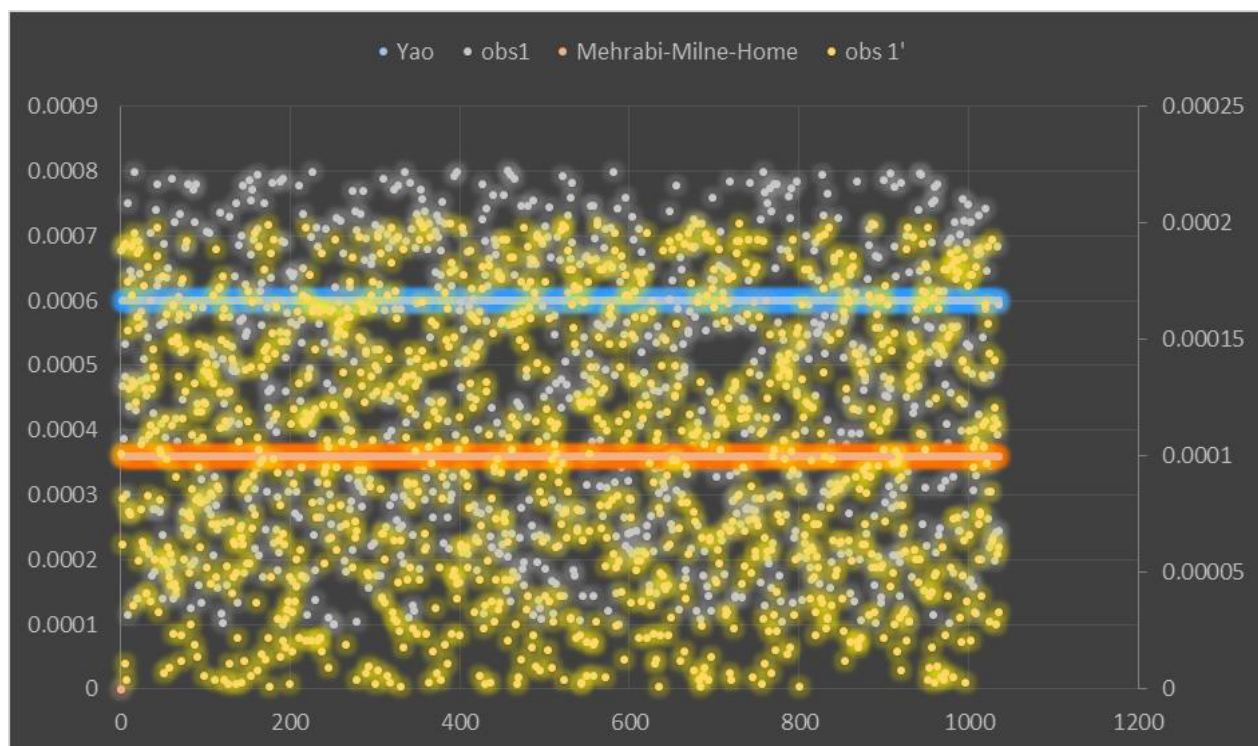


Figure 4-19Concentration realisation: Observation Point 1

Table 4-11Statistical information: Observation Point 1

	Standard Deviation	Mean	Min	Max	Range
Yao	2.008E-04	4.491E-04	1.000E-04	8.000E-04	7.000E-04
Mehrabi-Milne-Home	5.833E-05	1.005E-04	1.000E-06	2.000E-04	1.990E-04

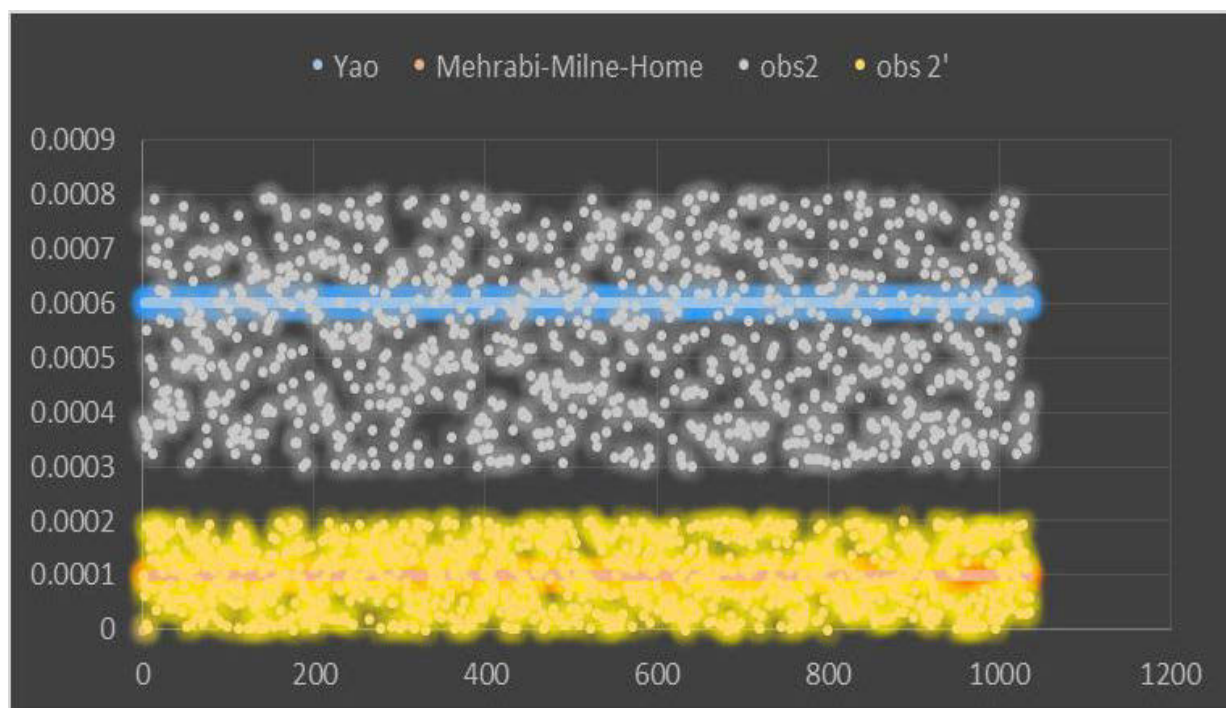


Figure 4-20Concentration realisation: Observation Point 2

Table 4-12Statistical information: Observation Point 2

	Standard Deviation	Mean	Min	Max	Range
Yao	1.423E-04	5.425E-04	3.000E-04	7.990E-04	4.990E-04
Mehrab-Milne-Home	5.833E-05	1.005E-04	1.000E-06	2.000E-04	1.990E-04

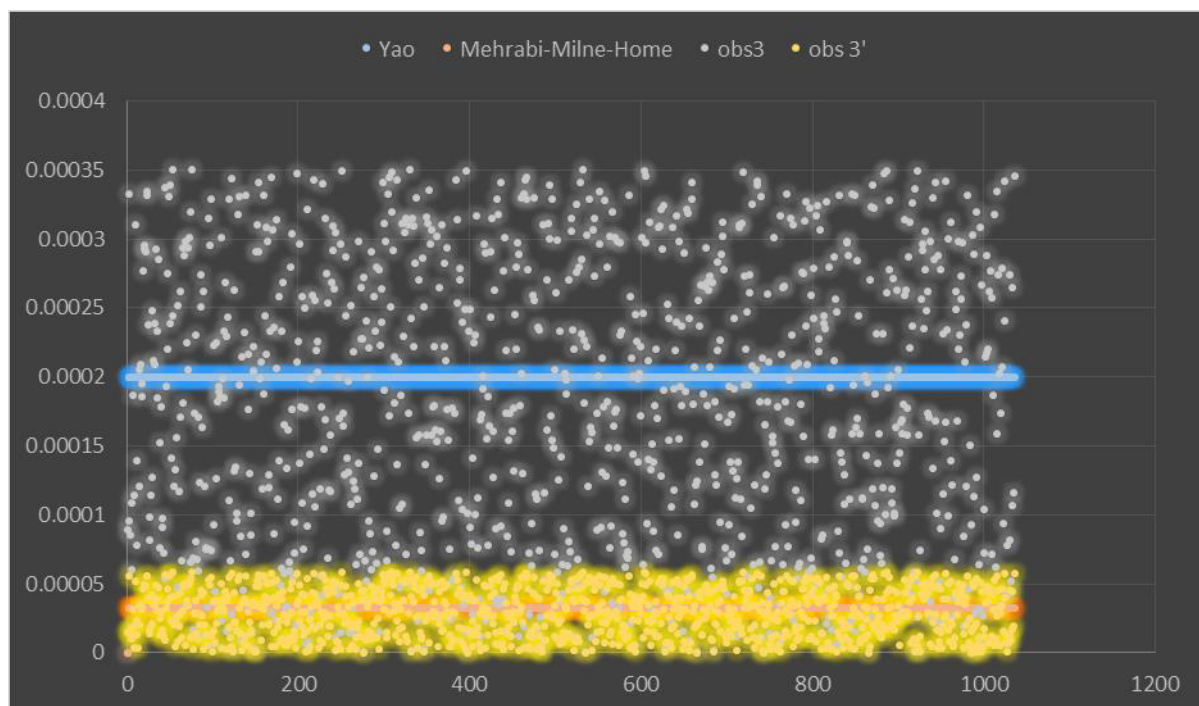


Figure 4-21Concentration realisation: Observation Point 3

Table 4-13Statistical information: Observation Point 3

	Standard Deviation	Mean	Min	Max	Range
Yao	1.026E-04	1.750E-04	1.000E-06	3.500E-04	3.490E-04
Mehrabi-Milne-Home	1.709E-05	2.916E-05	1.667E-07	5.833E-05	5.817E-05

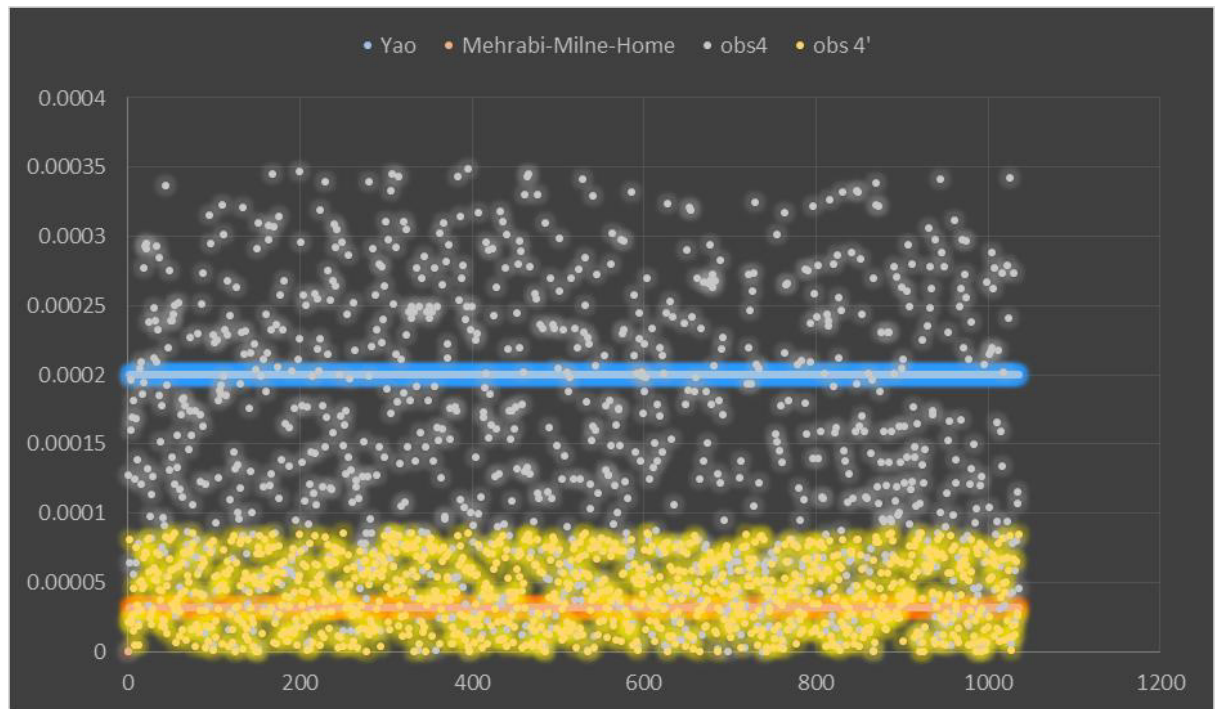


Figure 4-22Concentration realisation: Observation Point 4

Table 4-14Statistical information: Observation Point 4

	Standard Deviation	Mean	Min	Max	Range
Yao	9.441E-05	1.448E-04	2.450E-07	3.490E-04	3.488E-04
Mehrabi-Milne-Home	2.513E-05	4.287E-05	2.450E-07	8.575E-05	8.551E-05

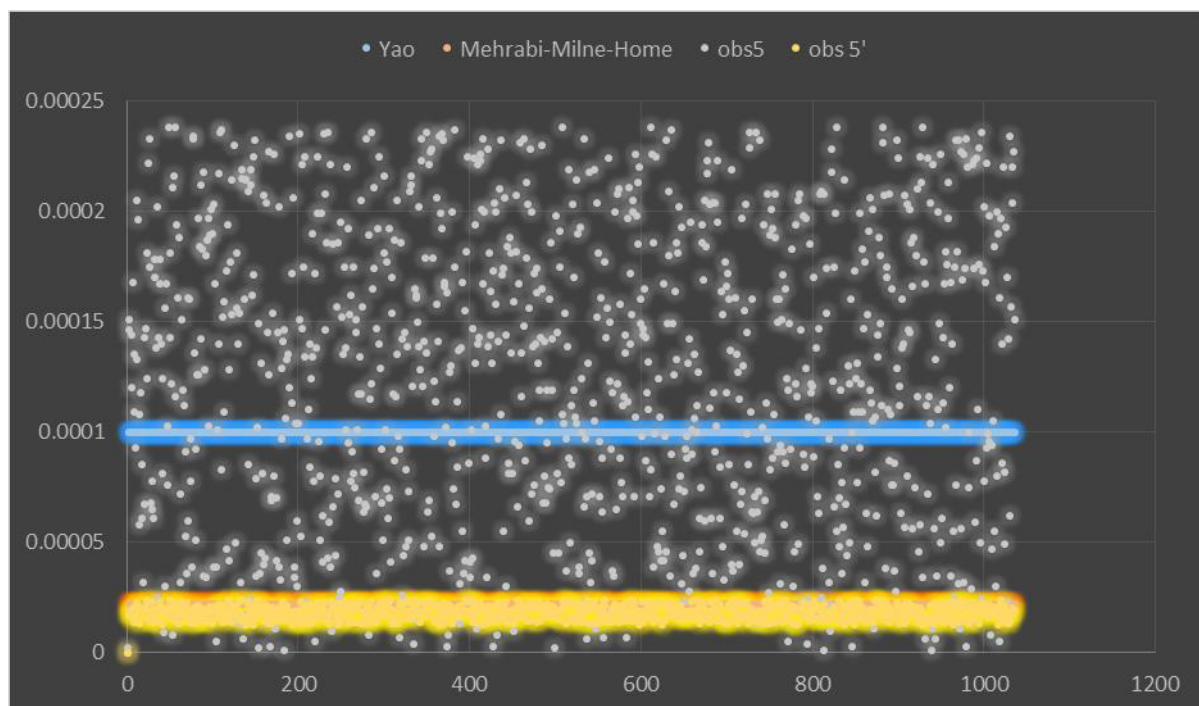


Figure 4-23Concentration realisation: Observation Point 5

Table 4-15Statistical information: Observation Point 5

	Standard Deviation	Mean	Min	Max	Range
Yao	6.722E-05	1.232E-04	1.000E-06	2.380E-04	2.370E-04
Mehrabi-Milne-Home	3.167E-06	1.821E-05	1.530E-09	2.380E-05	2.380E-05

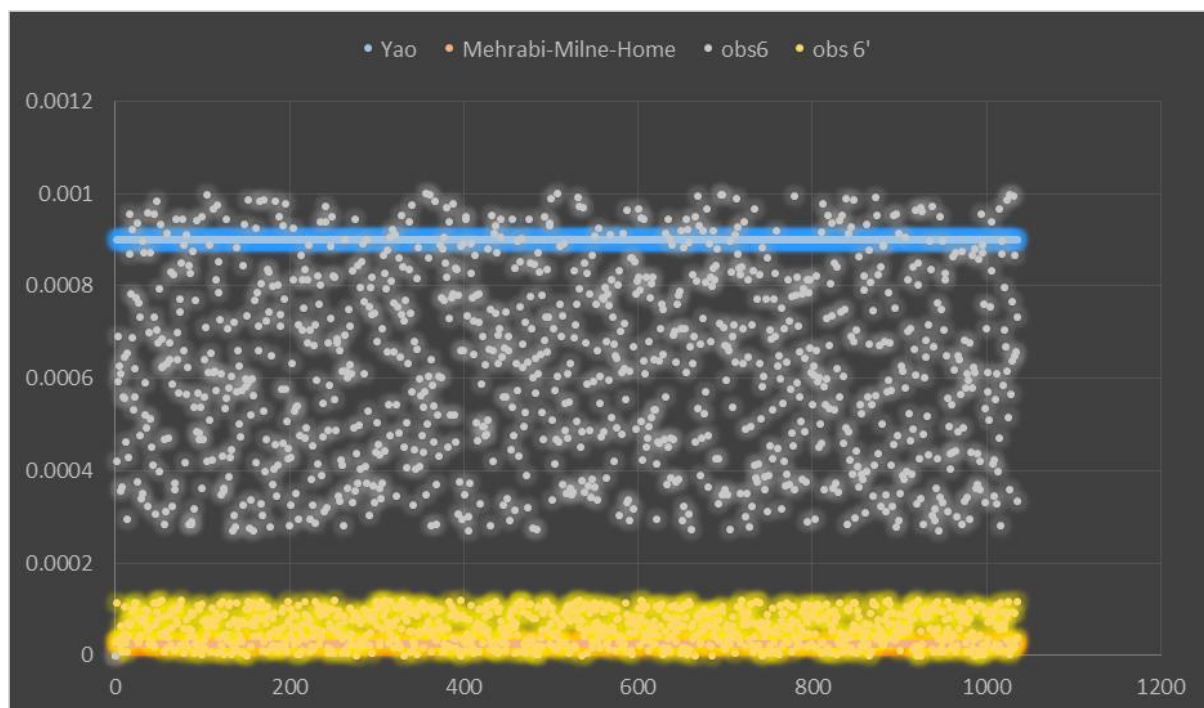


Figure 4-24Concentration realisation: Observation Point 6

Table 4-16Statistical information: Observation Point 6

	Standard Deviation	Mean	Min	Max	Range
Yao	2.071E-04	6.281E-04	6.400E-08	1.000E-03	9.999E-04
Mehrab-Milne-Home	3.486E-05	5.947E-05	3.399E-07	1.190E-04	1.186E-04

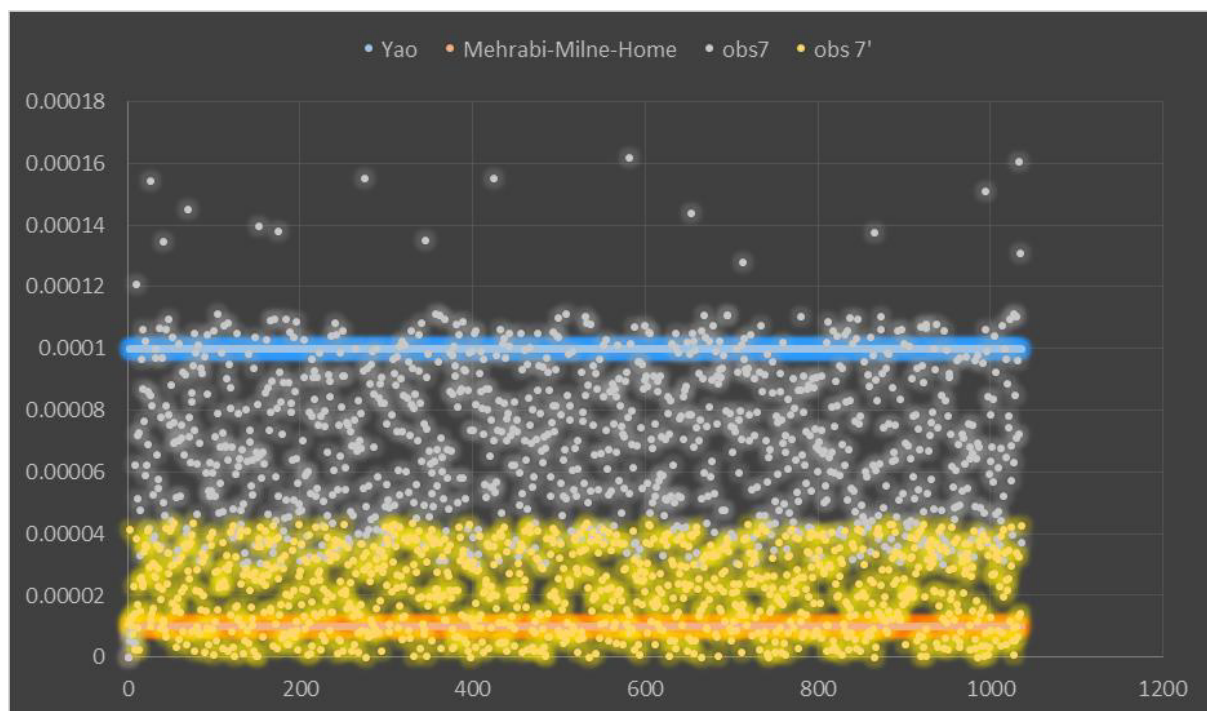


Figure 4-25Concentration realisation: Observation Point 7

Table 4-17Statistical information: Observation Point 7

	Standard Deviation	Mean	Min	Max	Range
Yao	2.508E-05	7.043E-05	7.901E-10	1.620E-04	1.620E-04
Mehrabi-Milne-Home	1.267E-05	2.161E-05	1.235E-07	4.323E-05	4.311E-05

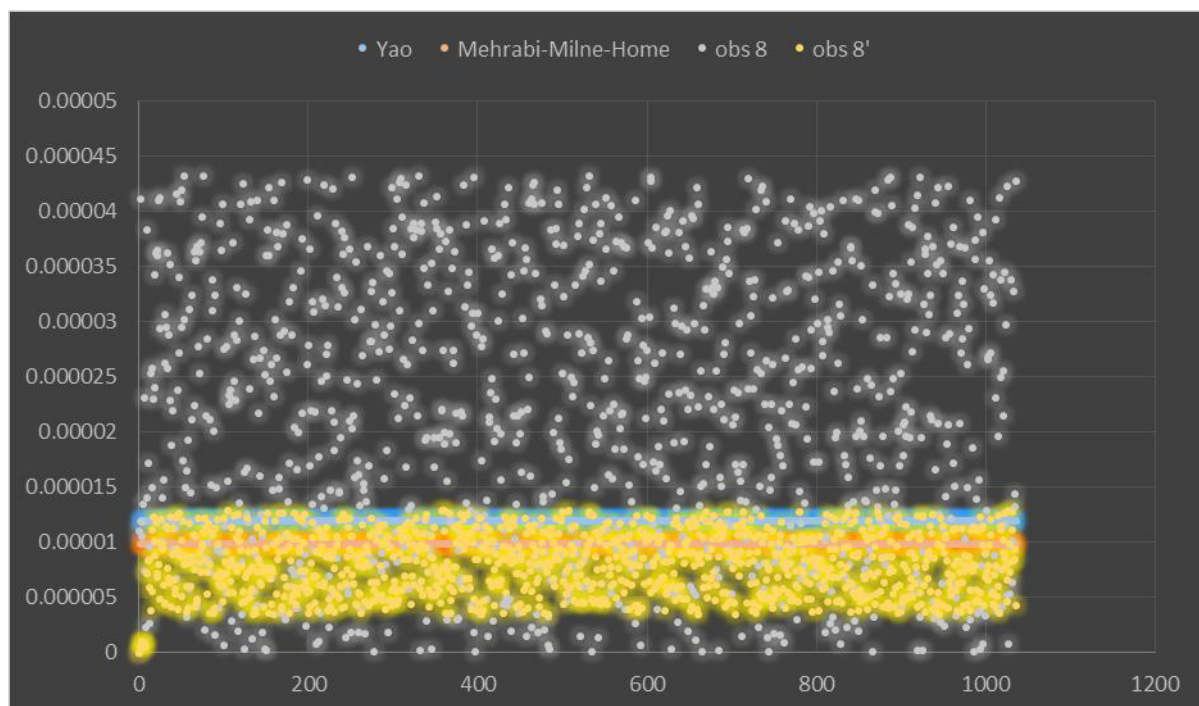


Figure 4-26Concentration realisation: Observation Point 8

Table 4-18Statistical information: Observation Point 8

	Standard Deviation	Mean	Min	Max	Range
Yao	1.267E-05	2.161E-05	1.235E-07	4.323E-05	4.311E-05
Mehrabi-Milne-Home	2.722E-06	8.028E-06	9.134E-11	1.285E-05	1.285E-05

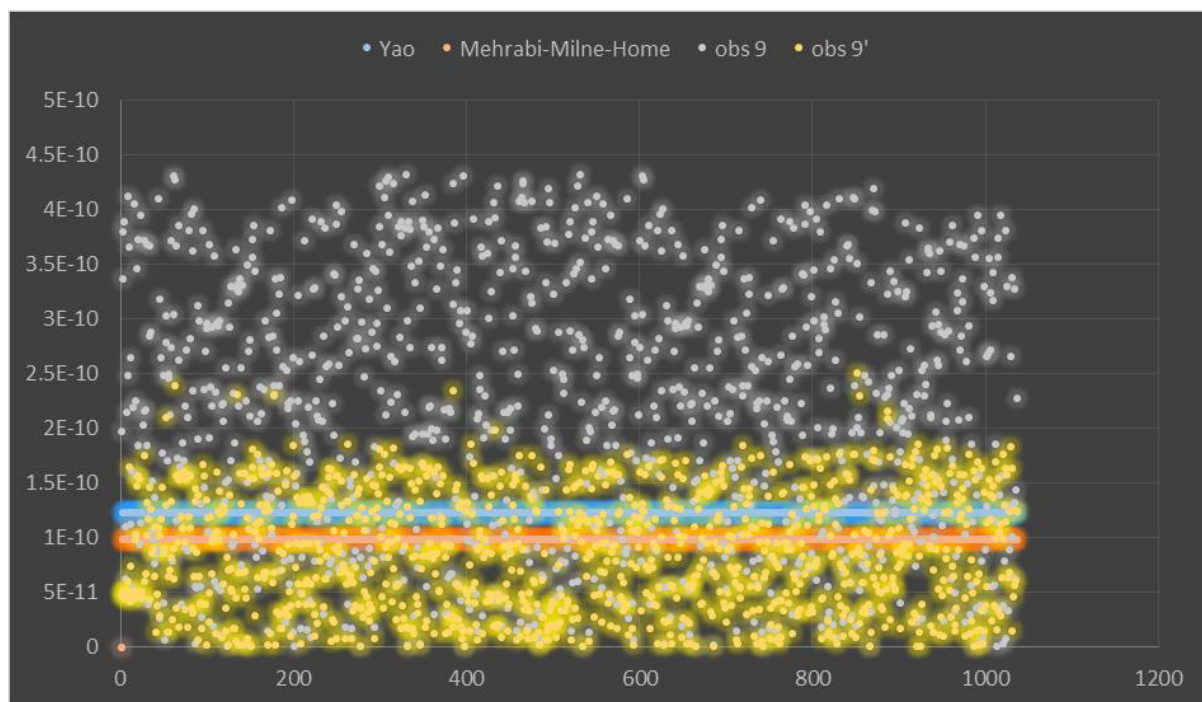


Figure 4-27Concentration realisation: Observation Point 9

Table 4-19Statistical information: Observation Point 9

	Standard Deviation	Mean	Min	Max	Range
Yao	1.202E-10	2.103E-10	1.235E-12	4.323E-10	4.31E-10
Mehrabi-Milne-Home	5.389E-11	8.691E-11	5.310E-13	2.853E-10	2.85E-10

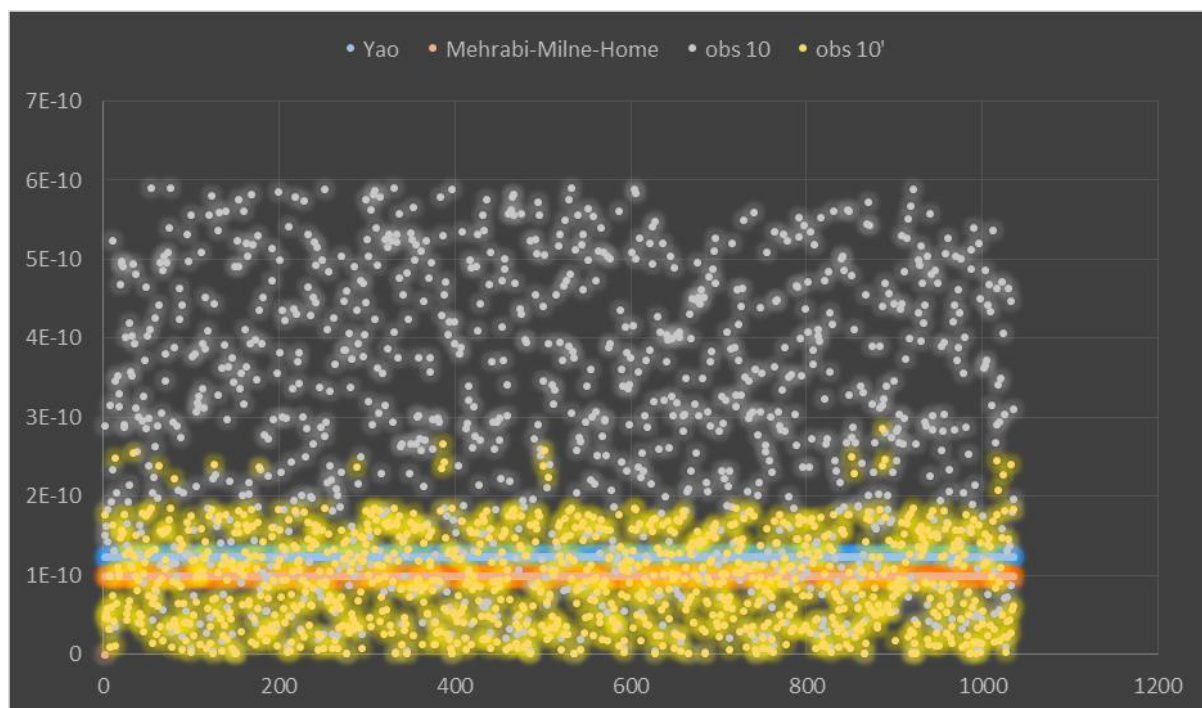


Figure 4-28Concentration realisation: Observation Point 10

Table 4-20Statistical information: Observation Point 10

	Standard Deviation	Mean	Min	Max	Range
Yao	1.676E-10	2.889E-10	1.688E-12	5.910E-10	5.893E-10
Mehrabi-Milne-Home	5.818E-11	9.509E-11	5.310E-13	2.853E-10	2.848E-10

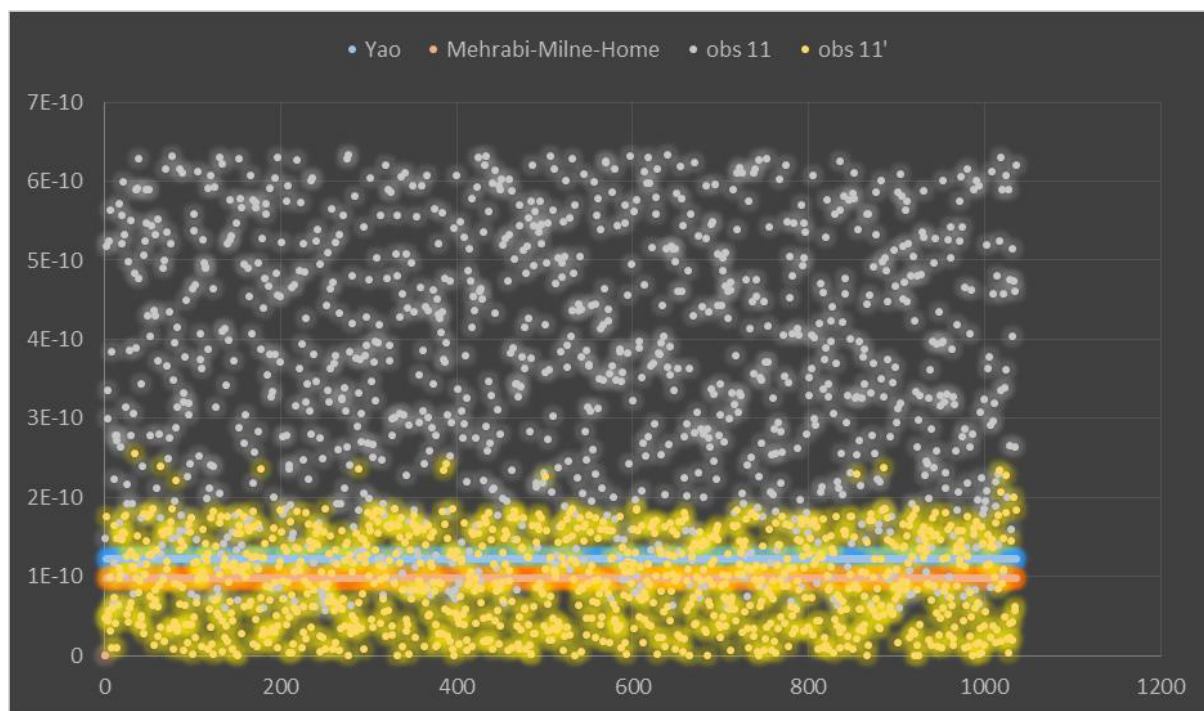


Figure 4-29Concentration realisation: Observation Point 11

Table 4-21Statistical information: Observation Point 11

	Standard Deviation	Mean	Min	Max	Range
Yao	1.662E-10	3.531E-10	5.698E-11	6.331E-10	5.762E-10
Mehrabi-Milne-Home	5.660E-11	9.424E-11	5.310E-13	2.556E-10	2.551E-10

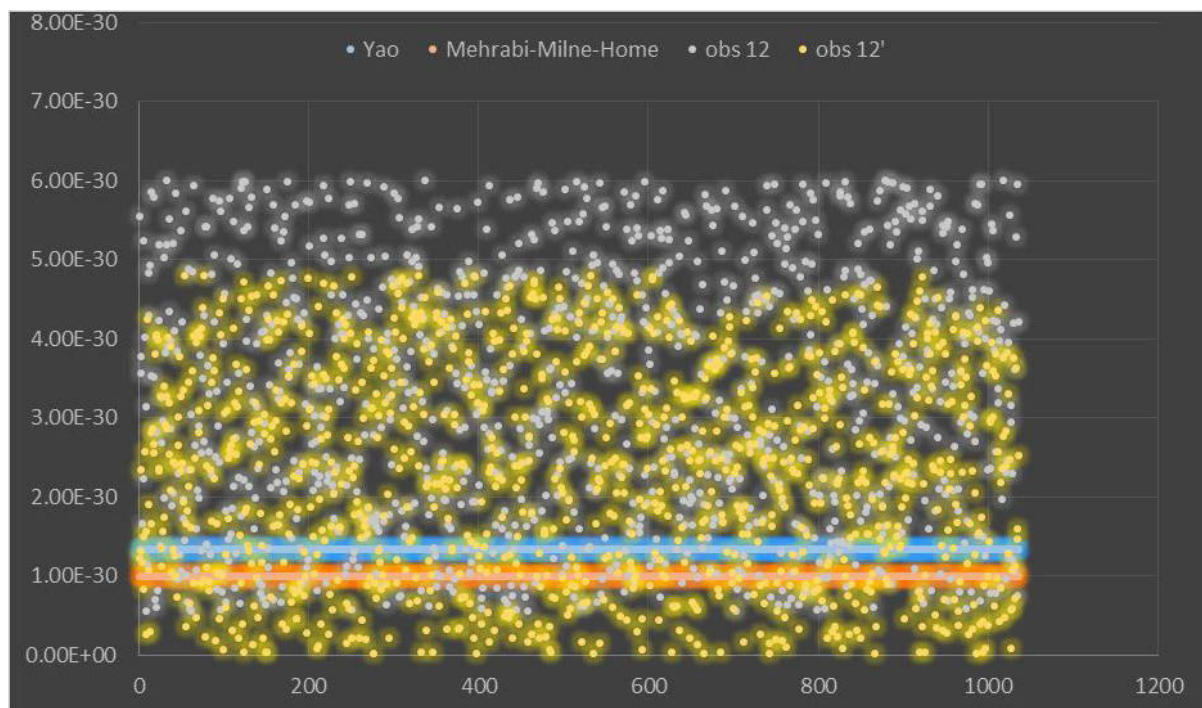


Figure 4-30Concentration realisation: Observation Point 12

Table 4-22Statistical information: Observation Point 12

	Standard Deviation	Mean	Min	Max	Range
Yao	1.619E-30	3.260E-30	5.460E-31	6.000E-30	5.454E-30
Mehrabi-Milne-Home	1.361E-30	2.347E-30	1.372E-32	4.801E-30	4.787E-30

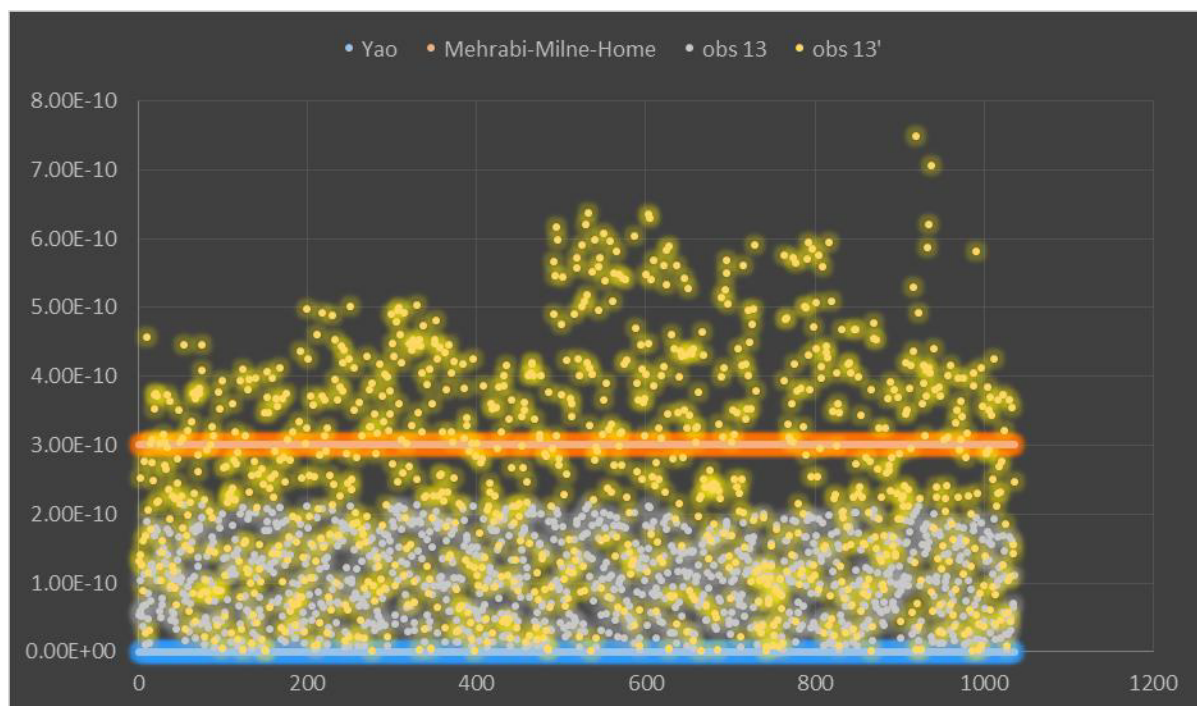


Figure 4-31Concentration realisation: Observation Point 13

Table 4-23Statistical information: Observation Point 13

	Standard Deviation	Mean	Min	Max	Range
Yao	6.033E-11	1.040E-10	6.079E-13	2.127E-10	2.121E-10
Mehrabi-Milne-Home	1.566E-10	2.495E-10	5.896E-13	7.496E-10	7.490E-10

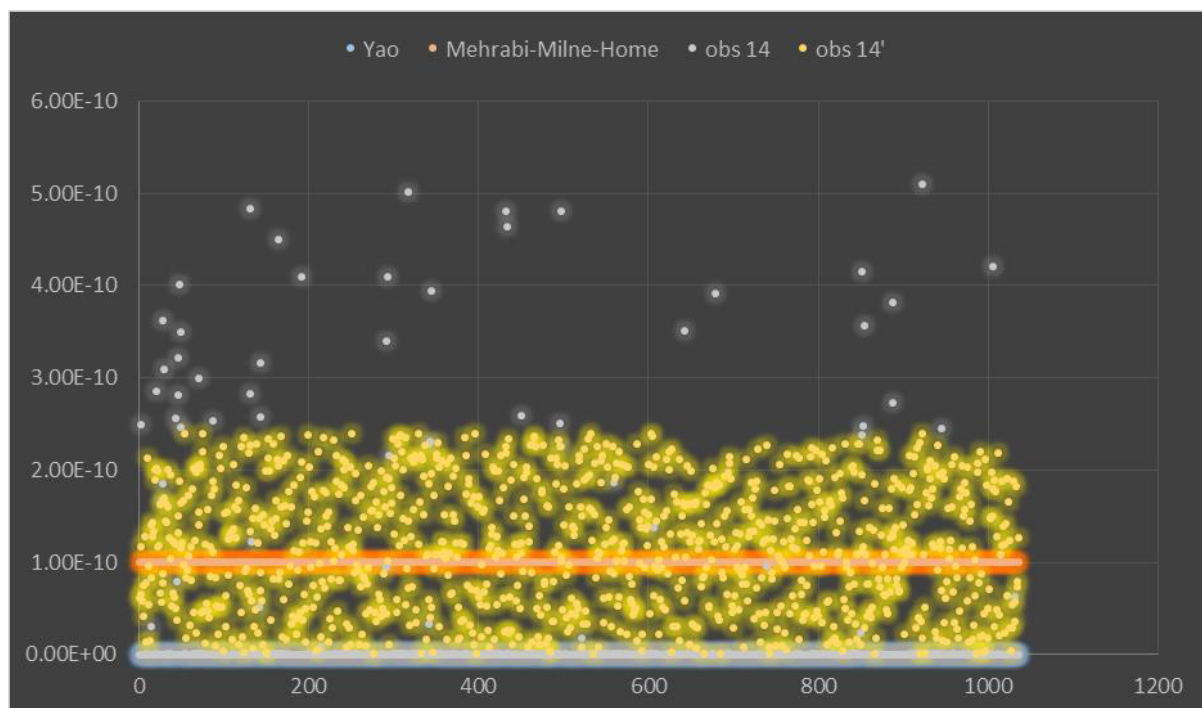


Figure 4-32Concentration realisation: Observation Point 14

Table 4-24Statistical information: Observation Point 14

	Standard Deviation	Mean	Min	Max	Range
Yao	6.955E-11	1.512E-11	1.461E-15	5.098E-10	5.098E-10
Mehrabi-Milne-Home	6.807E-11	1.173E-10	6.858E-13	2.400E-10	2.394E-10

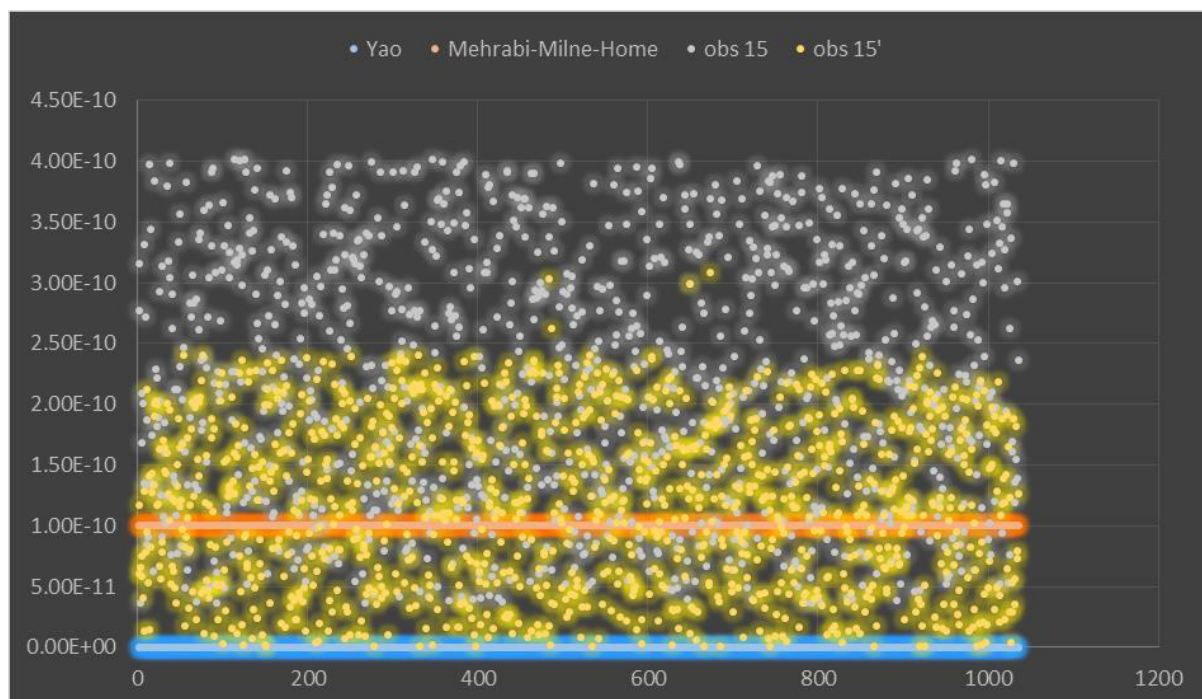


Figure 4-33Concentration realisation: Observation Point 15

Table 4-25Statistical information: Observation Point 15

	Standard Deviation	Mean	Min	Max	Range
Yao	1.046E-10	2.204E-10	3.613E-11	4.015E-10	3.653E-10
Mehrabi-Milne-Home	6.874E-11	1.179E-10	6.858E-13	3.089E-10	3.082E-10

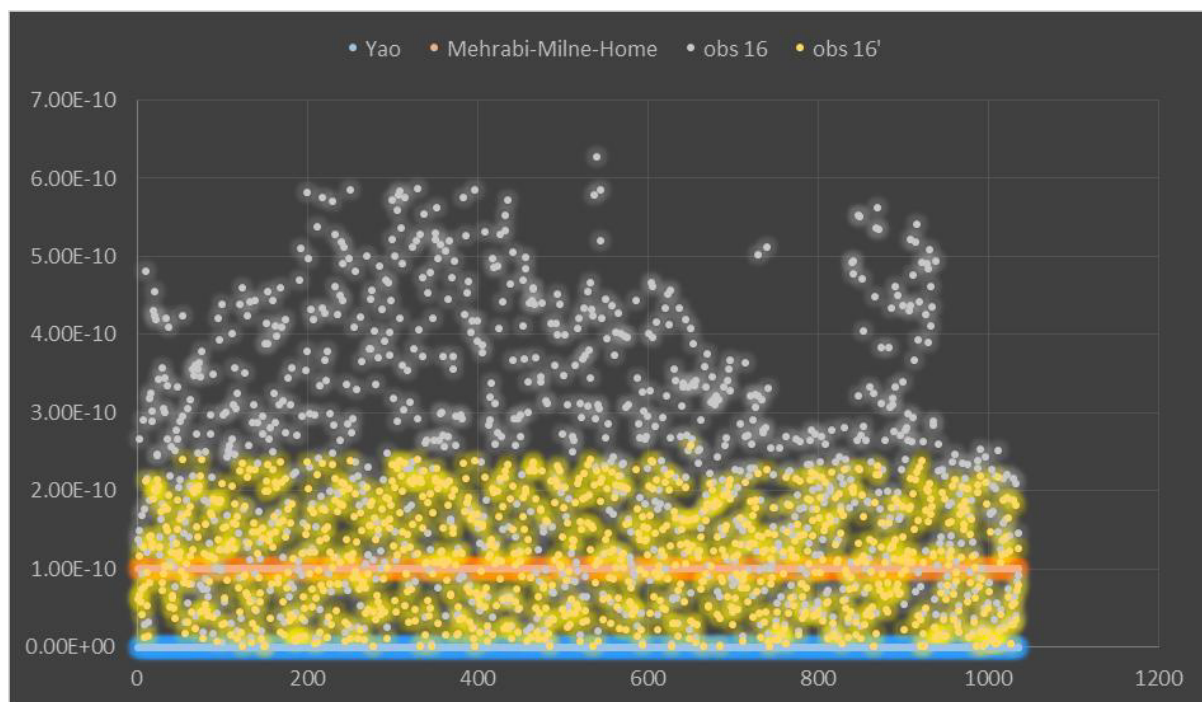


Figure 4-34Concentration realisation: Observation Point 16

Table 4-26Statistical information: Observation Point 16

	Standard Deviation	Mean	Min	Max	Range
Yao	1.501E-10	2.353E-10	7.899E-13	6.276E-10	6.268E-10
Mehrabi-Milne-Home	6.939E-11	1.152E-10	6.858E-13	2.589E-10	2.582E-10

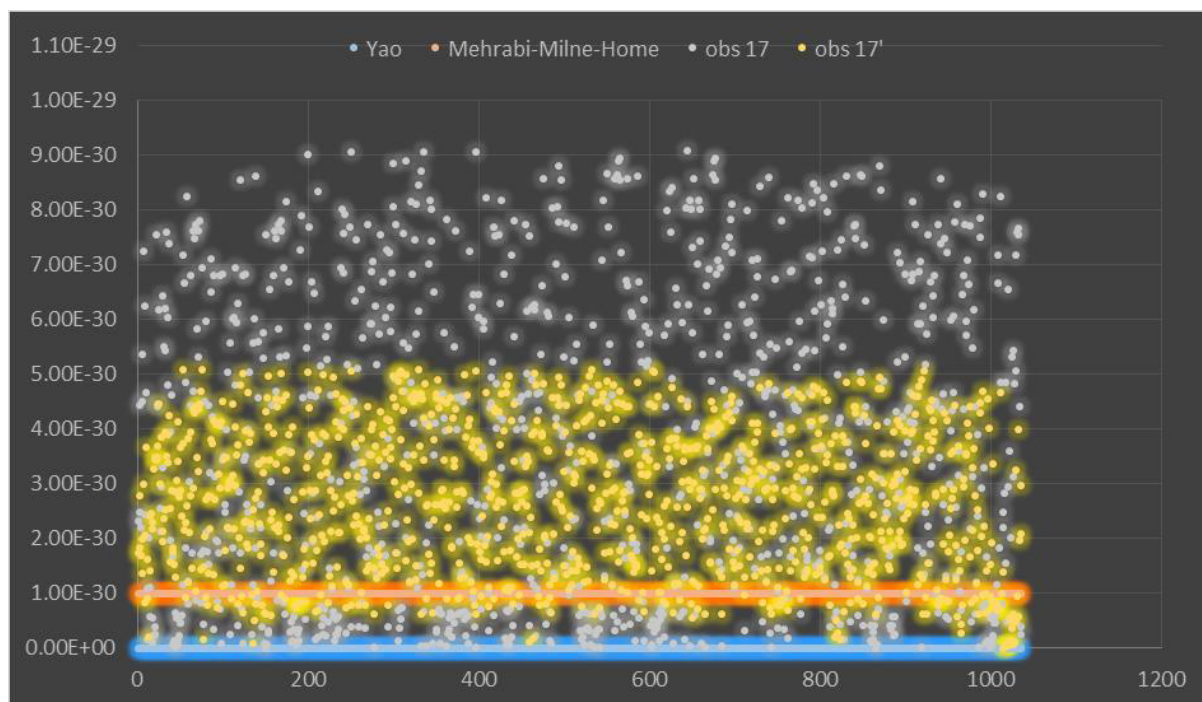


Figure 4-35Concentration realisation: Observation Point 17

Table 4-27Statistical information: Observation Point 17

	Standard Deviation	Mean	Min	Max	Range
Yao	2.727E-30	3.682E-30	2.109E-33	9.081E-30	9.078E-30
Mehrabi-Milne-Home	1.323E-30	2.641E-30	4.348E-33	5.084E-30	5.080E-30

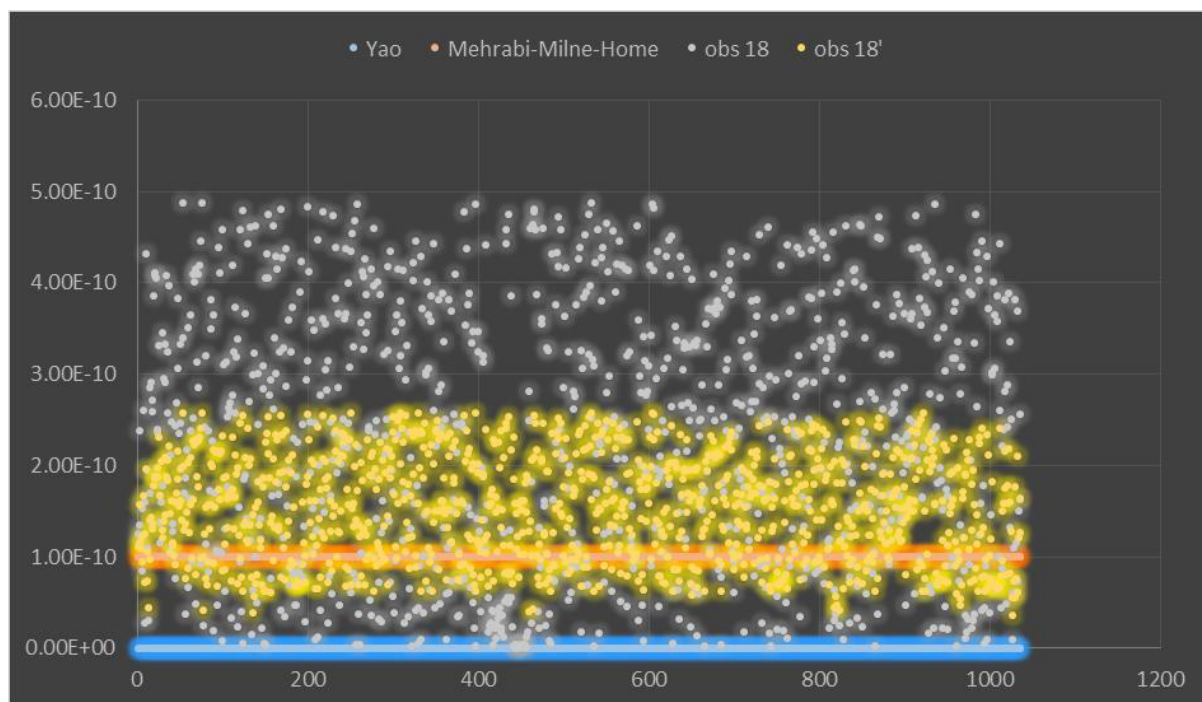


Figure 4-36Concentration realisation: Observation Point 18

Table 4-28Statistical information: Observation Point 18

	Standard Deviation	Mean	Min	Max	Range
Yao	1.414E-10	2.257E-10	3.327E-13	4.871E-10	4.867E-10
Mehrabi-Milne-Home	5.711E-11	1.522E-10	3.641E-11	2.583E-10	2.219E-10

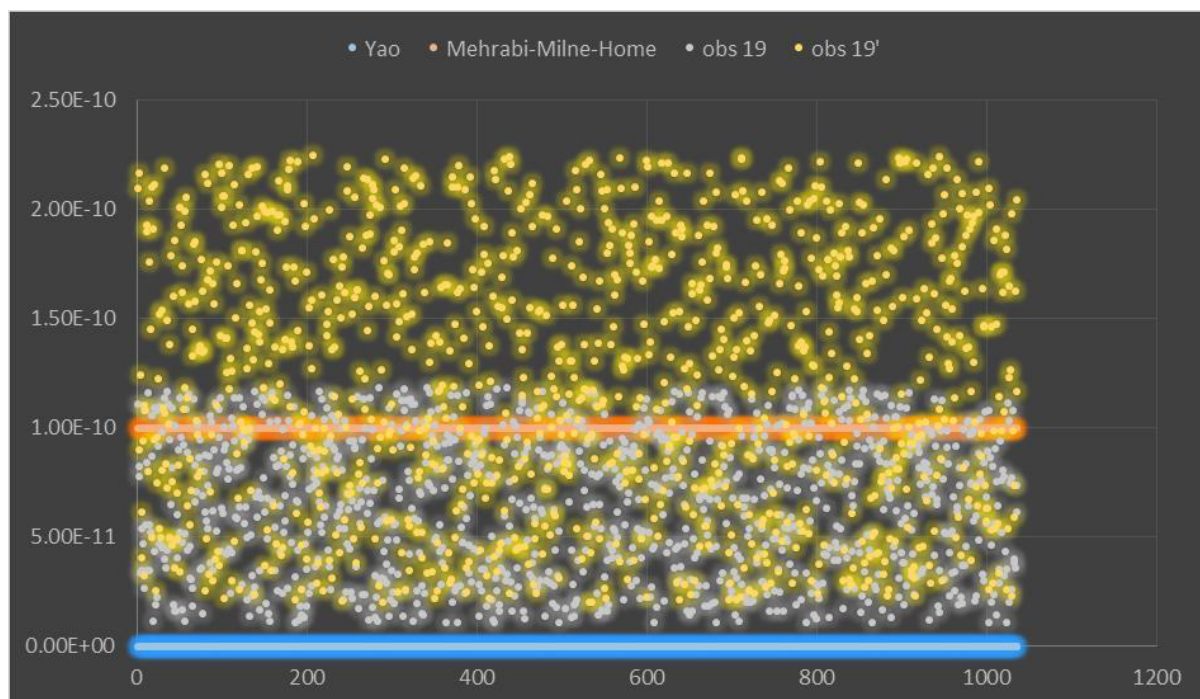


Figure 4-37Concentration realisation: Observation Point 19

Table 4-29Statistical information: Observation Point 19

	Standard Deviation	Mean	Min	Max	Range
Yao	3.161E-11	6.552E-11	1.065E-11	1.182E-10	1.076E-10
Mehrabi-Milne-Home	5.937E-11	1.234E-10	2.022E-11	2.247E-10	2.045E-10

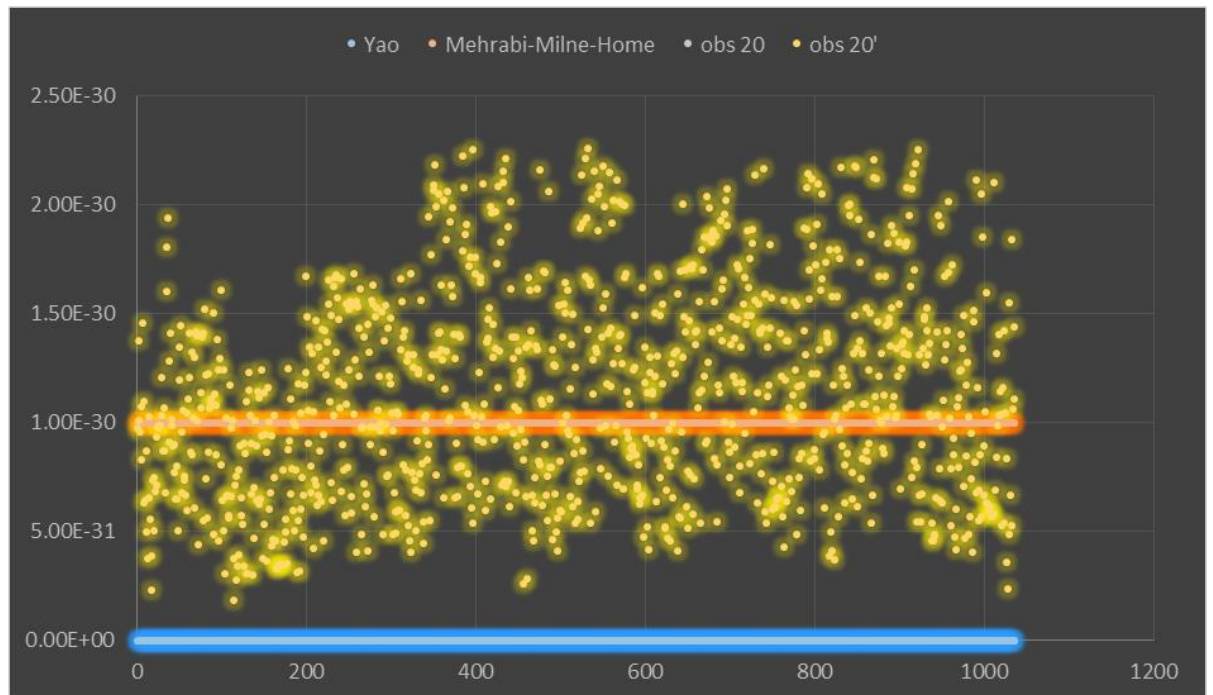


Figure 4-38Concentration realisation: Observation Point 20

Table 4-30Statistical information: Observation Point 20

	Standard Deviation	Mean	Min	Max	Range
Yao	0	0	0	0	0
Mehrabi-Milne-Home	4.740E-31	1.127E-30	1.876E-31	2.259E-30	2.071E-30

Over all, I can endorse other researchers argument in that numerous realizations of model heterogeneity, will ensure the coverage of all possible scenarios as long as the realisations are kept within a realistic range (i.e. when plausible constraints are defined and enforced for the random parameter selection mechanisms). However, challenges are faced with identification of the uncertainty sources as well as computational limitations both with technology and time availability. Monte Carlo is probably one of the very few workable tools for prediction of error propagation and the only well-founded drawback of using it, is being time-consuming.

On the other hand I have shown that by considering hydraulic conductivity heterogeneity in filtration rate simulations, the local bias is tangibly reduced (between 9% and 87%) which in turn, has caused a reduction in uncertainty within the final particle movement results. The predictions based on our equation offer narrower intervals while encompassing more data.

I kept the number of realizations around 1000 which makes this framework practical for the industry and government users. This feature of the framework will improve the likelihood of such sophisticated stochastic methods being used in policy making and management decisions. If adopted as a regulatory framework, this proposition will reduce the uncertainty in predicted data while offering more accuracy. It will expand the present standards of transport modelling in groundwater.

5 Concluding Remarks

“You have to start with the truth. The truth is the only way that we can get anywhere. Because any decision-making that is based upon lies or ignorance can't lead to a good conclusion.”

Julian Assange

This work was an effort to examine the existing modelling tools and equations for predictive simulations of cylindrical nanoparticle transport in saturated porous media; propose improvements to these methods; and, finally, demonstrate the effects of these propositions in a quantitative manner.

The main benefit of this research was building a bridge that joins the traditionally separate realms of research and the real world. I achieved this goal by up-scaling the well-understood equations at laboratory scale to make them usable for field scale applications. Introducing physical heterogeneity of the porous media was, in essence, a volume-averaging method which made this up-scaling effort possible.

The layout of this dissertation displays three major parts:

- the first of the three parts, was allocated to basic information on nanoparticles and their characteristics,
- the second part focused on the mathematical principles and governing equations for particle transport,
- the third and final part demonstrated the application of these equations in a modelling context along with their underlined uncertainties.

In the following sections, I will recap all that was pointed out in this work; sketch a mental diagram that connects all the dots and draws a pathway which links this work to previous work by other researchers; how I built on top of that work; where I see it is headed in the future; highlight all the key results and observations; and conclude with discussions on what those observations mean. I will share our point of view on where some of the remaining gaps are in this field and how future work can attempt to fill these gaps.

5.1 Recapping the Story

Let us recap the story and scan our journey to the wonderland of nanoparticles migration in aquifers from the beginning.

The journey started with defining basics and fundamental information on nanoparticles in general. I discussed their particular characteristics which have turned them into one of the most interesting and popular research topics over the past few decades. Generally speaking, the proportionally large surface area is the key to nanoparticles' super effectiveness compared to the bulk material of the same mass. I touched on the topic of aquifer remediation, and to illustrate this concept, I compared the effectiveness of reactive barrier walls of iron with an injection of iron nanoparticles.

Our next stop was describing the characteristics of some representative nanoparticles. I categorised these ultra-fine particles from various aspects, including their size, production processes, and associated surface treatments. I gave the reader an appreciation of which groups of particles qualify as nanoparticles, what defines an engineered nanoparticle and what are some of the applications they have been designed, produced and used for. I also shed some light on the levels (masses) of production to give the reader some idea of how many of these particles are produced, transported, and used globally.

A discussion of toxicity, or potential toxicity, was put forward based on toxicological studies of other researchers on a variety of engineered nanoparticles. The combination of these key points: the ever increasing usage of engineered nanoparticles in so many industries, the mass production of these materials by hundreds of tons annually, with strong prospect of increased production over time and, lastly, the risks associated with exposure to these materials, laid the foundations on which I highlighted the importance of understanding their transport in a natural aquatic subsurface environment.

Carbon nanotubes (CNTs) were identified as one of (if not) the most popular engineered nanoparticles. Praised for their versatility when it comes to chemical, physical, electrical, structural, and elastic properties, they are being mass produced by hundreds of tons, heading to thousands in the next few years. Worthy of a detour, I took you through the history of CNT, when it was observed for the first time and how it was synthesised, what characteristics it displays, what types does it fall into and how it is treated to form stable suspensions in water.

You fastened your seatbelt and, together, I took off to the land of mathematical equations which represent the natural system(s) considered in this work. We visited the traditional approaches to particle transport modelling, focused on cylindrical nanoparticles (with CNT as a generic example), and singled out Yao's modified version of the filtration theory as the most suitable equation for simulating the transport of cylindrical nanoparticles in a saturated porous media. This conclusion was founded on the work of several researchers before us. Together, we developed a sound understanding of what the conventional ways of simulating transport of nanoparticles are and what is missing from these approaches. Our next obvious step was to propose a technique to improve the current methods.

A discussion of natural heterogeneity was brought up. If a bridge is going to be built to link the real world to a research laboratory, where all experiments are performed under tightly controlled conditions and the porous media is homogeneous, the natural heterogeneity has to be introduced to the system simulation. This was the hurdle I needed to pass. The question was: how to consider porous media's heterogeneity? This was a particularly challenging obstacle while using an equation which essentially required the user to assume homogeneity by defining a single value as the mean collector diameter to represent the full body of the porous medium. These discussions presented a question of scale. Could the filtration theory represent a natural heterogeneous system (Darcy-scale system) closely enough?

Our first substantial contribution to solving this matter came about when I exhaustively reviewed numerous relationships between grain size, grain size distribution and permeability

parameters of a porous media in search of the most comprehensive equation which defined the correlation between these parameters. Researchers have explored and proposed these relationships since the early-1800s. I investigated a series of the most promising of several equations and bench-marked them against a set of real measured data from Australian soil samples to make this selection. The result of the selection was the Alyamani-Sen equation which was then appropriately reorganised to be suitable for up-scaling the filtration theory. With confidence in this mathematical modification, I re-developed the filtration theory, this time, with the inclusion of natural physical heterogeneity of the porous media. This up-scaling exercise not only makes the filtration theory suitable for a Darcy-scale simulation in terms of heterogeneity of any given natural system, but also it makes it conceivable for a modeller to consider the use of the newly developed equation as it uses parameters that are commonly measured during field investigations, such as hydraulic conductivity and porosity, instead of detailed pore-scale parameters only quantifiable under strictly controlled laboratory conditions.

At this point, I proposed a new equation to replace Yao's filtration theory. I claimed it would better simulate the transport of cylindrical nanoparticles as it was able to consider heterogeneity of the soil using permeability parameters. Inclusion of various types of heterogeneity, such as geochemical heterogeneity, was previously shown to have improved the agreement between computed and observed data. However, to the best of our knowledge, inclusion of the physical heterogeneity had never been investigated in this manner and hence it was not known to us just how different the results of a simulation were going to be between Yao's equation and our proposed equation. It was time to dive into the depths of the groundwater modelling boundless ocean.

Our second significant contribution occurred when I selected software packages, identified as industry-standard and developed a general intrusive rate-calculation algorithm to incorporate our equation into a Darcy-scale group of equations of reactive transport in saturated porous

media. I used PHT3D, coupling MT3DMS and PHREEQC to allow for a flexible structure of modular codes for calculations of rates for any species of interest. This rate calculation algorithm will be added to the official PHT3D database following the publication of the paper submitted to the Journal of Environmental Modelling and Software.

Using our new modelling code, I simulated a heterogeneous system in MODFLOW and created a hypothetical source of CNT in this system. I then inspected the results of three model scenarios: first; tracer transport (a non-reactive and non-adsorbing specie), second; CNT transport using Yao's equation, and third; CNT transport using our equation. A step by step visualization of the transport was provided to highlight the variations, not only in transported concentrations but also in transport patterns among the presented scenarios. I answered a question raised earlier: does it make a perceptible difference in the model results if we consider heterogeneity? Or are the outcomes similar to those of Yao's equation and negligibly different from the previous approaches? These illustrated variations confirm that our modification does result in significantly different outcomes.

I established that our equation makes a significant difference in the results of transport modelling, but naturally, I would like to show that these differences are correspondingly indicative of a better and more accurate outcome. Here, I raised the question of uncertainty; taking the reader through the basic concept of uncertainty, its roots and sources, and the ways of dealing with it. I examined many suppositions by other researchers who focused on uncertainty and concluded that, in the context of groundwater modelling, the main source of uncertainty is considered to be heterogeneity of the porous media. The objective was clear: demonstrate whether or not our inclusion of this type of heterogeneity has led to less uncertainty in the results.

I started our demonstration by defining constraints for hydraulic conductivity and running Monte Carlo Simulation for two scenarios of our model: Yao's version and ours. Random fields of hydraulic conductivity were generated (in excess of one thousand) and each

realization was run. The results were observed and compared over the 20 points selected within the model grid. I took you through the statistical analysis of these results as well as visually showing you the tighter confidence band offered by the band of results when our equation was in use. A simple and clear answer to the research question: our equation successfully introduced heterogeneity into the filtration theory by up-scaling this equation, it resulted in meaningfully different results for CNT transport, and it reduced the uncertainty associated with the transport model when heterogeneity of porous media is considered to be the main source of uncertainty.

5.2 Observations and Results

Let us state specific results and observations, noted as this work progressed; from the very first step of outlining the research question to equation development, testing and benchmarking the model, and to the final stage of stochastic simulations.

Starting with the statement of the problem (or the research question), I cited the works of many others and made the following key observations:

1. Water resources are globally stressed.
2. Groundwater resources should be protected as a safer source of water protected from excessive evaporation.
3. Groundwater pollution is showing an increasing trend.
4. New types of contaminants can go un-noticed as they are rarely tested for.
5. Managed aquifer recharge (MAR) has the potential to introduce these new contaminants by injecting urban run-off into aquifers.
6. Engineered nanoparticles (ENP) are a group of new and emerging contaminants which have recently been detected in groundwater, surface water, and aquatic animals.
7. Many ENPs have been tagged as toxic to human cells and the environment.
8. These ENPs have been mass produced for various products and also have been used for groundwater and soil remediation.

9. The communities are concerned about ENPs and there is a need to increase the extent of our knowledge about their fate and transport in the natural environment.
10. Combination of all the observations above, enabled us to highlight the importance and significance of the research objective: to better understand the transport of cylindrical NPs in aquifers.
11. Transport mechanism of colloids (including ENPs and other micro and nanocolloids) are important in many fields such as water treatment systems, contaminant transport in the soil column and aquifers, contamination treatment in aquifers, microorganism migration on aquifers, clinical testing and drug delivery.
12. Various treatments are necessary to make many aggregating ENPs dispersed for the purpose of use in products. These treatments can lead to long term dispersivity of ENPs in aquatic environments which increases their mobility and the risk of exposure.
13. Filtration of colloidal particles is governed by three main mechanisms: sedimentation, interception, and diffusion.
14. Particle shape has an impact on the filtration rate hence classical filtration theory was modified to account for the cylindrical shape of particles such as CNTs.
15. Particle orientation can also have an impact on filtration when aspect ratio of any given particle is not equal to 1.
16. Our particle flow modelling illustrated that physical heterogeneity causes dispersion. In a Darcy scale system dispersion is the dominant lateral transport mechanism substituting diffusion in a pore scale system. In other words, transport through heterogeneous media causes large scale spreading. This phenomenon was also observed and reported by Sampath (2006).
17. Filtration theory has an inherent shortcoming for simulating a Darcy scale system by using a single value for grain size to represent a large body of a porous medium.
18. Using laboratory measured samples, I showed that mean grain size cannot adequately represent the permeability of a porous medium.

19. Up-scaling of filtration theory is the key to representing natural heterogeneity of the porous media.
20. Alyamani-Sen equation offers the most accurate correlation between grain size and permeability and covers a wide range of soil types.
21. Single collector efficiency shows a better agreement with hydraulic conductivity values after the inclusion of heterogeneity.
22. I observed that particle mobility can increase when heterogeneity is considered.
23. Colloid transport modelling started in the early 1970s and many conceptual approaches have been proposed and tested to date.
24. The most common modelling theories today are: advection-dispersion equation, irreversible attachment, equilibrium adsorption, and kinetic adsorption.
25. I modelled CNTs using our equation and Yao's equation. Significant differences were observed between the two scenarios.
26. I estimated the uncertainty of each scenario and examined the reasons for lesser uncertainty associated with our equation.

5.3 Conclusions and Discussions

Based on the observations and results mentioned in the previous section, a number of conclusions were made.

By using hypothetical scenarios for CNT transport through saturated porous media with various proportions of side and end contact, I concluded that particle orientation can have a significant impact on the total filtration of the particles as they migrate through the porous medium. However, to the best of our knowledge, there is no established method or existing dataset that examines the orientation of cylindrical particles as they move through a water-saturated porous media. This is partially because of the fast random Brownian motion type

movement of the particles that has been examined in viscous, gluey matrix of polymer material.

Heterogeneity of porous media's permeability can be introduced into the filtration theory using up-scaling method of volume averaging. This inclusion of natural heterogeneity resulted in a better correlation between hydraulic conductivity and collector efficiency.

Up-scaled filtration theory transforms this equation to a practical model for a Darcy-scale real-world problem. It also makes the theory usable as it utilises the field-measured parameters instead of laboratory measured pore scale parameters.

Both filtration equations (Yao's and ours) result in particle sorption. This was benchmarked against a tracer with zero sorption tendency.

The up-scaled filtration theory for cylindrical nanoparticles results in different transport patterns as well as different concentrations showing that transport through a heterogeneous porous media causes a much larger scale smearing and spreading of the particles.

Inclusion of heterogeneity enhances the dilution of the concentration while increasing the total coverage of the spread.

Pore-scale diffusion has a small impact on longitudinal Darcy scale dispersion, though it has a slightly larger influence on transverse Darcy scale dispersion.

The use of our equation reduces the sensitivity of those parameters used in filtration rate calculation. With less sensitivity, the impact of errors on the final results becomes less significant, leading to more accurate results with less uncertainty.

Using our equation, the model results show a much narrower range of uncertainty at the selected points, indicating a reduction of uncertainties caused by the inherent uncertainty in natural heterogeneity of the porous media.

I also conclude that by defining sensible constraints, Monte Carlo stochastic modelling can become more practical in terms of computational demand and run times, and, hence can be adopted in policy making and resource management practices.

This work lays the foundations for a framework which will allow further advances in bridging the gap between research and practice when it comes to non-traditional emerging issues. It also promotes the introduction of a probabilistic modelling approach, backing decision support systems. This framework is illustrated in Figure 5-1.

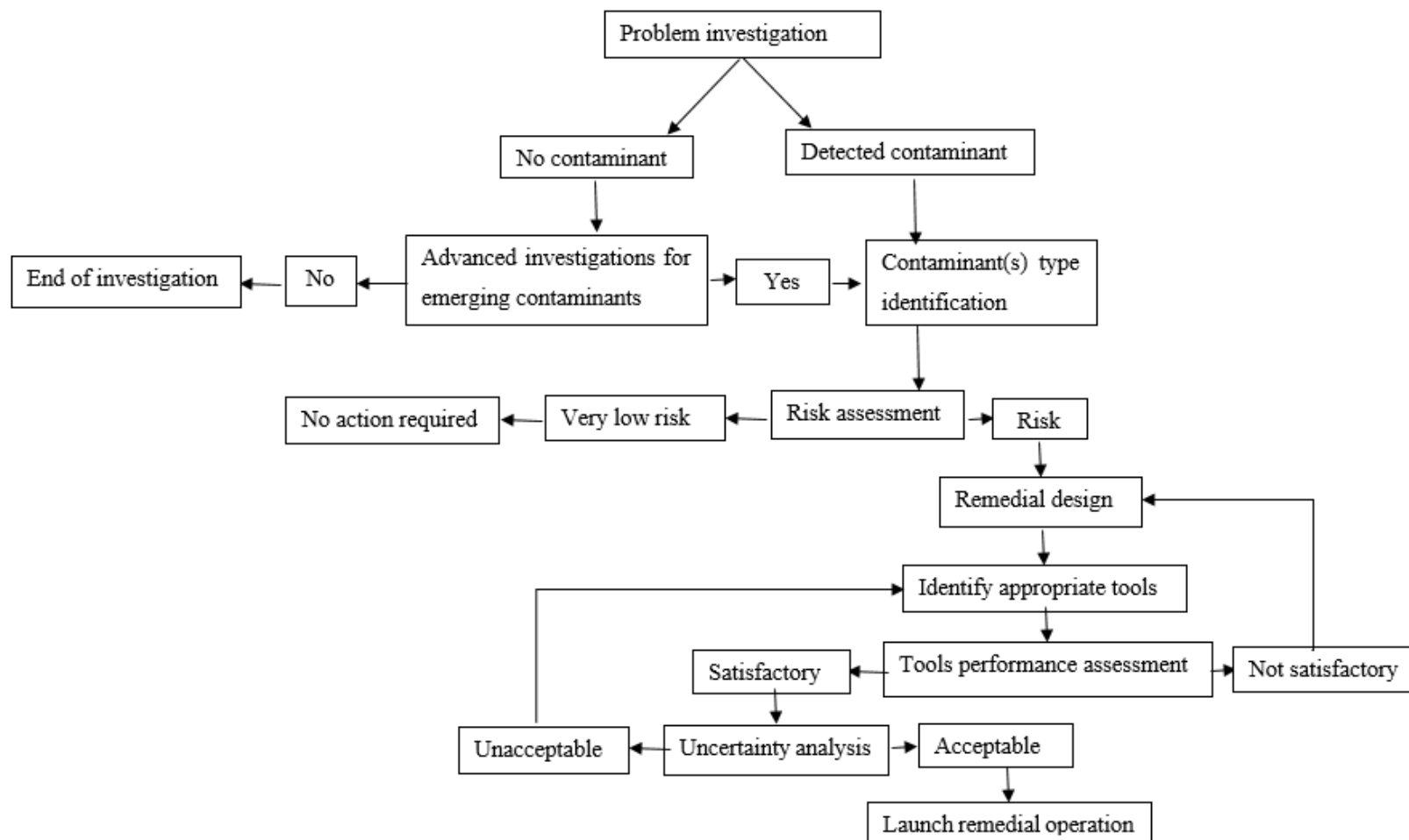


Figure 5-1 Proposed framework for assessment of emerging contaminants

5.4 Future Research

Engineered nanoparticles are a relatively new group of materials that are finding increasing popularity every day. There is still much unknown about their toxicity and other long-term adverse impacts in the environment. There is much need for developing detailed safe handling guidelines for various nanoparticles as well as environmental guidelines for various users (including but not limited to drinking water). At the same time, a large proportion of research work can focus on new applications for the existing ENPs and /or engineering new ones for specific purposes.

As mentioned in the previous section, the orientation of cylindrical nanoparticles can significantly alter the filtration rate but there are no studies to determine the factors that govern the orientation of these particle as they travel in an aqueous environment. This is a potential area for future research work.

It is conceivable to hypothesise that pore geometry would also affect the filtration of the particles, as it impacts the localised velocity fields. Further work is necessary to determine the relationship between pore geometry and filtration.

Benchmarking our equation against a 3D field-scale experimental dataset is very desirable and can be a potential research topic.

Let us end on a note of common sense: behind every sensible model, is a knowledgeable modeller supported by well measured data and robust information. When predicting the transport of a less known specie, in the absence of much real data, all precautions should be taken. Considering all possibilities within a set of realistic constraints can reduce the biases of human involvement and the errors of measurements (caused by tools or natural fluctuations) and give a more holistic image of the issue of concern. This approach is deemed particularly suitable for management decisions and policy making.

Appendix A- Original PHT3D Rates

Database

```
#####
# Description: PHREEQC-2 Database
# Modified to simulate transport of bacteria
#####

SOLUTION_MASTER_SPECIES
#
#element species      alk  gfw_formula  element_gfw
#
H      H+          -1.  H          1.008
H(0)   H2          0.0  H
H(1)   H+          -1.  0.0
E      e-          0.0  0.0      0.0
O      H2O         0.0  O          16.00
O(0)   O2          0.0  O
O(-2)  H2O         0.0  0.0
Ca      Ca+2        0.0  Ca          40.08      #Ca
Mg      Mg+2        0.0  Mg          24.312      #Mg
Na      Na+         0.0  Na          22.9898      #Na
K      K+           0.0  K          39.102      #K
Fe      Fe+2        0.0  Fe          55.847      #Fe
Fe(+2) Fe+2         0.0  Fe          #Fe2
Fe(+3) Fe+3        -2.0  Fe          #Fe3
Mn      Mn+2        0.0  Mn          54.938      #Mn
Mn(+2) Mn+2         0.0  Mn
Mn(+3) Mn+3         0.0  Mn
Al      Al+3        0.0  Al          26.9815      #Al
Ba      Ba+2        0.0  Ba          137.34      #Ba
Sr      Sr+2        0.0  Sr          87.62      #Sr
Si      H4SiO4       0.0  SiO2         28.0843      #Si
Cl      Cl-         0.0  Cl          35.453      #Cl
C      CO3-2        2.0  HCO3         12.0111
C(+4)  CO3-2        2.0  HCO3
C(-4)  CH4          0.0  CH4
Alkalinity CO3-2    1.0  Ca0.5(CO3)0.5  50.05
S      SO4-2        0.0  SO4          32.064
S(6)   SO4-2        0.0  SO4          #SO4
S(-2)  HS-          1.0  S
N      NO3-         0.0  N          14.0067
N(+5)  NO3-         0.0  N          #NO3
N(+3)  NO2-         0.0  N          #NO2
N(0)   N2           0.0  N
Amm     AmmH+       0.0  AmmH         17.0      #NH4
B      H3BO3        0.0  B          10.81
P      PO4-3        2.0  P          30.9738
F      F-           0.0  F          18.9984      #F
Br      Br-          0.0  Br          79.904      #Br
Zn      Zn+2        0.0  Zn          65.37      #Zn
Cd      Cd+2        0.0  Cd          112.4      #Cd
```

Pb	Pb+2	0.0	Pb	207.19	#Pb
Cu	Cu+2	0.0	Cu	63.546	#Cu
Cu(+2)	Cu+2	0.0	Cu		
Cu(+1)	Cu+1	0.0	Cu		
Orgc	Orgc	0.0	Orgc	30	
Tracer	Tracer	0.0	Tracer	1	
Tmp	Tmp	0.0	Tmp	1	
Orgc_sed_l	Orgc_sed_l	0.0	Orgc_sed_l	1	
Coliforms_m	Coliforms_m	0.0	Coliforms_m	1	
Ecoli_m	Ecoli_m	0.0	Ecoli_m	1	
Coliforms_im	Coliforms_im	0.0	Coliforms_im	1	
Ecoli_im	Ecoli_im	0.0	Ecoli_im	1	
Carbnano_m	Carbnano_m	0.0	Carbnano_m	1	
Carbnano_im	Carbnano_im	0.0	Carbnano_im	1	

SOLUTION_SPECIES

H+ = H+

log_k	0.000	
-gamma	9.0000	0.0000

e- = e-

log_k	0.000
-------	-------

H2O = H2O

log_k	0.000
-------	-------

Orgc_sed_l = Orgc_sed_l

log_k	0.000
-------	-------

Ca+2 = Ca+2

log_k	0.000	
-gamma	5.0000	0.1650

Mg+2 = Mg+2

log_k	0.000	
-gamma	5.5000	0.2000

Na+ = Na+

log_k	0.000	
-gamma	4.0000	0.0750

K+ = K+

log_k	0.000	
-gamma	3.5000	0.0150

Fe+2 = Fe+2

log_k	0.000	
-gamma	6.0000	0.0000

Mn+2 = Mn+2

log_k	0.000	
-gamma	6.0000	0.0000

Al+3 = Al+3

log_k	0.000	
-gamma	9.0000	0.0000

Ba+2 = Ba+2
log_k 0.000
-gamma 5.0000 0.0000

Sr+2 = Sr+2
log_k 0.000
-gamma 5.2600 0.1210

H4SiO4 = H4SiO4
log_k 0.000

Cl- = Cl-
log_k 0.000
-gamma 3.5000 0.0150

CO3-2 = CO3-2
log_k 0.000
-gamma 5.4000 0.0000

SO4-2 = SO4-2
log_k 0.000
-gamma 5.0000 -0.0400

NO3- = NO3-
log_k 0.000
-gamma 3.0000 0.0000

H3BO3 = H3BO3
log_k 0.000

PO4-3 = PO4-3
log_k 0.000
-gamma 4.0000 0.0000

F- = F-
log_k 0.000
-gamma 3.5000 0.0000

Br- = Br-
log_k 0.000
-gamma 3.0000 0.0000

Zn+2 = Zn+2
log_k 0.000
-gamma 5.0000 0.0000

Cd+2 = Cd+2
log_k 0.000

Pb+2 = Pb+2
log_k 0.000

Cu+2 = Cu+2
log_k 0.000
-gamma 6.0000 0.0000

Orgc = Orgc
log_k 0.000

Tracer = Tracer
 log_k 0.000

Tmp = Tmp
 log_k 0.000

Coliforms_m = Coliforms_m
 log_k 0.000

Ecoli_m = Ecoli_m
 log_k 0.000

Carbnano_m = Carbnano_m
 log_k 0.000

Coliforms_im = Coliforms_im
 log_k 0.000

Ecoli_im = Ecoli_im
 log_k 0.000

Carbnano_im = Carbnano_im
 log_k 0.000

H2O = OH- + H+
 log_k -14.000
 delta_h 13.362 kcal
 -analytic -283.971 -0.05069842 13323.0 102.24447 -1119669.0
 -gamma 3.5000 0.0000

2 H2O = O2 + 4 H+ + 4 e-
 log_k -86.08
 delta_h 134.79 kcal

2 H+ + 2 e- = H2
 log_k -3.15
 delta_h -1.759 kcal

numerical trick !!! See PHREEQC manual
 H2O + 0.01e- = H2O-0.01
 log_k -9

CO3-2 + H+ = HCO3-
 log_k 10.329
 delta_h -3.561 kcal
 -analytic 107.8871 0.03252849 -5151.79 -38.92561 563713.9
 -gamma 5.4000 0.0000

CO3-2 + 2 H+ = CO2 + H2O
 log_k 16.681
 delta_h -5.738 kcal
 -analytic 464.1965 0.09344813 -26986.16 -165.75951 2248628.9

CO3-2 + 10 H+ + 8 e- = CH4 + 3 H2O
 log_k 41.071
 delta_h -61.039 kcal

SO4-2 + H+ = HSO4-
 log_k 1.988

delta_h	3.85	kcal				
-analytic	-56.889		0.006473	2307.9	19.8858	0.0

HS- = S-2 + H+

log_k	-12.918				
delta_h	12.1	kcal			
-gamma	5.0000		0.0000		

SO4-2 + 9 H+ + 8 e- = HS- + 4 H2O

log_k	33.65				
delta_h	-60.140	kcal			
-gamma	3.5000		0.0000		

HS- + H+ = H2S

log_k	6.994				
delta_h	-5.300	kcal			
-analytical	-11.17		0.02386	3279.0	

NO3- + 2 H+ + 2 e- = NO2- + H2O

log_k	28.570				
delta_h	-43.760	kcal			
-gamma	3.0000		0.0000		

2 NO3- + 12 H+ + 10 e- = N2 + 6 H2O

log_k	207.080				
delta_h	-312.130	kcal			

#NH4+ = NH3 + H+

#	log_k	-9.252			
#	delta_h	12.48	kcal		
#	-analytic	0.6322	-0.001225	-2835.76	

AmmH+ = AmmH+

	log_k	0.0			
	-gamma	2.5		0.0	

AmmH+ = Amm + H+

	log_k	-9.252			
	delta_h	12.48	kcal		
	-analytic	0.6322	-0.001225	-2835.76	

#NO3- + 10 H+ + 8 e- = AmmH+ + 3 H2O

#	log_k	119.077			
#	delta_h	-187.055	kcal		
#	-gamma	2.5		0.0	

AmmH+ + SO4-2 = AmmHSO4-

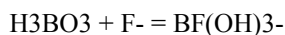
	log_k	1.11			
--	-------	------	--	--	--

#NH4+ + SO4-2 = NH4SO4-

#	log_k	1.11			
#					

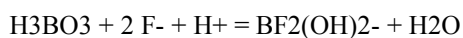
H3BO3 = H2BO3- + H+

	log_k	-9.240			
	delta_h	3.224	kcal		
#	-analytical	24.3919	0.012078	-1343.9	-13.2258



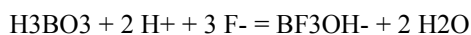
log_k -0.400

delta_h 1.850 kcal



log_k 7.63

delta_h 1.618 kcal



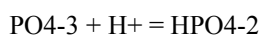
log_k 13.67

delta_h -1.614 kcal



log_k 20.28

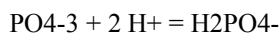
delta_h -1.846 kcal



log_k 12.346

delta_h -3.530 kcal

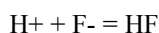
-gamma 4.0000 0.0000



log_k 19.553

delta_h -4.520 kcal

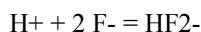
-gamma 4.5000 0.0000



log_k 3.18

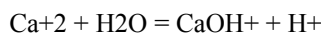
delta_h 3.18 kcal

-analytic -2.033 0.012645 429.01

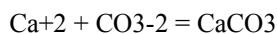


log_k 3.760

delta_h 4.550 kcal



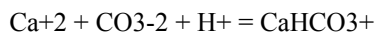
log_k -12.780



log_k 3.224

delta_h 3.545 kcal

-analytic -1228.732 -0.299440 35512.75 485.818

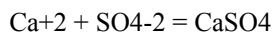


log_k 11.435

delta_h -0.871 kcal

-analytic 1317.0071 0.34546894 -39916.84 -517.70761 563713.9

-gamma 5.4000 0.0000

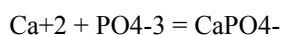


log_k 2.300

delta_h 1.650 kcal

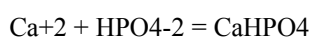


log_k 1.08



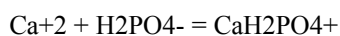
log_k 6.459

delta_h 3.100 kcal



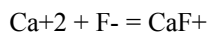
log_k 2.739

delta_h 3.3 kcal



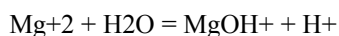
log_k 1.408

delta_h 3.4 kcal



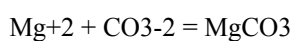
log_k 0.940

delta_h 4.120 kcal



log_k -11.440

delta_h 15.952 kcal



log_k 2.98

delta_h 2.713 kcal

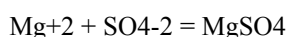
-analytic 0.9910 0.00667



log_k 11.399

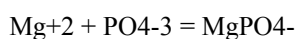
delta_h -2.771 kcal

-analytic 48.6721 0.03252849 -2614.335 -18.00263 563713.9



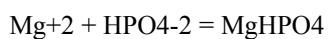
log_k 2.370

delta_h 4.550 kcal



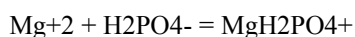
log_k 6.589

delta_h 3.100 kcal



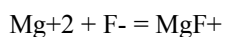
log_k 2.87

delta_h 3.3 kcal



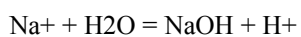
log_k 1.513

delta_h 3.4 kcal

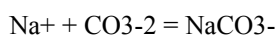


log_k 1.820

delta_h 3.200 kcal

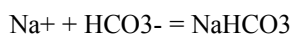


log_k -14.180

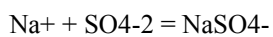


log_k 1.270

delta_h 8.910 kcal

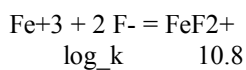
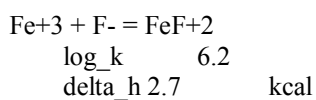
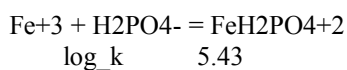
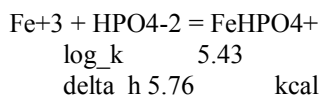
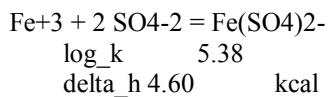
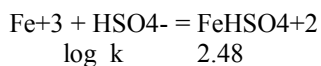
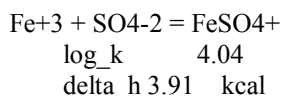
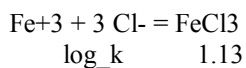
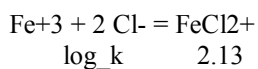
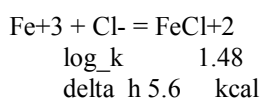
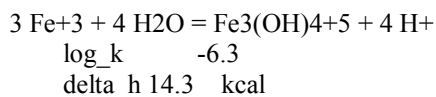
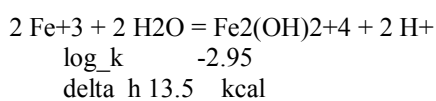
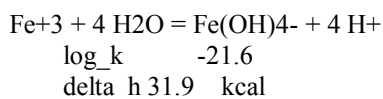
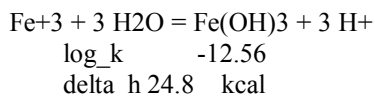
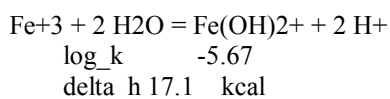
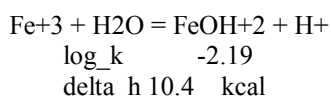


log_k -0.25



log_k 0.700

ΔH 1.120 kcal
 $\text{Na}^+ + \text{HPO}_4^{2-} = \text{NaHPO}_4^-$
 $\log K$ 0.29
 $\text{Na}^+ + \text{F}^- = \text{NaF}$
 $\log K$ -0.240
 $\text{K}^+ + \text{H}_2\text{O} = \text{KOH} + \text{H}^+$
 $\log K$ -14.460
 $\text{K}^+ + \text{SO}_4^{2-} = \text{KSO}_4^-$
 $\log K$ 0.850
 ΔH 2.250 kcal
 -analytical 3.106 0.0 -673.6
 $\text{K}^+ + \text{HPO}_4^{2-} = \text{KHPO}_4^-$
 $\log K$ 0.29
 $\text{Fe}^{2+} + \text{H}_2\text{O} = \text{FeOH}^+ + \text{H}^+$
 $\log K$ -9.500
 ΔH 13.200 kcal
 $\text{Fe}^{2+} + \text{Cl}^- = \text{FeCl}^+$
 $\log K$ 0.140
 $\text{Fe}^{2+} + \text{CO}_3^{2-} = \text{FeCO}_3$
 $\log K$ 4.380
 $\text{Fe}^{2+} + \text{HCO}_3^- = \text{FeHCO}_3^+$
 $\log K$ 2.0
 $\text{Fe}^{2+} + \text{SO}_4^{2-} = \text{FeSO}_4$
 $\log K$ 2.250
 ΔH 3.230 kcal
 $\text{Fe}^{2+} + \text{HSO}_4^- = \text{FeHSO}_4^+$
 $\log K$ 1.08
 $\text{Fe}^{2+} + 2\text{HS}^- = \text{Fe}(\text{HS})_2$
 $\log K$ 8.95
 $\text{Fe}^{2+} + 3\text{HS}^- = \text{Fe}(\text{HS})_3^-$
 $\log K$ 10.987
 $\text{Fe}^{2+} + \text{HPO}_4^{2-} = \text{FeHPO}_4$
 $\log K$ 3.6
 $\text{Fe}^{2+} + \text{H}_2\text{PO}_4^- = \text{FeH}_2\text{PO}_4^+$
 $\log K$ 2.7
 $\text{Fe}^{2+} + \text{F}^- = \text{FeF}^+$
 $\log K$ 1.000
 $\text{Fe}^{2+} = \text{Fe}^{3+} + \text{e}^-$
 $\log K$ -13.020
 ΔH 9.680 kcal
 -gamma 9.0000 0.0000



delta_h 4.8	kcal			
Fe+3 + 3 F- = FeF3				
log_k	14.0			
delta_h 5.4	kcal			
Mn+2 + H2O = MnOH+ + H+				
log_k	-10.590			
delta_h 14.400	kcal			
Mn+2 + Cl- = MnCl+				
log_k	0.610			
Mn+2 + 2 Cl- = MnCl2				
log_k	0.250			
Mn+2 + 3 Cl- = MnCl3-				
log_k	-0.310			
Mn+2 + CO3-2 = MnCO3				
log_k	4.900			
Mn+2 + HCO3- = MnHCO3+				
log_k	1.95			
Mn+2 + SO4-2 = MnSO4				
log_k	2.250			
delta_h 3.370	kcal			
Mn+2 + 2 NO3- = Mn(NO3)2				
log_k	0.600			
delta_h -0.396	kcal			
Mn+2 + F- = MnF+				
log_k	0.840			
Mn+2 = Mn+3 + e-				
log_k	-25.510			
delta_h 25.800	kcal			
Al+3 + H2O = AlOH+2 + H+				
log_k	-5.00			
delta_h 11.49	kcal			
-analytic	-38.253	0.0	-656.27	14.327
Al+3 + 2 H2O = Al(OH)2+ + 2 H+				
log_k	-10.1			
delta_h 26.90	kcal			
-analytic	88.500	0.0	-9391.6	-27.121
Al+3 + 3 H2O = Al(OH)3 + 3 H+				
log_k	-16.9			
delta_h 39.89	kcal			
-analytic	226.374	0.0	-18247.8	-73.597
Al+3 + 4 H2O = Al(OH)4- + 4 H+				
log_k	-22.7			
delta_h 42.30	kcal			
-analytic	51.578	0.0	-11168.9	-14.865

Al+3 + SO4-2 = AlSO4+
log_k 3.5
delta_h 2.29 kcal

Al+3 + 2SO4-2 = Al(SO4)2-
log_k 5.0
delta_h 3.11 kcal

Al+3 + HSO4- = AlHSO4+2
log_k 0.46

Al+3 + F- = AlF+2
log_k 7.000
delta_h 1.060 kcal

Al+3 + 2 F- = AlF2+
log_k 12.700
delta_h 1.980 kcal

Al+3 + 3 F- = AlF3
log_k 16.800
delta_h 2.160 kcal

Al+3 + 4 F- = AlF4-
log_k 19.400
delta_h 2.200 kcal

Al+3 + 5 F- = AlF5-2
log_k 20.600
delta_h 1.840 kcal

Al+3 + 6 F- = AlF6-3
log_k 20.600
delta_h -1.670 kcal

H4SiO4 = H3SiO4- + H+
log_k -9.83
delta_h 6.12 kcal
-analytic -302.3724 -0.050698 15669.69 108.18466 -1119669.0

H4SiO4 = H2SiO4-2 + 2 H+
log_k -23.0
delta_h 17.6 kcal
-analytic -294.0184 -0.072650 11204.49 108.18466 -1119669.0

H4SiO4 + 4 H+ + 6 F- = SiF6-2 + 4 H2O
log_k 30.180
delta_h -16.260 kcal

Ba+2 + H2O = BaOH+ + H+
log_k -13.470

Ba+2 + CO3-2 = BaCO3
log_k 2.71
delta_h 3.55 kcal
-analytic 0.113 0.008721

Ba+2 + HCO3- = BaHCO3+

log_k	0.982					
delta_h	5.56	kcal				
-analytical	-3.0938		0.013669	0.0	0.0	0.0

Ba+2 + SO4-2 = BaSO4

log_k	2.700					
-------	-------	--	--	--	--	--

Sr+2 + H2O = SrOH+ + H+

log_k	-13.290					
-gamma	5.0000	0.0000				

Sr+2 + CO3-2 + H+ = SrHCO3+

log_k	11.509					
delta_h	2.489	kcal				
-analytic	104.6391		0.04739549	-5151.79	-38.92561	563713.9
-gamma	5.4000	0.0000				

Sr+2 + CO3-2 = SrCO3

log_k	2.81					
delta_h	5.22	kcal				
-analytic	-1.019		0.012826			

Sr+2 + SO4-2 = SrSO4

log_k	2.290					
delta_h	2.080	kcal				

Cu+2 + e- = Cu+

log_k	2.720					
delta_h	1.650	kcal				
-gamma	2.5000	0.0000				

Cu+2 + H2O = CuOH+ + H+

log_k	-8.000					
-gamma	4.0000	0.0000				

Cu+2 + 2 H2O = Cu(OH)2 + 2 H+

log_k	-13.680					
-------	---------	--	--	--	--	--

Cu+2 + 3 H2O = Cu(OH)3- + 3 H+

log_k	-26.900					
-------	---------	--	--	--	--	--

Cu+2 + 4 H2O = Cu(OH)4-2 + 4 H+

log_k	-39.600					
-------	---------	--	--	--	--	--

Cu+2 + SO4-2 = CuSO4

log_k	2.310					
delta_h	1.220	kcal				

Zn+2 + H2O = ZnOH+ + H+

log_k	-8.96					
delta_h	13.4	kcal				

Zn+2 + 2 H2O = Zn(OH)2 + 2 H+

log_k	-16.900					
-------	---------	--	--	--	--	--

Zn+2 + 3 H2O = Zn(OH)3- + 3 H+

log_k	-28.400					
-------	---------	--	--	--	--	--

Zn+2 + 4 H2O = Zn(OH)4-2 + 4 H+

log_k -41.200

$\text{Zn}^{+2} + \text{Cl}^- = \text{ZnCl}^+$
log_k 0.43
delta_h 7.79 kcal

$\text{Zn}^{+2} + 2 \text{Cl}^- = \text{ZnCl}_2$
log_k 0.45
delta_h 8.5 kcal

$\text{Zn}^{+2} + 3 \text{Cl}^- = \text{ZnCl}_3^-$
log_k 0.5
delta_h 9.56 kcal

$\text{Zn}^{+2} + 4 \text{Cl}^- = \text{ZnCl}_4^{2-}$
log_k 0.2
delta_h 10.96 kcal

$\text{Zn}^{+2} + \text{CO}_3^{2-} = \text{ZnCO}_3$
log_k 5.3

$\text{Zn}^{+2} + 2 \text{CO}_3^{2-} = \text{Zn}(\text{CO}_3)_2^{2-}$
log_k 9.63

$\text{Zn}^{+2} + \text{HCO}_3^- = \text{ZnHCO}_3^+$
log_k 2.1

$\text{Zn}^{+2} + \text{SO}_4^{2-} = \text{ZnSO}_4$
log_k 2.37
delta_h 1.36 kcal

$\text{Zn}^{+2} + 2 \text{SO}_4^{2-} = \text{Zn}(\text{SO}_4)_2^{2-}$
log_k 3.28

$\text{Cd}^{+2} + \text{H}_2\text{O} = \text{CdOH}^+ + \text{H}^+$
log_k -10.080
delta_h 13.1 kcal

$\text{Cd}^{+2} + 2 \text{H}_2\text{O} = \text{Cd}(\text{OH})_2 + 2 \text{H}^+$
log_k -20.350

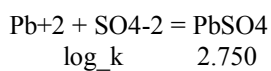
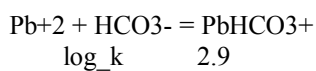
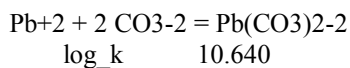
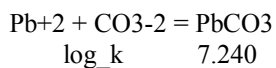
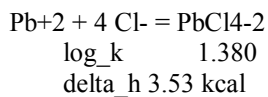
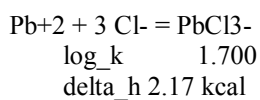
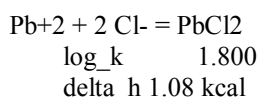
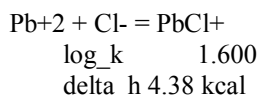
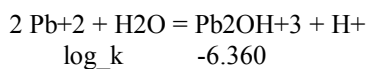
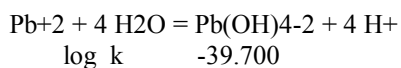
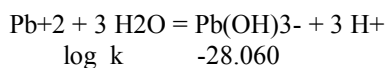
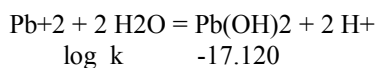
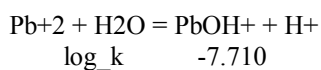
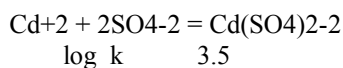
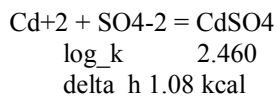
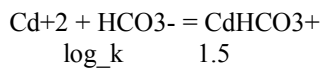
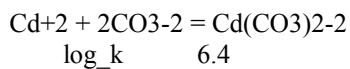
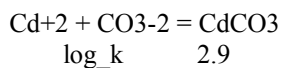
$\text{Cd}^{+2} + 3 \text{H}_2\text{O} = \text{Cd}(\text{OH})_3^- + 3 \text{H}^+$
log_k -33.300

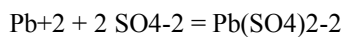
$\text{Cd}^{+2} + 4 \text{H}_2\text{O} = \text{Cd}(\text{OH})_4^{2-} + 4 \text{H}^+$
log_k -47.350

$\text{Cd}^{+2} + \text{Cl}^- = \text{CdCl}^+$
log_k 1.980
delta_h 0.59 kcal

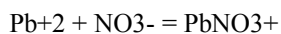
$\text{Cd}^{+2} + 2 \text{Cl}^- = \text{CdCl}_2$
log_k 2.600
delta_h 1.24 kcal

$\text{Cd}^{+2} + 3 \text{Cl}^- = \text{CdCl}_3^-$
log_k 2.400
delta_h 3.9 kcal





log_k 3.470



log_k 1.170

PHASES

Calcite



log_k -8.480

delta_h -2.297 kcal

-analytic -171.9065 -0.077993 2839.319 71.595

Aragonite

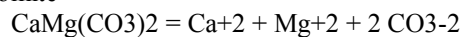


log_k -8.336

delta_h -2.589 kcal

-analytic -171.9773 -0.077993 2903.293 71.595

Dolomite



log_k -17.090

delta_h -9.436 kcal

Siderite



log_k -10.890

delta_h -2.480 kcal

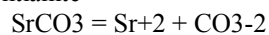
Rhodochrosite



log_k -11.130

delta_h -1.430 kcal

Strontianite



log_k -9.271

delta_h -0.400 kcal

-analytic 155.0305 0.0 -7239.594 -56.58638

Witherite

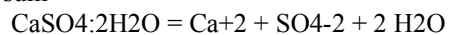


log_k -8.562

delta_h 0.703 kcal

-analytic 607.642 0.121098 -20011.25 -236.4948

Gypsum

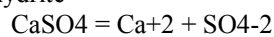


log_k -4.580

delta_h -0.109 kcal

-analytic 68.2401 0.0 -3221.51 -25.0627

Anhydrite

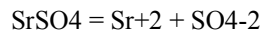


log_k -4.360

delta_h -1.710 kcal

-analytic 197.52 0.0 -8669.8 -69.835

Celestite

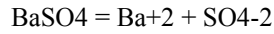


log_k -6.630

delta_h -1.037 kcal

-analytic -14805.9622 -2.4660924 756968.533 5436.3588 -40553604.0

Barite

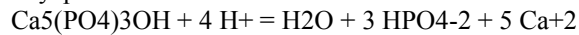


log_k -9.970

delta_h 6.350 kcal

-analytic 136.035 0.0 -7680.41 -48.595

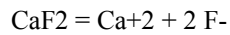
Hydroxyapatite



log_k -3.421

delta_h -36.155 kcal

Fluorite

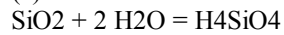


log_k -10.600

delta_h 4.690 kcal

-analytic 66.348 0.0 -4298.2 -25.271

SiO2(a)

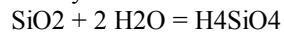


log_k -2.710

delta_h 3.340 kcal

-analytic -0.26 0.0 -731.0

Chalcedony

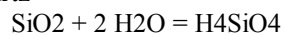


log_k -3.550

delta_h 4.720 kcal

-analytic -0.09 0.0 -1032.0

Quartz

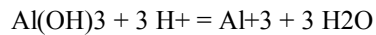


log_k -3.980

delta_h 5.990 kcal

-analytic 0.41 0.0 -1309.0

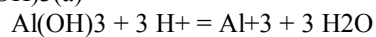
Gibbsite



log_k 8.110

delta_h -22.800 kcal

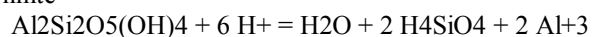
Al(OH)3(a)



log_k 10.800

delta_h -26.500 kcal

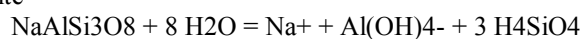
Kaolinite



log_k 7.435

delta_h -35.300 kcal

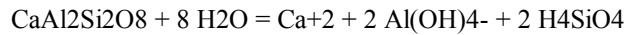
Albite



log_k -18.002

delta_h 25.896 kcal

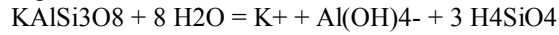
Anorthite



log_k -19.714

delta_h 11.580 kcal

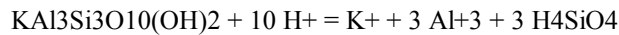
K-feldspar



log_k -20.573

delta_h 30.820 kcal

K-mica



log_k 12.703

delta_h -59.376 kcal

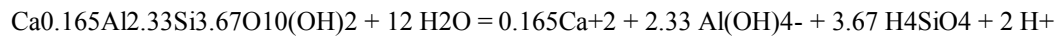
Chlorite(14A)



log_k 68.38

delta_h -151.494 kcal

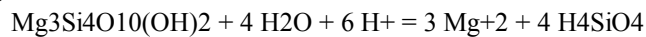
Ca-Montmorillonite



log_k -45.027

delta_h 58.373 kcal

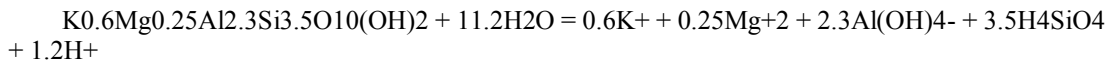
Talc



log_k 21.399

delta_h -46.352 kcal

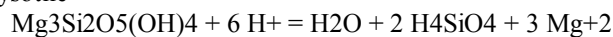
Illite



log_k -40.267

delta_h 54.684 kcal

Chrysotile



log_k 32.200

delta_h -46.800 kcal

-analytic 13.248 0.0 10217.1 -6.1894

#Sepiolite



log_k 15.760

delta_h -10.700 kcal

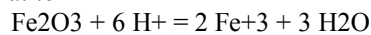
#

#Sepiolite(d)



log_k 18.660

Hematite



log_k -4.008

delta_h -30.845 kcal

Goethite

FeOOH + 3 H+ = Fe+3 + 2 H2O
log_k -1.000
delta_h -14.48 kcal

Fe(OH)3(a)
Fe(OH)3 + 3 H+ = Fe+3 + 3 H2O
log_k 4.891

Pyrite
FeS2 + 2 H+ + 2 e- = Fe+2 + 2 HS-
log_k -18.479
delta_h 11.300 kcal

FeS(ppt)
FeS + H+ = Fe+2 + HS-
log_k -3.915

Mackinawite
FeS + H+ = Fe+2 + HS-
log_k -4.648

Sulfur
S + 2H+ + 2e- = H2S
log_k 4.882
delta_h -9.5 kcal

Vivianite
Fe3(PO4)2·8H2O = 3 Fe+2 + 2 PO4-3 + 8 H2O
log_k -36.000

Pyrolusite
MnO2 + 4 H+ + 2 e- = Mn+2 + 2 H2O
log_k 41.380
delta_h -65.110 kcal

Hausmannite
Mn3O4 + 8 H+ + 2 e- = 3 Mn+2 + 4 H2O
log_k 61.030
delta_h -100.640 kcal

Manganite
MnOOH + 3 H+ + e- = Mn+2 + 2 H2O
log_k 25.340

Pyrochroite
Mn(OH)2 + 2 H+ = Mn+2 + 2 H2O
log_k 15.200

Halite
NaCl = Na+ + Cl-
log_k 1.582
delta_h 0.918 kcal

CO2(g)
CO2 = CO2
log_k -1.468
delta_h -4.776 kcal
-analytic 108.3865 0.01985076 -6919.53 -40.45154 669365.0

O2(g)
 O2 = O2
 # log_k -2.960
 # delta_h -1.844 kcal
 # log K from llnl.dat Aug 23, 2005
 log_k -2.8983
 -analytic -7.5001e+000 7.8981e-003 0.0000e+000 0.0000e+000 2.0027e+005

H2(g)
 H2 = H2
 log_k -3.150
 delta_h -1.759 kcal

H2O(g)
 H2O = H2O
 log_k 1.51
 delta_h -44.03 kJ
 # Stumm and Morgan, from NBS and Robie, Hemmingway, and Fischer (1978)

N2(g)
 N2 = N2
 log_k -3.260
 delta_h -1.358 kcal

H2S(g)
 H2S = H2S
 log_k -0.997
 delta_h -4.570 kcal

CH4(g)
 CH4 = CH4
 log_k -2.860
 delta_h -3.373 kcal

#NH3(g)
 # NH3 = NH3
 # log_k 1.770
 # delta_h -8.170 kcal

Amm(g)
 Amm = Amm
 log_k 1.7966
 -analytic -1.8758e+001 3.3670e-004 2.5113e+003 4.8619e+000 3.9192e+001

Melanterite
 $\text{FeSO}_4 \cdot 7\text{H}_2\text{O} = 7 \text{H}_2\text{O} + \text{Fe}^{+2} + \text{SO}_4^{-2}$
 log_k -2.209
 delta_h 4.910 kcal
 -analytic 1.447 -0.004153 0.0 0.0 -214949.0

Alunite
 $\text{KAl}_3(\text{SO}_4)_2(\text{OH})_6 + 6 \text{H}^+ = \text{K}^+ + 3 \text{Al}^{+3} + 2 \text{SO}_4^{-2} + 6\text{H}_2\text{O}$
 log_k -1.400
 delta_h -50.250 kcal

Jarosite-K
 $\text{KFe}_3(\text{SO}_4)_2(\text{OH})_6 + 6 \text{H}^+ = 3 \text{Fe}^{+3} + 6 \text{H}_2\text{O} + \text{K}^+ + 2 \text{SO}_4^{-2}$

log_k -9.210
delta_h -31.280 kcal

Zn(OH)₂(e)
 $\text{Zn(OH)}_2 + 2 \text{H}^+ = \text{Zn}^{+2} + 2 \text{H}_2\text{O}$
log_k 11.50

Smithsonite
 $\text{ZnCO}_3 = \text{Zn}^{+2} + \text{CO}_3^{-2}$
log_k -10.000
delta_h -4.36 kcal

Sphalerite
 $\text{ZnS} + \text{H}^+ = \text{Zn}^{+2} + \text{HS}^-$
log_k -11.618
delta_h 8.250 kcal

Willemite 289
 $\text{Zn}_2\text{SiO}_4 + 4\text{H}^+ = 2\text{Zn}^{+2} + \text{H}_4\text{SiO}_4$
log_k 15.33
delta_h -33.37 kcal

Cd(OH)₂
 $\text{Cd(OH)}_2 + 2 \text{H}^+ = \text{Cd}^{+2} + 2 \text{H}_2\text{O}$
log_k 13.650

Otavite 315
 $\text{CdCO}_3 = \text{Cd}^{+2} + \text{CO}_3^{-2}$
log_k -12.1
delta_h -0.019 kcal

CdSiO₃ 328
 $\text{CdSiO}_3 + \text{H}_2\text{O} + 2\text{H}^+ = \text{Cd}^{+2} + \text{H}_4\text{SiO}_4$
log_k 9.06
delta_h -16.63 kcal

CdSO₄ 329
 $\text{CdSO}_4 = \text{Cd}^{+2} + \text{SO}_4^{-2}$
log_k -0.1
delta_h -14.74 kcal

Cerrusite 365
 $\text{PbCO}_3 = \text{Pb}^{+2} + \text{CO}_3^{-2}$
log_k -13.13
delta_h 4.86 kcal

Anglesite 384
 $\text{PbSO}_4 = \text{Pb}^{+2} + \text{SO}_4^{-2}$
log_k -7.79
delta_h 2.15 kcal

Pb(OH)₂ 389
 $\text{Pb(OH)}_2 + 2\text{H}^+ = \text{Pb}^{+2} + 2\text{H}_2\text{O}$
log_k 8.15
delta_h -13.99 kcal

EXCHANGE_MASTER_SPECIES
X X-
EXCHANGE_SPECIES

$X^- = X^-$
log_k 0.0

$Na^+ + X^- = NaX$
log_k 0.0
-gamma 4.0 0.075

$K^+ + X^- = KX$
log_k 0.7
-gamma 3.5 0.015
delta_h -4.3 # Jardine & Sparks, 1984

$NH_4^+ + X^- = NH_4X$
log_k 0.6
-gamma 2.5 0.0
delta_h -2.4 # Laudelout et al., 1968

$AmmH^+ + X^- = AmmHX$
log_k 0.6
-gamma 2.5 0.0
delta_h -2.4 # Laudelout et al., 1968

$Ca^{+2} + 2X^- = CaX_2$
log_k 0.8
-gamma 5.0 0.165
delta_h 7.2 # Van Bladel & Gheyl, 1980

$Mg^{+2} + 2X^- = MgX_2$
log_k 0.6
-gamma 5.5 0.2
delta_h 7.4 # Laudelout et al., 1968

$Sr^{+2} + 2X^- = SrX_2$
log_k 0.91
-gamma 5.26 0.121
delta_h 5.5 # Laudelout et al., 1968

$Ba^{+2} + 2X^- = BaX_2$
log_k 0.91
-gamma 5.0 0.0
delta_h 4.5 # Laudelout et al., 1968

$Mn^{+2} + 2X^- = MnX_2$
log_k 0.52
-gamma 6.0 0.0

$Fe^{+2} + 2X^- = FeX_2$
log_k 0.44
-gamma 6.0 0.0

$Cu^{+2} + 2X^- = CuX_2$
log_k 0.6
-gamma 6.0 0.0

$Zn^{+2} + 2X^- = ZnX_2$
log_k 0.8
-gamma 5.0 0.0

$Cd^{+2} + 2X^- = CdX_2$

```

log_k 0.8
-gamma 0.0 0.0

Pb+2 + 2X- = PbX2
log_k 1.05
-gamma 0.0 0.0

Al+3 + 3X- = AlX3
log_k 0.41
-gamma 9.0 0.0

AlOH+2 + 2X- = AlOHX2
log_k 0.89
-gamma 0.0 0.0

```

RATES

```

#####
# Pyrite
#####
# rate equation Williamson & Rimstidt 1994, GCA 58
# parameters according to Appelo et al. 1998 , Appl. Geochem. 13
# using correct. factor FeS2 -> FeS and O2 -> NO3
# parm(1) = log10(A/V, 1/dm) parm(2) = exp for (m/m0)
# parm(3) = exp for O2 parm(4) = exp for H+

Pyrite
-start
6 if (m <= 1e-12) then goto 200
7 mTmp = 1000 * tot("Tmp")
9 si_pyr = SI("Pyrite")
10 sr_pyr = SR("Pyrite")
11 if (m <= 1e-15 and sr_pyr < 1) then goto 200
14 par1 = -6758.1
15 par2 = 16.1
18 invtemp = 1/(mTmp+273.15)
19 invtemp14 = 1/(14+273.15)
22 y14 = -exp(invtemp14*par1+par2)
23 yTmp = -exp(invtemp*par1+par2)
25 arrh_factor = yTmp/y14
30 rate_ox = (mol("O2"))^parm(3) * (mol("H+"))^parm(4)
40 rate_nitr = (mol("NO3-"))^parm(3) * (mol("H+"))^parm(4)
#45 surf_over_vol = log10(m*115) 115 = value used in Prommer & Stuyfzand, 2005
45 surf_over_vol = log10(m*parm(5))
52 f1 = 10^(-10.19 + surf_over_vol) * (m/m0)^parm(2)
60 moles_ox = f1 * rate_ox * arrh_factor * time
# limit O2 oxidation to maximal stoichiometry for FeS -> Fe+3 + SO4
62 m_o2 = mol("O2") * 4/9
64 if moles_ox > m_o2 then moles_ox = m_o2
70 moles_nitr = f1 * rate_nitr * arrh_factor * time
82 moles_0 = f1 * rate_0 * arrh_factor * time
90 moles = moles_ox + moles_nitr + moles_0
100 if (moles > m) then moles = m
200 save moles
-end

#####
#K-feldspar
#####

```

```

#
# Sverdrup, H.U., 1990, The kinetics of base cation release due to
# chemical weathering: Lund University Press, Lund, 246 p.
#
# Example of KINETICS data block for K-feldspar rate:
#   KINETICS 1
#   K-feldspar
#       -m0 2.16 # 10% K-fsp, 0.1 mm cubes
#       -m 1.94
#       -parms 1.36e4 0.1

K-feldspar
-start
1 rem specific rate from Sverdrup, 1990, in kmol/m2/s
2 rem parm(1) = 10 * (A/V, 1/dm) (recalc's sp. rate to mol/kgw)
3 rem parm(2) = corrects for field rate relative to lab rate
4 rem temp corr: from p. 162. E (kJ/mol) / R / 2.303 = H in H*(1/T-1/298)

10 dif_temp = 1/TK - 1/298
20 pk_H = 12.5 + 3134 * dif_temp
30 pk_w = 15.3 + 1838 * dif_temp
40 pk_OH = 14.2 + 3134 * dif_temp
50 pk_CO2 = 14.6 + 1677 * dif_temp
#60 pk_org = 13.9 + 1254 * dif_temp # rate increase with DOC
70 rate = 10^-pk_H * ACT("H+")^0.5 + 10^-pk_w + 10^-pk_OH * ACT("OH-")^0.3
71 rate = rate + 10^-pk_CO2 * (10^SI("CO2(g)))^0.6
#72 rate = rate + 10^-pk_org * TOT("Doc")^0.4
80 moles = parm(1) * parm(2) * rate * (1 - SR("K-feldspar")) * time
81 rem decrease rate on precipitation
90 if SR("K-feldspar") > 1 then moles = moles * 0.1
100 save moles
-end
#####
#Albite
#####
#
# Sverdrup, H.U., 1990, The kinetics of base cation release due to
# chemical weathering: Lund University Press, Lund, 246 p.
#
# Example of KINETICS data block for Albite rate:
#   KINETICS 1
#   Albite
#       -m0 0.43 # 2% Albite, 0.1 mm cubes
#       -parms 2.72e3 0.1

Albite
-start
1 rem specific rate from Sverdrup, 1990, in kmol/m2/s
2 rem parm(1) = 10 * (A/V, 1/dm) (recalc's sp. rate to mol/kgw)
3 rem parm(2) = corrects for field rate relative to lab rate
4 rem temp corr: from p. 162. E (kJ/mol) / R / 2.303 = H in H*(1/T-1/298)

10 dif_temp = 1/TK - 1/298
20 pk_H = 12.5 + 3359 * dif_temp
30 pk_w = 14.8 + 2648 * dif_temp
40 pk_OH = 13.7 + 3359 * dif_temp
#41 rem ^12.9 in Sverdrup, but larger than for oligoclase...
50 pk_CO2 = 14.0 + 1677 * dif_temp
#60 pk_org = 12.5 + 1254 * dif_temp # ...rate increase for DOC

```

```

70  rate = 10^-pk_H * ACT("H+")^0.5 + 10^-pk_w + 10^-pk_OH * ACT("OH-")^0.3
71  rate = rate + 10^-pk_CO2 * (10^SI("CO2(g)"))^0.6
#72  rate = rate + 10^-pk_org * TOT("Doc")^0.4
80  moles = parm(1) * parm(2) * rate * (1 - SR("Albite")) * time
81  rem decrease rate on precipitation
90  if SR("Albite") > 1 then moles = moles * 0.1
100  save moles
-end

#####
#Calcite
#####
#
# Plummer, L.N., Wigley, T.M.L., and Parkhurst, D.L., 1978,
# American Journal of Science, v. 278, p. 179-216.
#
# Example of KINETICS data block for calcite rate:
#
# KINETICS 1
# Calcite
# -tol 1e-8
# -m0 3.e-3
# -m 3.e-3
# -parms 5.0 0.6
Calcite
-start
1 REM Modified from Plummer and others, 1978
2 REM M = current moles of calcite
3 REM M0 = initial moles of calcite
4 REM parm(1) = Area/Volume, cm^2/L (or cm^2 per cell)
5 REM parm(2) = exponent for M/M0 for surface area correction
10 REM rate = 0 if no calcite and undersaturated
20 si_cc = SI("Calcite")
30 if (M <= 0 and si_cc < 0) then goto 300
40 k1 = 10^(0.198 - 444.0 / TK)
50 k2 = 10^(2.84 - 2177.0 / TK)
60 if TC <= 25 then k3 = 10^(-5.86 - 317.0 / TK)
70 if TC > 25 then k3 = 10^(-1.1 - 1737.0 / TK)
80 REM surface area calculation
90 t = 1
100 if M0 > 0 then t = M/M0
110 if t = 0 then t = 1
120 area = PARM(1) * (t)^PARM(2)
130 rf = k1 * ACT("H+") + k2 * ACT("CO2") + k3 * ACT("H2O")
140 REM 1e-3 converts mmol to mol
150 rate = area * 1e-3 * rf * (1 - 10^(2/3*si_cc))
160 moles = rate * TIME
170 REM do not dissolve more calcite than present
180 if (moles > M) then moles = M
190 if (moles >= 0) then goto 300
200 REM do not precipitate more Ca or C(4) than present
210 temp = TOT("Ca")
220 mc = TOT("C(4)")
230 if mc < temp then temp = mc
240 if -moles > temp then moles = -temp
300 SAVE moles
-end

#####

```



```

#Organic_C (as supplied by USGS)
#####
#
# Example of KINETICS data block for Organic_C rate:
#   KINETICS 1
#   Organic_C
#       -tol 1e-8
#       # m in mol/kgw
#       -m0 5e-3
#       -m 5e-3
Orgc_orig # Parkhurst & Appelo, 1999; Appelo & Postma, 2005
-start
1 rem    Additive Monod kinetics
2 rem    Electron acceptors: O2, NO3, and SO4

10 if(m <= 0) then goto 200
20 mO2 = mol("O2")
30 mNO3 = tot("N(5)")
40 mSO4 = tot("S(6)")
50 rate = 1.57e-9*mO2/(2.94e-4 + mO2) + 1.67e-11*mNO3/(1.55e-4 + mNO3)
60 rate = rate + 1.e-13*mSO4/(1.e-4 + mSO4)
70 moles = rate * time
80 if (moles > m) then moles = m
200 save moles
-end

#####
Orgc # (extended - see, e.g., Prommer et al. 2006, ES&T)
#####
-start
# 1      = parm(1) (not used)
2 k1_ox  = parm(2) # 1.57e-09
3 k1_nit = parm(3) # 8.00e-10
4 k1_sul  = parm(4) # 5e-11
5 k1_fe   = parm(5) # 5e-11
6 k1_mn   = parm(6) # 2.00e-10
7 resid  = parm(7) # 2e-05 residual (undegradable) fraction of DOC
10 mOrgc = mol("Orgc")
12 if(mOrgc < resid) then goto 15
13 m_deg_OrgC = mOrgc - resid
15 if(m_deg_OrgC <= 1e-10) then goto 200
16 mTmp = 1000 * tot("Tmp")
18 f_t  = EXP(-1.5 + 0.18 * mTmp * (1 - 0.5 * mTmp/35))
19 put(f_t,7)
20 mO2 = mol("O2")
25 mNO3 = tot("N(5)")
50 rate = f_t * k1_ox * mO2/(2.94e-4 + mO2)
52 k_inh_ox= 1e-5
55 rate = rate + f_t * k1_nit * mNO3/(1.55e-4 + mNO3) * (k_inh_ox/(m_O2 + k_inh_ox))
74 rate = rate * m_deg_OrgC / (1e-05 + m_deg_OrgC)
75 moles = rate * time
200 save moles
-end
#####
# Orgc_sed_1
#####
Orgc_sed_1
-start
3 temp_fac=get(7)

```

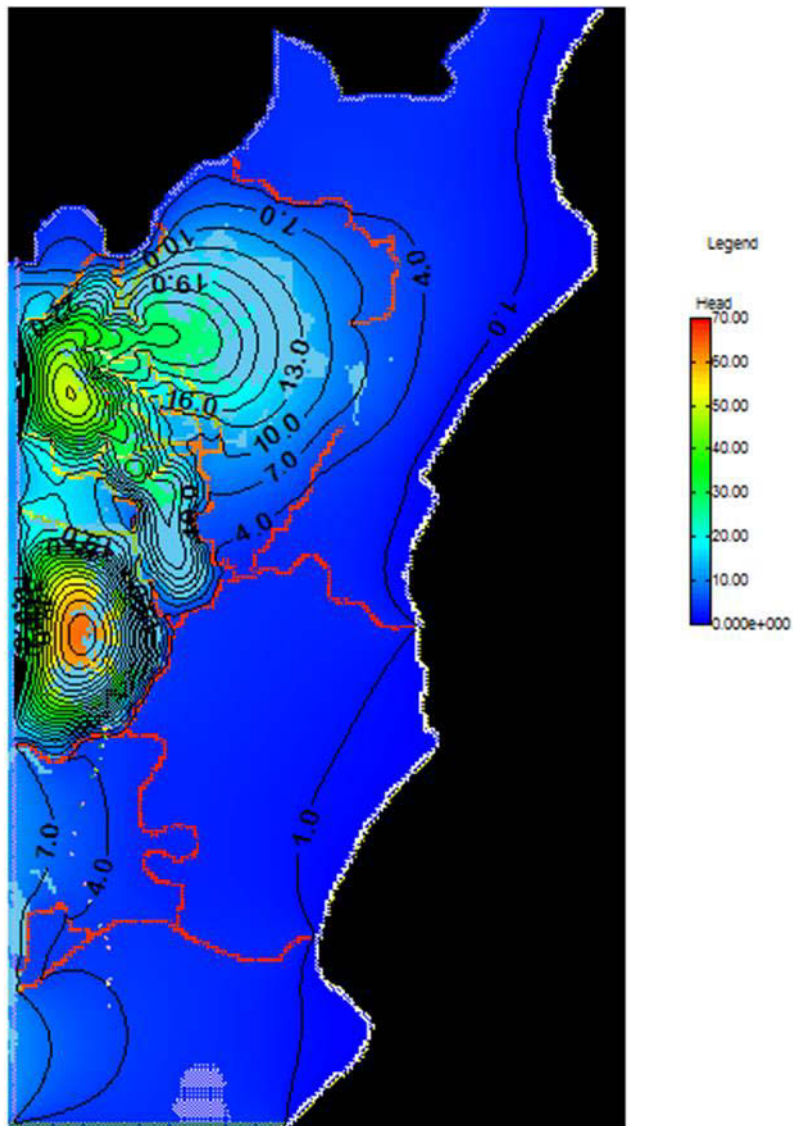
```

5 parm1= parm(1)*temp_fac
7 parm2= parm(2)*temp_fac
10 parm3= parm(3)*temp_fac
20 m_O2 = mol("O2")
30 m_NO3 = tot ("N(5)")
# 40 m_MnO2 = equi ("Pyrolusite")
45 m_orgc = tot("Orgc_sed_l")
47 if (m_orgc < 1e-9) then goto 200
50 r_ox=parm1
51 k_ox=1e-5
52 k_inh_ox=1e-5
53 r_nitr=parm2
54 k_nitr=1e-5
# 55 r_mn=parm3/86400 # Check time units
80 rate = r_ox*(m_O2/(m_O2 + k_ox))+ r_nitr*(m_NO3/(m_NO3+k_nitr))*(k_inh_ox/(m_O2 +
k_inh_ox)) #+ r_mn
90 moles = m_orgc/(m_orgc+1e-5)*rate*time
91 put(r_ox,1)
92 put(r_nitr,2)
# 93 put(r_mn,3)
94 put(k_ox,4)
95 put(k_nitr,5)
96 put(k_inh_ox,6)
100 if (moles > m) then moles = m
200 SAVE moles
-end
#####
#Pyrolusite
#####
#
# Postma, D. and Appelo, C.A.J., 2000, GCA 64, in press
#
# Example of KINETICS data block for Pyrolusite
# KINETICS 1-12
# Pyrolusite
# -tol 1.e-7
# -m0 0.1
# -m 0.1
Pyrolusite
-start
5 if (m <= 0.0) then goto 200
7 sr_pl = sr("Pyrolusite")
9 if abs(1 - sr_pl) < 0.1 then goto 200
10 if (sr_pl > 1.0) then goto 100
#20 rem initially 1 mol Fe+2 = 0.5 mol pyrolusite. k*A/V = 1/time (3 cells)
#22 rem time (3 cells) = 1.432e4. 1/time = 6.98e-5
30 Fe_t = tot("Fe(2)")
32 if Fe_t < 1.e-8 then goto 200
40 moles = 6.98e-5 * Fe_t * (m/m0)^0.67 * time * (1 - sr_pl)
50 if moles > Fe_t / 2 then moles = Fe_t / 2
70 if moles > m then moles = m
90 goto 200
100 Mn_t = tot("Mn")
110 moles = 2e-3 * 6.98e-5 * (1-sr_pl) * time
120 if moles <= -Mn_t then moles = -Mn_t
200 save moles
-end

END

```

Appendix B- Simulated Water Table Post-Calibration



Appendix C- Flow Model Raw Output

LISTING FILE: OH2Ka.out
UNIT 6

OPENING OH2Ka.bas
FILE TYPE:BAS UNIT 1

OPENING OH2Ka.bcf
FILE TYPE:BCF UNIT 11

OPENING OH2Ka.wel
FILE TYPE:WEL UNIT 12

OPENING OH2Ka.riv
FILE TYPE:RIV UNIT 14

OPENING OH2Ka.ghb
FILE TYPE:GHB UNIT 17

OPENING OH2Ka.rch
FILE TYPE:RCH UNIT 18

OPENING OH2Ka.oc
FILE TYPE:OC UNIT 22

OPENING OH2Ka.pg5
FILE TYPE:PG5 UNIT 19

OPENING OH2Ka.cbb
FILE TYPE:DATA(BINARY) UNIT 50

OPENING OH2Ka.hds
FILE TYPE:DATA(BINARY) UNIT 30

OPENING OH2Ka.ddn
FILE TYPE:DATA(BINARY) UNIT 31

1 MODFLOW-SURFACT Version 4.0
U.S. GEOLOGICAL SURVEY MODULAR FINITE-DIFFERENCE GROUND-WATER FLOW MODEL
(HYDROGEOLOGIC'S ENHANCED VERSION OF USGS MODFLOW HYDROLOGIC MODELING SYSTEM)

MODFLOW Data Set Created by Groundwater Vistas

3 LAYERS 60 ROWS 34 COLUMNS
1 STRESS PERIOD(S) IN SIMULATION
MODEL TIME UNIT IS DAYS
CALCULATE FLOW BETWEEN ADJACENT CONSTANT-HEAD CELLS

I/O UNITS:
ELEMENT OF IUNIT: 1 2 3 4 5 6 7 8 9 10 11 12 13 14 15 16 17 18 19 20
PACKAGE NAME : BCF WEL DRN RIV EVT TLK GHB RCH SIP DE4 SOR OC PG4 STR PG2 HFB BTN LAK IBS
CHD
I/O UNIT: 11 12 0 14 0 0 17 18 0 0 0 22 0 0 0 0 0 0 0 0

ELEMENT OF IUNIT: 21 22 23 24 25 26 27 28 29 30 31 32 33 34 35 36 37 38 39 40
PACKAGE NAME : FWL ATO PCN HCN OLF CHF PRL OBS GFD FHB IPT RCT SLC LMG PG5 RES WL5 SFR LK3
GAG
I/O UNIT: 0 0 0 0 0 0 0 0 0 0 0 0 0 19 0 0 0 0 0

ELEMENT OF IUNIT: 41 42 43 44 45 46
PACKAGE NAME : ET2 LUP SUB ZNB CFP TMP
I/O UNIT: 0 0 0 0 0 0

BAS5 -- BASIC MODEL PACKAGE, VERSION 5, 1/1/95 INPUT READ FROM UNIT 1
ARRAYS RHS AND BUFF WILL HAVE SEPARATE MEMORY ALLOCATIONS
INITIAL HEAD WILL BE KEPT THROUGHOUT THE SIMULATION
89784 ELEMENTS IN X ARRAY ARE USED BY BAS
89784 ELEMENTS OF X ARRAY USED

BCF4 -- BLOCK-CENTERED FLOW PACKAGE, VERSION 4, 7/9/92 INPUT READ FROM UNIT 11
 STEADY-STATE SIMULATION
 CELL-BY-CELL FLOWS WILL BE RECORDED ON UNIT 50
 HEAD AT CELLS THAT CONVERT TO DRY= -0.10000E+31
 WETTING CAPABILITY IS NOT ACTIVE
 UPSTREAM DIFFERENCING USED FOR RELATIVE PERMEABILITY
 LEAKANCE VALUES WILL BE READ IN BCF FILE
 ANISOTROPY WITHIN EACH LAYER IS UNIFORM
 RECTANGULAR MODFLOW GRID IS USED
 LAYER AQUIFER TYPE INTERBLOCK T

1	1	0-HARMONIC
2	5	0-HARMONIC
3	5	0-HARMONIC

22440 ELEMENTS IN X ARRAY ARE USED BY BCF
 112224 ELEMENTS OF X ARRAY USED

WEL1 -- WELL PACKAGE, VERSION 5, 9/1/93 INPUT READ FROM 12
 MAXIMUM OF 6 WELLS
 CELL-BY-CELL FLOWS WILL BE RECORDED ON UNIT 50
 24 ELEMENTS IN X ARRAY ARE USED FOR WELLS
 112248 ELEMENTS OF X ARRAY USED

RSF4 -- RECHARGE SEEPAGE FACE PACKAGE, 12/23/95 INPUT READ FROM UNIT 18
 OPTION 3 -- RECHARGE TO HIGHEST ACTIVE NODE IN EACH VERTICAL COLUMN
 CELL-BY-CELL FLOW TERMS WILL BE RECORDED ON UNIT 50
 MAXIMUM OF 0 SEEPAGE-FACE BOUNDARY NODES
 MAXIMUM OF 0 SEEPAGE-FACE BOUNDARY NODES
 4080 ELEMENTS OF X ARRAY USED FOR RSF4 PACKAGE
 116328 ELEMENTS OF X ARRAY USED

RIV1 -- RIVER PACKAGE, VERSION 1, 9/1/87 INPUT READ FROM UNIT 14
 MAXIMUM OF 105 RIVER NODES
 CELL-BY-CELL FLOWS WILL BE RECORDED ON UNIT 50
 630 ELEMENTS IN X ARRAY ARE USED FOR RIVERS
 116958 ELEMENTS OF X ARRAY USED

GHB1 -- GHB PACKAGE, VERSION 1, 9/1/87 INPUT READ FROM UNIT 17
 MAXIMUM OF 43 HEAD-DEPENDENT BOUNDARY NODES
 CELL-BY-CELL FLOW WILL BE RECORDED ON UNIT 50
 215 ELEMENTS IN X ARRAY ARE USED FOR HEAD-DEPENDENT BOUNDARIES
 117173 ELEMENTS OF X ARRAY USED

0PCG5 -- ITERATIVE SPARSE MATRIX SOLVER, VERSION 01, 06/21/02 INPUT READ FROM UNIT 19
 MAXIMUM OF 100 CALLS OF SOLUTION ROUTINE
 MAXIMUM OF 600 INTERNAL ITERATIONS PER CALL TO SOLUTION ROUTINE
 0

SOLUTION BY ITERATIVE SPARSE MATRIX SOLVER

0 MAXIMUM NUMBER OF CALLS TO PCG5 ROUTINE = 100
 MAXIMUM ITERATIONS PER CALL TO PCG5 = 600
 ONLY ACTIVE NODES INCLUDED IN THE SOLVER = 1
 HEAD CHANGE CRITERION FOR CLOSURE = 0.10000E-02
 SOLVER SUMMARY PRINTOUT INDEX = 0
 NATURAL ORDERING (0=OFF;1=ON) = 0
 LEVEL OF ILU FACTORIZATION = 1
 ACCELERATION METHOD = 1
 INDEX FOR BOTTOM DAMPING (IDMPBOT) = 1
 631000 ELEMENTS IN X ARRAY ARE USED BY PCG
 748173 ELEMENTS OF X ARRAY USED
 !!!X ARRAY Allocated for 748184 Elements
 !!!RX AND IR ARRAYS Allocated for 22 Elements

BAS5 -- BASIC MODEL PACKAGE, VERSION 5, 1/1/95 INPUT READ FROM UNIT 1
 1
 MODFLOW Data Set Created by Groundwater Vistas

BOUNDARY ARRAY FOR LAYER 1
 READING ON UNIT 1 WITH FORMAT: (25I3)

BOUNDARY ARRAY FOR LAYER 2
READING ON UNIT 1 WITH FORMAT: (25I3)

BOUNDARY ARRAY = 0 FOR LAYER 3

NUMBER OF ACTIVE NODES IN BAS
1191 FOR LAYER 1
1192 FOR LAYER 2
0 FOR LAYER 3
TOTAL NUMBER OF ACTIVE NODES = 2383

AQUIFER HEAD WILL BE SET TO 999.00 AT ALL NO-FLOW NODES (IBOUND=0).

DATUM ADJUSTMENT IS 0.00000

INITIAL HEAD FOR LAYER 1
READING ON UNIT 1 WITH FORMAT: (10e12.4)

INITIAL HEAD FOR LAYER 2
READING ON UNIT 1 WITH FORMAT: (10e12.4)

INITIAL HEAD FOR LAYER 3
READING ON UNIT 1 WITH FORMAT: (10e12.4)
OOC -- OUTPUT CONTROL PACKAGE INPUT READ FROM UNIT 22

OUTPUT CONTROL IS SPECIFIED EVERY TIME STEP
HEAD PRINT FORMAT CODE IS 0 DRAWDOWN PRINT FORMAT CODE IS 0

HEADS WILL BE SAVED ON UNIT 30 DRAWDOWNS WILL BE SAVED ON UNIT 31

OUTPUT CONTROL IS SPECIFIED EVERY TIME STEP

BCF4 -- BLOCK-CENTERED FLOW PACKAGE, VERSION 4, 7/9/92 INPUT READ FROM UNIT 11

COLUMN TO ROW ANISOTROPY = 1.000000

DELR = 1000.000

DELC = 1000.000

HYD. COND. ALONG ROWS = 0.2000000E-01 FOR LAYER 1

BOTTOM FOR LAYER 1
READING ON UNIT 11 WITH FORMAT: (10e12.4)

VERT HYD COND /THICKNESS FOR LAYER 1
READING ON UNIT 11 WITH FORMAT: (10e12.4)

TRANSMIS. ALONG ROWS = 0.2000000E-01 FOR LAYER 2

VERT HYD COND /THICKNESS FOR LAYER 2
READING ON UNIT 11 WITH FORMAT: (10e12.4)

TRANSMIS. ALONG ROWS FOR LAYER 3
READING ON UNIT 11 WITH FORMAT: (10e12.4)
red-black ordering: nblack,nred = 1273 1110
fill in LU factors: nfill,nfilu = 6915 6915
integer workspace used: 23690

BAS5 -- BASIC MODEL PACKAGE, VERSION 5, 1/1/95 INPUT READ FROM UNIT 1
 1 STRESS PERIOD NO. 1, LENGTH = 1461.000

NUMBER OF TIME STEPS = 1

MULTIPLIER FOR DELT = 1.200

INITIAL TIME STEP SIZE = 1461.000

WEL1 -- WELL PACKAGE, VERSION 5, 9/1/93 INPUT READ FROM 12

6 WELLS

LAYER ROW COL STRESS RATE WELL NO.

1	51	6	0.0000	1
2	51	6	0.0000	2
3	51	6	0.0000	3
1	51	6	0.0000	4
2	51	6	0.0000	5
3	51	6	0.0000	6

RSF4 -- RECHARGE SEEPAGE FACE PACKAGE, 12/23/95 INPUT READ FROM UNIT 18

RECHARGE = 0.1000000E-02

0 SEEPAGE-FACE BOUNDARY NODES

RIV1 -- RIVER PACKAGE, VERSION 1, 9/1/87 INPUT READ FROM UNIT 14

105 RIVER REACHES

LAYER ROW COL STAGE CONDUCTANCE BOT. ELEV. REACH NO.

1	1	25	4.506	485.0	1.506	1
1	1	26	4.283	1138.	1.283	2
1	1	27	4.081	649.0	1.081	3
1	2	24	4.880	1086.	1.880	4
1	2	25	4.655	717.0	1.655	5
1	3	22	5.453	1105.	2.453	6
1	3	23	5.175	1086.	2.175	7
1	3	24	5.030	116.0	2.030	8
1	4	22	5.719	1069.	2.719	9
1	4	23	5.989	1174.	2.989	10
1	5	23	6.271	1002.	3.270	11
1	6	23	6.523	1000.	3.523	12
1	7	16	9.221	960.0	6.221	13
1	7	17	8.994	987.0	5.994	14
1	7	20	7.536	1062.	4.536	15
1	7	21	7.282	1001.	4.282	16
1	7	22	7.033	1001.	4.032	17
1	7	23	6.777	1044.	3.777	18
1	8	15	9.552	1058.	6.552	19
1	8	16	9.399	317.0	6.399	20
1	8	17	8.764	886.0	5.764	21
1	8	18	8.631	181.0	5.631	22
1	8	19	7.868	1247.	4.868	23
1	8	20	7.683	91.00	4.683	24
1	9	14	9.922	863.0	6.922	25
1	9	15	9.758	448.0	6.758	26
1	9	18	8.428	1429.	5.428	27
1	9	19	8.130	995.0	5.130	28
1	10	12	10.55	897.0	7.548	29
1	10	13	10.31	1004.	7.313	30
1	10	14	10.13	637.0	7.128	31
1	11	10	11.26	1298.	8.257	32
1	11	11	11.00	1006.	7.998	33
1	11	12	10.77	850.0	7.770	34
1	12	9	11.62	1321.	8.621	35

1	12	10	11.45	36.00	8.452	36
1	13	3	14.15	1715.	11.15	37
1	13	8	11.95	1100.	8.953	38
1	13	9	11.81	159.0	8.805	39
1	14	1	14.74	1028.	11.74	40
1	14	2	14.56	386.0	11.56	41
1	14	3	13.89	38.00	10.89	42
1	14	4	13.76	1184.	10.76	43
1	14	8	12.18	663.0	9.182	44
1	15	1	14.91	386.0	11.91	45
1	15	4	13.53	541.0	10.53	46
1	15	5	13.37	694.0	10.37	47
1	15	7	12.52	1069.	9.519	48
1	16	5	13.22	656.0	10.22	49
1	16	6	13.00	1012.	9.996	50
1	16	7	12.76	845.0	9.764	51
1	49	7	2.878	61.80	1.878	52
1	49	8	2.796	303.0	1.796	53
1	49	9	2.656	303.0	1.656	54
1	49	10	2.503	316.8	1.503	55
1	49	11	2.400	166.2	1.400	56
1	49	15	1.562	110.7	0.5624	57
1	49	16	1.474	292.2	0.4737	58
1	50	6	3.091	282.3	2.091	59
1	50	7	2.977	281.4	1.977	60
1	50	11	2.308	197.7	1.308	61
1	50	12	2.211	251.4	1.211	62
1	50	14	1.754	70.50	0.7541	63
1	50	15	1.663	324.0	0.6626	64
1	50	16	1.389	49.80	0.3888	65
1	50	17	1.325	293.4	0.3253	66
1	51	4	3.389	129.6	2.389	67
1	51	5	3.260	352.8	2.260	68
1	51	6	3.176	82.50	2.176	69
1	51	12	2.108	190.8	1.108	70
1	51	13	2.013	306.6	1.013	71
1	51	14	1.853	326.1	0.8525	72
1	51	17	1.143	519.0	0.1429	73
1	52	3	3.578	272.1	2.578	74
1	52	4	3.470	221.1	2.470	75
1	53	1	3.926	305.4	2.926	76
1	53	2	3.795	314.7	2.795	77
1	53	3	3.679	132.3	2.678	78
1	40	6	2.741	125.8	1.741	79
1	40	7	2.710	151.1	1.710	80
1	40	8	2.654	193.6	1.654	81
1	41	1	2.962	142.8	1.962	82
1	41	2	2.959	21.30	1.959	83
1	41	4	2.829	138.6	1.829	84
1	41	5	2.795	161.2	1.795	85
1	41	6	2.763	34.50	1.763	86
1	41	8	2.612	153.9	1.612	87
1	42	2	2.932	183.3	1.932	88
1	42	3	2.891	182.7	1.891	89
1	42	4	2.853	43.95	1.853	90
1	42	8	2.575	175.8	1.575	91
1	43	8	2.531	152.4	1.531	92
1	44	8	2.484	152.4	1.484	93
1	44	10	2.356	77.55	1.356	94
1	45	8	2.440	188.1	1.440	95
1	45	9	2.397	199.4	1.398	96
1	45	10	2.372	116.7	1.372	97
1	45	11	2.308	109.8	1.308	98
1	46	8	2.149	204.9	1.149	99
1	46	9	2.215	180.0	1.215	100
1	46	10	2.262	179.7	1.262	101
1	46	11	2.289	44.10	1.289	102
1	47	9	2.094	154.4	1.094	103
1	47	10	2.062	130.8	1.062	104
1	48	10	2.023	151.5	1.023	105

GHB1 -- GHB PACKAGE, VERSION 1, 9/1/87 INPUT READ FROM UNIT 17

43 HEAD-DEPENDENT BOUNDARY NODES

LAYER ROW COL ELEVATION CONDUCTANCE BOUND NO.

1	16	1	20.00	1000.	1
1	17	1	20.00	1000.	2
1	18	1	20.00	1000.	3
1	19	1	20.00	1000.	4
1	20	1	20.00	1000.	5
1	21	1	20.00	1000.	6
1	22	1	20.00	1000.	7
1	23	1	20.00	1000.	8
1	24	1	20.00	1000.	9
1	25	1	20.00	1000.	10
1	26	1	20.00	1000.	11
1	27	1	20.00	1000.	12
1	28	1	20.00	1001.	13
1	29	1	20.00	1000.	14
1	30	1	20.00	1000.	15
1	31	1	20.00	1000.	16
1	32	1	20.00	1000.	17
1	33	1	20.00	1000.	18
1	34	1	20.00	1000.	19
1	35	1	20.00	1000.	20
1	36	1	20.00	1000.	21
1	37	1	20.00	1000.	22
1	38	1	20.00	1000.	23
1	39	1	20.00	1000.	24
1	40	1	20.00	1000.	25
1	42	1	20.00	1000.	26
1	43	1	20.00	1000.	27
1	44	1	20.00	1000.	28
1	45	1	20.00	1000.	29
1	46	1	20.00	1000.	30
1	47	1	20.00	1000.	31
1	48	1	20.00	1000.	32
1	49	1	20.00	1000.	33
1	50	1	20.00	1000.	34
1	51	1	20.00	1000.	35
1	52	1	20.00	1000.	36
1	54	1	20.00	1000.	37
1	55	1	20.00	1000.	38
1	56	1	20.00	1000.	39
1	57	1	20.00	1000.	40
1	58	1	20.00	1000.	41
1	59	1	20.00	1000.	42
1	60	1	20.00	850.0	43

real workspace requirement: 49322
free storage for 84 orthogonal vectors = 217395
storage used for 10 orthogonal vectors = 28017

Iterations

nitr	ohm	rms	rrms
0	0.00000D+00	3.16228D+05	1.00000D+00
1	7.09784D-01	9.56794D+04	3.02565D-01
2	4.48484D+00	6.94067D+04	2.19483D-01
3	2.02386D+00	3.76990D+04	1.19215D-01
4	2.18983D+00	9.56417D+03	3.02446D-02
5	1.69441D+00	4.03314D+03	1.27539D-02
6	1.55529D+00	1.54113D+03	4.87348D-03
7	1.50034D+00	5.16754D+02	1.63412D-03
8	1.36724D+00	1.92128D+02	6.07560D-04
9	1.36861D+00	8.81908D+01	2.78884D-04
10	1.53797D+00	3.24488D+01	1.02612D-04
11	1.73567D+00	1.66941D+01	5.27912D-05

Convergence in 11 iterations
free storage for 84 orthogonal vectors = 217395
storage used for 10 orthogonal vectors = 28017

Iterations

nitr	ohm	rms	rrms
0	0.00000D+00	1.91778D+09	1.00000D+00
1	1.04264D+00	6.10683D+08	3.18432D-01

2	1.52697D+00	2.56959D+08	1.33988D-01
3	1.41531D+00	1.45317D+08	7.57736D-02
4	1.96560D+00	9.94357D+07	5.18494D-02
5	2.27382D+00	6.64821D+07	3.46662D-02
6	2.37567D+00	4.15860D+07	2.16845D-02
7	1.85408D+00	3.06484D+07	1.59812D-02
8	2.11609D+00	2.45111D+07	1.27810D-02
9	2.57194D+00	2.06080D+07	1.07458D-02
10	2.10238D+00	1.84491D+07	9.62002D-03
11	2.67016D+00	1.58379D+07	8.25845D-03
12	8.54016D-01	1.44339D+07	7.52635D-03
13	3.75350D+00	1.25677D+07	6.55328D-03
14	6.01032D+00	1.03596D+07	5.40187D-03
15	3.11487D+00	8.29271D+06	4.32412D-03
16	2.74180D+00	7.65245D+06	3.99026D-03
17	2.58603D+00	5.00664D+06	2.61065D-03
18	1.92539D+00	3.33283D+06	1.73786D-03
19	1.94092D+00	2.26001D+06	1.17845D-03
20	3.07193D+00	1.65785D+06	8.64463D-04
21	2.14596D+00	8.84928D+05	4.61434D-04
22	1.66768D+00	4.41433D+05	2.30179D-04
23	1.67603D+00	3.10612D+05	1.61964D-04
24	1.84276D+00	2.28797D+05	1.19303D-04
25	1.92770D+00	2.12644D+05	1.10880D-04
26	3.25402D+00	2.01692D+05	1.05169D-04
27	4.65301D+00	2.03613D+05	1.06171D-04
28	3.33045D+00	2.56522D+05	1.33760D-04
29	2.60143D+00	2.55593D+05	1.33275D-04
30	5.19637D+00	2.14048D+05	1.11613D-04
31	3.90558D+00	1.97988D+05	1.03238D-04
32	2.73334D+00	1.48716D+05	7.75457D-05

Convergence in 32 iterations
free storage for 84 orthogonal vectors = 217395
storage used for 10 orthogonal vectors = 28017

Iterations			
nitr	ohm	rms	rrms
0	0.00000D+00	4.12005D+05	1.00000D+00
1	9.92746D-01	1.15677D+05	2.80765D-01
2	2.39189D+00	9.27797D+04	2.25191D-01
3	2.69483D+00	8.66586D+04	2.10334D-01
4	2.95187D+00	5.35078D+04	1.29872D-01
5	1.94118D+00	3.45201D+04	8.37856D-02
6	2.05797D+00	2.32520D+04	5.64361D-02
7	2.03254D+00	1.89764D+04	4.60587D-02
8	2.40839D+00	1.47089D+04	3.57009D-02
9	1.66427D+00	1.29446D+04	3.14186D-02
10	2.48251D+00	1.08202D+04	2.62623D-02
11	4.36984D+00	5.49949D+03	1.33481D-02
12	1.22775D+00	4.58347D+03	1.11248D-02
13	2.42500D+00	3.98619D+03	9.67510D-03
14	2.42493D+00	3.20506D+03	7.77919D-03
15	3.14890D+00	2.10568D+03	5.11082D-03
16	2.24181D+00	9.91373D+02	2.40622D-03
17	2.20198D+00	6.65328D+02	1.61486D-03
18	2.37249D+00	2.82262D+02	6.85093D-04
19	1.74956D+00	1.78297D+02	4.32754D-04
20	2.04501D+00	1.26940D+02	3.08102D-04
21	2.77451D+00	9.79364D+01	2.37707D-04
22	2.72584D+00	6.02407D+01	1.46214D-04
23	1.34333D+00	3.63773D+01	8.82934D-05

Convergence in 23 iterations
free storage for 84 orthogonal vectors = 217395
storage used for 10 orthogonal vectors = 28017

Iterations			
nitr	ohm	rms	rrms
0	0.00000D+00	4.05610D+06	1.00000D+00
1	1.07433D+00	1.39308D+06	3.43454D-01
2	1.45216D+00	6.74658D+05	1.66331D-01
3	1.47899D+00	4.00824D+05	9.88200D-02
4	1.83563D+00	2.18293D+05	5.38184D-02
5	1.62101D+00	1.52353D+05	3.75614D-02
6	1.57045D+00	1.37434D+05	3.38833D-02

7	2.20304D+00	1.31371D+05	3.23886D-02
8	2.95929D+00	1.25615D+05	3.09693D-02
9	3.79527D+00	1.15689D+05	2.85221D-02
10	3.37796D+00	1.04692D+05	2.58109D-02
11	3.22941D+00	9.53006D+04	2.34956D-02
12	1.14561D+00	9.03103D+04	2.22653D-02
13	1.97098D+00	8.62519D+04	2.12647D-02
14	5.53071D+00	8.15073D+04	2.00950D-02
15	4.36464D+00	7.49032D+04	1.84668D-02
16	3.19493D+00	6.63246D+04	1.63518D-02
17	2.57700D+00	5.90558D+04	1.45597D-02
18	3.14002D+00	5.54872D+04	1.36799D-02
19	3.06039D+00	4.94702D+04	1.21965D-02
20	3.08036D+00	3.75928D+04	9.26821D-03
21	2.38950D+00	2.23300D+04	5.50528D-03
22	1.99731D+00	1.26560D+04	3.12023D-03
23	2.13164D+00	1.11511D+04	2.74920D-03
24	2.56553D+00	1.01353D+04	2.49879D-03
25	1.99204D+00	8.36091D+03	2.06132D-03
26	1.98458D+00	6.71727D+03	1.65609D-03
27	1.89564D+00	6.01375D+03	1.48264D-03
28	3.22268D+00	5.52086D+03	1.36112D-03
29	2.07000D+00	5.16407D+03	1.27316D-03
30	3.98760D+00	4.83416D+03	1.19182D-03
31	3.16896D+00	4.48247D+03	1.10512D-03
32	2.29491D+00	4.28352D+03	1.05607D-03
33	5.56517D+00	3.71597D+03	9.16142D-04
34	1.12133D+00	3.52295D+03	8.68556D-04
35	2.53004D+00	3.37341D+03	8.31687D-04
36	3.06645D+00	3.25550D+03	8.02618D-04
37	3.89022D+00	3.00700D+03	7.41351D-04
38	3.82788D+00	2.70639D+03	6.67240D-04
39	3.38810D+00	2.22525D+03	5.48619D-04
40	2.72135D+00	1.94298D+03	4.79025D-04
41	3.21693D+00	1.65543D+03	4.08133D-04
42	2.70061D+00	1.23058D+03	3.03389D-04
43	2.28672D+00	7.72179D+02	1.90375D-04
44	1.76860D+00	5.92806D+02	1.46152D-04
45	1.74773D+00	5.33320D+02	1.31486D-04
46	3.66687D+00	4.38848D+02	1.08195D-04
47	2.01487D+00	3.33824D+02	8.23016D-05

Convergence in 47 iterations
free storage for 84 orthogonal vectors = 217395
storage used for 10 orthogonal vectors = 28017

Iterations

nitr	ohm	rms	rrms
0	0.00000D+00	1.60909D+05	1.00000D+00
1	9.96152D-01	3.45395D+04	2.14652D-01
2	1.57477D+00	1.87831D+04	1.16731D-01
3	1.69204D+00	9.69853D+03	6.02735D-02
4	1.67172D+00	5.06579D+03	3.14823D-02
5	1.96823D+00	3.02879D+03	1.88230D-02
6	1.73757D+00	2.14598D+03	1.33366D-02
7	2.54635D+00	1.54494D+03	9.60132D-03
8	2.57894D+00	9.94819D+02	6.18250D-03
9	1.88177D+00	6.96064D+02	4.32583D-03
10	2.11279D+00	5.23744D+02	3.25491D-03
11	3.23693D+00	3.24988D+02	2.01971D-03
12	1.37428D+00	2.33568D+02	1.45156D-03
13	2.24083D+00	1.86754D+02	1.16062D-03
14	2.66367D+00	1.45524D+02	9.04390D-04
15	2.24382D+00	1.17020D+02	7.27246D-04
16	2.44463D+00	9.70226D+01	6.02966D-04
17	2.81085D+00	7.53835D+01	4.68486D-04
18	2.36166D+00	5.87702D+01	3.65239D-04
19	2.46913D+00	4.53954D+01	2.82119D-04
20	2.24833D+00	3.60196D+01	2.23851D-04
21	2.83957D+00	3.03506D+01	1.88620D-04
22	3.46979D+00	2.14360D+01	1.33218D-04
23	1.37722D+00	1.69614D+01	1.05410D-04
24	2.34312D+00	1.34139D+01	8.33631D-05

Convergence in 24 iterations
free storage for 84 orthogonal vectors = 217395

storage used for 10 orthogonal vectors = 28017

Iterations

nitr	ohm	rms	rrms
0	0.00000D+00	5.68197D+04	1.00000D+00
1	9.98540D-01	7.77525D+03	1.36841D-01
2	1.31669D+00	5.07161D+03	8.92578D-02
3	2.13295D+00	3.80162D+03	6.69067D-02
4	2.22516D+00	2.98208D+03	5.24831D-02
5	2.96596D+00	1.81508D+03	3.19444D-02
6	1.90069D+00	8.82426D+02	1.55303D-02
7	1.67164D+00	5.21062D+02	9.17044D-03
8	1.97378D+00	3.31321D+02	5.83109D-03
9	1.83911D+00	2.48343D+02	4.37072D-03
10	2.09888D+00	2.11461D+02	3.72162D-03
11	2.66933D+00	1.88325D+02	3.31443D-03
12	1.39177D+00	1.75533D+02	3.08930D-03
13	2.79882D+00	1.61073D+02	2.83481D-03
14	4.62064D+00	1.31836D+02	2.32025D-03
15	3.56797D+00	8.78786D+01	1.54662D-03
16	2.00669D+00	5.23609D+01	9.21526D-04
17	1.99537D+00	3.11180D+01	5.47662D-04
18	1.91036D+00	2.10439D+01	3.70363D-04
19	2.16897D+00	1.43036D+01	2.51737D-04
20	2.19211D+00	9.38107D+00	1.65102D-04
21	2.38376D+00	5.77948D+00	1.01716D-04
22	2.01727D+00	1.92490D+00	3.38773D-05

Convergence in 22 iterations

free storage for 84 orthogonal vectors = 217395

storage used for 10 orthogonal vectors = 28017

Iterations

nitr	ohm	rms	rrms
0	0.00000D+00	2.36111D+04	1.00000D+00
1	9.97539D-01	2.92090D+03	1.23709D-01
2	1.23118D+00	1.50557D+03	6.37656D-02
3	1.81776D+00	7.75708D+02	3.28535D-02
4	1.33731D+00	5.79850D+02	2.45584D-02
5	2.17850D+00	5.19716D+02	2.20115D-02
6	2.66710D+00	4.58849D+02	1.94336D-02
7	3.83484D+00	3.68236D+02	1.55959D-02
8	2.64891D+00	2.92690D+02	1.23963D-02
9	2.55903D+00	2.16876D+02	9.18534D-03
10	1.91560D+00	1.71348D+02	7.25708D-03
11	2.82880D+00	1.31937D+02	5.58790D-03
12	1.73850D+00	1.16500D+02	4.93412D-03
13	3.48173D+00	8.23337D+01	3.48707D-03
14	2.18192D+00	5.44806D+01	2.30741D-03
15	1.83639D+00	4.31843D+01	1.82898D-03
16	1.91165D+00	3.83728D+01	1.62520D-03
17	3.43076D+00	3.28841D+01	1.39274D-03
18	2.74965D+00	2.74144D+01	1.16108D-03
19	3.43838D+00	1.99517D+01	8.45013D-04
20	2.78022D+00	1.00821D+01	4.27008D-04
21	1.55732D+00	5.75436D+00	2.43714D-04
22	2.26651D+00	3.46827D+00	1.46892D-04
23	1.44951D+00	2.50546D+00	1.06113D-04
24	2.39638D+00	1.67232D+00	7.08278D-05

Convergence in 24 iterations

free storage for 84 orthogonal vectors = 217395

storage used for 10 orthogonal vectors = 28017

Iterations

nitr	ohm	rms	rrms
0	0.00000D+00	9.26522D+03	1.00000D+00
1	9.99017D-01	9.58279D+02	1.03428D-01
2	1.28659D+00	5.90048D+02	6.36841D-02
3	1.90314D+00	3.84132D+02	4.14596D-02
4	1.98446D+00	2.68998D+02	2.90331D-02
5	2.48503D+00	1.74291D+02	1.88113D-02
6	1.95077D+00	1.07645D+02	1.16182D-02
7	2.23461D+00	6.43014D+01	6.94008D-03
8	2.05441D+00	2.94721D+01	3.18093D-03
9	1.48142D+00	1.62111D+01	1.74967D-03

10	1.97663D+00	1.09694D+01	1.18394D-03
11	2.73273D+00	5.85660D+00	6.32105D-04
12	1.26180D+00	3.82939D+00	4.13308D-04
13	2.18454D+00	2.72022D+00	2.93595D-04
14	2.06940D+00	2.04275D+00	2.20475D-04
15	2.06939D+00	1.67874D+00	1.81187D-04
16	2.30326D+00	1.42805D+00	1.54130D-04
17	2.96617D+00	1.19119D+00	1.28565D-04
18	2.84445D+00	9.66264D-01	1.04289D-04
19	3.25281D+00	6.26012D-01	6.75658D-05

Convergence in 19 iterations
free storage for 84 orthogonal vectors = 217395
storage used for 10 orthogonal vectors = 28017

Iterations

nit	ohm	rms	rrms
0	0.00000D+00	7.06067D+03	1.00000D+00
1	1.00092D+00	2.83240D+02	4.01152D-02
2	1.21423D+00	1.26495D+02	1.79154D-02
3	1.50054D+00	6.23732D+01	8.83390D-03
4	1.55713D+00	2.91383D+01	4.12685D-03
5	1.59551D+00	2.32891D+01	3.29843D-03
6	2.62306D+00	1.79366D+01	2.54036D-03
7	2.75818D+00	1.14280D+01	1.61855D-03
8	2.05063D+00	7.73485D+00	1.09548D-03
9	2.00702D+00	5.98246D+00	8.47293D-04
10	2.04740D+00	5.02564D+00	7.11780D-04
11	2.79980D+00	4.24732D+00	6.01546D-04
12	1.27721D+00	4.03458D+00	5.71416D-04
13	4.94986D+00	3.51866D+00	4.98346D-04
14	2.80897D+00	2.88617D+00	4.08768D-04
15	3.17605D+00	2.07935D+00	2.94498D-04
16	2.46297D+00	1.12528D+00	1.59373D-04
17	1.90108D+00	5.73888D-01	8.12796D-05

Convergence in 17 iterations
free storage for 84 orthogonal vectors = 217395
storage used for 10 orthogonal vectors = 28017

Iterations

nit	ohm	rms	rrms
0	0.00000D+00	6.80217D+03	1.00000D+00
1	1.00346D+00	1.27546D+02	1.87507D-02
2	1.19148D+00	6.04250D+01	8.88319D-03
3	1.42084D+00	3.65910D+01	5.37931D-03
4	2.00972D+00	2.52727D+01	3.71539D-03
5	2.23012D+00	2.08910D+01	3.07123D-03
6	2.67513D+00	1.70358D+01	2.50447D-03
7	2.29473D+00	1.34709D+01	1.98039D-03
8	2.55634D+00	1.17848D+01	1.73250D-03
9	3.27728D+00	9.70575D+00	1.42686D-03
10	2.78089D+00	6.73272D+00	9.89790D-04
11	2.20348D+00	4.73301D+00	6.95809D-04
12	1.62787D+00	3.99812D+00	5.87771D-04
13	3.27627D+00	3.00774D+00	4.42174D-04
14	2.44132D+00	1.98280D+00	2.91495D-04
15	1.71472D+00	1.53742D+00	2.26019D-04
16	1.98177D+00	1.37414D+00	2.02016D-04
17	3.38249D+00	1.18495D+00	1.74202D-04
18	2.96800D+00	9.52194D-01	1.39984D-04
19	2.56039D+00	6.95069D-01	1.02183D-04
20	2.67593D+00	4.94422D-01	7.26860D-05

Convergence in 20 iterations
free storage for 84 orthogonal vectors = 217395
storage used for 10 orthogonal vectors = 28017

Iterations

nit	ohm	rms	rrms
0	0.00000D+00	6.72495D+03	1.00000D+00
1	1.00709D+00	9.88206D+01	1.46946D-02
2	1.23572D+00	4.25644D+01	6.32933D-03
3	1.40928D+00	2.73242D+01	4.06311D-03
4	1.87200D+00	1.44591D+01	2.15006D-03
5	1.86721D+00	1.26690D+01	1.88387D-03
6	2.83997D+00	1.16470D+01	1.73191D-03

7	3.21019D+00	9.07160D+00	1.34895D-03
8	2.75912D+00	6.73375D+00	1.00131D-03
9	2.24208D+00	5.15506D+00	7.66557D-04
10	2.22943D+00	4.08590D+00	6.07573D-04
11	3.12547D+00	2.88278D+00	4.28670D-04
12	1.38362D+00	2.38131D+00	3.54101D-04
13	2.92626D+00	1.89764D+00	2.82179D-04
14	2.57157D+00	1.41536D+00	2.10464D-04
15	2.02796D+00	1.09233D+00	1.62430D-04
16	2.27104D+00	8.65139D-01	1.28646D-04
17	2.10052D+00	7.42241D-01	1.10371D-04
18	3.20155D+00	6.52989D-01	9.70994D-05

Convergence in 18 iterations
free storage for 84 orthogonal vectors = 217395
storage used for 10 orthogonal vectors = 28017

Iterations

nitr	ohm	rms	rrms
0	0.00000D+00	6.69520D+03	1.00000D+00
1	1.00446D+00	6.11218D+01	9.12921D-03
2	1.18586D+00	2.94008D+01	4.39133D-03
3	1.43184D+00	2.02606D+01	3.02614D-03
4	1.90317D+00	8.71156D+00	1.30117D-03
5	2.00502D+00	7.58081D+00	1.13228D-03
6	2.83425D+00	6.89044D+00	1.02916D-03
7	2.52010D+00	4.52423D+00	6.75743D-04
8	2.41625D+00	3.51895D+00	5.25592D-04
9	2.01135D+00	3.04061D+00	4.54149D-04
10	2.84502D+00	2.65588D+00	3.96684D-04
11	4.05482D+00	1.83639D+00	2.74285D-04
12	1.33736D+00	1.44226D+00	2.15417D-04
13	2.40574D+00	1.24591D+00	1.86089D-04
14	2.64219D+00	1.07233D+00	1.60164D-04
15	2.43932D+00	8.92648D-01	1.33327D-04
16	2.99556D+00	6.84171D-01	1.02188D-04
17	2.06640D+00	5.56798D-01	8.31638D-05

Convergence in 17 iterations
free storage for 84 orthogonal vectors = 217395
storage used for 10 orthogonal vectors = 28017

Iterations

nitr	ohm	rms	rrms
0	0.00000D+00	6.68393D+03	1.00000D+00
1	1.00083D+00	3.30324D+01	4.94207D-03
2	1.14628D+00	2.04926D+01	3.06594D-03
3	1.44817D+00	1.33658D+01	1.99969D-03
4	1.87442D+00	5.07760D+00	7.59673D-04
5	1.99415D+00	4.68571D+00	7.01042D-04
6	3.01954D+00	4.62736D+00	6.92311D-04
7	2.57788D+00	2.75120D+00	4.11615D-04
8	2.38752D+00	2.19916D+00	3.29023D-04
9	2.04726D+00	1.89213D+00	2.83087D-04
10	3.00684D+00	1.66623D+00	2.49288D-04
11	3.90658D+00	1.12232D+00	1.67913D-04
12	1.30146D+00	8.13616D-01	1.21727D-04
13	2.36693D+00	6.86232D-01	1.02669D-04
14	2.67614D+00	5.95201D-01	8.90496D-05

Convergence in 14 iterations
free storage for 84 orthogonal vectors = 217395
storage used for 10 orthogonal vectors = 28017

Iterations

nitr	ohm	rms	rrms
0	0.00000D+00	6.67939D+03	1.00000D+00
1	9.98425D-01	2.40216D+01	3.59638D-03
2	1.13300D+00	1.54068D+01	2.30661D-03
3	1.48952D+00	9.86362D+00	1.47673D-03
4	1.86689D+00	3.54056D+00	5.30073D-04
5	2.01221D+00	3.42271D+00	5.12428D-04
6	3.07443D+00	3.59803D+00	5.38677D-04
7	2.64920D+00	2.03231D+00	3.04266D-04
8	2.55395D+00	1.69579D+00	2.53884D-04
9	2.12360D+00	1.38055D+00	2.06688D-04
10	2.99551D+00	1.21513D+00	1.81922D-04

```

11 3.38980D+00 8.30110D-01 1.24279D-04
12 1.31661D+00 5.70636D-01 8.54324D-05
Convergence in 12 iterations
free storage for 84 orthogonal vectors = 217395
storage used for 10 orthogonal vectors = 28017

```

Iterations

nitr	ohm	rms	rrms
0	0.00000D+00	6.67728D+03	1.00000D+00
1	9.96794D-01	2.60881D+01	3.90699D-03
2	1.12397D+00	1.18237D+01	1.77073D-03
3	1.53335D+00	7.70883D+00	1.15449D-03
4	1.87419D+00	2.44781D+00	3.66587D-04
5	2.04414D+00	2.44360D+00	3.65957D-04
6	2.85498D+00	2.64022D+00	3.95404D-04
7	2.54594D+00	1.36641D+00	2.04636D-04
8	2.68485D+00	1.21688D+00	1.82242D-04
9	2.13579D+00	9.56886D-01	1.43305D-04
10	2.97988D+00	8.43581D-01	1.26336D-04
11	3.21340D+00	6.29455D-01	9.42681D-05

```

Convergence in 11 iterations
free storage for 84 orthogonal vectors = 217395
storage used for 10 orthogonal vectors = 28017

```

Iterations

nitr	ohm	rms	rrms
0	0.00000D+00	6.67627D+03	1.00000D+00
1	9.95523D-01	3.16345D+01	4.73836D-03
2	1.11215D+00	9.01506D+00	1.35031D-03
3	1.56598D+00	5.99593D+00	8.98096D-04
4	1.88444D+00	1.86421D+00	2.79230D-04
5	2.11891D+00	1.85941D+00	2.78510D-04
6	2.79727D+00	2.09821D+00	3.14279D-04
7	2.46594D+00	9.50705D-01	1.42401D-04
8	2.66483D+00	9.24275D-01	1.38442D-04
9	2.15439D+00	7.07565D-01	1.05982D-04
10	3.08256D+00	6.10444D-01	9.14349D-05

```

Convergence in 10 iterations
free storage for 84 orthogonal vectors = 217395
storage used for 10 orthogonal vectors = 28017

```

Iterations

nitr	ohm	rms	rrms
0	0.00000D+00	6.67578D+03	1.00000D+00
1	9.94664D-01	3.63628D+01	5.44697D-03
2	1.10509D+00	7.17593D+00	1.07492D-03
3	1.59036D+00	4.81514D+00	7.21286D-04
4	1.90691D+00	1.67458D+00	2.50844D-04
5	2.19432D+00	1.55745D+00	2.33298D-04
6	2.93752D+00	1.93200D+00	2.89404D-04
7	2.54649D+00	7.81280D-01	1.17032D-04
8	2.71117D+00	8.72826D-01	1.30745D-04
9	2.21537D+00	6.11489D-01	9.15982D-05

```

Convergence in 9 iterations
free storage for 84 orthogonal vectors = 217395
storage used for 10 orthogonal vectors = 28017

```

Iterations

nitr	ohm	rms	rrms
0	0.00000D+00	6.67550D+03	1.00000D+00
1	9.94237D-01	3.88197D+01	5.81525D-03
2	1.10283D+00	6.24580D+00	9.35630D-04
3	1.60342D+00	4.06798D+00	6.09389D-04
4	1.87951D+00	1.46285D+00	2.19137D-04
5	2.19206D+00	1.21859D+00	1.82546D-04
6	2.98786D+00	1.67782D+00	2.51339D-04
7	2.61042D+00	5.71207D-01	8.55676D-05

```

Convergence in 7 iterations
free storage for 84 orthogonal vectors = 217395
storage used for 10 orthogonal vectors = 28017

```

Iterations

nitr	ohm	rms	rrms
0	0.00000D+00	6.67537D+03	1.00000D+00

1	9.93811D-01	4.14844D+01	6.21454D-03
2	1.10211D+00	5.12153D+00	7.67227D-04
3	1.61150D+00	4.11185D+00	6.15973D-04
4	2.04234D+00	1.71025D+00	2.56203D-04
5	2.76640D+00	1.58019D+00	2.36719D-04
6	3.02858D+00	1.91957D+00	2.87560D-04
7	2.29598D+00	5.23685D-01	7.84502D-05

Convergence in 7 iterations
free storage for 84 orthogonal vectors = 217395
storage used for 10 orthogonal vectors = 28017

Iterations

nitr	ohm	rms	rrms
0	0.00000D+00	6.67529D+03	1.00000D+00
1	9.93654D-01	4.24448D+01	6.35850D-03
2	1.10075D+00	5.02602D+00	7.52930D-04
3	1.60790D+00	3.64883D+00	5.46618D-04
4	1.92736D+00	1.53814D+00	2.30423D-04
5	2.62659D+00	1.23821D+00	1.85491D-04
6	3.23829D+00	1.75853D+00	2.63438D-04
7	2.56460D+00	3.86718D-01	5.79328D-05

Convergence in 7 iterations
free storage for 84 orthogonal vectors = 217395
storage used for 10 orthogonal vectors = 28017

Iterations

nitr	ohm	rms	rrms
0	0.00000D+00	6.67523D+03	1.00000D+00
1	9.93636D-01	4.25213D+01	6.37002D-03
2	1.09353D+00	4.76009D+00	7.13098D-04
3	1.60242D+00	3.25996D+00	4.88367D-04
4	1.89780D+00	1.39495D+00	2.08974D-04
5	2.56317D+00	1.06975D+00	1.60257D-04
6	3.18458D+00	1.51918D+00	2.27585D-04
7	2.46960D+00	2.50292D-01	3.74956D-05

Convergence in 7 iterations
free storage for 84 orthogonal vectors = 217395
storage used for 10 orthogonal vectors = 28017

Iterations

nitr	ohm	rms	rrms
0	0.00000D+00	6.67520D+03	1.00000D+00
1	9.93577D-01	4.28960D+01	6.42617D-03
2	1.09414D+00	4.58062D+00	6.86214D-04
3	1.60609D+00	3.19666D+00	4.78886D-04
4	1.93931D+00	1.41187D+00	2.11510D-04
5	2.61387D+00	1.09635D+00	1.64243D-04
6	3.06200D+00	1.47738D+00	2.21323D-04
7	2.41212D+00	1.80303D-01	2.70109D-05

Convergence in 7 iterations
free storage for 84 orthogonal vectors = 217395
storage used for 10 orthogonal vectors = 28017

Iterations

nitr	ohm	rms	rrms
0	0.00000D+00	6.67518D+03	1.00000D+00
1	9.93496D-01	4.34250D+01	6.50543D-03
2	1.09549D+00	4.58299D+00	6.86571D-04
3	1.61148D+00	3.21700D+00	4.81934D-04
4	1.94588D+00	1.45109D+00	2.17386D-04
5	2.64467D+00	1.11211D+00	1.66604D-04
6	3.03778D+00	1.52151D+00	2.27936D-04
7	2.43999D+00	1.37153D-01	2.05467D-05

Convergence in 7 iterations
free storage for 84 orthogonal vectors = 217395
storage used for 10 orthogonal vectors = 28017

Iterations

nitr	ohm	rms	rrms
0	0.00000D+00	6.67517D+03	1.00000D+00
1	9.93431D-01	4.38540D+01	6.56971D-03
2	1.09485D+00	4.66750D+00	6.99233D-04
3	1.61125D+00	3.20553D+00	4.80216D-04
4	1.93155D+00	1.45245D+00	2.17589D-04

5	2.63489D+00	1.11562D+00	1.67130D-04
6	3.04606D+00	1.51356D+00	2.26744D-04
7	2.46060D+00	1.06931D-01	1.60192D-05

Convergence in 7 iterations
free storage for 84 orthogonal vectors = 217395
storage used for 10 orthogonal vectors = 28017

Iterations

nitr	ohm	rms	rrms
0	0.00000D+00	6.67517D+03	1.00000D+00
1	9.93432D-01	4.38446D+01	6.56831D-03
2	1.09384D+00	4.60181D+00	6.89393D-04
3	1.61148D+00	3.21568D+00	4.81739D-04
4	1.92638D+00	1.42597D+00	2.13623D-04
5	2.62776D+00	1.10313D+00	1.65259D-04
6	3.02497D+00	1.51487D+00	2.26942D-04
7	2.45882D+00	9.07366D-02	1.35932D-05

Convergence in 7 iterations
free storage for 84 orthogonal vectors = 217395
storage used for 10 orthogonal vectors = 28017

Iterations

nitr	ohm	rms	rrms
0	0.00000D+00	6.67516D+03	1.00000D+00
1	9.93442D-01	4.37786D+01	6.55844D-03
2	1.09423D+00	4.68097D+00	7.01252D-04
3	1.61088D+00	3.24992D+00	4.86868D-04
4	1.92998D+00	1.41811D+00	2.12445D-04
5	2.64427D+00	1.16267D+00	1.74179D-04
6	3.00166D+00	1.52376D+00	2.28273D-04
7	2.44420D+00	7.85179D-02	1.17627D-05

Convergence in 7 iterations
free storage for 84 orthogonal vectors = 217395
storage used for 10 orthogonal vectors = 28017

Iterations

nitr	ohm	rms	rrms
0	0.00000D+00	6.67516D+03	1.00000D+00
1	9.93421D-01	4.39152D+01	6.57891D-03
2	1.09490D+00	4.67835D+00	7.00860D-04
3	1.61065D+00	3.25153D+00	4.87110D-04
4	1.92408D+00	1.43578D+00	2.15093D-04
5	2.63030D+00	1.15414D+00	1.72901D-04
6	2.99636D+00	1.54350D+00	2.31230D-04
7	2.47174D+00	6.26187D-02	9.38086D-06

Convergence in 7 iterations
free storage for 84 orthogonal vectors = 217395
storage used for 10 orthogonal vectors = 28017

Iterations

nitr	ohm	rms	rrms
0	0.00000D+00	6.67516D+03	1.00000D+00
1	9.93322D-01	4.45754D+01	6.67780D-03
2	1.09184D+00	4.85534D+00	7.27375D-04
3	1.61400D+00	3.26784D+00	4.89553D-04
4	1.92072D+00	1.47136D+00	2.20423D-04
5	2.64306D+00	1.19612D+00	1.79190D-04
6	2.99570D+00	1.55179D+00	2.32473D-04
7	2.46050D+00	6.08691D-02	9.11875D-06

Convergence in 7 iterations
free storage for 84 orthogonal vectors = 217395
storage used for 10 orthogonal vectors = 28017

Iterations

nitr	ohm	rms	rrms
0	0.00000D+00	6.67515D+03	1.00000D+00
1	9.93407D-01	4.40072D+01	6.59268D-03
2	1.09555D+00	4.91212D+00	7.35881D-04
3	1.61267D+00	3.32821D+00	4.98597D-04
4	1.91651D+00	1.33108D+00	1.99409D-04
5	2.65981D+00	1.24356D+00	1.86296D-04
6	2.96819D+00	1.61104D+00	2.41349D-04
7	2.44660D+00	1.01225D-01	1.51644D-05

Convergence in 7 iterations

free storage for 84 orthogonal vectors = 217395
storage used for 10 orthogonal vectors = 28017

Iterations

nitr	ohm	rms	rrms
0	0.00000D+00	6.67515D+03	1.00000D+00
1	9.93431D-01	4.38468D+01	6.56865D-03
2	1.09404D+00	4.90762D+00	7.35208D-04
3	1.61188D+00	3.29358D+00	4.93408D-04
4	1.91117D+00	1.46221D+00	2.19052D-04
5	2.62734D+00	1.26384D+00	1.89336D-04
6	2.98964D+00	1.57526D+00	2.35989D-04
7	2.49928D+00	4.85239D-02	7.26934D-06

Convergence in 7 iterations
free storage for 84 orthogonal vectors = 217395
storage used for 10 orthogonal vectors = 28017

Iterations

nitr	ohm	rms	rrms
0	0.00000D+00	6.67515D+03	1.00000D+00
1	9.93331D-01	4.45148D+01	6.66873D-03
2	1.08941D+00	4.88792D+00	7.32256D-04
3	1.61651D+00	3.55637D+00	5.32777D-04
4	1.92550D+00	1.41841D+00	2.12491D-04
5	2.65955D+00	1.35794D+00	2.03432D-04
6	2.96666D+00	1.66608D+00	2.49595D-04
7	2.44347D+00	6.80854D-02	1.01998D-05

Convergence in 7 iterations
free storage for 84 orthogonal vectors = 217395
storage used for 10 orthogonal vectors = 28017

Iterations

nitr	ohm	rms	rrms
0	0.00000D+00	6.67515D+03	1.00000D+00
1	9.93256D-01	4.50169D+01	6.74395D-03
2	1.09094D+00	4.93972D+00	7.40016D-04
3	1.61623D+00	3.27422D+00	4.90509D-04
4	1.90110D+00	1.53433D+00	2.29857D-04
5	2.61403D+00	1.26454D+00	1.89440D-04
6	2.98072D+00	1.67122D+00	2.50365D-04
7	2.49333D+00	3.41196D-02	5.11144D-06

Convergence in 7 iterations
free storage for 84 orthogonal vectors = 217395
storage used for 10 orthogonal vectors = 28017

Iterations

nitr	ohm	rms	rrms
0	0.00000D+00	6.67515D+03	1.00000D+00
1	9.93497D-01	4.34068D+01	6.50274D-03
2	1.09731D+00	4.59151D+00	6.87851D-04
3	1.61455D+00	3.96603D+00	5.94148D-04
4	1.91597D+00	1.42328D+00	2.13220D-04
5	2.67388D+00	1.14374D+00	1.71344D-04
6	2.99496D+00	1.86384D+00	2.79221D-04
7	2.49669D+00	1.80619D-01	2.70584D-05

Convergence in 7 iterations
free storage for 84 orthogonal vectors = 217395
storage used for 10 orthogonal vectors = 28017

Iterations

nitr	ohm	rms	rrms
0	0.00000D+00	6.67515D+03	1.00000D+00
1	9.92960D-01	4.69963D+01	7.04048D-03
2	1.07748D+00	6.06459D+00	9.08532D-04
3	1.62148D+00	3.30792D+00	4.95557D-04
4	1.90495D+00	1.24523D+00	1.86547D-04
5	2.64219D+00	1.67909D+00	2.51543D-04
6	2.96327D+00	1.59382D+00	2.38769D-04
7	2.35193D+00	1.02939D-01	1.54213D-05

Convergence in 7 iterations
free storage for 84 orthogonal vectors = 217395
storage used for 10 orthogonal vectors = 28017

Iterations

nitr	ohm	rms	rrms
0	0.00000D+00	6.67515D+03	1.00000D+00
1	9.94019D-01	3.99268D+01	5.98141D-03
2	1.10992D+00	6.02052D+00	9.01931D-04
3	1.60055D+00	3.04797D+00	4.56614D-04
4	1.88394D+00	1.12490D+00	1.68520D-04
5	2.70355D+00	1.52307D+00	2.28170D-04
6	3.02143D+00	1.72436D+00	2.58326D-04
7	2.41464D+00	2.71808D-01	4.07194D-05

Convergence in 7 iterations
free storage for 84 orthogonal vectors = 217395
storage used for 10 orthogonal vectors = 28017

Iterations

nitr	ohm	rms	rrms
0	0.00000D+00	6.67515D+03	1.00000D+00
1	9.92657D-01	4.90145D+01	7.34283D-03
2	1.08387D+00	5.13560D+00	7.69361D-04
3	1.64636D+00	3.80565D+00	5.70122D-04
4	1.91439D+00	1.89875D+00	2.84451D-04
5	2.50979D+00	1.60724D+00	2.40779D-04
6	2.89913D+00	1.73899D+00	2.60517D-04
7	2.73364D+00	3.52705D-02	5.28385D-06

Convergence in 7 iterations

0
36 ITERATIONS FOR TIME STEP 1 IN STRESS PERIOD 1

MAXIMUM HEAD CHANGE FOR EACH ITERATION:

HEAD CHANGE HEAD CHANGE HEAD CHANGE HEAD CHANGE HEAD CHANGE
LAYER,ROW,COL LAYER,ROW,COL LAYER,ROW,COL LAYER,ROW,COL LAYER,ROW,COL

```

-----
0.3613E+06 -0.3612E+06 0.1901E+05 -0.1542E+05 -1109.
( 1, 7, 17) ( 1, 7, 17) ( 1, 17, 20) ( 1, 17, 20) ( 1, 49, 14)
-524.2 -237.8 -42.96 -13.90 -8.001
( 1, 3, 25) ( 1, 3, 25) ( 1, 3, 25) ( 1, 49, 14) ( 1, 14, 9)
-5.007 -3.386 -2.245 -1.580 -1.112
( 1, 39, 8) ( 1, 39, 8) ( 1, 39, 8) ( 1, 39, 8) ( 1, 39, 8)
-0.7829 -0.5698 -0.3918 -0.3004 -0.2140
( 1, 40, 9) ( 1, 40, 9) ( 1, 40, 9) ( 1, 40, 9) ( 1, 40, 9)
-0.1488 -0.1067 -0.7692E-01 -0.5497E-01 -0.3917E-01
( 1, 40, 9) ( 1, 40, 9) ( 1, 40, 9) ( 1, 40, 9) ( 1, 40, 9)
-0.2802E-01 -0.2004E-01 -0.1433E-01 -0.1025E-01 -0.7284E-02
( 1, 40, 9) ( 1, 40, 9) ( 1, 40, 9) ( 1, 40, 9) ( 1, 40, 9)
-0.5261E-02 -0.3719E-02 -0.2722E-02 -0.1900E-02 -0.1391E-02
( 1, 40, 9) ( 1, 40, 9) ( 1, 40, 9) ( 1, 40, 9) ( 1, 40, 9)
-0.9724E-03
( 1, 40, 9)

```

00C -- OUTPUT CONTROL PACKAGE INPUT READ FROM UNIT 22

HEAD/DRAWDOWN PRINTOUT FLAG = 1 TOTAL BUDGET PRINTOUT FLAG = 1
CELL-BY-CELL FLOW TERM FLAG = 1

OUTPUT FLAGS FOR ALL LAYERS ARE THE SAME:

HEAD DRAWDOWN HEAD DRAWDOWN
PRINTOUT PRINTOUT SAVE SAVE

```

-----
0 0 1 1
UBUDSV SAVING " CONSTANT HEAD" ON UNIT 50 AT TIME STEP 1, STRESS PERIOD 1
UBUDSV SAVING "FLOW RIGHT FACE " ON UNIT 50 AT TIME STEP 1, STRESS PERIOD 1
UBUDSV SAVING "FLOW FRONT FACE " ON UNIT 50 AT TIME STEP 1, STRESS PERIOD 1
UBUDSV SAVING "FLOW LOWER FACE " ON UNIT 50 AT TIME STEP 1, STRESS PERIOD 1
UBUDSV SAVING " WELLS" ON UNIT 50 AT TIME STEP 1, STRESS PERIOD 1
UBUDSV SAVING " RECHARGE" ON UNIT 50 AT TIME STEP 1, STRESS PERIOD 1
UBUDSV SAVING " RIVER LEAKAGE" ON UNIT 50 AT TIME STEP 1, STRESS PERIOD 1
UBUDSV SAVING " HEAD DEP BOUNDS" ON UNIT 50 AT TIME STEP 1, STRESS PERIOD 1

```

HEAD WILL BE SAVED ON UNIT 30 AT END OF TIME STEP 1, STRESS PERIOD 1

DRAWDOWN WILL BE SAVED ON UNIT 31 AT END OF TIME STEP 1, STRESS PERIOD 1

1
VOLUMETRIC BUDGET FOR ENTIRE MODEL AT END OF TIME STEP 1 IN STRESS PERIOD 1

CUMULATIVE VOLUMES		L**3	RATES FOR THIS TIME STEP		L**3/T

IN:			IN:		
---			---		
STORAGE =	0.0000		STORAGE =	0.0000	
CONSTANT HEAD =	1.6146E-12		CONSTANT HEAD =	1.1051E-15	
WELLS =	0.0000		WELLS =	0.0000	
RECHARGE =	1645085952.0000		RECHARGE =	1126000.0000	
RIVER LEAKAGE =	0.0000		RIVER LEAKAGE =	0.0000	
HEAD DEP BOUNDS =	0.0000		HEAD DEP BOUNDS =	0.0000	
TOTAL IN = 1645085952.0000			TOTAL IN = 1126000.0000		
OUT:			OUT:		
----			----		
STORAGE =	0.0000		STORAGE =	0.0000	
CONSTANT HEAD =	92406920.0000		CONSTANT HEAD =	63249.0898	
WELLS =	0.0000		WELLS =	0.0000	
RECHARGE =	0.0000		RECHARGE =	0.0000	
RIVER LEAKAGE =	1316913024.0000		RIVER LEAKAGE =	901377.8125	
HEAD DEP BOUNDS =	235766160.0000		HEAD DEP BOUNDS =	161373.1406	
TOTAL OUT = 1645086104.0000			TOTAL OUT = 1126000.0430		
IN - OUT = -152.0000			IN - OUT = -4.2969E-02		
PERCENT DISCREPANCY = 0.00			PERCENT DISCREPANCY = 0.00		

%%%%%%%%% STEADY STATE FLOW %%%%%%%%%

TIME SUMMARY AT END OF TIME STEP			1 IN STRESS PERIOD			1
SECONDS	MINUTES	HOURS	DAYS	YEARS		

TIME STEP LENGTH	1.2623040E+08	2103840.	35064.00	1461.000	4.000000	
STRESS PERIOD TIME	1.2623040E+08	2103840.	35064.00	1461.000	4.000000	
TOTAL TIME	1.2623040E+08	2103840.	35064.00	1461.000	4.000000	

1

***** SIMULATION TIME = 0.218750 SECS *****

***** END OF SIMULATION *****

Appendix D- Glossary

List of acronyms

AFM Atomic Force Microscopy

BTC Break Through Curve

CFT Colloid Filtration Theory

CNT Carbon Nanotube

DNAPL Dense Non Aqueous-Phase Liquid

ENP Engineered Nanoparticle

FEFLOW Finite Element Flow Model

MAR Managed Aquifer Recharge

MODFLOW Modular Finite-Difference Flow Model

MWCNT Multi Walled Carbon Nanotube

NZVI Nano-Scale Zero Valent Iron

Pe Peclet Number (dimensionless)

PRB Permeable Reactive Barrier

SCE Single Collector Efficiency

SEM Scanning Electron Microscope

SWCNT Single Walled Carbon Nanotube

TEM Transmission Electron Microscope

USGS United States Geological Survey

Terminology guide

Adsorption: the attachment of colloids, controlled by a kinetic process.

Advection: the movement of miscible or suspended contaminants at the same velocity as the groundwater flow.

Artificial recharge: the directed and enhanced recharge to groundwater which would not have occurred without human intervention.

Break through curve: A plot of relative concentration versus time, where relative concentration is defined as C/C_0 with C as the concentration at a point in the groundwater flow domain, and C_0 as the source concentration.

Colloid: a homogeneous non-crystalline substance consisting of large molecules or ultramicroscopic particles of one substance dispersed through a second substance.

Desorption: the detachment of colloids, controlled by a kinetic process.

Dispersion: the spreading of the contaminant over a larger area than would be predicted solely from the average groundwater velocity vectors.

Equilibrium: the state of a reversible chemical reaction in which its forward and reverse reactions occur at equal rates so that the concentration of the reactants and products remains the same.

Finite element: this method finds approximate solutions to boundary value problems for differential equations.

Finite-difference: this methods approximate the solutions to differential equations by approximating derivatives of these equations.

Grey water: the relatively clean waste water from baths, sinks, washing machines, and other kitchen appliances.

Heterogeneous: diverse in character or content

Homogeneous: Similar in character or content

Nanomaterials: a material having particles or constituents of nanoscale dimensions, or one that is produced by nanotechnology.

Nanoremediation: a particular remedial design, in which, nanomaterials or nanotechnology is in use.

Nanotechnology: the branch of technology that deals with dimensions and tolerances of less than 100 nanometres, especially the manipulation of individual atoms and molecules.

Oxidation: the interaction between oxygen molecules and all the different substances they may contact.

Retardation: the continuous decrement of velocity; a negative acceleration, delaying progress.

Stochastic modelling: estimating probability distributions of potential outcomes by allowing for random variation in one or more inputs over time.

Unsaturated [soil]: soil in which the pore spaces contain water at less than atmospheric pressure.

Viscosity: the state of being thick, sticky, and semi-fluid in consistency, due to internal friction.

Bibliography

- Abbasi, S., Carreau, P.J. & Derdouri, A. 2010, 'Flow induced orientation of multiwalled carbon nanotubes in polycarbonate nanocomposites: Rheology, conductivity and mechanical properties', *Polymer*, vol. 51, pp. 922-35.
- Anderson, M.P. 1979, 'Using models to simulate the movement of contaminants through groundwater flow systems', *CRC Critical Rev. Environmental Control*, vol. 9, no. 2, pp. 97-156.
- Anderson, M.P. 1984, 'Movement of contaminants in groundwater: groundwater transport -- advection and dispersion', *Groundwater Contamination*, National Academy Press, Washington, DC, pp. 37-45.
- Andricevic, R. & Kitanidis, P.K. 1990, 'Optimization of the pumping schedule in aquifer remediation under uncertainty', *Water Resources Research*, vol. 26, no. 5, pp. 878-85.
- Aravind, S.S. & Ramaprabhu, S. 2012, 'Synthesis and thermal transport studies of nanofluids based on metal decorated photochemically oxidized multiwalled carbon nanotubes', *Journal of Nanoscience and Nanotechnology*, vol. 12, no. 8, pp. 6615-20.
- Arnold, W.A. & Roberts, A.L. 2000, 'Pathways and kinetics of chlorinated ethylene and chlorinated acetylene reaction with Fe(0) particles', *Environmental Science and Technology*, vol. 34, pp. 1794-805.
- Bagtzoglou, A.C., Dougherty, D.E. & Tompson, A.F.B. 1992, 'Application of particle methods to reliable identification of groundwater pollution sources ', *Water Resources Management*, vol. 6, pp. 15-23.
- Bales, R.C., Hinkle, S.R., Kroeger, T.W., Stocking, K. & Gerba, C.P. 1991, 'Bacteriophage adsorption during transport through porous media: chemical perturbations and reversibility', *Environmental Science and Technology*, vol. 25, no. 12, pp. 2088-95.
- Ballio, F. & Guadagnini, A. 2004, 'Convergence assessment of numerical Monte Carlo simulations in groundwater hydrology', *Water Resources Research*, vol. 40, no. W04603, pp. doi: 10.1029/2003 WR002876.
- Banfield, J.F. & Zhang, H.Z. 2001, 'Nanoparticles in the environment', *Mineral Geochemistry*, vol. 44, pp. 1-58.
- Barnett, B., Townley, L.R., Post, V., Evans, R.E., Hunt, R.J., Peeters, L., Richardson, S., Werner, A.D., Knapton, A. & Boronkay, A. 2012, *Australian groundwater*

modelling guidelines, Report Number Waterlines Report No. 82, National Water Commission, Canberra, AUstralia.

- Battaglin, W.A., Thurman, E.M., Kalkhoff, S.J. & Porter, S.D. 2003, 'Herbicides and transformation products in surface waters of the Midwestern United States', *American Water Resources Association*, vol. 39, pp. 743-56.
- Battiato, I. 2010. *Hybrid models of transport in crowded environments*. Engineering Sciences w/ Spec in Computational Science, University of California, San Diego, USA.
- Bear, J. 1972, *Dynamics of fluids in porous media*, American Elsevier Publishing Company, New York.
- Bear, J. 1979, *Hydraulics of groundwater*, McGraw-Hill, New York.
- Beven K.J. & Binley, A. 1992, 'The future of distributed models: model calibration and uncertainty prediction', *Hydrological Processes*, vol. 6, pp. 279-98.
- Bhattacharjee, S., Ryan, J. & Elimelech, M. 2002, 'Virus transport in physically and geochemically heterogeneous subsurface porous media', *Journal of Contaminant Hydrology*, vol. 57, pp. 161-87.
- Bianco, A., Kostarelos, K. & Prato, M. 2005, 'Applications of carbon nanotubes in drug delivery', *Current Opinion in Chemical Biology*, vol. 9, no. 6, pp. 674-9.
- Boxall, A.B.A. 2012, *New and emerging water pollutants arising from agriculture*, OECD, York, UK.
- Brooks, K. 2000. *In-situ reductive dehalogenation of DNAPLS by the use of emulsified zero-valent nanoscale and microscale iron particles*. PhD, University of Central Florida, Orlando, Florida, USA.
- Bryant, S.L. & Thompson, K.E. 2001, 'Theory, modeling and experiment in reactive transport in porous media', *Science*, vol. 6, no. 3, pp. 217-22.
- Burrough, P.A. 1986, *Principals of geographical information systems for land resources assessment*, Clarendon Press, Oxford.
- Carrera, J. & Neuman, S.P. 1986, 'Estimation of aquifer parameters under steady-state and transient condition: 1. Background and Statistical framework', *Water Resources Research*, vol. 22, no. 2, pp. 199-210.
- Chen, J., Hamon, M.A., Hu, H., Chen, Y.S., Rao, A.M., Eklund, P.C. & Haddon, R.C. 1998, 'Solution properties of single-walled carbon nanotubes', *Science*, vol. 282, pp. 95-8.

- Christensen, S. & Cooley, R.L. 1999a, 'Evaluation of confidence intervals for a steady-state leaky aquifer model', *Advances in Water Resources*, vol. 22, no. 8, pp. 807-17.
- Christensen, S. & Cooley, R.L. 1999b, 'Evaluation of prediction intervals for expressing uncertainties in groundwater flow model predictions', *Water Resources Research*, vol. 35, no. 9, pp. 2627-39.
- Cooley, R.L. & Christensen, S. 2006, 'Bias and uncertainty in regression-calibrated models of groundwater flow in heterogeneous media', *Advances in Water Resources*, vol. 29, no. 5, pp. 639-56.
- Cooley, R.L. 2004, 'A theory for modeling ground-water flow in heterogeneous media', *U.S. Geological Survey Professional Paper*, pp. 1679-220.
- Corapcioglu, M.Y. & Jiang, S. 1993, 'Colloid-facilitated groundwater contaminant transport', *Water Resources Research*, vol. 29, no. 7, pp. 2215-26.
- Cullen, E., O'Carroll, D., Yanful, E. & Sleep, B. 2010, 'Simulation of the subsurface mobility of carbon nanoparticles at the field scale', *Advances in Water Resources*, vol. 33, pp. 361-71.
- Darvini, G. & Salandin, P. 2006, 'Nonstationary flow and non ergodic transport in random porous media', *Water Resources Research*, vol. 42, no. 12, pp. W12409.
- Datta, B., Beegle, J.E., Kavvas, M.L. & Orlog, G.T. 1989, *Development of an expert system embedding pattern recognition technique for groundwater pollution source identification. Technical report*, National Technical Information Service, Springfield, Virg.
- de Heer, W.A., Bacsa, W.S., Chatelain, A., Garfin, T., Humphrey- Baker, R., Forro, L. & Ugarte, D. 1995, 'Aligned carbon nanotube films: Production and optical and electronic properties', *Science*, vol. 268, no. 5212, pp. 845-7.
- Diallo, M.S., Glinka, C.J., Goddard, W.A. & Johnson, J.H. 2005, 'Characterisation of nanoparticles and colloids in aquatic systems 1. small angle neutron scattering investigations of Suwanee River fulvic acid aggregates in aqueous solutions', *Nanoparticle Resources*, vol. 7, no. (4-5), pp. 435-48.
- Doherty, J. 2003, 'Groundwater model calibration using pilot points and regularization', *Ground Water*, vol. 41, no. 2, pp. 170-7.
- Doherty, J. 2014, *Model-independent parameter estimation and uncertainty analysis*, Echo Valley Graphics, Inc., USA, viewed 02/07 2014, <<http://www.pesthomepage.org/PEST.php>>.
- Draper, R.N. & Smith, H. 1998, *Applied regression analysis*, 1st edn, John Wiley and Sons, New York.

- Dresselhaus, M.S., Dresselhaus, G. & Eklund, P.C. 1996, *Science of fullerenes and carbon nanotubes*, First edn, Academic Press, San Diego, CA.
- Elimelech, M. & Ryan, J.N. 2002, *Interactions between soil particles and microorganisms: impact on the terrestrial ecosystem*, John Wiley & Sons, New York.
- Fan, Z. & Advani, S.G. 2005, 'Characterization of orientation state of carbon nanotubes in shear flow', *Polymer*, vol. 46, pp. 5232-40.
- Fetter, C.W. 2001, *Applied hydrogeology*, 4th edn, Prentice Hall, New Jersey.
- Fornberg, B. 1998, 'Calculation of weights in finite difference formulas', *SIAM Review*, vol. 40, pp. 685-91.
- Gaganis, P. & Smith, L. 2006, 'Evaluation of the uncertainty of groundwater model predictions associated with conceptual errors: A per-datum approach to model calibration', *Advances in Water Resources*, vol. 29, no. 4, pp. 503-14.
- Garg, A. & Sinnott, S.B. 1998, 'Effect of chemical functionalization on the mechanical properties of carbon nanotubes', *Chemio Physical Letters*, vol. 295, pp. 273-8.
- Gavaskar, A.R., Gupta, N., Sass, B.M., Janosy, R.J. & O'Sullivan, D. 1998, *Permeable barriers for groundwater remediation design, construction, and monitoring*, First edn, Battelle Press, Columbus, OH.
- Geiger, C.L., Clausen, C.A., Clausen, K., Huntley, C., Filipek, C., Reinhart, L., Quinn, D.R., Krug, J., O'Hara, T., Major, S. & Brooks, D. 2003, *Nanoscale and microscale iron emulsions for treating DNAPL. In chlorinated solvent and DNAPL remediation innovative strategies for subsurface cleanup*, American Chemical Society, Washington, DC.
- Gelhar, L.W. 1993, *Stochastic subsurface hydrology*, Prentice-Hall, Englewood Cliffs, NJ.
- Gelhar, L.W. 1993, *Stochastic subsurface hydrology*, NJ: Prentice-, Englewood Cliffs.
- Gelhar, L.W., Gutjahr, A.L. & Naff, R.L. 1979, 'Stochastic analysis of macrodispersion in a stratified aquifer', *Water Resources Research*, vol. 15, pp. 1387-97.
- Gerba, C.P., Wallis, C. & Melnick, J.L. 1975, 'Microbiological hazards of household toilets: Droplet production and the fate of residual organisms', *Applied Microbiology*, vol. 30, no. 2, pp. 229-37.

- Gomez-Hernandez, J.J., Sahuquillo, A. & Capilla, J.E. 1997, 'Stochastic simulation of transmissivity fields conditional to both transmissivity and piezometric data: 1-Theory', *Journal of Hydrology*, vol. 204, no. 1-4, pp. 162-74.
- Gorelick, S.M. 1983, 'A review of distributed parameter groundwater management modelling method ', *Water Resources Research*, vol. 19, no. 2, pp. 305-19.
- Gorelick, S.M., Evans, B. & Remson, I. 1983, 'Identifying sources of groundwater pollution: an optimization approach', *Water Resources Research*, vol. 19, no. 3, pp. 779-90.
- Gould, P. 1970, 'Is Stalistic Infems the Geographical Name for a Wild Goose?', *Economic Geography*, vol. 46, no. 2, pp. 439-48.
- Granqvist, C.G., Buhrman, R.A., Wyns, J. & Sievers, A.J. 1976, 'Far-infrared absorption in ultrafine Al particles', *Physics Review Letters*, vol. 37, no. 10, pp. 625-9.
- Grassian, V.H., O'Shaughnessy, P.T., Dodd, A.A., Pettibone, J.M. & Thorne, P.S. 2008, 'Titanium dioxide nanoparticles', *Environmental Health Perspective*, vol. 116, no. 4, pp. 152-3.
- Griffitt, R.J., Luo, J., Gao, J., Bonzongo, J.C. & Barber, D.S. 2008, 'Effects of particle composition and species on toxicity of metallic nanomaterials in aquatic organisms', *Environmental Toxicology and Chemistry*, vol. 27, pp. 1972-8.
- Guo, W., Ciptadjaya, C.G.E., Liu, M., Simms, C.M. & Obare, S.O. 2008, 'Modulating the reactivity of nanocrystalline TiO₂ for the degradation of organophosphorus pesticides', *Advanced Oxid. Technology*, vol. 11, pp. 459-62.
- Gupta, H.V., Sorooshian, S. & Yapo, P.O. 1998, 'Toward Improved Calibration of Hydrologic Models: Multiple and Noncommensurable Measures of Information', *Water Resources Research*, vol. 34, no. 4, pp. 751-63.
- Harding, S.E. & Colfen, H. 1995, 'Inversion formulas for ellipsoid of revolution macromolecular shape functions', *Analytical Biochemistry*, vol. 228, no. 1, pp. 131-42.
- Hazani, M., Naaman, R., Hennrich, F. & Kappes, M.M. 2003, 'Confocal fluorescence imaging of DNA-functionalized carbon nanotubes', *Nanotechnology Letters*, vol. 3, pp. 153-5.
- Hazen, A. 1892, *Some physical properties of sands and gravels, with special reference to their use in filtration*, Report Number Pub. Doc. No. 34, 539-556, 24th Annual report, Massachusetts State Board of Health.
- Hilder, T.A. & Hill, J.M. 2008, 'Carbon nanotubes as drug delivery nanocapsules', *Current Applied Physics*, vol. 8, no. 3-4, pp. 258-61.

- Hilding, J., Grulke, E.A., Zhang, Z.G. & Lockwood, F. 2003, 'Dispersion of carbon nanotubes in liquids', *Journal of Dispersion Science and Technology*, vol. 24, no. 1, pp. 1-41.
- Hill, M.C. 1998, *Methods and guidelines for effective model calibration*, Report Number 98-4005, US Geological Survey, Water-Resources Investigations, USA.
- Hill, M.C. & Tiedeman, C.R. 2007, *Effective Groundwater Model Calibration, with Analysis of Sensitivities, Predictions, and Uncertainty*, Wiley and Sons, New York.
- Honeyman, B.D. 1999, 'Colloidal culprits in contamination', *Nature*, vol. 397, pp. 23-4.
- Huang, W.J., Taylor, S., Fu, K.F., Lin, Y., Zhang, D.H., Hanks, T.W., Rao, A.M. & Sun, Y.P. 2002, 'Attaching proteins to carbon nanotubes via diimide-activated amidation', *Nanotechnology Letters*, vol. 2, pp. 311-4.
- Huard, D. & Mailhot, A. 2006, 'A Bayesian perspective on input uncertainty in model calibration: application to hydrological model "abc"', *Water Resources Research*, vol. 42, no. WR004661, pp. doi: 10.1029/2005WR004661.
- Hughes, T.V. & Chambers, C.R. 1889, *Manufacture of carbon filaments*, USA, viewed 405480 .
- Ibaraki, M. & Sudicky, E.A. 1995, 'Colloid-facilitated contaminant transport in discretely fractured porous media: 1. Numerical formulation and sensitivity analysis', *Water Resources Research*, vol. 31, no. 12, pp. 2945-60.
- Iijima, S. 1991, 'Helical microtubules of graphitic carbon', *Nature*, vol. 354, pp. 56-8.
- Iwasaki, T. 1937, 'Some notes on sand filtration', *Journal of American Water Works Assoc.*, vol. 29, pp. 1591-7.
- Jaisi, D., Saleh, N., Blake, R. & Elimelech, M. 2008, 'Transport of single-walled carbon nanotubes in porous media: filtration mechanisms and reversibility', *Environmental Science and Technology*, vol. 42, pp. 8317-23.
- Jattasingh, S.J. 2009. *Wettability for environmental remediation: A study using zinc oxide nanorod films*. PhD, University of Auckland: Civil and Environmental Engineering, Auckland, NZ.
- Jiang, L.Q., Gao, L. & Sun, J. 2003, 'Production of aqueous colloidal dispersions of carbon nanotubes', *Journal of Colloid Interface Science*, vol. 260, pp. 89-94.
- Johnson, P.R. & Elimelech, M. 1995, 'Dynamics of colloid deposition in porous media: Blocking based on random sequential adsorption', *Langmuir*, vol. 11, no. 3, pp. 801-12.

- Juhler, R.K., Sorensen, S.R. & Larsen, L. 2001, 'Analysing the transformation products of herbicide residence in environmental samples', *Water Resources*, vol. 35, pp. 1371-8.
- Jung, D.H., Ko, Y.K. & Jung, H.T. 2004, 'Aggregation behavior of chemically attached poly(ethylene glycol) to single-walled carbon nanotubes (SWNTs) ropes', *Material Science Engineering*, vol. 24, no. C, pp. 117-21.
- Kahn, M.G.C., Banerjee, S. & Wong, S.S. 2002, 'Solubilization of oxidized single-walled carbon nanotubes in organic and aqueous solvents through organic derivatization', *Nanotechnology Letters*, vol. 2, pp. 1215-8.
- Kapoor, V. & Kitanidis, P.K. 1997, 'Advection-diffusion in spatially random flows: Formulation of concentration covariance', *Stochastic Hydrology and Hydraulics*, vol. 11, pp. 397-422.
- Karn, B., Kuiken, T. & Otto, M. 2011, 'Nanotechnology and in situ remediation: a review of the benefits and potential risks', *Environmental Health Perspect*, vol. 117, no. 12, pp. 1813-31.
- Kavetski, D., Franks, S. & Kuczera, G. 2002, 'Confronting input uncertainty in environmental modelling. In: Gupta, H.V., Sorooshian, S., Rousseau, A.N., Turcotte, R. (Eds.), Calibration of Watershed Models', *AGU Water Science and Applications Series*, pp. 49-68.
- Kersting, A.B., Efur, D.W., Finnegan, D.L. & Rokop, D.J. 1999, 'Migration of the plutonium in groundwater at Nevada test site', *Nature*, vol. 397, pp. 56-9.
- Kessler, J.H. & Hunt, J.R. 1994, 'Dissolved and colloidal contaminant transport in a partially clogged fracture', *Water Resources Research*, vol. 30, no. 4, pp. 1195-206.
- Ko, C.H. & Elimelech, M. 2000, 'The “shadow effect” in colloid transport and deposition dynamics in granular porous media: Measurements and mechanisms', *Environmental Science and Technology*, vol. 34, no. 17, pp. 3681-9.
- Kolpin, D.W., Furlong, E.T., Meyer, M.T., Thurman, E.M., Zaugg, S.D., Barber, L.B. & Buxton, H.T. 2002, 'Pharmaceuticals, hormones, and other organic wastewater contaminants in US streams', *Environmental Science and Technology*, vol. 36, pp. 1202-11.
- Kong, J., Franklin, N., Zhou, C., Chapline, M., Peng, S., Cho, K. & Dai, H. 2000, 'Nanotube molecular wires as chemical sensors', *Science*, vol. 287, no. 5453, pp. 622-5.
- Kozeny, J. 1927, 'Über kapillare leitung des wassers in boden. Sitzungsber Akad (In German).', *Wiss.Wien Math.Naturwiss.Kl.*, vol. 136, no. Abt.2a, pp. 271-306.

- Kretzschmar, R., Barmettler, K., Grolimund, D., Yan, Y., Borokovec, M. & Sticher, H. 1997, 'Experimental determination of colloid deposition rates and collision efficiencies in natural porous media', *Water Resources Research*, vol. 33, no. 5, pp. 1129-37.
- Lagana, A., Bacaloni, A., De Leva, I., Faberi, A., Giovanna, F. & Marino, A. 2001, 'Occurrence and determination of herbicides and their major transformation products in environmental waters', *Analytica Chimica Acta*, vol. 462, pp. 187-98.
- Le Gallo, Y., Bildstein, O. & Brosse, E. 1998, 'Coupled reaction-flow modeling of diagenetic changes in reservoir permeability, porosity and mineral compositions', *Journal of Hydrology*, vol. 209, no. 1-4, pp. 366-88.
- Li, P.S. 2002, 'Diazinon and its degradation products in agricultural water courses in British Columbia', *Bull. Environmental Contaminants Toxicology*, vol. 69, pp. 59-65.
- Li, Y.S., Wang, Y.G., Pennell, K.D. & Abriola, L.M. 2008, 'Investigation of the transport and the deposition of fullerene C60 nanoparticles in quartz sands under varying flow conditions', *Environmental Science and Technology*, vol. 42, no. 19, pp. 7174-80.
- Lichtner, P.C. & Tartakovsky, D.M. 2003, 'Stochastic analysis of effective rate constant for heterogeneous reactions', *Stochastic Environmental Resources Risk Assessment*, vol. 17, no. 6, pp. 419-29.
- Lin, D., Tian, X., Wu, F. & Xing, B. 2010, 'Fate and Transport of engineered nanomaterials in the environment', *Journal of Environmental Quality*, vol. 39, no. 6, pp. 1896-908.
- Lindqvist, R., Cho, J.S. & Enfield, C.G. 1994, 'A kinetic model for cell density dependent bacterial transport in porous media', *Water Resources Research*, vol. 30, no. 12, pp. 3291-9.
- Lisunova, M.O., Lebovka, N.I., Melezhyk, E.V. & Boiko, Y.P. 2006, 'Stability of the aqueous suspensions of nanotubes in the presence of nonionic surfactant', *Journal of Colloid Interface Science*, vol. 299, pp. 740-6.
- Liu, X., O'Carroll, d., Petersen, E., Huang, Q. & Anderson, L. 2009, 'Mobility of multiwalled carbon nanotubes in porous media', *Journal of Contaminant Hydrology*, vol. 43, no. 21, pp. 8153-8.
- Loveland, J.P., Bhattacharjee, S., Ryan, J. & Elimelech, M. 2003, 'Colloid transport in a geochemically heterogeneous porous medium: aquifer tank experiment and modeling', *Journal of Contaminant Hydrology*, vol. 65, pp. 161-82.
- Lövestam, G., Rauscher, H., Roebben, G., Sokull Klüttgen, B., Gibson, N., Putaud, J.P. & Stamm, H. 2010, *Considerations on a definition of nanomaterial for*

regulatory purposes, Report Number 36, Publications Office of the European Union, JRC European Commission, Luxembourg.

- Lührmann, L., Noseck, U. & Tix, C. 1998, 'Model of contaminant transport in porous media in the presence of colloids applied to actinide migration in column experiments', *Water Resources Research*, vol. 34, no. 3, pp. 421-6.
- Macdonald, M.G. & Harbaugh, A.W. 2003, 'The History of MODFLOW', *Groundwater*, vol. 41, no. 2, pp. 280-3.
- Madsen, H. 2003, 'Parameter estimation on distributed hydrological catchment modelling using automatic calibration with multiple objectives', *Advances in Water Resources*, vol. 26, no. 2, pp. 205-16.
- Masch, F.D. & Denny, K.J. 1966, 'Grain-size distribution and its effects on the permeability of unconsolidated sands', *Water Resources Research*, vol. 2, pp. 665-7.
- Mawdsley, J.L. & Bardgett, R.D. 1995, 'Pathogens in livestock waste. Their potential for movement through soil and environmental-pollution', *Applied Soil Ecology*, vol. 2, no. 1, pp. 1-15.
- Maxwell, M., Welty, C. & Tompson, A.F.B. 2003, 'Streamline-based simulation of virus transport resulting from long term artificial recharge in a heterogeneous aquifer', *Advances in Water Resources*, vol. 26, pp. 1075-96.
- Maynard, A.D., Aitken, R.J., Butz, T., Colvin, V., Donaldson, K., Oberdorster, G., Philbert, M.A., Ryan, J., Seaton, A., Stone, V., Tinkle, S.S., Tran, L., Walker, N.J. & Warheit, D.B. 2006, 'Safe handling of nanotechnology', *Nature*, vol. 444, pp. 267-9.
- McCarthy, J.F. 1989, 'Subsurface transport of contaminants', *Environmental Science and Technology*, vol. 23, no. 5, pp. 496-502.
- McDowell-Boyer, L.M. 1992, 'Flow of micron-sized particles in saturated porous media under steady conditions', *Environmental Science and Technology*, vol. 26, pp. 586-93.
- Medema, G.L. & Juhasz-Holterman, M.H.A. 2000, 'Removal of micro-organisms by bank filtration in a gravel-sand soil', *the International Riverbank Filtration Conference*, eds W. Julich & J. Schubert, IAWR, Dusseldorf, Germany, .
- Mehrabi, S. & Milne-Home, W. 2012, 'Representation of Heterogeneity in Single Collector Efficiency Equation for Multi-Walled Carbon Nanotubes', *International Journal of Theoretical and Applied Nanotechnology*, vol. 1, pp. 75-86.

- Michalak, A.M. & Kitanidis, P.K. 2003, 'A method for enforcing parameter non negativity in bayesian inverse problems with an application to contaminant source identification', *Water Resources Research*, vol. 39, no. 2, pp. 1033-46.
- Mintmire, J.W. & White, C.T. 1995, 'Electronic and structural properties of carbon nanotubes', *Carbon*, vol. 33, no. 7, pp. 893-902.
- Molla, S.H. 2009. *AC electrokinetic manipulation of colloids during filtration*. University of Alberta (Canada), ProQuest, UMI Dissertations Publishing, Alberta, Canada.
- Monteiro, S.C. & Boxall, A.B.A. 2009, 'Factors affecting the degradation of pharmaceuticals in agricultural soils', *Environmental Toxicology and Chemistry*, vol. 28, no. 12, pp. 2546-54.
- Monthioux, M. & Kuznetsov, V.L. 2006, 'Who should be given the credit for the discovery of carbon nanotubes?', *Carbon*, vol. 44, pp. 1621-3.
- Monthioux, M., Smith, B.W., Burteaux, B., Claye, A., Fischer, J.E. & Luzzi, D.E. 2001, 'Sensitivity of single-wall carbon nanotubes to chemical processing: an electron microscopy investigation', *Carbon*, vol. 39, pp. 1251-72.
- Moore, C. & Doherty, J. 2005, 'The role of the calibration process in reducing model predictive error', *Water Resources Research*, vol. 41, no. W05020, pp. doi:10.1029/2004WR003501.
- Morales-Casique, E., Neuman, S.P. & Guadagnini, A. 2006a, 'Non-local and localized analyses of non-reactive solute transport in bounded randomly heterogeneous porous media: Theoretical framework', *Journal of Advanced Water Resources*, vol. 29, no. 8, pp. 1238-55.
- Morales-Casique, E., Neuman, S.P. & Guadagnini, A. 2006b, 'Nonlocal and localized analyses of nonreactive solute transport in bounded randomly heterogeneous porous media: Computational analysis', *Journal of Advanced Water Resources*, vol. 29, no. 9, pp. 1399-416.
- Mulvey, J.M., Vanderbei, R.J. & Zenios, S.A. 1995, 'Robust optimization of large-scale systems', *Operations Research*, vol. 23, no. 2, pp. 264-81.
- Nelson, K.E. & Ginn, T.R. 2005, 'Colloid filtration theory and the happel sphere-in-cell model revisited with direct numerical simulation of colloids', *Langmuir*, vol. 21, pp. 2173-84.
- Nelson, K.E. & Ginn, T.R. 2011, 'New collector efficiency equation for colloid filtration in both natural and engineered flow conditions', *Water Resources Research*, vol. 47, no. W05543, pp. 1-17.

- Neuman, S.P. 2003, 'Maximum likelihood Bayesian averaging of alternative conceptual-mathematical models', *Stochastic Environmental Research and Risk*, vol. 17, no. 5, pp. 291-305.
- Neuman, S.P. & Wierenga, P.J. 2003, *A comprehensive strategy of hydrogeologic modeling and uncertainty analysis for nuclear facilities and sites*, Report Number NUREG/CR-6805, prepared for U.S. Nuclear Regulatory Commission, Washington, DC.
- Neuman, S.P. & Yakowitz, S. 1979, 'A statistical approach to the inverse problem of aquifer hydrology, 1. Theory', *Water Resources Research*, vol. 15, pp. 845-60.
- Oberlin, A., Endo, M. & Koyama, T. 1976, 'Filamentous growth of carbon through benzene decomposition', *Journal of Crystal Growth*, vol. 32, pp. 35-349.
- Odom, T.W., Huang, J.L., Kim, P. & Lieber, C.M. 1998, 'Atomic structure and electronic properties of single-walled carbon nanotubes', *Nature*, vol. 391, pp. 62-4.
- Pan, Z.W., Xie, S.S., Chang, B.H., Wang, C.Y., Lu, L., Liu, W., Zhou, M.Y. & Li, W.Z. 1998, 'Very long carbon nanotubes', *Nature*, vol. 394, pp. 631-2.
- Panday, S., Langevin, C.D., Niswonger, R.G., Ibaraki, M. & Hughes, J.D. 2013, *MODFLOW-USG version 1: An unstructured grid version of MODFLOW for simulating groundwater flow and tightly coupled processes using a control volume finite-difference formulation*, Report Number Techniques and Methods 6-A45, U.S. Geological Survey, Reston, Virginia.
- Pang, S. 1996. *Colloid retention and flow in porous media*. The University of Texas at Austin, ProQuest, UMI Dissertations Publishing, Austin, USA .
- Parratt, L.G. 1961, *Probability and experimental errors in science: An elementary survey*, 1st edn, Wiley, New York.
- Poeter, E. & Hill, M.C. 1998, *Documentation of UCODE, a computer code for universal inverse modeling*, Report Number WRIR 98-4080, USGS, USA.
- Pompeo, F. & Resasco, D.E. 2002, 'Water solubilization of single-walled carbon nanotubes by functionalization with glucosamine', *Nanotechnology Letters*, vol. 2, pp. 369-73.
- Powell, R.M., Blowes, D.W., Gillham, R.W., Schultz, D., Sivavec, T., Puls, R.W., Vogan, J.L., Powell, P.D. & Landis, R. September 1998, *Permeable reactive barrier technologies for contaminant remediation*, Report Number EPA/600/R-98/125, U.S. Printing Office, Washington, DC.
- Quinn, J., O'Hara, S., Krug, T., Geiger, C. & Clausen, C. May 2004, 'Evaluating the distribution of emulsified zero-valent iron for four different injection

techniques', *Fourth International Conference on Remediation of Chlorinated and Recalcitrant Compounds. Monterey, CA.*, .

- Radushkevich, L.V. & Lukyanovich, V.M. 1952, 'O strukture ugleroda, obrazujucesja pri termiceskom razlozenii okisi ugleroda na zeleznom kontakte', *Zurn. Fisic. Chim.*, vol. 26, pp. 88-95.
- Rajagopalan, R. & Tien, C. 1976, 'Trajectory analysis of deep-bed filtration with the sphere-in-cell porous media model', *AIChE Journal*, vol. 22, no. 3, pp. 523-33.
- Rajan, C.S. 2011, 'Nanotechnology in groundwater remediation', *International Journal of Environmental Science and Development*, vol. 2, no. 3.
- Refsgaard, J.C., van der Sluijs, J. P., Brown, J. & van der Keur, P. 2006, 'A framework for dealing with uncertainty due to model structure error', *Advances in Water Resources*, vol. 29, no. 11, pp. 1586-97.
- Robert, W. & Powellet, R.B. 1992, 'Transport of inorganic colloids through natural aquifer material: Implications for contaminant transport', *Environmental Science and Technology*, vol. 26, pp. 614-21.
- Roy, S.B. & Dzombak, A. 1997, 'Chemical factors influencing colloid-facilitated transport of contaminants in porous media ', *Environmental Science and Technology*, vol. 31, pp. 656-64.
- Saiers, J.E. & Hornberger, G.M. 1996, 'The role of colloidal kaolinite in the transport of cesium through laboratory sand columns', *Water Resources Research*, vol. 32, no. 1, pp. 33-41.
- Saito, R., Dresselhaus, G. & Dresselhaus, M.S. 1998, *Physical properties of carbon nanotubes*, First edn, Imperial College Press, London.
- Saito, R., Fujita, M., Dresselhaus, G. & Dresselhaus, M.S. 1992, 'Electronic-structure of chiral graphene tubules', *Applied Physics Letters*, vol. 60, pp. 2204-6.
- Salandin, P. & Fiorotto, V. 1998, 'Solute transport in highly heterogeneous aquifers', *Water Resources Research*, vol. 34, no. 5, pp. 949-61.
- Salandin, P. & Fiorotto, V. 2000, 'Dispersion tensor evaluation in heterogeneous media for finite Peclet values', *Water Resources Research*, vol. 36, pp. 1449-55.
- Saleh, N.B., Pfefferle, L.D. & Elimelech, M. 2008, 'Aggregation kinetics of multiwalled carbon nanotubes in aquatic systems: measurements and environmental implications', *Environmental Science and Technology*, vol. 42, pp. 7963-9.
- Salzmann, C.G., Llewellyn, S.A., Tobias, G., Ward, M.A.H., Huh, Y. & Green, M.L.H. 2007, 'The role of carboxylated carbonaceous fragments in the

functionalization and spectroscopy of a single-walled carbon-nanotube material', *Advanced Materials*, vol. 19, pp. 883-7.

Sampath, P.V. 2006. *Effects of heterogeneity on groundwater flow and contaminant transport - a visualization library*. Master of Science, Michigan State University, Michigan.

Sano, M., Kamino, A., Okamura, J. & Shinkai, S. 2001b, 'Self-organising of PEO-graft-single-walled carbon nanotube in solutions and Langmuir-Blodgett films', *Langmuir*, vol. 17, pp. 5125-8.

Scheibe, T.D., Dong, H. & Xie, Y. 2007, 'Correlation between bacterial attachment rate coefficients and hydraulic conductivity and its effect on field-scale bacterial transport', *Advances in Water Resources*, vol. 30, pp. 1571-82.

Schijven, J.F. & Hassanizadeh, S.M. 2000, 'Removal of viruses by soil passage: Overview of modeling, processes, and parameters', *Critical Reviews in Environmental Science and Technology*, vol. 30, no. 1, pp. 49-127.

Seaman, J.C. & Bertsch, P.M. 1997, 'Characterization of colloids mobilized from southeastern coastal plain sediments', *Environmental Science and Technology*, vol. 31, pp. 2782-90.

Skaggs, T.H. & Kabala, Z.J. 1994, 'Recovering the release history of a groundwater contaminant', *Water Resources Research*, vol. 30, no. 1, pp. 71-9.

Smith, B.W., Benes, Z., Luzzi, D.E., Fischer, J.E., Walters, D.A., Casavant, M.J., Schmidt, J. & Smalley, R.E. 2000, 'Structural anisotropy of magnetically aligned single wall carbon nanotube films', *Applied Physics Letters*, vol. 77, no. 5, pp. 663.

Smith, J.E. & Perdek, J.M. 2004, 'Assessment and management of watershed microbial contaminants', *Critical Reviews in Environmental Science and Technology*, vol. 34, pp. 2771-81.

Smith, V.J. & Charbeneau, R.J. 1990, 'Probabilistic soil contamination exposure assessment procedures', *Journal of Environmental Engineering, ASCE*, vol. 116, no. 1143el, pp. 163.

Snodgrass, M.F. & Kitanidis, P.K. 1997, 'A geostatistical approach to contaminant source identification', *Water Resources Research*, vol. 33, no. 4, pp. 537-46.

Srinivasan, C. 2008, 'Carbon nanotubes in cancer therapy', *Current Science*, vol. 94, pp. 300.

Sun, N., Elimelech, M., Sun, N.Z. & Ryan, J.N. 2001, 'A novel two-dimensional model for colloid transport in physically and geochemically heterogeneous porous media', *Journal of Contaminant Hydrology*, vol. 49, pp. 173-99.

- Swartz, C.H. & Gschwend, P.M. 1999, 'Field studies of in situ colloid mobilization in a southeastern coastal plain aquifer', *Water Resources Research*, vol. 35, no. 7, pp. 2213-23.
- Szecsody, J.E., Zachara, J.M., Chilakapati, A., Jardine, P.M. & Ferency, A.S. 1998, 'Importance of flow and particle-scale heterogeneity on CoII/III/EDTA reactive transport', *Journal of Hydrology*, vol. 209, no. 1-4, pp. 112-36.
- Tartakovsky, A.M., Meakin, P., Scheibe, T.D. & Eichler West, R.M. 2007, 'Simulation of reactive transport and precipitation with smoothed particle hydrodynamics', *Journal of Computational Physics*, vol. 222, pp. 654-72.
- Tinsley Oden, J. 2010, 'Finite element method', *Scholarpedia*, vol. 5, no. 5, viewed 12/12/2013, <http://www.scholarpedia.org/article/Finite_element_method>.
- Tonkin, M., Doherty, J. & Moore, C. 2007, 'Efficient nonlinear predictive error variance for highly parameterized models', *Water Resources Research*, vol. 43, no. W07429, pp. doi: 10.1029/2006WR005348.
- Townley, L.R. & Wilson, J.L. 1985, 'Computationally efficient algorithms for parameter estimation and uncertainty propagation in numerical models of groundwater flow', *Water Resources Research*, vol. 21, no. 12, pp. 1851-60.
- Trefry, M.G. & Muffels, C. 2007, 'FEFLOW: A finite-element ground water flow and transport modeling tool', *Groundwater*, vol. 45, no. 5, pp. 525-8.
- Tufenkji, N. 2007, 'Colloid and microbe migration in granular environments: A discussion of modelling methods', in F.H. Frimmel, F. Von der Kammer & H.C. Flemming (eds), *Colloidal transport in Porous Media*, 1st edn, vol. 1, Springer, pp. 119-42.
- Tufenkji, N. & Elimelech, M. 2004, 'Deviation from the classical colloid filtration theory in the presence of repulsive DLVO interactions', *Langmuir*, vol. 20, pp. 10818-28.
- Tufenkji, N., Redman, J. & Elimelech, M. 2003, 'Interpreting deposition patterns of microbial particles in laboratory-scale column experiments', *Environmental Science and Technology*, vol. 37, pp. 616-23.
- Tyagi, A. & Haan, C.T. 2001, 'Uncertainty analysis using first-order approximation method', *Water Resources Research*, vol. 37, no. 6, pp. 1847-58.
- Uma, K.O., Egboka, B.C.E. & Onuoha, K.M. 1989, 'New Statistical Grain-Size Method for Evaluating the Hydraulic Conductivity of Sandy Aquifers', *Journal of Hydrology*, vol. Amsterdam, pp. 367-86.
- Vasco, D.W., Peterson, J.E. & Majer, E.L. 1996, 'A simultaneous inversion of seismic travel times and amplitudes for velocity and attenuation', *Geophysics*, vol. 61, no. 6, pp. 1738-57.

- Vecchia, A.V. & Cooley, R.L. 1987, 'Simultaneous confidence and prediction intervals for nonlinear regression models with application to a groundwater flow model', *Water Resources Research*, vol. 23, no. 7, pp. 1237-50.
- Velikanov, M.A. 1965, *Measurement errors and empirical relations*, 1st edn, Israel Program for Scientific Translations, Springfield, Va.
- Vrugt, J.A., Diks, C.G.H., Gupta, H.V., Bouten, W. & Verstraten, J.M. 2005, 'Improved treatment of uncertainty in hydrologic modeling: Combining the strengths of global optimization and data assimilation', *Water Resources Research*, vol. 41, no. W01017, pp. doi: 10.1029/2004 WR003059.
- Vrugt, J.A., Gupta, H.V., Bastidas, W., Bouten, W. & Sorooshian, S. 2003, 'Effective and efficient algorithm for multi-objective optimization of hydrologic models', *Water Resources Research*, vol. 39, no. 8, pp. 1214.
- Vukovic, M. & Soro, A. 1992, *Determination of hydraulic conductivity of porous media from grain-size composition*, first edn, Water Resources Publications, Littleton, Colorado.
- Wada, Y., van Beek, L.P.H., Sperna Weiland, F.C., Chao, B.F., Wu, Y. & Bierkens, M.F.P. 2012, 'Past and future contribution of global groundwater depletion to sea-level rise', *Geophysical Research Letters*, vol. 39, no. 9, pp. - L09402.
- Wagner, B.J. 1992, 'Simultaneous parameter estimation and contaminant source characterization for coupled groundwater flow and contaminant transport modelling', *Journal of Hydrology*, vol. 135, pp. 275-300.
- Wagner, B.J. 1999, 'Evaluating data-worth for ground-water management under uncertainty', *Journal of Water Resources Planning and Management*, vol. 125, no. 5, pp. 281-8.
- Wagner, B.J. & Gorelick, S.M. 1989, 'Reliable aquifer remediation in the presence of spatially variable hydraulic conductivity: From data to design', *Water Resources Research*, vol. 25, no. 10, pp. 2211-25.
- Wan, J. & Wilson, J.L. 1994, 'Colloid transport in unsaturated porous media', *Water Resources Research*, vol. 30, no. 4, pp. 857-64.
- Watkins Jr., D.W. & McKinney, D.C. 1997, 'Finding robust solutions to water resources problems', *Journal of Water Resources Planning and Management*, vol. 123, no. 1, pp. 49-58.
- Wong, E.W., Sheehan, P.E. & Lieber, C.M. 1997, 'Nanobeam mechanics: Elasticity, strength, and toughness of nanorods and nanotubes', *Science*, vol. 277, no. 5334, pp. 1971-5.

- Woodbury, A.D. & Ulrych, T.J. 2000, 'A full Bayesian approach to the groundwater inverse problem for steady state flow', *Water Resources Research*, vol. 36, no. 8, pp. 2081-93.
- Yang, M., Yang, Y., Liu, Y., Shen, G. & Yu, R. 2006, 'Platinum nanoparticles-doped solgel/ carbon nanotubes composite electrochemical sensors and biosensors', *Biosensors and Bioelectronics*, vol. 21, no. 7, pp. 1125-31.
- Yao, K.M. 1968. *Influence of suspended particle size on the transport aspect of water filtration*. PhD, University of North Carolina, Chapel Hill, North Carolina. USA.
- Yao, K., Habibian, M.T. & O'Melia, C.R. 1971, 'Water and waste water filtration: Concepts and applications', *Environmental Science and Technology*, vol. 5, pp. 1105-12.
- Zadeh, L.A. 2005, *Toward a generalized theory of uncertainty(GTU)—An outline*, Computer Science Division and the Electronics Research Laboratory, Department of EECS, University of California, Berkeley, CA 94720-1776, USA, To appear in Information Sciences, .
- Zhao, B., Hu, H., Yu, A.P., Perea, D. & Haddon, R.C. 2005, 'Synthesis and characterization of water soluble single-walled carbon nanotube graft copolymers', *Journal of the American Chemical Society*, vol. 127, pp. 8197-203.
- Zheng, C. & Wang, P.P. 1999, *MT3DMS: A modular three-dimensional multispecies transport model for simulation of advection, dispersion, and chemical reactions of contaminants in groundwater systems; Documentation and user's guide*, Report Number Contract Report SERDP-99-1, US Army Corps of Engineers, Alabama.
- Zheng, M., Jagota, A., Semke, E.D., Diner, B.A., Mclean, R.S., Lustig, S.R., Richardson, R.E. & Tassi, N.G. 2003, 'DNA-assisted dispersion and separation of carbon nanotubes', *Nature Materials*, vol. 2, pp. 338-42.
- Zimmerman, D.A., de Marsily, G., Gotway, C.A., Marietta, M.G., Axness, C.L., Beauheim, R.L., Bras, R.L., Carrera, J., Dagan, G., Davies, P.B., Gallegos, D.P., Galli, A., Gomez-Hernandez, J.J., Grindrod, P., Gutjahr, A.L., Kitanidis, P.K., LaVenue, A.M., McLaughlin, D., Neuman, S.P., RamaRao, B.S., Ravenne, C. & Rubin, Y. 1998, 'A comparison of seven geostatistically based inverse approaches to estimate transmissivities for modeling advective transport by groundwater flow', *Water Resources Research*, vol. 34, no. 6, pp. 1373-413.
- Zimmerman, L.R., Schneider, R.J. & Thurman, E.M. 2002, 'Analysis and detection of the herbicides dimethenamid and flufenacet and their sulfonic and oxanilic acid degradates in natural water', *Journal of Agricultural and Food Chemistry*, vol. 50, pp. 1045-52.

